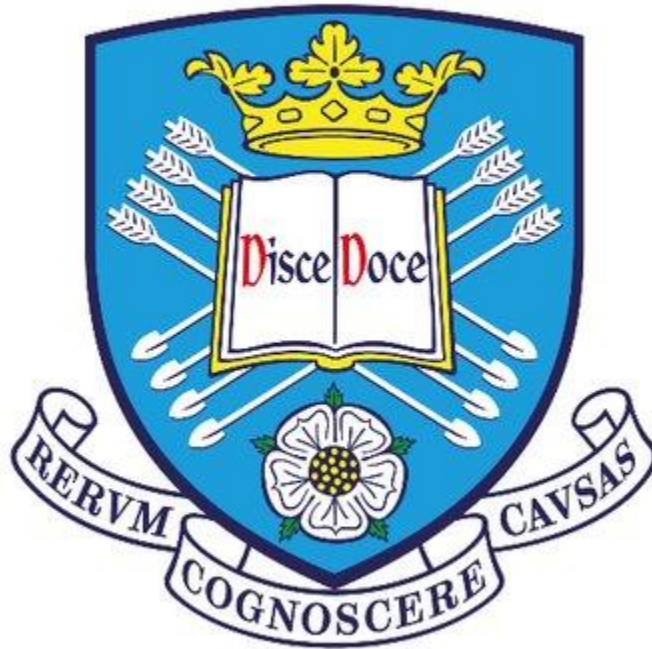


**The Application of Spatial Complementary Code  
Keying in Point-to-Point MIMO Wireless  
Communications Systems**



**Ibrahim Ali Kh Shati**

**Department of Electronic and Electrical Engineering**

**University of Sheffield**

A thesis submitted for the degree of Doctor of Philosophy

**August 2018**

*Dedicated to:*

*To my dear father Ali.*

*To my lovely mother Fatima.*

*To my small wonderful family, my wife Saliha and my kids Ali and Fatima and Farah.*

*To my brothers and sisters.*

## **Abstract**

Due to the increasing data speeds of wireless communications, there is a considerable concern about the means of sending data with lower costs and less complexity including by applying advanced coding mechanisms.

Current solutions based on techniques such as Spatial Modulation, while achieving low complexity, suffer from limited spectral efficiency. This arises from the use of restricted code sets that limit the data rate.

A spatial coding-modulation scheme based on complementary code keying (CCK) sequences with non-conventional phases in the spatial domain applied to MIMO-OFDM systems has been previously presented. Spatial CCK modulation is presented in this study where CCK is processed as a coded modulation technique applied in the spatial domain. Spatial CCK modulation is implemented for various Wi-Fi configurations of Multiple Input Multiple Output (MIMO) systems. CCK codes can achieve higher spectral efficiencies through the deployment of larger code sets. These codes improve BER performance based on the number of codeword pairs in any CCK set with large Euclidean distance. This means that low complexity detection scheme can be used effectively. The previous research, which explored spectral efficiencies of 2, 4 and 8 bit/s/Hz with CCK codes, which also has limited spectral efficiency, is defined in this thesis as an enhanced spatial CCK system.

This work extends the previous work to 11 bit/s/Hz with length 16 CCK codewords and tests this system with different detectors: zero forcing (ZF) and minimum mean square error (MMSE) and the optimal maximum likelihood detection (ML).

This research proposes spatial CCK modulation with conventional QPSK modulation phase order in CCK codewords of lengths 2, 4, 8 and 16 with wideband Rayleigh and Rician IEEE channels MIMO-OFDM system model.

The Exponential Kronecker correlation is applied as a mathematical model of correlation between antenna channels in both transmit and receive antennas, which provides more realistic channel scenarios.

The 4-phase spatial CCK system is extended to an 8-phase spatial CCK system, which is novel. This is done by applying 8-PSK modulation phases to increase the number of codewords to exploit the salient property of CCK codes in the spatial domain, such codes have many codewords with large Euclidean distances. This leads to higher spectral efficiencies in the cases of length 2, 4, 8 and 16 CCK codewords compared with the 4-phase case.

An analytical framework has been developed to evaluate the system using the CCK modulation with length 2, 4, 8 and 16 CCK codewords by constructing an analytical model of 4-phase CCK, modified CCK and 8-phase CCK under narrowband uncorrelated and correlated wireless fading channels with the optimal detection (ML) scheme. The performance of SCCK was compared with the state of the art such as spatial modulation (SM) and spatial multiplexing (SMX) with the same detector and channel conditions.

Finally, for the first time, the performance of SCCK is tested in an analytical model, whereby the performance improvement in the case of spectral efficiency compared with SM system and BER performance of SCCK principle compared with both SM and SMX schemes is validated.

# Acknowledgment

“Praise be to Allah, the Cherisher and Sustainer of the worlds;”

My deepest gratitude goes to my supervisor, Professor Timothy O’Farrell, for his support, patient, encouragement and advice throughout my PhD. His huge enthusiasm on research and fathomless knowledge in many areas has deeply inspired me. I fully appreciate his continuous support and encouragements, especially during my difficult times in work and life.

My sincere thanks go to my second supervisor Dr. Mohammed Benaissa for his support, and Dr. Abdelhamid Younis Alhassi, for his encouragement, assistance, and insightful comments. My thanks also go to Mike Croucher EPSRC Research Software Engineering Fellow at university of Sheffield for his great help in Matlab simulation and his comments and assistance in pointing out the simulation errors.

I offer my sincerest gratitude to my family for their unflagging love and support throughout my life; this thesis would have been impossible without them. I am indebted to my parents, Ali Shati and Fatima Shati, for their care, love, knowledge and support and my lovely wife Saliha Jalboub.

Last but not least, I would like to thank my lifelong friends for tirelessly supporting me in their own magical ways throughout my studies especially my colleague Stephen Henthorn for his support during the writing up stage.

“Those who do not thank people, they do not thank Allah”

(The Prophet Muhammad (pbuh))

## Table of Contents

Abstract .....	III
Acknowledgment .....	V
List of Figures .....	XI
List of Tables .....	XXI
List of abbreviations .....	XXII
Chapter 1                      Introduction .....	1
1.1 Chapter motivation and overview .....	1
1.2 Thesis problem statement and areas of novelty and originality .....	3
1.3 The aim of the thesis .....	6
1.4 Thesis objectives .....	6
1.5 Thesis outlines.....	7
1.6 List of expected Publications .....	8
Chapter 2                      Background .....	9
2.1 Chapter Overview .....	9
2.2 Wi-Fi overview .....	9
2.3 Wi-Fi standards .....	10
2.3.1 802.11b .....	10
2.3.2 802.11a .....	10
2.3.3 802.11g .....	11
2.3.4 802.11n .....	11
2.3.5 802.11ac.....	11
2.4 Complementary code keying.....	12
2.4.1 Auto correlative property of Binary complementary sequences .....	12
2.4.2 Generation of complementary sequences .....	14

2.4.3	Polyphase complementary codes .....	15
2.4.4	Complementary code keying modulation .....	17
2.5	Principles of OFDM .....	18
2.5.1	Advantages of OFDM .....	21
2.5.2	Limitations of OFDM .....	21
2.6	Space diversity .....	22
2.6.1	Alamouti space-time block coding for transmit diversity .....	22
2.6.2	Summary of Alamouti's scheme .....	24
2.7	MIMO Principles.....	24
2.8	Spatial multiplexing (SMX) .....	26
2.9	Vertical-Bell Laboratories Layered Space-Time (V-BLAST) Coding .....	26
2.10	Multipath fading.....	27
2.11	Channel correlation .....	30
2.12	Detection .....	31
2.12.1	Zero-Forcing (ZF) Detectors .....	31
2.12.2	Minimum Mean-Square Error (MMSE) Method .....	32
Chapter 3	Literature review .....	33
3.1	Chapter Overview .....	33
3.2	Spatial diversity.....	33
3.3	The evolution from MIMO to spatial modulation-MIMO .....	34
3.4	Theory of spatial modulation (SM).....	35
3.4.1	Summary of spatial modulation.....	38
3.5	Spatial Complementary Code Keying Theory .....	39
3.5.1	Conventional Spatial Complementary Code Keying.....	40
3.6	Contemporary WLAN Techniques .....	42

3.7	Summary .....	47
Chapter 4	spatial complementary code keying .....	48
4.1	Chapter Overview .....	48
4.2	An investigation of CCK with different Spectral efficiencies .....	49
4.2.1	4-bit/s/Hz Spatial Complementary Code Keying .....	49
4.2.2	6- bit/s/Hz Spatial Complementary Code Keying. ....	49
4.2.3	8- bit/s/Hz Spatial Complementary Code Keying. ....	50
4.2.4	10- bit/s/Hz Spatial Complementary Code Keying. ....	51
4.3	Largest minimum distance between Complementary Codes .....	51
4.4	Spatial Complementary Code Keying Modulation System .....	52
4.5	Simulation modeling. ....	55
4.5.1	Spatial CCK for different detection schemes Results. ....	57
4.5.2	Spatial CCK under different wireless channels with different RMS delay spread results .....	65
4.5.3	Correlated channel effect results .....	72
4.6	Bit error rate analysis of Spatial Complementary Code Keying compared to SMX and SM with narrowband fading channels. ....	79
4.6.1	BER performance results discussion .....	86
4.7	Summary .....	93
Chapter 5	System performance comparison of spatial CCK, SM and SMX .....	94
5.1	Chapter overview .....	94
5.2	Introduction .....	94
5.3	Spatial Multiplexing (SMX).....	95
5.3.1	Maximum–Likelihood Receiver for SMX .....	96
5.4	Spatial Modulation .....	96
5.4.1	SM Operating Principle .....	97

5.4.2	Maximum–Likelihood Receiver for SM .....	97
5.5	Analytical ABER performance of SM and SMX.....	98
5.6	Results discussion .....	98
5.6.1	Analytical performance of SM, SMX.....	98
5.6.2	Comparing the ABER performance of SCCK, SM and SMX .....	98
5.6.3	Comparing exemplar results of CCK-SM MIMO-OFDM systems with different spectral efficiency results with Rayleigh wideband channel and different detection schemes .....	110
5.7	Summary .....	116
Chapter 6	Modified spatial complementary code keying .....	117
6.1	Chapter Overview .....	117
6.2	Modified spatial Complementary Code Keying Modulation system.....	118
6.2.1	2-bit/s/Hz Modified Spatial Complementary Code Keying with codeword length 2-Chip. ....	118
6.2.2	4-bit/s/Hz Modified Spatial Complementary Code Keying with code word length 4-Chip .....	118
6.2.3	8-bit/s/Hz Modified Spatial Complementary Code Keying with code word length 8-Chip .....	121
6.2.4	11-bit/s/Hz Modified Spatial Complementary Code Keying with code word length 16-Chip .....	121
6.3	The Minimum Euclidean Distance between Complementary Codes.....	121
6.4.	Results and Discussions .....	122
6.4.1	Spatial CCK for different detection schemes Results .....	123
6.4.2	Modified Spatial CCK under different wireless channels with different RMS delay spread results .....	128
6.4.3	Correlated channel effect Results .....	133
6.5	Bit error rate analysis of Modified SCCK system for narrow band channel .....	138

6.5.1 Modified SCCK results discussion.....	138
6.6 Summary .....	142
Chapter 7 High order phase spatial complementary code keying.....	144
7.1 Chapter Overview .....	144
7.2 High order phase spatial Complementary Code Keying Modulation system .....	144
7.2.1 6-bit/s/Hz High order Spatial Complementary Code Keying.....	145
7.2.2 9- bit/s/Hz High order Spatial Complementary Code Keying.....	146
7.2.3 12- bit/s/Hz High order Spatial Complementary Code Keying.....	146
7.2.4 15- bit/s/Hz High order Spatial Complementary Code Keying.....	146
7.2.5 Minimum Distance Characteristics between Complementary Codewords. ....	146
7.3 Theoretical and simulations BER performance results for 8-phase SCCK with narrowband channel .....	147
7.3.1 Analytical and simulation results comparison.....	147
7.4 Simulations results for 8-phase SCCK with wideband IEEE fading channels. ....	155
7.4.1 Comparison between conventional 4-phase and 8-phase SCCK with detection schemes under wideband IEEE fading channel. ....	156
7.5. Summary .....	159
Chapter 8 Conclusions and Future Work.....	160
8.1 Conclusions .....	160
8.2 Future work .....	163
References .....	165

## List of Figures

Figure 2.1: Block diagram of a MIMO wireless communication system [12] .....	9
Figure 2.2: Complementary sequences .....	13
Figure 2.3: Flow chart of binary complementary code generation [17] .....	15
Figure 2.4: Flow chart of Polyphase complementary code generation [17] .....	17
Figure 2.5: OFDM Transmitter .....	19
Figure 2.6: Multipath received signal .....	20
Figure 2.7: OFDM receiver .....	21
Figure 2.8: Alamouti transmit-diversity scheme with $N_t = 2$ and $N_r = 1$ .....	23
Figure 2.9: Typical MIMO system [30] .....	25
Figure 2.10: Exponentially decaying channel impulse response .....	28
Figure 2.11: Frequency selective channel representation in time-frequency domain [1] .....	29
Figure 3.1: Spatial modulation with OFDM .....	38
Figure 3.2: Block diagram of conventional spatial SCCK modulation. ....	41
Figure 4.1: Block diagram of spatial CCK modulation with wideband channel .....	53
Figure 4.2: BER versus $E_b/N_0$ for spatial conventional SCCK over uncorrelated Rayleigh channel and different detection schemes with $m = 4$ , where $N_t = 2$ and $N_r = 2$ and RMS delay spread=50 ns. ....	59
Figure 4.3: BER versus $E_b/N_0$ for spatial conventional SCCK over uncorrelated Rayleigh channel and different detection schemes with $m = 4$ , where $N_t = 2$ and $N_r = 4$ and RMS delay spread=50 ns. ....	59
Figure 4.4: BER versus $E_b/N_0$ for spatial conventional SCCK over uncorrelated Rayleigh channel and different detection schemes with $m = 4$ , where $N_t = 2$ and $N_r = 8$ and RMS delay spread=50 ns. ....	60
Figure 4.5: BER versus $E_b/N_0$ for spatial conventional SCCK over uncorrelated Rayleigh channel and different receive antennas and ML detection with $m = 4$ , where $N_t = 2$ and $N_r = 1, 2, 4$ and 8 and RMS delay spread=50 ns. ....	60

Figure 4.6: BER versus Eb/No for spatial conventional SCCK over uncorrelated Rayleigh channel and different detection schemes with  $m = 6$ , where  $N_t = 4$  and  $N_r = 4$  and RMS delay spread=50 ns. .... 61

Figure 4.7: BER versus Eb/No for spatial conventional SCCK over uncorrelated Rayleigh channel and different detection schemes with  $m = 6$ , where  $N_t = 4$  and  $N_r = 8$  and RMS delay spread=50 ns. .... 62

Figure 4.8 BER versus Eb/No for spatial conventional SCCK over uncorrelated Rayleigh channel and different receive antennas and ML detection with  $m = 6$ , where  $N_t = 4$  and  $N_r = 1, 2$  and  $4$  and RMS delay spread=50 ns. .... 63

Figure 4.9: BER versus Eb/No for spatial conventional SCCK over uncorrelated Rayleigh channel and different detection schemes with  $m = 8$ , where  $N_t = 8$  and  $N_r = 8$  and RMS delay spread=50 ns. .... 64

Figure 4.10: BER versus Eb/No for spatial conventional SCCK over uncorrelated Rayleigh channel and different detection schemes with  $m = 10$ , where  $N_t = 16$  and  $N_r = 16$  and RMS delay spread=50 n. .... 65

Figure 4.11: BER versus Eb/No for spatial conventional SCCK over uncorrelated Rayleigh/Rician channel and different detection schemes with  $m = 4$ , where  $N_t = 2$  and  $N_r = 2$  and RMS delay spread=50 ns. .... 66

Figure 4.12: BER versus Eb/No for spatial conventional SCCK over uncorrelated Rayleigh channel and ZF detection scheme with  $m = 4$ , where  $N_t = 2$  and  $N_r = 2$  and RMS delay spread=50,100,150 ns. .... 67

Figure 4.13: BER versus Eb/No for spatial conventional SCCK over uncorrelated Rayleigh channel and MMSE detection scheme with  $m = 4$ , where  $N_t = 2$  and  $N_r = 2$  and RMS delay spread=50,100,150 ns. .... 67

Figure 4.14: BER versus Eb/No for spatial conventional SCCK over uncorrelated Rician IEEE channel and ZF detection scheme with  $m = 4$ , where  $N_t = 2$  and  $N_r = 2$  and RMS delay spread=50,100,150 ns. .... 68

Figure 4.15: BER versus Eb/No for spatial conventional SCCK over uncorrelated Rayleigh/Rician IEEE channel and different detection schemes with  $m = 6$ , where  $N_t = 4$  and  $N_r = 4$  and RMS delay spread=50 ns. .... 69

Figure 4.16: BER versus  $E_b/N_0$  for spatial conventional SCCK over uncorrelated Rayleigh/Rician IEEE channel and ZF detection scheme with  $m = 6$ , where  $N_t = 4$  and  $N_r = 4$  and RMS delay spread=50,100,150 ns. .... 70

Figure 4.17: BER versus  $E_b/N_0$  for spatial conventional SCCK over uncorrelated Rayleigh/Rician IEEE channel and MMSE detection scheme with  $m = 6$ , where  $N_t = 4$  and  $N_r = 4$  and RMS delay spread=50,100,150 ns. .... 70

Figure 4.18: BER versus  $E_b/N_0$  for spatial conventional CCK over uncorrelated Rayleigh/Rician channel and ZF detection scheme with  $m = 8$ , where  $N_t = 8$  and  $N_r = 8$  and RMS delay spread=50,100,150 ns. .... 71

Figure 4.19: BER versus  $E_b/N_0$  for spatial conventional SCCK over uncorrelated Rayleigh/Rician channel and ZF detection scheme with  $m = 10$ , where  $N_t = 16$  and  $N_r = 16$  and RMS delay spread=50,100,150 ns. .... 72

Figure 4.20: BER versus  $E_b/N_0$  for spatial conventional SCCK over correlated/uncorrelated Rayleigh channel and different detection schemes with  $m = 4$ , where  $N_t = 2$  and  $N_r = 2$  and RMS delay spread=50 ns and  $c=0.5$ . .... 73

Figure 4.21: BER versus  $E_b/N_0$  for spatial conventional SCCK over correlated/uncorrelated Rician channel and different detection schemes with  $m = 4$ , where  $N_t = 2$  and  $N_r = 2$  and RMS delay spread=50 ns and  $c=0.5$ . .... 74

Figure 4.22: BER versus  $E_b/N_0$  for spatial conventional SCCK over correlated/uncorrelated Rayleigh channel and different detection schemes with  $m = 6$ , where  $N_t = 4$  and  $N_r = 4$  and RMS delay spread=50 ns and  $c=0.5$ . .... 75

Figure 4.23: BER versus  $E_b/N_0$  for spatial conventional SCCK over correlated/uncorrelated Rayleigh channel and different detection schemes with  $m = 6$ , where  $N_t = 4$  and  $N_r = 4$  and RMS delay spread=50 ns and  $c=0.5$ . .... 75

Figure 4.24: BER versus  $E_b/N_0$  for spatial conventional SCCK over correlated/uncorrelated Rayleigh channel and different detection schemes with  $m = 8$ , where  $N_t = 8$  and  $N_r = 8$  and RMS delay spread=50 ns and correlation factor=0.5. .... 76

Figure 4.25: BER versus $E_b/N_0$ for spatial conventional CCK over correlated/uncorrelated Rician channel and different detection schemes with $m = 8$ , where $N_t = 8$ and $N_r = 8$ and RMS delay spread=50 ns and $c=0.5$ .....	77
Figure 4.26: BER versus $E_b/N_0$ for spatial conventional SCCK over correlated/uncorrelated Rician channel and ZF detection scheme with $m = 8$ , where $N_t = 8$ and $N_r = 8$ and RMS delay spread=50,100,150 ns and $c=0.5$ .....	78
Figure 4.27: BER versus $E_b/N_0$ for spatial conventional SCCK over correlated/uncorrelated Rician-Rayleigh channel and ZF, MMSE detection schemes with $m = 10$ , where $N_t = 16$ and $N_r = 16$ and RMS =50 ns and $c=0.5$ .....	79
Figure 4.28: spatial CCK modulation system with 4-phases and narrowband Rayleigh channel..	80
Figure 4.29: BER versus $E_b/N_0$ for SCCK over uncorrelated/correlated Rayleigh channel, where $m= 4$ and $N_t=N_r = 2$ . (Dashed line) Simulation, (solid line) Analytical.....	87
Figure 4.30: BER versus $E_b/N_0$ for SCCK over uncorrelated/correlated Rician channel, where $m =4$ and $N_t=N_r=2$ . (Dashed line) simulation, (solid line) Analytical.....	87
Figure 4.31: BER versus $E_b/N_0$ for SCCK over uncorrelated/correlated Rayleigh channel, where $m = 6$ and $N_t=N_r = 4$ . (Dashed line) Simulation, (solid line) Analytical.....	88
Figure 4.32: BER versus $E_b/N_0$ for SCCK over uncorrelated/correlated Rician channel, where $m=6$ and $N_t=N_r = 4$ . (Dashed line) Simulation, (solid line) Analytical.....	89
Figure 4.33: BER versus $E_b/N_0$ for SCCK over uncorrelated/correlated Rayleigh channel, where $m = 8$ and $N_t=N_r = 8$ . (Dashed line) Simulation, (solid line) Analytical.....	90
Figure 4.34: BER versus $E_b/N_0$ for SCCK over uncorrelated/correlated Rician channel, where $m = 8$ and $N_t=N_r = 8$ . (Dashed line) Simulation, (solid line) Analytical.....	90
Figure 4.35: BER versus $E_b/N_0$ for SCCK over uncorrelated/correlated Rayleigh channel compared with SM, where $m = 6, 10$ and $N_t=N_r = 16$ . (Dashed line) Simulation, (solid line) Analytical.....	91

Figure 4.36: BER versus  $E_b/N_0$  for SCCK over uncorrelated Rician channel compared with SM, where  $m = 6, 10$  and  $N_t=N_r = 16$ . (Dashed line) Simulation, (solid line) Analytical.....92

Figure 5.1: The SM unique three dimensional constellation diagram, where the second two bits from left to right identify the active antenna, which describes the spatial constellation. These are represented in parentheses. The signal constellation point that is to be transmitted is defined by the remaining two bit set [99] ..... 96

Figure 5.2: BER versus  $E_b/N_0$  for SMX and SM and SCCK over uncorrelated Rayleigh channel, where  $m = 4, 3, 4$  respectively and  $N_t = N_r = 2$ . (Dashed line) Simulation, (solid line) Analytical ..... 99

Figure 5.3: BER versus  $E_b/N_0$  for SMX and SM and SCCK over uncorrelated Rayleigh channel, where  $m = 8, 4, 6$  respectively and  $N_t = N_r = 4$ , (Dashed line) Simulation, (solid line) Analytical ..... 100

Figure 5.4: BER versus  $E_b/N_0$  SM and SCCK over uncorrelated Rayleigh channel, where  $m = 5, 8$  respectively and  $N_t = N_r = 8$ . (Dashed line) Simulation, (solid line) Analytical ..... 101

Figure 5.5: BER versus  $E_b/N_0$  SM and SCCK over uncorrelated Rayleigh channel, where  $m = 6, 10$  respectively and  $N_t = N_r = 16$ . (Dashed line) Simulation, (solid line) Analytical ..... 102

Figure 5.6: BER versus  $E_b/N_0$  for SM and SCCK over correlated Rayleigh channel, where  $m = 3, 4$  respectively and  $N_t = N_r = 2$ . (Dashed line) Simulation, (solid line) Analytical.....103

Figure 5.7: BER versus  $E_b/N_0$  for SM and SCCK over correlated Rayleigh channel, where  $m = 4, 6$  respectively and  $N_t = N_r = 4$ , (Dashed line) Simulation, (solid line) Analytical.....103

Figure 5.8: BER versus  $E_b/N_0$  SM and SCCK over correlated Rayleigh channel, where  $m = 5, 8$  respectively and  $N_t = N_r = 8$ . (Dashed line) Simulation, (solid line) Analytical.....104

Figure 5.9: BER versus  $E_b/N_0$  SM and SCCK over correlated Rayleigh channel, where  $m = 6, 10$  respectively and  $N_t = N_r = 16$ . (Dashed line) Simulation, (solid line) Analytical.....105

Figure 5.10: BER versus  $E_b/N_0$  for SMX and SM and SCCK over uncorrelated Rician channel, where  $m = 4, 3, 4$  respectively and  $N_t = N_r = 2$  and  $K=3dB$ . (Dashed line) Simulation, (solid line) Analytical.....106

Figure 5.11: BER versus  $E_b/N_0$  for SM and SCCK over uncorrelated Rician channel, where  $m=4, 6$  respectively and  $N_t=N_r=4$  and  $K=3\text{dB}$ . (Dashed line) Simulation, (solid line) Analytical..107

Figure 5.12: BER versus  $E_b/N_0$  for SM and SCCK over uncorrelated Rician channel, where  $m=5, 8$  respectively and  $N_t=N_r=8$  and  $K=3\text{dB}$ . (Dashed line) Simulation, (solid line) Analytical..108

Figure 5.13: BER versus  $E_b/N_0$  for SM and SCCK over correlated Rician channel, where  $m=4$  and  $N_t=N_r=2$  and  $K=3\text{dB}$ . (Dashed line) Simulation, (solid line) Analytical.....109

Figure 5.14: BER versus  $E_b/N_0$  for SM and SCCK over correlated Rician channel, where  $m=4, 6$  respectively and  $N_t=N_r=4$  and  $K=3\text{dB}$ . (Dashed line) Simulation, (solid line) Analytical....109

Figure 5.15: BER versus  $E_b/N_0$  for SM and SCCK over correlated Rician channel, where  $m=5, 8$  respectively and  $N_t=N_r=8$  and  $K=3\text{dB}$ . (Dashed line) Simulation, (solid line) Analytical...110

Figure 5.16: BER versus  $E_b/N_0$  for MIMO-OFDM-SM and MIMO-OFDM-SCCK over uncorrelated IEEE channel, where  $m=4, 6$  respectively and  $N_t=N_r=4$  and different detection scheme for SM with same modulation.....111

Figure 5.17: BER versus  $E_b/N_0$  for MIMO-OFDM-SM and MIMO-OFDM-SCCK over uncorrelated IEEE channel, where  $m=6$  and  $N_t=N_r=4$  with different modulation order.....112

Figure 5.18: BER versus  $E_b/N_0$  for MIMO-OFDM-SM and MIMO-OFDM-SCCK over uncorrelated IEEE Rician channel, where  $m=4, 4, 6$  respectively and  $N_t=N_r=4$ , ZF detection scheme and  $K=3\text{dB}$  for SM with same modulation order.....113

Figure 5.19: BER versus  $E_b/N_0$  for MIMO-OFDM-SM and MIMO-OFDM-SCCK over correlated IEEE channel, where  $m=4, 4, 6$  respectively and  $N_t=N_r=4$  and ZF detection scheme for SM with same modulation order.....114

Figure 5.20: BER versus  $E_b/N_0$  for MIMO-OFDM-SM and MIMO-OFDM-SCCK over correlated Rician IEEE channel, where  $m=4, 4, 6$  respectively and  $N_t=N_r=4$ , ZF detection scheme and  $K=3\text{dB}$  for SM with same modulation order.....115

Figure 5.21: BER versus  $E_b/N_0$  for MIMO-OFDM-SM and MIMO-OFDM-SCCK over uncorrelated wideband Rayleigh channel, where  $m=10$  and  $N_t=N_r=16$  and ZF detection scheme with different modulation order.....116

Figure 6.1: Matrix shows all possible 4-bit/s/Hz spectral efficiency for modified SCCK with code word length 4 [7].....	119
Figure 6.2: Matrix showing the selected 4-bit/s/Hz spectral efficiency for modified SCCK subset [7].....	120
Figure 6.3: BER versus $E_b/N_0$ for spatial modified CCK over uncorrelated Rayleigh channel and different detection schemes with $m = 2$ , where $N_t = 2$ and $N_r = 2$ and RMS delay spread=50 ns.....	123
Figure 6.4: BER versus $E_b/N_0$ for spatial modified SCCK over uncorrelated Rayleigh channel and different detection schemes with $m = 2$ , where $N_t = 2$ and $N_r = 4$ and RMS delay spread=50 ns.....	124
Figure 6.5: BER versus $E_b/N_0$ comparison between for spatial conventional/modified 2CCK over uncorrelated Rayleigh channel and different detection schemes with $m = 2, 4$ respectively, where $N_t = 2$ and $N_r = 2$ and RMS delay spread=50 ns.....	125
Figure 6.6: BER versus $E_b/N_0$ for spatial modified CCK over uncorrelated Rayleigh channel and different detection schemes with $m = 4$ , $N_t = 4$ and $N_r = 4$ and RMS delay spread=50 ns.....	126
Figure 6.7: BER versus $E_b/N_0$ comparison between for spatial conventional/modified 4-SCCK over uncorrelated Rayleigh channel and optimal detection schemes with $m = 4, 6$ respectively, where $N_t = 4$ and $N_r = 4$ and RMS delay spread=50 ns.....	126
Figure 6.8: BER versus $E_b/N_0$ for spatial modified CCK over uncorrelated Rayleigh channel and different detection schemes with $m = 11$ , where $N_t = 16$ and $N_r = 16$ and RMS delay spread=50 ns.....	127
Figure 6.9: BER versus $E_b/N_0$ comparison between for spatial conventional/modified 16-SCCK over uncorrelated Rayleigh channel and optimal detection schemes with $m = 10, 11$ , where $N_t = 16$ and $N_r = 16$ and RMS delay spread=50 ns.....	128
Figure 6.10: BER versus $E_b/N_0$ for spatial modified SCCK over uncorrelated Rayleigh/Rician channel and different detection schemes with $m = 2$ , where $N_t = 2$ and $N_r = 2$ and RMS delay spread=50 ns.....	129

Figure 6.11: BER versus $E_b/N_0$ for spatial modified SCCK over uncorrelated Rayleigh channel and optimal detection scheme with $m = 2$ , where $N_t = 2$ and $N_r = 2$ and RMS delay spread=50,100,150 ns.....	130
Figure 6.12: BER versus $E_b/N_0$ comparison between spatial conventional/modified 2CCK over uncorrelated Rayleigh/Rician channel and optimal detection schemes with $m = 4, 2$ respectively, where $N_t = 2$ and $N_r = 2$ and RMS delay spread=50 ns.....	130
Figure 6.13: BER versus $E_b/N_0$ for modified 4-SCCK over uncorrelated Rayleigh/Rician channel and different detection schemes with $m = 4$ , where $N_t = 4$ and $N_r = 4$ and RMS delay spread=50 ns.....	131
Figure 6.14: BER versus $E_b/N_0$ comparison between for spatial conventional/modified 4-SCCK over uncorrelated Rayleigh/Rician channel and different detection schemes with $m = 6, 4$ respectively, where $N_t = 4$ and $N_r = 4$ and RMS delay spread=50 ns.....	132
Figure 6.15: BER versus $E_b/N_0$ for modified 16-SCCK over uncorrelated Rayleigh/Rician channel and different detection schemes with $m = 11$ , where $N_t = 12$ and $N_r = 12$ and RMS delay spread=50 ns.....	133
Figure 6.16: BER versus $E_b/N_0$ for modified 2-SCCK over correlated/uncorrelated Rician channel and ZF detection schemes with $m = 2$ , where $N_t = 2$ and $N_r = 2$ and RMS delay spread=50 ns and correlation factor=0.5.....	134
Figure 6.17: BER versus $E_b/N_0$ comparison between for conventional/modified 4-SCCK over uncorrelated/correlated Rayleigh/Rician channel and different detection schemes with $m = 4, 2$ respectively, where $N_t = 2$ and $N_r = 2$ and RMS delay spread=50 ns.....	135
Figure 6.18: BER versus $E_b/N_0$ for modified 4-SCCK over correlated/uncorrelated Rician channel and ZF detection schemes with $m = 4$ , where $N_t = 4$ and $N_r = 4$ and RMS delay spread=50 ns and $c=0.5$ .....	136
Figure 6.19: BER versus $E_b/N_0$ comparison between for conventional/modified 4-SCCK over uncorrelated/correlated Rayleigh/Rician channel and different detection schemes with $m = 6, 4$ respectively, where $N_t = 4$ and $N_r = 4$ and RMS delay spread=50 ns and $c=0.5$ .....	136

Figure 6.20: BER versus $E_b/N_0$ for spatial modified 4-SCCK over correlated/uncorrelated Rician channel and ZF detection schemes with $m = 11$ , where $N_t = 16$ and $N_r = 16$ and RMS delay spread=50 ns and correlation factor=0.5.....	137
Figure 6.21: BER versus $E_b/N_0$ comparison between for conventional/modified 16-SCCK over correlated Rician channel and ML detection scheme with $m = 11$ , where $N_t = 16$ and $N_r = 16$ and RMS delay spread=50 ns.....	138
Figure 6.22: BER versus $E_b/N_0$ for SCCK over uncorrelated/correlated Rayleigh channel, $m = 4, 2$ respectively, where $N_t = N_r = 2$ . (Dashed line) Simulation, (solid line) Analytical.....	139
Figure 6.23: BER versus $E_b/N_0$ for SCCK over uncorrelated/correlated Rician channel, $m = 4, 2$ respectively and $N_t = N_r = 2$ . (Dashed line) Simulation, (solid line) Analytical.....	140
Figure 6.24: BER versus $E_b/N_0$ for SCCK over uncorrelated/correlated Rayleigh channel $m = 6, 4$ respectively and $N_t = N_r = 4$ . (Dashed line) Simulation, (solid line) Analytical.....	141
Figure 6.25: BER versus $E_b/N_0$ for SCCK over uncorrelated/correlated Rician channel, where $m = 6, 4$ respectively and $N_t = N_r = 4$ . (Dashed line) Simulation, (solid line) Analytical.....	141
Figure 6.26: analytical BER versus $E_b/N_0$ for conventional/modified SCCK over correlated Rayleigh channel, where $m = 10, 11$ respectively and $N_t = N_r = 16$ .....	142
Figure 7.1: spatial CCK modulation system with 8-phases and narrowband Rayleigh channel..	145
Figure 7.2: Theoretical BER versus $E_b/N_0$ for SCCK modulation over uncorrelated Rayleigh/Rician channels with $K = 3$ dB, where $m = 6$ and $N_t = N_r = 2$ . (Solid line) analytical, (Dashed line) simulation.....	148
Figure 7.3: Theoretical BER versus $E_b/N_0$ for SCCK modulation over correlated Rayleigh/Rician channels with $K = 3$ dB, where $m = 6$ and $N_t = N_r = 2$ . (Solid line) analytical, (Dashed line) simulation.....	149
Figure 7.4: Theoretical BER versus $E_b/N_0$ for SCCKM and SMX over uncorrelated Rayleigh channels, where $m = 6$ and $N_t = N_r = 2$ . (Dashed line) simulation, (Solid line) Analytical....	150
Figure 7.5: Theoretical BER versus $E_b/N_0$ for SCCK and SM over uncorrelated Rayleigh channels, where $N_t = N_r = 2$ . (Dashed line) simulation, (Solid line) Analytical .....	151

Figure 7.6: Theoretical BER versus Eb/No for SCCK modulation over uncorrelated/correlated Rayleigh channels, where $m = 9$ and $Nt = Nr = 4$ . (Solid line) analytical, (Dashed line) simulation .....	152
Figure 7.7: Theoretical BER versus Eb/No for SCCK modulation over uncorrelated/correlated Rician channels, where $m = 9$ and $Nt = Nr = 4$ . (Solid line) analytical, (Dashed line) simulation .....	152
Figure 7.8: Theoretical BER versus Eb/No for SCCKM and SM over uncorrelated Rayleigh channels, where $Nt = Nr = 4$ . (Dashed line) simulation, (Solid line) Analytical.....	153
Figure 7.9: Theoretical BER versus Eb/No for SCCK modulation over uncorrelated Rayleigh channel, where $Nt = Nr = 8$ . (Solid line) analytical, (Dashed line) simulation .....	154
Figure 7.10: Theoretical BER versus Eb/No for SCCK and SM modulation comparison over uncorrelated Rayleigh channel, where $Nt = Nr = 8$ . (Solid line) analytical, (Dashed line) simulation.....	155
Figure 7.11: BER versus Eb/No comparison between conventional 4 and 8 phase SCCK over uncorrelated Rician channel and ZF detection scheme with $m = 4, 6$ respectively, where $Nt = Nr = 2$ and RMS delay spread=50 ns. ....	156
Figure 7.12: BER versus Eb/No comparison between conventional 4 and 8 phase SCCK over uncorrelated Rayleigh channel and ZF detection scheme with $m = 6, 9$ respectively, where $Nt = Nr = 4$ and RMS delay spread=50 ns .....	157
Figure 7.13: BER versus Eb/No comparison between conventional 4-8 phase SCCK over uncorrelated Rayleigh channel and ZF detection schemes with $m = 8, 12$ respectively, where $Nt = Nr = 8$ and RMS delay spread=50 ns .....	158
Figure 7.14: BER versus Eb/No comparison between conventional 4 and 8 phase SCCK over uncorrelated Rayleigh channel and ZF detection scheme with $m = 10, 15$ respectively, where $Nt = Nr = 16$ and RMS delay spread=50 ns .....	159

## List of Tables

Table 1.1: Array size of 16x16 SCCK with different frequencies.....	5
Table 2.1:Tabulation of autocorrelation functions for a pair of complementary codes[13].....	14
Table 3.1: spatial modulation using BPSK and 4 transmit antennas.....	36
Table 3. 2: spatial modulation using 4-QAM and 2 transmit antennas. ....	36
Table 3. 3: Phase Allocation for 8-bit CCK modulation .....	42
Table 3. 4: Bit phase correspondence .....	42
Table 4.1: The Euclidean distance comparison between the code words of 8-SCCK.....	52
Table 4.2: System Simulation Parameters .....	55
Table 6.1: System Simulation Parameters .....	122
Table 7.1:The Euclidean distance comparison between the codewords of high order 2-SCCK	147

## List of abbreviations

<b>1G</b>	first generation
<b>2G</b>	second generation
<b>3G</b>	third generation
<b>3GPP</b>	third generation partnership project
<b>4G</b>	fourth generation
<b>8-PSK</b>	eight phase shift keying
<b>ABER</b>	average bit error ratio
<b>AMPS</b>	advance mobile telephone systems
<b>ARQ</b>	automatic repeat request
<b>AWGN</b>	additive white Gaussian noise
<b>B4G</b>	beyond 4G
<b>BER</b>	bit error rate
<b>Bit/s/Hz</b>	Bits per second per Hertz
<b>BPSK</b>	binary phase shift keying
<b>BW</b>	Bandwidth
<b>CCK</b>	complementary code keying
<b>CDF</b>	cumulative distribution function
<b>CDMA</b>	code–division multiple access
<b>CFO</b>	carrier frequency offset
<b>CP</b>	cyclic prefix
<b>CSI</b>	channel state information
<b>D–AMPS</b>	digital advanced mobile phone services
<b>D–BLAST</b>	diagonal Bell Labs layered space–time
<b>DL</b>	downlink
<b>DSL</b>	digital subscriber line
<b>DSP</b>	digital signal processing
<b>ED</b>	Euclidian distance
<b>EE</b>	energy efficiency
<b>EGC</b>	equal gain combining

<b>FDD</b>	frequency division duplex
<b>FDE</b>	frequency domain equalisation
<b>FDM</b>	frequency-division <i>multiplexing</i>
<b>FDMA</b>	frequency–division multiple access
<b>FEC</b>	forward error correction
<b>FFT</b>	fast Fourier transform
<b>F-GNSM</b>	fully generalized special modulation
<b>Fig</b>	figure
<b>FIR</b>	finite impulse response
<b>FO</b>	frequency offset
<b>FWT</b>	Fast Walsh Transform
<b>GNSM</b>	generalised spatial modulation
<b>GPRS</b>	general packet radio service
<b>GSM</b>	global system for mobile
<b>GSSK</b>	generalised space shift keying
<b>IAS</b>	inter-antenna synchronization
<b>IBDFE</b>	iterative block decision feedback equalisation
<b>ICI</b>	inter channel interference
<b>IEEE</b>	institute of electrical and electronics engineers
<b>IFFT</b>	inverse fast Fourier transform
<b>IFI</b>	inter frame interference
<b>IF</b>	intermediate frequency
<b>i.i.d.</b>	identical and independently distributed
<b>IMT–2000</b>	international mobile telecommunications 2000 project
<b>IMT–Advanced</b>	international mobile telecommunications–advanced
<b>ISI</b>	inter-symbol interference
<b>ISM</b>	industrial, scientific and medical
<b>ITU</b>	international telecommunications union
<b>ITU–R</b>	radio communications sector of ITU
<b>LOS</b>	line of sight

<b>LSB</b>	least significant bit
<b>LS</b>	least squares
<b>LTE</b>	long term evolution
<b>MGF</b>	moment-generation function
<b>MISO</b>	multiple-input single-output
<b>MIMO</b>	multiple-input multiple-output
<b>ML</b>	maximum-likelihood
<b>MMSE</b>	minimum mean squared error
<b>MOK</b>	M-ary orthogonal keying
<b>MRC</b>	maximal ratio combining
<b>MRRC</b>	maximum receive ratio combining
<b>MSB</b>	most significant bit
<b>NAS</b>	network attached storage
<b>NB</b>	narrowband
<b>NLOS</b>	non-line of sight
<b>OFDM</b>	orthogonal frequency division multiplexing
<b>OFDMA</b>	orthogonal frequency division multiple access
<b>P2P</b>	point to point
<b>PAM</b>	pulse amplitude modulation
<b>PA</b>	power amplifier
<b>PAPR</b>	peak-to-average power ratio
<b>PEP</b>	pairwise error probability
<b>PDF</b>	probability distribution function
<b>PHY</b>	Physical Layer Network
<b>PIC</b>	parallel interference cancellation
<b>PSK</b>	phase shift keying
<b>QAM</b>	quadrature amplitude modulation
<b>QPSK</b>	quadrature phase shift keying
<b>QoS</b>	quality of service
<b>RF</b>	radio frequency
<b>RMS</b>	root mean square

<b>SISO</b>	single input single output
<b>SC</b>	spatial correlation
<b>SCCK</b>	spatial complementary code keying
<b>SDMA</b>	space division multiple access
<b>SE</b>	spectral efficiency
<b>SEP</b>	symbol error probability
<b>SIMO</b>	single input multiple output
<b>SIC</b>	successive interference cancellation
<b>SM</b>	spatial modulation
<b>SMX</b>	spatial multiplexing
<b>SNR</b>	signal to noise ratio
<b>SOFDM</b>	spread orthogonal frequency division multiplexing
<b>SSK</b>	space shift keying
<b>STC</b>	space time coding
<b>STBC</b>	space time block coding
<b>STBC–SM</b>	space time block coding spatial modulation
<b>TDD</b>	time division duplex
<b>TDMA</b>	time division multiple access
<b>TO</b>	timing offset
<b>UHF</b>	ultra-high frequency
<b>UL</b>	user equipment
<b>UL</b>	uplink
<b>UMTS</b>	universal mobile telephone system
<b>V–BLAST</b>	vertical Bell Labs layered space–time
<b>VGSM</b>	variable generalised spatial modulation
<b>Wi-Fi</b>	wireless fidelity
<b>WiMAX</b>	worldwide interoperability for microwave access
<b>WLAN</b>	wireless local area networks
<b>ZP</b>	zero padded

# Chapter 1

# Introduction

## 1.1 Chapter motivation and overview

RF wireless communication is defined as a connection between two end nodes using radio waves. Wireless communication has provided advantages as it enables the ease of communication across relatively vast areas. Being wireless, there is no need for either wired communication or any other physical links. Wireless networks exploit RF transceiver units between multiple users in the office or throughout the network. This is currently known as modern wireless communication with various propagation channels. There are two common types of wireless communications[1]:

- Cellular networks: these include global system for mobile GSM, code division multiple access CDMA, time division multiple access TDMA and long term evolution LTE[2].
- Wireless Local Area Networks (WLAN): these mostly conform to the Wi Fi (IEEE 802.11) standard[3].

Orthogonal frequency division multiplexing (OFDM) is used as the basic mechanism to send the data among multiple transmitters and receivers. Considerable research has been carried out on the use of multiple input multiple output MIMO with OFDM as MIMO-OFDM system. Practically, it has been seen as the alternative to a single carrier as well as to single input-single output (SISO) systems. SISO systems have simplicity in construction since they are based on the connection between a single transmitter and receiver. Therefore, the fundamental property of using MIMO OFDM is based on dividing the data stream to be transmitted in parallel using OFDM mechanism. It is essential to introduce the core parameters for assessing these mechanisms. These are the amount of data transferred per unit of time (capacity), and the bit error rate performance (BER). In terms of flexibility with channel coding, MIMO OFDM provides more capacity than SISO with a low BER by using forward error correction coding as well as interleaving. The performance of forward error correction (FEC) is based on transmitting the data with protected bits, referred to as redundancy, to the other side. The function of these extra bits is to recover the data when an error occurs without need for packet retransmission. Compared with the alternative mechanism of Automatic Repeat Request (ARQ), this process can save more bandwidth, reduce packet losses and give low latency. Since its inception, FEC has played a major role in providing significant performance improvements in MIMO OFDM. This performance, combined with new types of

codes, can be evaluated on an Additive White Gaussian Noise (AWGN) channel. AWGN is defined as a channel model that has linear addition with a constant spectral power density and Gaussian distributed amplitude. At higher data rates, the issue of inter carrier interference (ICI) occurs when there is interference between the transmission and the receiver face. This results in an inability to extract the code correctly. For this reason, there is a guard interval that is used between two symbols to tackle the issue of ICI and it is precisely related to the channel; thereby the data can be restored [4].

Recent decades have witnessed intensive research in the field of data transmission in wireless communication systems. This is due to the ever-increasing demand for multimedia to be delivered by wireless mechanisms. One key issue in this regard is the multipath phenomenon which results in signal fading. This is equivalent to random variation in the gain of the channel, a variation that is caused by multipath scattering. Previously, multipath scattering was a major issue in wireless communications systems. However, with the implementation of multiple antennas at both the transmitter and the receiver (MIMO), the associated rich scattering environment has the capability to increase the data rate by creating a multiplicity of independent channels. This results in reducing the required cost without the need for additional bandwidth [1]. This feature has provided significant growth in wireless solutions. As seen in mobile technology the number of subscribers is large. A clear trend has been established to use mobile cellular telephony instead of fixed lines. Globally mobile cellular subscriptions have increased four-fold by the end of 2017 compared to the fixed lines. A major change has been seen with both vendors and mobile network operators in respect of the quality of an efficient network design fabrication [5].

Over the last ten years, there has been a vast improvement in terms of the speed related to each standard. Long Term Evolution (LTE) was the first release of OFDM technology in the Third Generation Partnership Project (3GPP) in December, 2008. In addition, the commercial application of this experienced significant improvement two years after its invention. Following this, LTE-Advanced was released in March, 2011. This created compatibility between LTE and the International Telecommunication Union (ITU) fourth generation in the wireless communication technology: IMT-Advanced. The data services are the main interest of all mobile generations. They show the distinction in the improvement of features in each generation such as 3G and later, 4G. However, looking ahead to the fifth generation, there will be more channel diversity due to the demand for more capacity. This shows a development proportional to the rate

of demand as well as an increase in population density, as observed on the continent of Asia. In certain situations, traffic and data services can be improved with device-to-device communications; for instance, smart grids, smart homes, cities and e-health. The future of this technology will require greater sustainability of the network technology compared to present networking. In short, if we are not able to deliver a new model which exceeds the potential achievements with LTE-Advanced, there will be no successful commercialisation of 5G [6].

The key element that guide research in future wireless communication systems is high spectral efficiency and Throughput improvement[7] . As a result, spatial complementary code keying SCCK modulation is proposed as a solution offering higher spectral efficiency than spatial modulation SM [8] with BER performance improvement compared with spatial modulation SM and spatial multiplexing SMX systems, which are explored in this research.

## 1.2 Thesis problem statement and areas of novelty and originality

As a result of the rapid evolution in wireless communications networks, especially in WLANs, there has been a considerable amount of research to improve systems in terms of spectral efficiency and complexity. As a point of comparison for current systems in terms of these criteria, spatial modulation (SM) is less complex but has lower spectral efficiency and less reliable system performance compared with SMX. As discussed in [8], the spectral efficiency increases with the base-2 logarithm of the total number of transmit antennas used in spatial modulation (SM). This is a significant disadvantage compared to Vertical-Bell Laboratories Layered Space-Time (V-BLAST) where the spectral efficiency linearly increases with the number of transmit antennas. For instance, if there is a MIMO system with eight transmit and receive antennas, by utilising V-BLAST with 16 QAM, a spectral efficiency of 32 bit/s/Hz can be achieved. However, with the same configuration and modulation order in SM, the spectral efficiency is only 7 bit/s/Hz. In order for SM to obtain the same spectral efficiency as that for V-BLAST with 16 QAM, it requires  $2^{28}$  transmit antennas, which is not feasible.

The complexity and the spectral efficiency of the proposed complementary code keying CCK system is considered as moderate compared with SM and V-BLAST as a result of spectral efficiency equations for the three systems, which are:

For spatial modulation [8]

$$m = \log_2(N_t) + \log_2(M) \text{ bit/s/Hz} \quad (1.1)$$

For spatial complementary code keying modulation [9]

$$m = (1 + \log_2(N_t))\log_2(M) \text{ bit/s/Hz} \quad (1.2)$$

And for spatial multiplexing [8]

$$m = N_t \log_2(M) \text{ bit/s/Hz} \quad (1.3)$$

Where  $m$  is the spectral efficiency of the system,  $N_t$  is the number of transmit antennas,  $M$  is the number of symbols in the modulation scheme, and  $\log_2(M)$  is the modulation order.

CCK codes have a useful distance property when used in the spatial domain. This property indicates that the number of codewords with large Euclidean distances between each pair of codewords is more than the number that have a small Euclidean distance. This helps to achieve reliable system performance with high spectral efficiency. It should be noted that CCK codes are quite resistant to the destructive effects of channel impairments [9]. This helps to improve the BER performance. Added to this is the fact that increasing the phase order of the CCK code by applying eight phase shift keying (8PSK) increases the number of codewords with the large Euclidean distance property, thereby giving higher spectral efficiency compared with systems such as SM.

In terms of spectral efficiency comparison between SCCK, SM and SMX in the previous example of a system with 16 modulation symbols and eight transmit/receive antennas, then SCCK requires 128 transmit antennas compared with  $2^{28}$  transmit antennas in SM system, which means less complexity than SMX as well as less cost than SMX. In this research CCK up to 8 modulation symbols has been studied. Reference [9] applies non-conventional phases and concentrates on improving the system BER performance. These non-conventional phases are allocated instead of applying 4-phases in length 2 and 4 CCK codeword generation cases, but length 8 codeword generation applies the conventional 4-phases.

The relationship between the frequency of operation and the physical size of the arrays at certain frequencies in this research is considered. For example, taking the frequencies 2.45GHz in 802.11g, 5.9 GHz in 802.11a and 28 GHz which corresponds to a millimeter wave channel [10], and work out the physical size of 4x4, 8x8 and 16x16 arrays (assuming half-wavelength spacing).

For the 2.45GHz band, we could say that some of those sizes are practical only at a wireless access point, rather than in a wireless mobile device because of the large separation of the antenna at 2.45 GHz.

For example, for {16, 16} SCCK

$$\lambda = \frac{c}{f} \quad (1.4)$$

where  $\lambda$  is the wave length in  $m$  and  $c$  is the speed of light which equal  $3 \times 10^8 m/s$  and  $f$  is the frequency in Hz

The table 1.1 below shows the array size (unit measured by meter) of the SCCK system is controlled by the range of frequency:

Frequency (GHz)	Wavelength ( $\lambda$ ) m	Array Type	Array Size {Nt,Nr}	Array size
			{16,16}	
2.45	0.1224	ULA	16X1	$(\lambda/2) \times 16 = 0.9792$
		UPA	4X4	$((\lambda/2) \times 4)^2 = 0.0599$
5.9	0.0508	ULA	16X1	$(\lambda/2) \times 16 = 0.4064$
		UPA	4X4	$((\lambda/2) \times 4)^2 = 0.0103$
28	0.0107	ULA	16X1	$(\lambda/2) \times 16 = 0.0848$
		UPA	4X4	$((\lambda/2) \times 4)^2 = 0.00045$

**Table 1.1:** Array size of 16x16 SCCK with different frequencies

The increased array size at 2.45 GHz can be practical in mobile stations such as laptops (e.g. placing them in the lid of the device). However, frequencies up to 2.45 GHz are impractical for the smaller mobile ubiquities. The wavelength as measured in equation 1.4 shows the reciprocal relationship with the frequency, thus the lower requirement of wavelength between the antennas of the array. As shown in Table 1.1, the higher frequencies such as 5.9 GHz or 28 GHz could mitigate the effect and decrease the required space of the array size. This is more likely to be practical for wireless devices, such as tablets, and mobile phones. However, this thesis does not concentrate on the application of the millimeter wave channel but it focus on the spatial coding.

### 1.3 The aim of the thesis

The aim of this research is to explore the application of conventional CCK (i.e. 4-phase CCK) codes (a unit magnitude complex code) in spatial MIMO wireless communications system.

In this current research, these spatial CCK concepts will be proved mathematically and validated by simulation. The obtained results will be compared with the established SM and SMX schemes, in order to prove that our new scheme can provide higher capacity with good BER performance.

### 1.4 Thesis objectives

Specific objectives are to compare CCK with SM and SMX using:

- 1- Conventional CCK codes (4-phases), which applies the conventional QPSK phases in the generation of the CCK codewords of each 2, 4,8,16 CCK codeword lengths.
- 2- Higher order CCK codes (8-phase): here 8-phases based on 8-PSK for higher number of bits per codeword.
- 3- Regenerated modified CCK codes based on [8], which applied by non-conventional phases instead of the standard 4-phases of conventional CCK except the case of generating 8CCK codeword length. For example, applying 2-phases for 2CCK codeword length and 3-phases for 4CCK codeword length and 4 phases for 8CCK codeword length as discussed in [8], as a result of that we will expected 5 phases for 16 CCK codeword length and generate the codewords based on these phases as will be discussed in Chapter 6.
- 4- Comparison of performance in Rayleigh and Rician channels which represent the system performance in non-line of sight (NLOS) and line of sight (LOS) cases respectively.
- 5- Performance in the presence of channel correlation at both the transmit side ( $N_t$ ) and the receive side ( $N_r$ ), which provides more realistic channel scenarios.
- 6- Comparison of the performance of detection schemes such as zero forcing (ZF), minimum mean square error (MMSE) and the optimal maximum likelihood detection (ML).
- 7- Evaluating wideband (WB) SCCK by simulation only in an MIMO-OFDM scenario.
- 8- Evaluating narrowband spatial complementary code keying NB-SCCK by simulation and analysis.

## 1.5 Thesis outlines

**Chapter Two** includes the basic background of materials related to the system. This chapter also discusses the fundamental aspects of the proposed system. Moreover, it includes the previous theories that have been explored in the field of Wi-Fi network enhancement.

**Chapter Three** presents a review of the work that has been done related to the novel system based on spatial complementary code keying modulation. A literature review of the system is provided including the state of art of the CCK modulation and how the new system is related to the existing SM and SMX schemes.

**Chapter Four** evaluates the proposed spatial CCK system in the conventional case with 4-phases and applies CCK codewords in the proposed system. Channel correlation is applied to model more realistic scenarios. The Kronecker model is used as a mathematical description. It is known that this model does not capture all possible scenarios of correlation to their full extent, but since the interest of using a different spatial multiplexing techniques is a comparative study, its use is considered justified [6]. The results are discussed and compared for different wireless channels and different detection schemes. Analytical BER is presented for the narrowband MIMO system and the results are compared with simulation results.

**Chapter Five** compares the bit error rate performance of the proposed spatial MIMO-OFDM-CCK against a MIMO-OFDM-SM system. This comparison ensures the same channel and detection conditions. The results of this comparison demonstrates the advantages of CCK systems compared with the state-of-the-art. The comparison includes the analytical BER of conventional CCK compared with SM and SMX in a narrowband channel [11].

**Chapter Six** models the modified spatial complementary code keying system in [7] and advances that work by including the length 16CCK codeword. Modified CCK depends on choosing specific phases that generate codewords with a large Euclidian distance property. This feature improves the BER performance of the system. However, enhancing the BER performance comes at the cost of decreasing the spectral efficiency. The key point of the chapter is to exploit the properties of the

codewords to improve the BER performance. This system is tested in different wideband wireless channels and different receiver detectors. New analytical results for NB channels are compared with the 4-phase conventional CCK system.

**Chapter Seven** considers the 8-phase SCCK scheme, which gives higher spectral efficiencies than the previous cases discussed in Chapters 4 and 6. 8-PSK phases produce more codewords than conventional and modified CCK. This provides more codewords with large Euclidian distance than 4-phase SCCK investigated in Chapter 4. The results are discussed and compared for different wireless channels and different detection schemes in the case of wideband channels. Analytical BER is presented for the narrowband MIMO system and the results are compared with simulation results.

**Chapter Eight** concludes the thesis by summarising the research outcomes and listing the research contributions of the work. In addition, possible future research directions are suggested.

## **1.6 List of expected Publications**

- 1- Journal paper ‘Spatial complementary code keying for high capacity point-to-point MIMO wireless communication systems’ (to be submitted).
- 2- Journal letter ‘High order Spatial CCK system’ (to be submitted).

# Chapter 2

# Background

## 2.1 Chapter Overview

The following chapter outlines the fundamental principles of point-to-point (P2P) MIMO, including the modulation schemes and mechanisms that are required to introduce the system proposed in this study. As a preliminary overview, Fig 2.1 shows the fundamental process of wireless communication in a point-to-point MIMO system[12] .

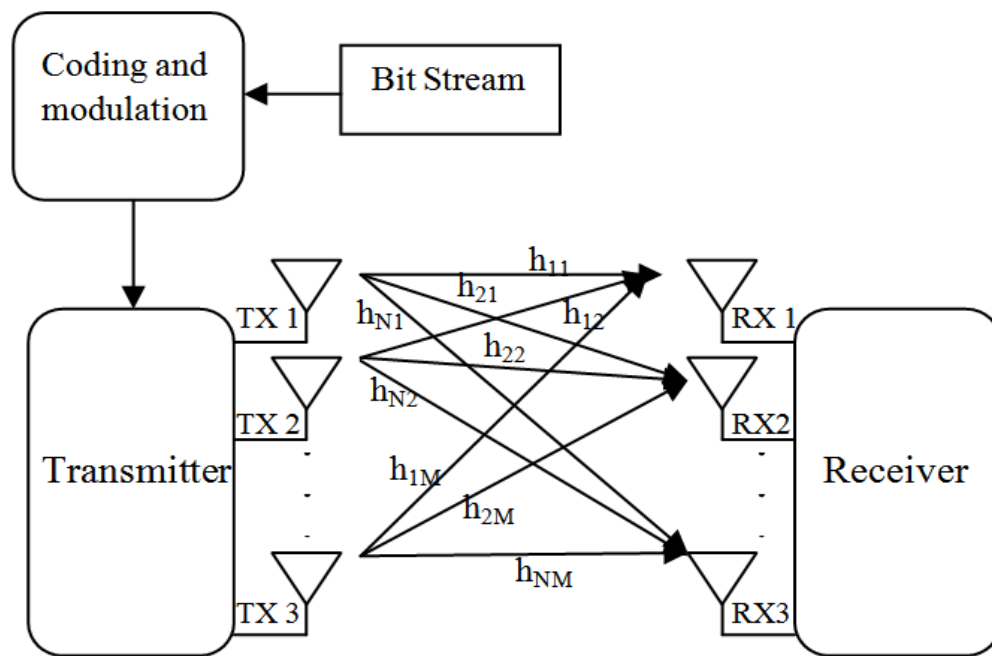


Figure 2.1: Block diagram of a MIMO wireless communication system [12]

## 2.2 Wi-Fi overview

Wi-Fi networking mechanisms permit devices, such as computers, to connect or communicate wirelessly with a wireless signal. This system depends on one of the 802.11 standards. Wi-Fi Alliance adopts the IEEE version of these standards:

802.11a, 802.11b, 802.11g, 802.11n and 802.11ac

Wi-Fi describes the method of linking computer networks wirelessly. Nearly all current computer models are manufactured with Wi-Fi chips, permitting users to detect and connect to Wi-Fi routers.

Moreover, this technique supports many applications, such as the majority of mobile devices, video game systems, and other standalone devices made possible as a result of the ability of these devices to connect with wireless networks. In addition, the establishment of any Wi-Fi connection with a router allows network communication between the router and other devices. However, this procedure must be done in conjunction with the router being connected to the Internet (via a DSL or cable modem) in order to link these devices with an internet connection. Thus, Wi-Fi connections are now ubiquitous, even without Internet access [13, 14].

## **2.3 Wi-Fi standards**

The 802.11 standards are a set of specifications developed by the Institute of Electrical and Electronic Engineers (IEEE). They are defined as a through-the-air interface between a wireless user and a base station access point or between two or more wireless users [14].

### **2.3.1 802.11b**

The 802.11b standard was established in 1999 to enhance the original 802.11 standard data rate, with data rates up to 11 Mbit/s. This standard exploited complementary code keying (CCK) modulation. However, it suffers from interference from other products operating in the 2.4 GHz band, such as cordless telephones, microwave ovens, Bluetooth devices, and baby monitors, amongst others. The most important feature of this standard is the low cost with good signal range. However, interference with other home appliances on the unregulated frequency band and the slow maximum speed are its major drawbacks [13].

### **2.3.2 802.11a**

The 802.11a standard was released in 1999 and operates in the 5 GHz frequency band. This standard supports the transfer of data up to a maximum of 54 Mbit/s and a minimum of 6.75 Mbit/s.

The required speed support for devices that exploit this standard is 6, 12 and 24 Mbit/s. Moreover, there might be optional speeds up to 54 Mbit/s and might include 48, 36, 18 and 9 Mbit/s data rates. These differences occur as a result of Forward Error Correction (FEC) levels as well as various modulation techniques. In other words, coding rate and modulation order are adapted to change data rate [13].

### **2.3.3 802.11g**

This standard operates in the same band as 802.11b, but with an additional feature that consists of the same OFDM based transmission scheme as 802.11a. This leads to a maximum bit rate of 54 Mbit/s at the physical layer, especially with forward error correction (FEC) codes, as well as a 24 Mbit/s average user-level data throughput. 802.11g hardware is fully integrated with 802.11b hardware. This gives a good signal range, which is not easily obstructed and a fast-maximum speed. The main drawback of this standard is that it is more expensive than 802.11b. Moreover, as a result of its use of an ISM frequency band, home appliances may still interfere with the signal[13].

### **2.3.4 802.11n**

The most important development of this modern standard is in exploiting the properties of MIMO. Two-stream (or two antenna) MIMO allows data rates of up to 300 Mbit/s, as well as three-streams up to 450 Mbit/s and four-streams up to 600 Mbit/s. This standard offers the fastest maximum speed with the best signal integrity and is robust against signal interference from outside sources. However, it is more expensive than 802.11g and the utilisation of multiple channels may interfere with other 802.11 b/g networks [13].

### **2.3.5 802.11ac**

The IEEE 802.11ac is an extended form of 802.11n, thus keeping backward compatibility with the previous standard. Theoretically, the maximum data rate is 600 Mbit/s when using a 40MHz bandwidth including 4 spatial streams. However, most subscriber devices are restricted to 2 streams. The 6.93 Gbit/s rate uses a 160 MHz bandwidth, in 802.11ac, which supports up to eight spatial streams and uses coding mechanism (MCS9) with 256QAM modulation compared with IEEE 802.11n that support 4 spatial streams and 64 QAM [13, 14].

As can be seen with the standards described above, wireless communication techniques tend to develop ever-increasing data throughput capabilities. The increase in data rates is achieved through improvements in the physical layer protocols. Consequently, there is a significant body of literature which explains these communications systems and the variations in the RF equipment needed. Presently, two of the most important areas in wireless standards are IEEE 802.11ax (WLAN) and 3GPP LTE-Advanced in cellular communications.

Moreover, point-to-point (P2P) wireless links, the subject of this thesis, are usually applied between two line of sight (LOS) locations to maximize the performance of the wireless link. For point-to-point wireless links working in the 5 GHz band (for example in 5.4 GHz or the 5.8 license-free bands) or in the 4.9 GHz public safety band it is suggested to deploy the P2P line in clear LOS because, above 2.4 GHz, LOS operations provide a much more reliable wireless link.

P2P wireless link at frequencies around 900 MHz or in the Ultra high frequency (UHF) band (400 MHz) can work reliably in non-line of sight conditions (NLOS P2P wireless links) [13, 14].

## **2.4 Complementary code keying**

Resulting from close cooperation between Intersil and the IEEE standards body, two WiFi specifications were created based on direct sequence spread spectrum (DSSS) techniques [13]. The first, known as the IEEE802.11 DSSS standard, used the length 11 Barker sequence with Binary Phase Shift Keying (BPSK) and Quadrature Phase Shift Keying (QPSK) modulation to obtain 1 Mbit/s and 2 Mbit/s data rates, respectively [15]. The second was the IEEE 802.11b standard, which introduced the use of Complementary Code Keying (CCK) to obtain data rates of 5.5 Mbit/s and 11 Mbit/s. The use of CCK codes were recommended by Intersil because of their superior performance in frequency selective multipath propagation with a RAKE receiver. The CCK codes used in 802.11b were based on 8-bit or 8-chip complex codewords. However, the CCK construct is more general and allows for other codeword lengths to be created in powers of two. For example, in this research lengths of 2, 4, 8 and 16 have been used, where lengths 4 and 16 have, in fact, never been generated or explored previously [16]. CCK codewords can in principle be generated for any power of two using the Walsh-Hadamard construct.

### **2.4.1 Auto correlation property of Binary complementary sequences**

In 1949, Golay first proposed the complementary codes. Initially, CCK codes were used in Infrared Spectrometry to control a series of open and closed slits in a multi-slit spectrometer [17]. Subsequently, the codes were used as block codes in communication systems such as IEEE 802.11b.

The unique correlation properties of these codes suit their use in radar applications. As shown in Fig 2.2, two identical fixed length pairs of sequences, which are characterised by the feature of the number of pairs of unlike elements with any given separation in one sequence is equal to the

number of pairs of like elements with the same separation in the other sequence. These sequences are complementary sequences and symmetrical [15].

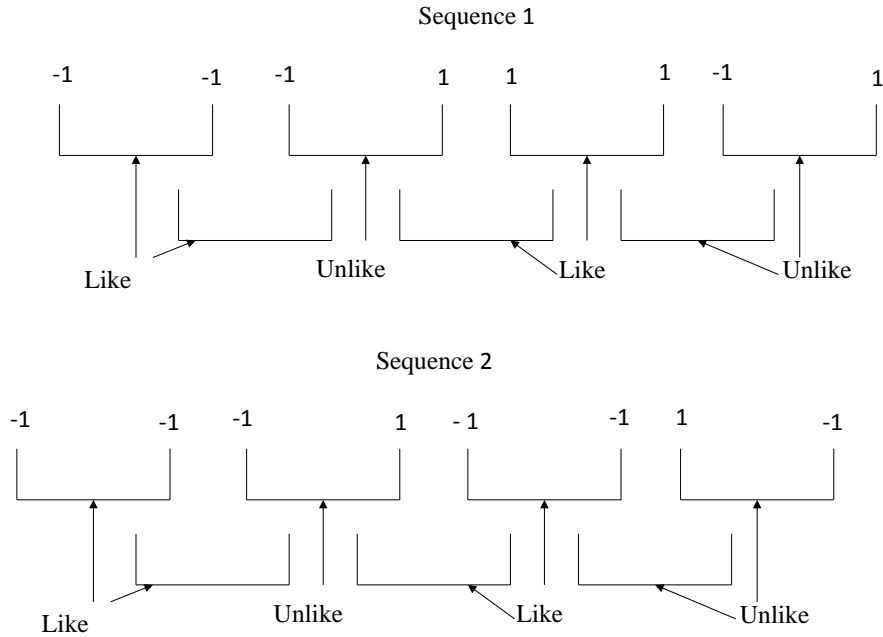


**Figure 2.2:** Complementary sequences

As formulated in [17],  $A_i$  and  $B_i$  are two complementary sequence elements where  $i = \{1, 2, \dots, n_0\}$

The autocorrelation functions  $C_j$  and  $D_j$  of the two sequences  $A_i$  and  $B_i$  are given by:

$$C_j = \sum_{i=1}^{n_0-j} A_i A_{i+j} \quad \text{and} \quad D_j = \sum_{i=1}^{n_0-j} B_i B_{i+j} \quad (2.1)$$

In general, the sequences  $A_i$  and  $B_i$  are complementary when:

$$C_j + D_j = \begin{cases} 0 & j \neq 0 \\ 2n_0 & j = 0 \end{cases} \quad (2.2)$$

Where  $n_0$  is the length of the sequence.

Table 2.1 tests the sequences  $A_i$  and  $B_i$  for the property of autocorrelation of two binary sequences [17]. At zero correlation shift the two complementary sequences have the maximum value of correlation and the minimum quantity of correlation in all other shifts.

Shift	Sequence 1								$c_i$	Sequence 2								$d_i$	$c_i+d_i$
	Code									Code									
0	-1	-1	-1	1	1	1	-1	1	8	-1	-1	-1	1	-1	-1	1	-1	8	16
	-1	-1	-1	1	1	1	-1	1		-1	-1	-1	1	-1	-1	1	-1		
1	-1	-1	-1	1	1	1	-1	1	0	-1	-1	-1	1	-1	-1	1	-1	0	0
	1	-1	-1	-1	1	1	1	-1		-1	-1	-1	-1	1	-1	-1	1		
2	-1	-1	-1	1	1	1	-1	1	0	-1	-1	-1	1	-1	-1	1	-1	0	0
	-1	1	-1	-1	-1	1	1	1		1	-1	-1	-1	-1	1	-1	-1		
3	-1	-1	-1	1	1	1	-1	1	-4	-1	-1	-1	1	-1	-1	1	-1	4	0
	1	-1	1	-1	-1	-1	1	1		-1	1	-1	-1	-1	-1	1	-1		
4	-1	-1	-1	1	1	1	-1	1	0	-1	-1	-1	1	-1	-1	1	-1	0	0
	1	1	-1	1	-1	-1	-1	1		-1	-1	1	-1	-1	-1	-1	1		
5	-1	-1	-1	1	1	1	-1	1	-4	-1	-1	-1	1	-1	-1	1	-1	4	0
	1	1	1	-1	1	-1	-1	-1		1	-1	-1	1	-1	-1	-1	-1		
6	-1	-1	-1	1	1	1	-1	1	0	-1	-1	-1	1	-1	-1	1	-1	0	0
	-1	1	1	1	-1	1	-1	-1		-1	1	-1	-1	1	-1	-1	-1		
7	-1	-1	-1	1	1	1	-1	1	0	-1	-1	-1	1	-1	-1	1	-1	0	0
	-1	-1	1	1	1	-1	1	-1		-1	-1	1	-1	-1	1	-1	-1		

**Table 2.1:**Tabulation of autocorrelation functions for a pair of complementary codes[17]

## 2.4.2 Generation of complementary sequences

The method of generating complementary sequences is founded on a “nucleus” out of which all complementary codes with longer length are obtained. This method only utilises complementary codes with lengths of powers of two [18]. Two preliminary sequences can be generated by exploiting the basic generation rule of  $A_{n_0} = A_{n_0-1}B_{n_0-1}$  and  $B_{n_0} = A_{n_0-1}\bar{B}_{n_0-1}$  where  $\bar{B}$  represents the sequence complement of  $B$  [17-19].

$$A_0 = 1, B_0 = 1 \quad (2.3)$$

$$A_1 = \{1 \ 1\}, B_1 = \{1 \ -1\} \quad (2.4)$$

$$A_2 = \{1 \ 1 \ 1 \ -1\}, B_2 = \{1 \ 1 \ -1 \ 1\} \quad (2.5)$$

$$A_3 = \{1 \ 1 \ 1 \ -1 \ 1 \ 1 \ -1 \ 1\}, B_3 = \{1 \ 1 \ 1 \ -1 \ -1 \ -1 \ 1 \ -1\} \quad (2.6)$$

$$A_4 = \{111-111-11111-1-1-1 \ 1 \ -1\}, B_4 = \{1 \ 1 \ 1 \ -1 \ 1 \ 1 \ -1 \ 1 \ -1 \ -1 \ -1 \ 1 \ 1 \ 1 \ -1 \ 1\} \quad (2.7)$$

The flow chart in Fig 2.3 presents the code generation of complementary code in eight sequences.

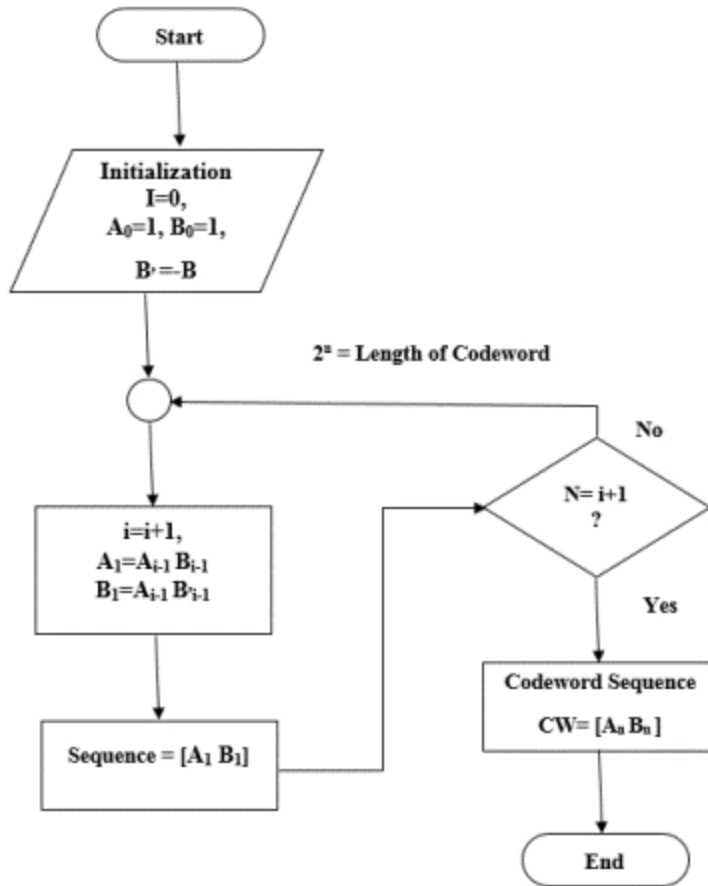


**Figure 2.3:** Flow chart of binary complementary code generation [17]

### 2.4.3 Polyphase complementary codes

Polyphase complementary codes maintain the complementary property described previously, but their elements are unity magnitude complex numbers with an associated phase  $\theta$  [15, 20]:

$$\text{And } p(t) = \begin{cases} 1 & \text{for } 0 \leq t \leq T \\ 0 & \text{for } \textit{otherwise} \end{cases} \quad (2.8)$$

where  $p(t)$  is the sum of the aperiodic autocorrelations of two complementary sequences and  $T$  is the period.

The length of the Polyphase complementary code equals the length of the codeword and it is denoted as  $N_c$ . The number of generating phases is  $1 + \log_2 N_c$  subset. For instance, a codeword

with length 8 chips will contain four subsets, i.e. subset “1”, subset “10”, subset “1100”, and subset “11110000”, in one matrix as formulated in equation (2.9) and the flowchart result of  $P_{n_r, m_c}$ , where  $n_r$  number of rows and  $m_c$  number of columns as explained.

$$P_{8,4} = \begin{bmatrix} 1 & 1 & 1 & 1 \\ 1 & 0 & 1 & 1 \\ 1 & 1 & 0 & 1 \\ 1 & 0 & 0 & 1 \\ 1 & 1 & 1 & 0 \\ 1 & 0 & 1 & 0 \\ 1 & 1 & 0 & 0 \\ 1 & 0 & 0 & 0 \end{bmatrix} \quad (2.9)$$

Equation (2.10) represents the polyphase matrix constructed from subsets shown in Fig 2.4, then this matrix is multiplied by  $e^{j\theta}$  and  $\phi_i$ , which are the CCK phases.

$$\theta = \begin{bmatrix} 1 & 1 & 1 & 1 \\ 1 & 0 & 1 & 1 \\ 1 & 1 & 0 & 1 \\ 1 & 0 & 0 & 1 \\ 1 & 1 & 1 & 0 \\ 1 & 0 & 1 & 0 \\ 1 & 1 & 0 & 0 \\ 1 & 0 & 0 & 0 \end{bmatrix} \begin{bmatrix} \phi_1 \\ \phi_2 \\ \phi_3 \\ \phi_4 \end{bmatrix} = \begin{bmatrix} \phi_1 + \phi_2 + \phi_3 + \phi_4 \\ \phi_1 + 0 + \phi_3 + \phi_4 \\ \phi_1 + \phi_2 + 0 + \phi_4 \\ \phi_1 + 0 + 0 + \phi_4 \\ \phi_1 + \phi_2 + \phi_3 + 0 \\ \phi_1 + 0 + \phi_3 + 0 \\ \phi_1 + \phi_2 + 0 + 0 \\ \phi_1 + 0 + 0 + 0 \end{bmatrix} \quad (2.10)$$

The result of this process corresponds one to one with the binary complementary code. The minus sign in the equation (2.11) is applied because of the Golay Kernel for CCK code generation definition [21].

$$C_8 = e^{j\theta}$$

$$C_8 = \{e^{j(\phi_1+\phi_2+\phi_3+\phi_4)}, e^{j(\phi_1+\phi_3+\phi_4)}, e^{j(\phi_1+\phi_2+\phi_4)}, \\ , -e^{j(\phi_1+\phi_4)}, e^{j(\phi_1+\phi_2+\phi_3)}, e^{j(\phi_1+\phi_3)}, -e^{j(\phi_1+\phi_2)}, e^{j(\phi_1)}\} \quad (2.11)$$

The flow chart of the generation process of the polyphase complementary codes is shown in Fig 2.4.

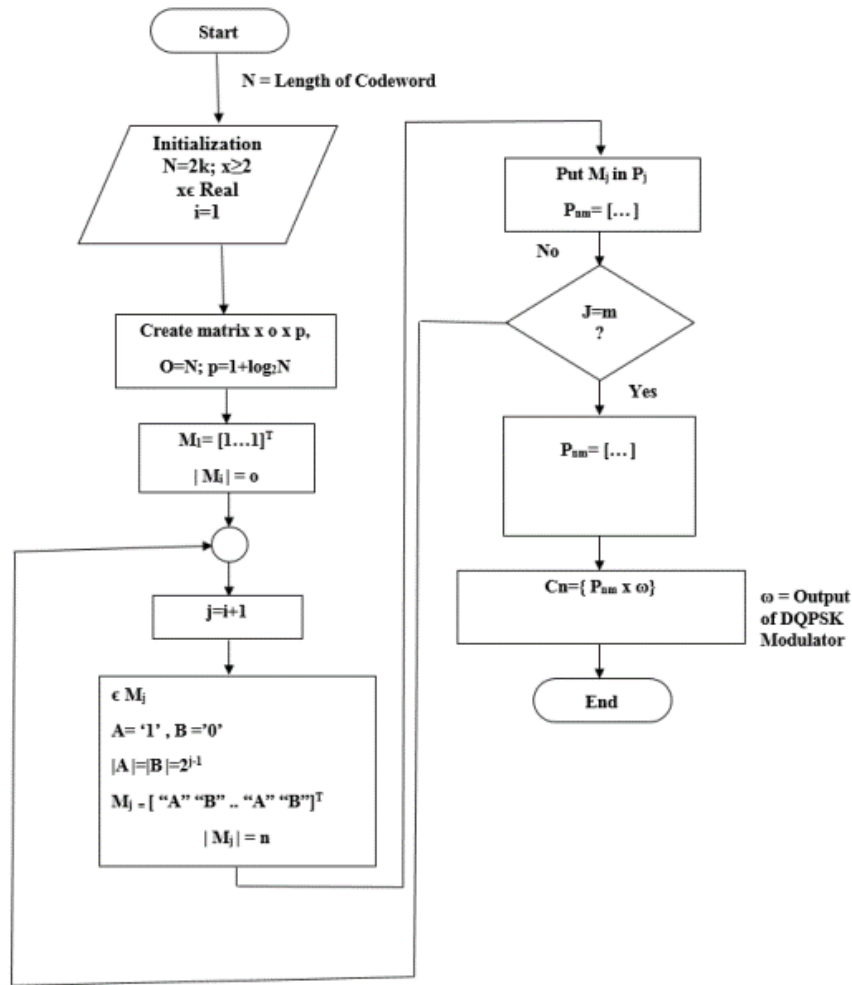


Figure 2.4: Flow chart of Polyphase complementary code generation [17]

## 2.4.4 Complementary code keying modulation

The principle of complementary code keying (CCK) modulation is based on the Complementary sequences. It was first used as an 8-bit (chip) spreading sequence and denoted one symbol in IEEE 802.11b with a chip rate of 11 Mchps. Also, it was used in a spread spectrum system to increase the data rate to 5.5Mbps and 11Mbps [17, 21, 22].

### 2.4.4.1 Complementary code keying in direct sequence spread spectrum

Time domain correlation is the fundamental property of the direct sequence spread spectrum[17].

Correlation properties improve the system performance in a multipath channel by reducing the Inter-Symbol-Interference effect, which leads to the use of spreading codes in the IEEE802.11

standard. Complementary codes of the IEEE 802.11 use 8 complex chips that can achieve a chipping rate of 11 Mchip/s.

Moreover, the symbol rate of CCK was modified in [17] to  $\sim 1.375$  MSs. As in the typical QPSK modulation, the bandwidth utilisation was improved [17, 18]. This led to enhancing the throughput to 5.5 Mbit/s and 11Mbit/s.

#### 2.4.4.2 Complementary code keying and M-ary Keying

CCK generates waveforms from multiple complementary codes, which are sent over a channel in a series of bits [16, 23]. The effective integration between modulation and coding to improve coding gain is defined as M-ary Bi orthogonal Keying (MOK) [22, 23]. The bio-orthogonal waveforms, interpreted as  $M$  symbols of  $\log_2 M$  bits, are defined by  $M$  codewords.

## 2.5 Principles of OFDM

OFDM is a parallel data transmission scheme, which avoids inter symbol interference (ISI). The frequency selective fading property of wireless channels introduces inter symbol interference (ISI) to the received wavelengths due to the effect of multipath echoes. The frequency band is partitioned into lower rate parallel sub-carriers. The subcarriers are orthogonal to each other. The flat fading effect of a sub-carrier offers many advantages as it is easy to correct compared with wideband single carrier frequency selective fading. Furthermore, a cyclic prefix (CP) protects the signal from ISI by a buffer region or guard interval. The addition of CP lowers the effective data rates [24].

If the consideration is made to have subcarriers of  $e^{j2\pi k f_c t}$  where  $1 \leq t \leq T$ , and  $k$  is an integer value in  $\{1, 2, 3, \dots, N\}$ ,  $f_c$  is the carrier spacing frequency, and  $T = \frac{1}{f_c}$  is the symbol period. The carriers are orthogonal in the duration  $T$ . The orthogonality of these carriers is over  $N$  samples.

This complex subcarriers give a complex base band representation determined by  $e^{\frac{j2\pi kn}{N}}$ .

If we modulate the  $k^{th}$  carrier by a complex symbol  $X_k$ , and collect the first  $N$  samples, we get the  $k^{th}$  modulated carrier sequence, given by [28]

$$x_n^k = X_k e^{\frac{j2\pi kn}{N}} \quad (2.12)$$

The sum of all the modulated carrier sequences scaled by  $\frac{1}{N}$  is

$$x_n = \frac{1}{N} \sum_{k=0}^{N-1} X_k e^{\frac{j2\pi kn}{N}}, 0 \leq n \leq N-1 \quad (2.13)$$

Therefore, the obtained  $N$  samples correspond to a set of  $N$  complex symbols.

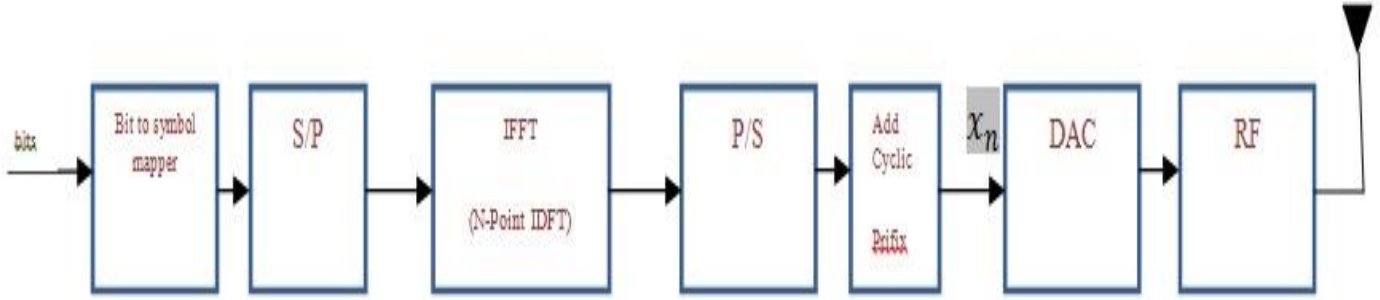


**Figure 2.5: OFDM Transmitter**

To overcome the interference produced by the symbols of the preceding frame when the sequence is sent over the multipath channel, the last  $N_g$  samples of  $x_n$  must be placed before the first sample. The  $N_g$  samples are known as Cyclic Prefix (CP) and should approximately be equal to the delay spread of the channel.

After including the CP, the sequence sent is given by:

$$x_n^c = \frac{1}{N} \sum_{k=0}^{N-1} X_k e^{\frac{j2\pi kn}{N}} \quad -N_g \leq n \leq N - 1 \quad (2.14)$$

Equation 2.16 refers to the OFDM signal where carriers divide into to subcarriers. Also, the Eqn. (2.14) is called the inverse Discrete Fourier Transform (IDFT) equation.

An OFDM transmitter consists of a bit to symbol mapper, serial-to-parallel converter, IDFT unit and CP insertion unit followed by a parallel-to-serial converter as shown in Fig 2.5. The output is transformed to an analogue signal using a DAC, then up converted to radio frequency and sent.

An L-path frequency selective channel has impulse response  $h = [h_0, h_1, \dots, h_{L-1}]$ . The signal at the input of the receiver is given by:

$$r_n = \frac{1}{N} \sum_{\lambda=0}^{L-1} h_\lambda x_{n-\lambda}^c + w_n \quad (2.15)$$

where  $w_n$  is the additive white Gaussian noise (AWGN) as shown in Fig 2.6.

After RF down conversion utilising the synchronous carriers and the conversion from analog to digital ADC, receiver output is given by:

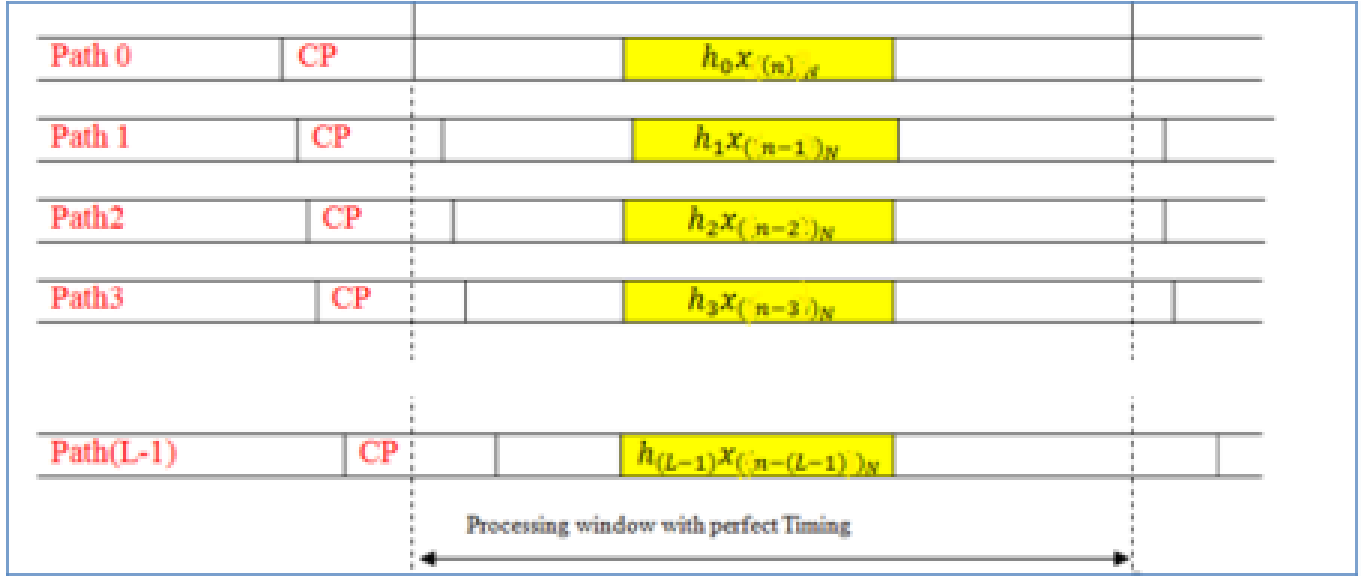


Figure 2.6: Multipath received signal

$$y_n = \frac{1}{N} \sum_{\lambda=0}^{L-1} h_{\lambda} x_{((n-\lambda))_N} + w_n \quad 0 \leq n \leq N - 1 \quad (2.16)$$

Which is the circular convolution of  $h$  and  $x$  where  $x = \{x_0, x_1, x_2, \dots, x_{N-1}\}$ . As shown in Fig 2.6 the discrete time complex baseband processing part of the receiver of OFDM system achieves synchronization. The  $k$  <sup>th</sup> output of N-point DFT unit in the receiver is represented by:

$$Y_k = X_k H_k + W_k \quad (2.17)$$

where  $H_k$  is the value of the  $k$  <sup>th</sup> subcarrier represented by:

$$H_k = \sum_{\lambda=0}^{L-1} h_{\lambda} e^{\frac{-j2\pi k n}{N}} \quad (2.18)$$

The  $k$  <sup>th</sup> sent symbol is revealed using  $Y_k H_k^*$ . The OFDM receiver is shown in Fig 2.7 [28].

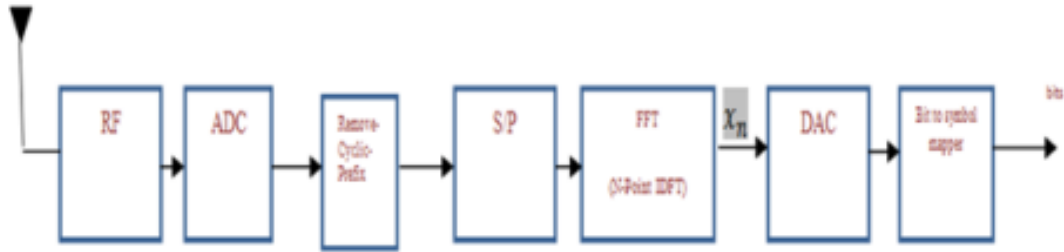


Figure 2.7: OFDM receiver

### 2.5.1 Advantages of OFDM

OFDM signaling provides the following advantages: the presence of a Cyclic Prefix (CP), the effectively matched synchronisation, and the good immunity to inter-symbol interference. In addition, circular convolution is achieved using linear convolution and the channel impulse response. As a result, the utilisation of the bandwidth is more effective compared to the traditional frequency-division multiplexing FDM. Finally, the multi-user communication systems in OFDM can be achieved by allocating various groups of subcarriers to different subscribers, similar to Orthogonal Frequency Division Multiple Access (OFDMA) used in LTE.

Because of its low cost and fast digital signal processing (DSP), which can calculate the FFT/IFFT efficiently, OFDM is simple, economic and can be compactly implemented. Therefore, it is suitable for various present and future wireless communication standards [24].

### 2.5.2 Limitations of OFDM

In OFDM error sensitivity to the synchronisation of the carrier frequency is high. The distinction between the transmitted carrier frequency and recovered carrier at the destination is defined as carrier frequency offset (CFO). A non-zero CFO represents inter-carrier interference, which occurs due to the loss of the subcarriers' orthogonality. This leads to the degradation of bit error rate performance. To overcome this degradation, it is essential to use accurate carrier frequency estimation and tracking techniques. Alternatively, inter symbol interference (ISI) cancellation techniques can be applied at the receiver to enhance the performance when there is an absence of narrow carrier frequency tracking, for instance, where the CFOs are large.

OFDM can also be sensitive to timing synchronisation errors. The amount of misalignment of the processing window is defined as Timing Offset (TO). Non-zero TOs give rise to interference of

adjacent and current frame samples. This increases the bit error rate. When TOs are higher, interference cancellation techniques can be applied at the receiver to enhance the performance.

One of the most serious issues in OFDM is its high peak-to-average power ratio (PAPR), which reduces the power amplifier efficiency. OFDM contains a throughput penalty in both the frequency and time domains resulted from adding the guard subcarriers. The fundamental reason for this is the implementation of Cyclic Prefix (CP), which is used in OFDM to add more bits to the OFDM sample to cancel interference [24].

## **2.6 Space diversity**

The gain resulting from systems that exploit multiple antennas at the transmitter and/or the receiver is of much interest [25]. As a result of the selection of the spatial separation between multiple antennas, the diversity branches benefit from uncorrelated fading [26]. In contrast to time and frequency diversity, space diversity has a very attractive property for high data rate wireless communications in that it does not require more bandwidth [27]. Different combining techniques, such as Equal Gain Combining (EGC), Maximum-Ratio Combining (MRC) and Selection Combining (SC), may be exploited at the receiver in space diversity. Moreover, codes that take advantage of diversity through space as well as time, such as space-time codes, can also be utilised at the sender side [28].

### **2.6.1 Alamouti space-time block coding for transmit diversity**

The Alamouti space-time block coding scheme is a simple scheme used to increase the reliability of transmission, which can be implemented with MISO and MIMO systems giving  $N_t \geq 2$  and any given number of receive antennas. One of its benefits is to harness the diversity in the spatial channel with no need for Channel State Information (CSI) at the transmission side. The maximum diversity of order  $N_T \times N_R$  is obtained in the case of a full diversity system, which is delivered in the channel. Full diversity cannot be achieved by all space time block codes (STBC).

The STBC can be categorised in terms of spatial rate and diversity gain, the former of which is also known as Spatial Multiplexing (SMX) and is defined as the expected number of different symbols transmitted per time period of a symbol [27]. Fig 2.8 presents the Alamouti system based on the simple state, where  $N_T=2$ ,  $N_R= 1$ .

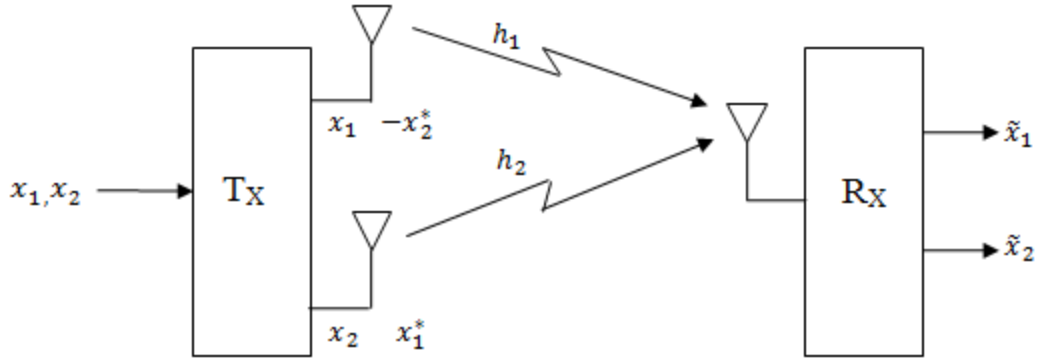


**Figure 2.8:** Alamouti transmit-diversity scheme with  $N_t = 2$  and  $N_r = 1$

Supposing the flat fading channel remains constant over two consecutive symbol periods, for two transmit symbols  $x_1$  and  $x_2$  the following matrix  $X$ , which defines the Alamouti coding can be formed:

$$X = \begin{bmatrix} x_1 & -x_2^* \\ x_2 & x_1^* \end{bmatrix} \quad (2.19)$$

Where the symbols  $x_1$ , which is sent from antenna 1, and another signal  $x_2$  which is sent from antenna 2 in the first time period. For the second time period, antenna 1 sends signal  $-x_2^*$  and signal  $x_1^*$  is sent from antenna 2. Therefore, the received symbols in two adjacent time slots are written as follows:

$$y_1 = (h_1 x_1 + h_2 x_2) + n_1 \quad (2.20)$$

And

$$y_2 = (-h_1 x_2^* + h_2 x_1^*) + n_2 \quad (2.21)$$

Since  $h_1, h_2$  represent the gain for each channel from two transmit antennas towards one receive antenna and  $n_1, n_2$  representing AWGN independent complex variables with unity variance and zero mean, then, they are combined using the combiner, which contains perfect CSI and thus recognizes the values of the channel gain generating the following signals:

$$\tilde{x}_1 = h_1^* y_1 + h_2 y_2^* \quad (2.22)$$

And

$$\tilde{x}_2 = h_2^* y_1 - h_1 y_2^* \quad (2.23)$$

So that:

$$\begin{aligned} \tilde{x}_1 &= h_1^* ((h_1 x_1 + h_2 x_2) + n_1) + h_2 ((-h_1 x_2^* + h_2 x_1^*) + n_2^*) \\ &= (|h_1|^2 + |h_2|^2)x_1 + h_1^* n_1 + h_2 n_2^* \end{aligned} \quad (2.24)$$

And similarly:

$$\tilde{x}_2 = (|h_1|^2 + |h_2|^2)x_2 + h_2^* n_1 - h_1 n_2^* \quad (2.25)$$

Thus,  $x_1$  is separated from  $x_2$  [27, 29, 30].

## 2.6.2 Summary of Alamouti's scheme

The characteristics of Alamouti's Scheme are as follows:

- 1) - There is no need for CSI feedback from the receiver to the transmitter to achieve full transmit diversity.
- 2) - There is no bandwidth increase; in other words, the redundancy is used in space across multiple antennas, not time or frequency.
- 3) – The detectors are less complex than spatial multiplexing (SMX).

## 2.7 MIMO Principles

As a result of their characteristics, Multiple Input Multiple Output (MIMO) systems have been widely discussed in research during recent years. The use of multiple antennas at both transmitter and receiver sides – known as transmit-receive diversity – is the defining feature of MIMO. Simpler variations of these systems also exist in which multiple antennas are used either only at the transmitter side (MISO), or only at the receiver side (SIMO).

A MIMO system with a typical narrowband is represented in Fig 2.9 [31, 32].

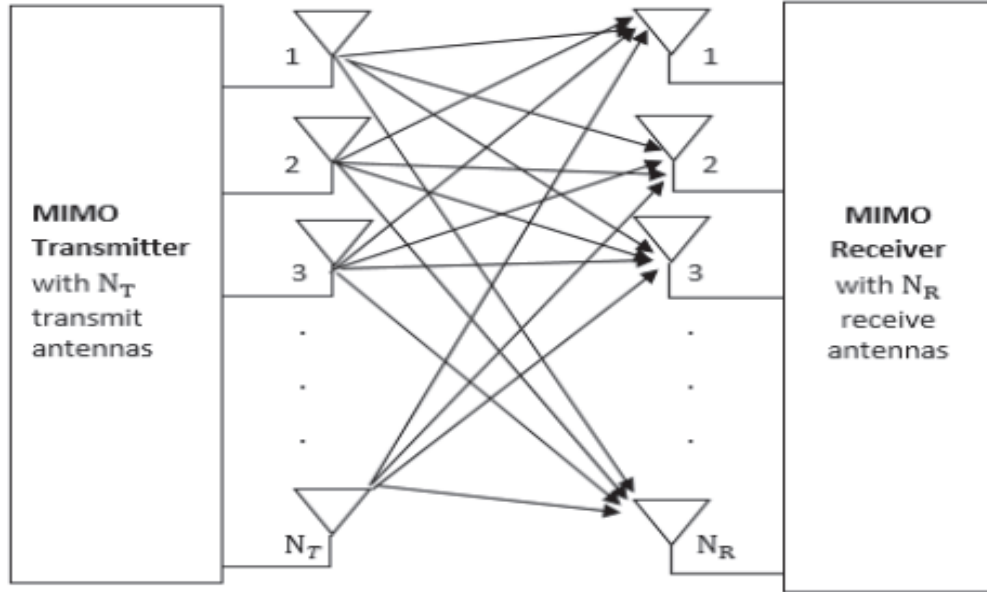


**Figure 2.9:** Typical MIMO system [30]

The most common advantages offered by the MIMO system are array gain, diversity, spatial multiplexing gain and interference minimisation.

Fig 2.9 shows a MIMO fading channel for a MIMO communication system with  $N_T$  transmit and  $N_R$  receive antennas in which each of the receiving antennas detects all the sent signals. The MIMO channel is viewed as a  $N_T \times N_R$  matrix [31, 33-35]. Over the bandwidth of interest for frequency-flat fading, the  $N_T \times N_R$  MIMO channel matrix at a certain moment of time is expressed as [31]:

$$H = \begin{bmatrix} h_{1,1} & h_{1,2} & \dots & h_{1,N_R} \\ h_{2,1} & h_{2,2} & \dots & h_{2,N_R} \\ \vdots & \vdots & \ddots & \vdots \\ h_{N_T,1} & h_{N_T,2} & \dots & h_{N_T,N_R} \end{bmatrix} \quad (2.26)$$

where  $h_{ij}$  is the gain of SISO channel between the  $i^{th}$  receive and  $j^{th}$  transmit antenna pair. The  $j^{th}$  column of  $H$  is often represented by the spatial signature of the  $j^{th}$  transmit antenna through the receive antenna array. As with SISO channels, the common model that includes the MIMO channel with independent gains in which the Rayleigh distributed random variables' amplitudes are  $h_{ij}$ . Thus, the following equation represents the receiving signal [31]

$$y = \sqrt{\frac{E_s}{N_T}} Hx + n \quad (2.27)$$

where  $y$  is the received signal vector of  $N_R \times 1$ ,  $x$  is the  $N_T \times 1$  transmitted signal vector,  $n$  is the Additive White Gaussian Noise AWGN, and  $\sqrt{\frac{E_s}{N_T}}$  normalizes the total transmitted energy ( $E_s$ ). Each transmit-receive antenna pair can be treated as a parallel sub-channel (i.e. a SISO channel). When the sending process is done over parallel channels that lead to only one channel for each antenna pair, the result is to increase the capacity in proportion to the number of transmit-receive pairs [31].

## 2.8 Spatial multiplexing (SMX)

Spatial Multiplexing (SMX) is a technique that simultaneously sends data streams independently over  $Nt$  transmit antennas. Compared to a single-antenna system, this enhances the total bit rate by multiplexing data streams without extra bandwidth or extra transmission power. By comparing this with a single antenna system, the gain in terms of bit rate is defined as a multiplexing gain [36, 37]. Bell Labs Layered Space-Time (BLAST) scheme was the first recognised spatial-multiplexing system [38, 39]. Diagonal BLAST and its subsequent development, Vertical BLAST, are two variations on Bell Labs layered Space-Time. With V-BLAST, whole signals related to individual layers are sent from the same antennas. However, in the case of D-BLAST, there is a shift in the time before the transmission. The purpose behind the shift is to reduce the complexity of decoding. V-BLAST was designed following D-BLAST to minimise inefficiency and complexity [38-40].

## 2.9 Vertical-Bell Laboratories Layered Space-Time (V-BLAST)

### Coding

Compared to SISO channels, the flat fading MIMO channels that contain many transmit and receive antennas have proven to provide large spectral efficiencies [41, 42] Capacity is linearly proportional to the number of transmit antennas when the number of receive antennas is more than or equal to the number of transmit antennas. This capacity is achievable through the Diagonal BLAST that was proposed by Foschini [41]. This method makes use of multi-element antenna arrays on both sides of the wireless link [41, 42]. There are two detection algorithms; namely, Zero-Forcing (ZF) [43] and Minimum Mean Squared Error (MMSE). Successive Interference Cancellation (SIC) provides the basis for BLAST detection schemes [43, 44]. SIC, Parallel

Interference Cancellation (PIC) and other BLAST detectors are usually affected by error propagation, which results in low efficiency transmit energies, which is improvable if the layers previously detected are cancelled appropriately. The utilisation of channel coding and interleaving can reduce the propagation errors of BLAST detectors [45-47]

## 2.10 Multipath fading

Multipath fading occurs when multiple versions of the same signal arrive with different amounts of delay and attenuation at the receiver.

The time period for which the impulse response of the channel remains unchanged is the channel coherence time  $T_c$ . The time interval between the shortest and the longest paths in a multipath channel represents the multipath delay spread  $T_m$  [31]. Equation 2.28 describes the time varying nature of the channel.

$$h(\tau, t) = \sum_{l=0}^{L(t)-1} \alpha_l(t) e^{-j\phi_l(t)} \delta(\tau - \tau_l(t)) = \sum_{l=0}^{L(t)-1} h_l(t) \delta(\tau - \tau_l(t)) \quad (2.28)$$

Generally, two models represent multipath fading, narrowband and wideband. Multipath elements are not resolvable in narrowband fading, whereas these elements can be separated in broadband fading [34]. Moreover, in both flat and frequency selective cases, the signal bandwidth of a flat fading model is smaller than the coherence bandwidth of the channel; this leads to the same attenuation level for all frequency elements. However, if the signal bandwidth is greater than the channel coherence bandwidth, this results in frequency selective fading. Slow and fast are two classifications of fading, depending on their time domain features.

The signal that is transmitted through a channel follows a Rayleigh distribution defined as a Rayleigh fading. The probability density function  $\rho_R$  is defined in equation (2.29) as:

$$\rho_R(r) = \frac{r}{P_r} e^{-\frac{r^2}{P_r}} \quad \text{and} \quad r > 0 \quad (2.29)$$

where  $\rho_R$  is the probability density function of the random variable  $r$  and  $P_r$  is the Rayleigh average power.

The Rayleigh fading is used when a channel with no line of sight consists of many tracks. Another type of fading is Rician fading. The Rician fading occurs when one of the paths, typically a line of sight signal, is not faded and often is the strongest path.

The general formula of a Rician channel is:

$$H_{Rician} = \sqrt{\frac{K}{K+1}} h_{LOS} + \sqrt{\frac{1}{1+K}} H_{Rayleigh} \quad (2.30)$$

where  $h_{LOS} = [1 \ 0 \ \dots \ 0]$  is defined as a vector, with all zero components, except for the first component being set to one;  $K$  is defined as the Rician factor where  $\sqrt{\frac{K}{K+1}}$  is the mean power of the  $LOS$  component; and  $\sqrt{\frac{1}{1+K}}$  is the mean power of the Rayleigh components [8, 48].

In the case of a wideband channel, such as the IEEE wireless fading channel, the impulse response of the channel model contains complex time domain samples. The magnitude of the time samples is Rayleigh distributed and decays exponentially. Figure (2.10) shows the impulse response of a typical channel model where the magnitude is the power delay profile, which gives the intensity of the received signal of the channel paths and the delay spread time in nanoseconds and discussed in Chapter 3.

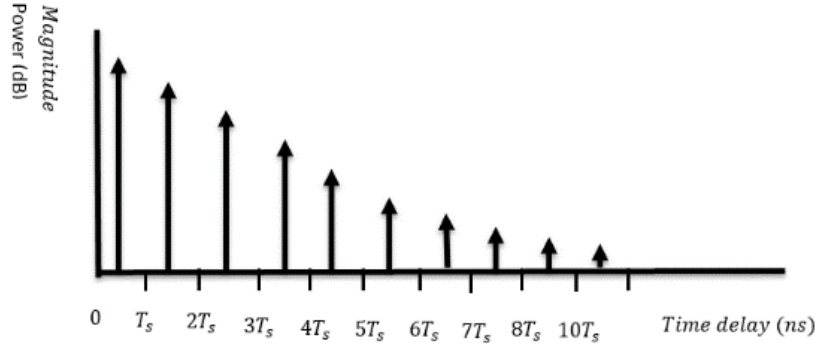


**Figure 2.10:** Exponentially decaying channel impulse response

Fig 2.10 shows an exponentially decaying frequency selective channel [9, 48], which describe in more details the nature of this IEEE channel, with sampling frequency of 80MHz and  $T_s = \frac{1}{80 \times 10^{-6}}$ . Based on the sampling frequency and the channel delay spread the channel finite impulse response (FIR) filter is applied to a raised cosine pulse shaping filter with a typical roll off factor of 0.5. The pulse shaping keeps the bandwidth usage in control. The pulse shaping output is down-sampled to 20MHz to respond with the sample period of 50 ns and avert extra frequency diversity. A root mean square (RMS) delay spread of 50 ns is a reasonable choice for an indoor office environment

[29]. Where  $H(\tau, t)$  denotes the channel and is of dimension  $N_T \times N_R$  where the number of receive antennas is  $N_R$ . And  $1 \times p$  is the size of the number of channel coefficients between each transmit-receive pair, which is a vector, where  $p$  denotes the number of channel coefficients between each transmit-receive pair. And by employing the  $N_R$  demodulators at the receiver OFDM demodulation will be used on the rows of the obtained received signal matrix  $R_c(t)$ .

$$H(\tau, t) = \begin{bmatrix} h_{1,1}(\tau, t) & h_{1,2}(\tau, t) & \dots & h_{1,N_T}(\tau, t) \\ h_{2,1}(\tau, t) & h_{2,2}(\tau, t) & \dots & h_{2,N_T}(\tau, t) \\ \vdots & \vdots & \ddots & \vdots \\ h_{N_R,1}(\tau, t) & h_{N_R,2}(\tau, t) & \dots & h_{N_R,N_T}(\tau, t) \end{bmatrix} \quad (2.31)$$

The following equation described the channel in time domain. In the case of frequency domain, the channel is defined by the frequency response using the Fourier transform of the channel in the time domain, which represents the channel as a function of frequency. Fig 2.11 shows the representation of the frequency selective channel in time and frequency domains; where  $H(f)$  is the frequency response of the channel  $h(t)$  that has the paths  $P_1, P_2,$  and  $P_3$  in delay times  $t_1, t_2,$  and  $t_3$ , respectively. In addition

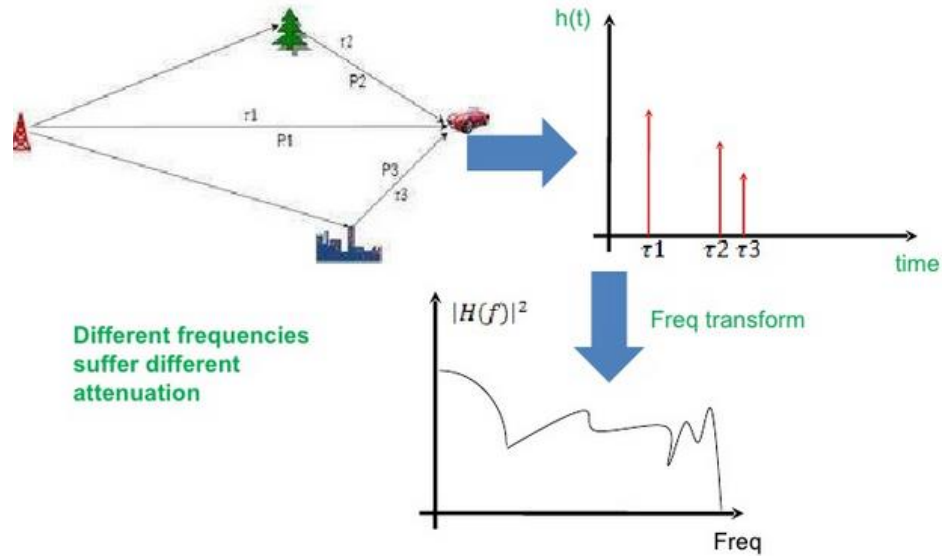


Figure 2.11: - Frequency selective channel representation in time-frequency domain [1]

$H(f)$  is the  $N_R \times N_T$  discrete time-invariant frequency response channel matrix calculated using the fast Furrier transform of the time domain channel matrix.

## 2.11 Channel correlation

In MIMO systems, the individual sub-channels can correlate. The paths between transmit antennas or receive antennas cause the channel matrix to have closely correlated elements. The correlation degrades the system BER performance [49].

In [49, 50], the correlation between different MIMO channel elements is assumed to be modelled where the correlation between receive antennas and transmit antennas is independent. They assume the immediate surroundings of the antenna array gives the correlation between array elements and have no effect on correlations observed between the elements of the array at the other end of the link. This approach is acceptable for indoor environments.

The antenna signal correlation of the MIMO channel model for Rayleigh fading is given by:

$$H = R_{N_R}^{\frac{1}{2}} H R_{N_T}^{\frac{1}{2}} \quad (2.32)$$

where  $H$  is a stochastic  $N_R \times N_T$  matrix of the channel, which can be a Rayleigh fading channel with independent identically distributed (i.i.d.) complex Gaussian zero-mean unit variance elements.  $R_{N_R}$  ( $N_R \times N_R$  Dimensions) and  $R_{N_T}$  ( $N_T \times N_T$  dimensions) denote the correlation observed on the transmitter and receiver side, respectively.

Such a correlation model in [51] covers a wide range of best-case to worst-case scenarios of correlation effects. To meet the requirements of representing the system in the real world, we can use a correlation matrix produced using an exponential decay model:

$$R_c = \begin{bmatrix} 1 & r_c & r_c^2 & \dots & r_c^{n_c-1} \\ r_c & 1 & r_c & \ddots & \vdots \\ r_c^2 & r_c & 1 & \ddots & r_c^2 \\ \vdots & \ddots & \ddots & \ddots & r_c \\ r_c^{n_c-1} & \dots & r_c^2 & r_c & 1 \end{bmatrix} \quad (2.33)$$

$$\text{Where } r_c = \exp(-\beta) \quad (2.34)$$

And  $\beta$  is defined as a correlation decay coefficient,  $n_c$  is the number of transmit or receive antennas, and  $R_c$  represents either the transmit or receive correlation matrix.

A MIMO system with  $R_c$  transmit or receive antennas and  $n$  parallel independent sub-channels has a system dimensionality of  $n_c$ . The maximum MIMO channel capacity is achieved under the

previous conditions. The channel capacity decreases if some, or all, of the sub-channels are correlated. Certain advantages might be provided by utilising spatial dimensions through  $N_T$  transmit and  $N_R$  receive antennas [49].

## 2.12 Detection

Detection means recovering information of interest that is contained in a modulated signal, in this section the ZF and MMSE detectors are discussed because of their use in the proposed system.

### 2.12.1 Zero-Forcing (ZF) Detectors

Direct matrix inversion is one of the important methods of decoding and detection. A pseudo-inverse matrix, which can be utilised for both square and non-square matrices, is a common expression to represent this situation for any received signals. Multiplying received signal  $y$  with the pseudo inverse of the channel matrix leads to the removal of the interference. This procedure is known as the Zero Forcing (ZF) detection. The following equation describes the ZF process.

$$y = \sqrt{\frac{E_s}{N_T}} H_x + n \quad (2.35)$$

Where  $y$  is the  $N_R \times 1$  received signal vector,  $H_x$  is the  $N_T \times 1$  transmitted signal vector,  $n$  is the AWGN, and the factor  $\sqrt{\frac{E_s}{N_T}}$  ensures that the total transmitted energy is  $E_s$  [52].

Hence, the ZF combiner weight  $G_{ZF}$  is given by [38, 52-55] as:

$$G_{ZF} = \sqrt{\frac{N_T}{E_s}} (H^H H)^{-1} H^H \quad (2.36)$$

Where  $H^P = (H^H H)^{-1} H^H$  defined a pseudo inverse of the channel matrix,  $H$  is the wireless channel matrix, and  $H^H$  is the complex conjugate transpose of the wireless channel  $H$ . For  $2 \times 2$  channel, the  $H^H H$  term is represented by [52, 54] as:

$$H^H H = \begin{bmatrix} h_{11}^* & h_{21}^* \\ h_{12}^* & h_{22}^* \end{bmatrix} \begin{bmatrix} h_{11} & h_{12} \\ h_{21} & h_{22} \end{bmatrix} = \begin{bmatrix} |h_{11}|^2 + |h_{21}|^2 & h_{11}^* h_{12} + h_{21}^* h_{22} \\ h_{12}^* h_{11} + h_{22}^* h_{21} & |h_{12}|^2 + |h_{22}|^2 \end{bmatrix} \quad (2.37)$$

So the interfering signal is cancelled by multiplying the received signal  $y$ , which is represented in Eq. (2.37) with the ZF weight  $G_{ZF}$  resulting in an estimated received vector  $\tilde{x}$  [52]. Thus:

$$\tilde{x} = G_{ZF}y = G_{ZF} \left( \sqrt{\frac{E_s}{N_T}} Hx + n \right) = x + G_{ZF}n \quad (2.38)$$

Noise increase is the most common disadvantage of the zero-forcing solution. Moreover, the noise amplification is large if the matrix  $H^H H$  has very small eigenvalues, which leads to the possibility of its inverse containing very large values [53].  $(N_R - N_T + 1)$  is the diversity gain (diversity order) that is accomplished utilising this detection method [43, 46]. Minimum Mean-Square Error (MMSE) is comparable to this method with slightly better performance, as the SNR is taken into consideration to calculate the matrix inversion [54].

### 2.12.2 Minimum Mean-Square Error (MMSE) Method

An MMSE receiver is described as an enhancement of the ZF receiver. MMSE endeavours to achieve an equilibrium between spatial interference suppression and noise by reducing the anticipated value of the mean square error between vector  $Hx$  (transmitted vector) and linear combination of the received vector  $G_{MMSE} y$  [30, 38] as:

$$\min E\{(x - G_{MMSE}y)^2\} \quad (2.39)$$

Where  $G_{MMSE}$  is an  $N_R \times N_T$  matrix presenting the MMSE combiner weights, which is given by [52, 56] as:

$$G_{MMSE} = \sqrt{\frac{N_T}{E_s}} \left( H^H H + \frac{N_o}{E_s} I_{NT} \right)^{-1} H^H \quad (2.40)$$

Where  $E_s$  is the transmit energy,  $N_o$  is the 1-sided noise power spectral density, and  $I_{N_T}$  is an  $N_R \times N_T$  identity matrix. An estimated received vector  $\tilde{x}$  is thus given by [57] :

$$\tilde{x} = G_{MMSE}y = x + G_{MMSE}n \quad (2.41)$$

As the SNR becomes large, the MMSE detector converges with the ZF detector. However, at low SNR, it compensates for the inversion of the smallest eigenvalues [38].

## Chapter 3

## Literature review

### 3.1 Chapter Overview

This chapter presents a review of the open literature related to spatial block coding based on complementary code keying (CCK) sequences. CCK can achieve higher spectral efficiencies through the deployment of larger code sets and BER improvement compared with spatial modulation (SM). This chapter includes a brief discussion of SM, which is the state of the art with which the SCCK modulation is compared in terms of BER performance.

### 3.2 Spatial diversity

As previously explained, the main aim of spatial multiplexing techniques is to achieve higher bit rates with enhanced error performance compared to systems using single antennas. This is achieved on the foundations of both a coding gain and a diversity gain. Improving SNR is the key consideration when utilising spatial diversity techniques. This procedure is carried out when spatial diversity is used in conjunction with an adaptive modulation or channel coding scheme [58].

Macroscopic and microscopic diversity are two common types of spatial diversity. In wireless communication scenarios these types of diversity have a relationship with shadowing effects as a result of the major obstacles that might be between the transmitter and the receiver (such as large buildings or walls). To be more specific, multiple transmit or receive antennas with large-scale separation lead to a gain due to the macroscopic diversity. In this situation, the probability that all paths are simultaneously obstructed is smaller than for a single path. The availability of microscopic (small-scale) diversity is in the environment where constructive and deconstructive superposition of signals due to scattering causes multipath fading: this is known as rich-scattering. This type of diversity can be gained by employing multiple almost co-located antennas [58]. A small fraction of the wavelength is sufficient between antenna intervals to provide links that fade independently. The possibility of all links being simultaneously in deep fade decreases with the number of utilised antennas and leads to diversity gains, which are comparable to macroscopic diversity.

Using macroscopic diversity in wireless communication systems is not new but dates back to the 1970s. Moreover, utilising multiple receive antennas to gain microscopic diversity (diversity

reception) dates from the 1950s and was exploited until the 1990s before transmit diversity techniques evolved [58].

### **3.3 The evolution from MIMO to spatial modulation-MIMO**

Traditional MIMO communications have taken the advantages of using multiple antennas at the transmitter by transmitting multiple data streams simultaneously from MIMO antennas. Therefore, all antennas are active at any given time. By adequately selecting the transmission or precoding matrices, gains from both multiplexing and transmit diversity can be achieved utilising MIMO. The main purpose of this is to activate all antennas simultaneously, providing spectral efficiency (SE) optimisation. However, this selection does not lead to energy efficiency (EE) optimisation [59-61]. For instance, under realistic base station (BS) power consumption and compared to the basic case of a single transmitting antenna, MIMO systems gain higher data rates as well as improved error performance [62].

Additional notes for MIMO systems are listed below [62]:

1. They raise the complexity of signal processing at the receiver. This is required to counteract the interference caused by multiple data streams.
2. Synchronisation requirements between several antennas contribute to exploiting the advantages of space-time codes as well as a multiuser MIMO transmission.
3. They can transmit multiple data streams due to the use of multiple RF stages at the transmitter side.
4. There is an independent power amplifier for each channel or signal, which recede the consuming power at the transmitter, where the power amplifier is inefficient as a result of the stringent linearity demands of phase or amplitude modulation.

Despite this information, a major challenge is inherent in the design of MIMO systems. This is the limitation due to multiple RF active chains, which are a target for reducing complexity. Other challenges include reducing the inter-antenna interference and the inter channel interference (ICI). It should also be noted that the signal processing at the receiver is complex when aiming to improve the EE. A single RF chain MIMO is thus explored in recent research. The basic reason for this is to understand the gains of MIMO systems, such as spatial multiplexing and diversity, based on

many antenna elements. The reason behind a shift from multiple to single RF in MIMO design comes from the assumption of a large number of antennas at the BSs, considering the complexity and power consumption required in the multiple RF case, particularly in the millimeter wave region [62].

Due to these considerations, SM has recently been suggested as a future transmission concept that is related to the single-RF chain large-scale MIMO wireless family. SM can be understood as a MIMO that possesses a many more radiation elements compared with the number of RF transmit chains. The SM-MIMO has the advantages of antenna arrays at the transmitter side while applying a restricted number of RF chains. The clear distinction of SM-MIMO is the use of extra symbols on an “SM constellation diagram” since every constellation element is transmitted by one or a subset of antennas. These characteristics aid high rate MIMO implementation with reduced complexity and signal processing as well as improved EE. Current analytical and simulation studies have demonstrated that SM-MIMOs have a built-in possibility of outperforming several state-of-the-art MIMO mechanisms provided that an adequately large number of antennas are used at the transmitter and that only a few of them are active simultaneously [62].

The rationale for SM-MIMO system design is summarised in the following points:

1. Delivery of performance constraints along with a reduction in the number of active antennas to raise the EE by minimising the circuit power consumption at the sender side (single RF MIMO basics).
2. Given the deployment and size constraints, it increases the number of passive antennas to raise both the SE and EE by minimising the transit power consumed (large-scale MIMO principle). This is achieved by capitalising on multiplexing gains presented by adding the extra bits onto the “SM constellation diagram” [62].

### **3.4 Theory of spatial modulation (SM)**

Spatial modulation was first presented by Haas [8, 63], and comprises two principles: first, the sending of information over the channel in the choice of the transmit antenna; second, the information symbol transmitted depends on the constellation [8, 64]. Moreover, there is the possibility of exploiting an arbitrary number of transmit antennas in parallel using different modulation schemes such as BPSK or M-QAM. This produces various combinations that form

SM configuration presented in Tables 3.1 and 3.2. It is clear from these tables that the dynamic variation of transmit symbols is based on the modulation order. For more clarification, consider four transmit antennas with BPSK modulation,  $(\pm 1)$ . This procedure can produce 8 code words and represents a 3-bit data sequence [8, 65]. Following this, there is a sorting process of the consecutive bits since there would be an allocation for a single transmit antenna representing each pair of two bits. It can be seen that there is exploitation of both the constellation symbol and number of transmit antennas for each of the codewords. This procedure might be substituted by 2 transmit antennas with 4-QAM modulation [63, 64] for the same spectral efficiency.

<b>Data Sequence <math>B(k)</math> (Grey Code)</b>	<b>Transmit Antenna Index</b>	<b>Transmit Symbol BPSK</b>
000	1	-1
001	1	+1
011	2	+1
010	2	-1
110	3	+1
100	3	-1
101	4	-1
111	4	+1

**Table 3.1:** spatial modulation using BPSK and 4 transmit antennas.

<b>Data Sequence <math>B(k)</math> (Grey Code)</b>	<b>Transmit Antenna Index</b>	<b>Transmit Symbol 4-QAM</b>
000	1	$-1 + j$
001	1	$+1 + j$
011	1	$+1 - j$
010	1	$-1 - j$
110	2	$+1 - j$
100	2	$-1 - j$
101	2	$-1 + j$
111	2	$+1 + j$

**Table 3. 2:** spatial modulation using 4-QAM and 2 transmit antennas.

Fig 3.1 shows the block diagram of SM system, according to the principles of spatial modulation, both  $(\pm 1 \pm j)$  for 4-QAM and the transmit antennas that are utilised to send the information are the distinguishing symbols  $B(k)$ , which are mapped from each row of input data  $(k)$  [66]. This mapping procedure depends on the spatial modulation scheme, which gives a new matrix  $s(k)$  of size  $N_t \times N_{sub}$  where  $N_t$  is the number of transmit antennas and  $N_{sub}$  is the number of OFDM sub-channels. Each row of the modulated matrix  $s(k)$  represents the transmit signal of its matching antenna. The OFDM process is applied for each row of  $k$ ; then, these OFDM symbols, denoted by  $x(t)$ , are sent through a time variant wireless channel [8, 55]. The channel is shown in equation (3.1) as a block matrix with dimensions  $N_t \times N_r$ , each vector of this matrix is a  $1 \times P_c$  vector where  $P_c$  defines the channel coefficients between each transmit–receive pair [44, 67].

As shown in Fig 3.1, the transmit signal  $x(t)$  is sent through the IEEE fading channel and the AWGN noise  $n(t)$  is added at the receive side yielding the receive signal  $r(t)$  as:

$$r(t) = H(\tau, t) \otimes x(t) + n(t) \quad (3.1)$$

Where  $\otimes$  defines the convolution process and  $H(\tau, t)$  defines the channel matrix.

At the receiver, the opposite procedure is performed as shown in Fig 3.1, firstly by applying OFDM demodulation process and removing the cyclic prefix, the demodulation signal  $R(k)$  is recovered as shown in equation (3.2).

$$R(k) = [R(1) R(2) \dots R(k) \dots R(N_r)]^T \quad (3.2)$$

Where  $k$  is the index or position of an element in  $R(k)$ .

The demodulated signal  $R(k)$  passes to the channel equalisation shown in equation (3.3) as ZF equalisation. Two important steps in processing the received signals are 1) locating the active antenna for each sub-channel, 2) discovering the sent modulation symbol.

$$f(k) = H^{-1}(k)r(k) \quad (3.3)$$

Study [8] used the Hermitian transpose of the channel frequency response for each channel when detecting the active antenna for each sub-channel. To achieve the channel frequency response of the channel taps, the response might be zero padded to extend to  $N_{sub}$  length symbols.

Transformation to the frequency domain is done by the fast Fourier transform (FFT). Moreover, the symbol detection, which is maximum value detector as presented in equation (3.4).

$$\hat{i} = \text{argmax} (|f_j(k)|) \quad (3.4)$$

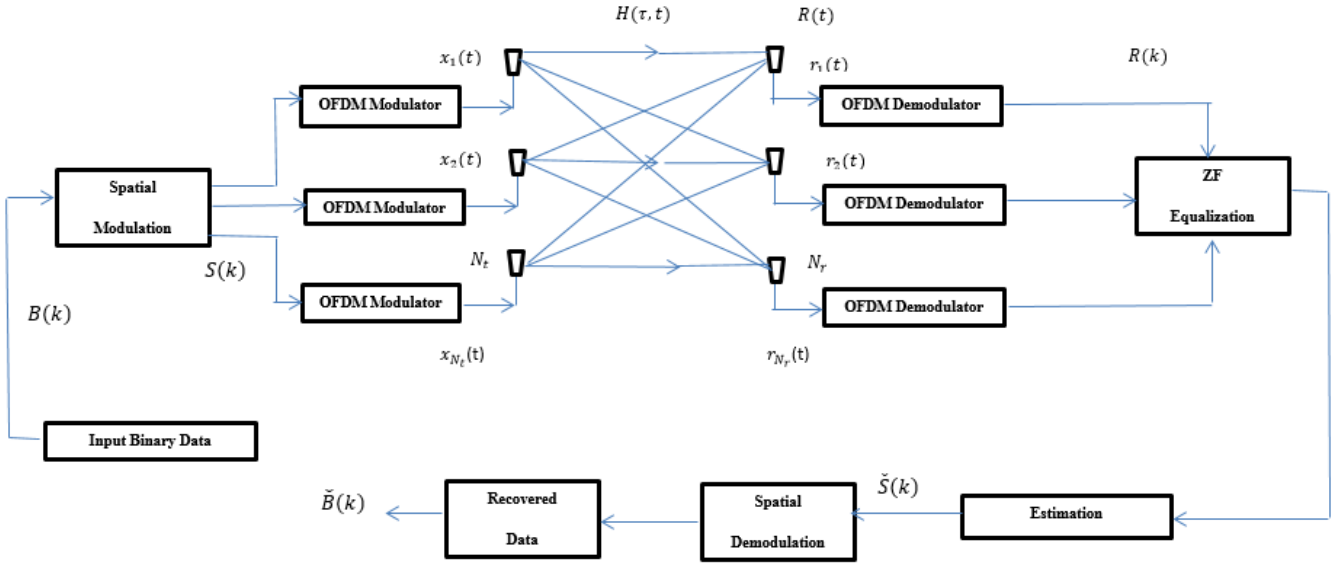


Figure 3.1: Spatial modulation with OFDM

Estimation and quantization is the next stage in the receiver. These techniques depend on the modulation scheme in terms of the index, which has the maximum absolute value that would be quantised as was shown in equation (3.5). The transmit bit sequence is determined utilising both the group transmit antenna number and the detected symbol depending on the SM mapping table (see tables (3.1) and (3.2)). It is important to confirm that the results of the data stream under the condition of estimations are accurate to get the recovered data [8, 68].

$$\check{B}(k) = Q[f_{j=i}(k)] \quad (3.5)$$

### 3.4.1 Summary of spatial modulation

One of the main properties of frequency selective fading channels is the plurality of propagation paths. This might lead to a noticeable effect caused by cross-correlation between these paths in terms of the estimated transmit antenna index. Channel characteristics and allocated antenna spacing are the two main factors on which this correlation depends.

To alleviate the impact of channel correlation, the mechanism of spatial modulation exhibits the system of a single active antenna for each of the sub-channels individually at any given time. This consists of increasing antenna spacing and reducing correlation. In addition, the principle of a single active antenna for each sub-channel dictates that only one of a group of recognisable constellation points is active in the case of the spatial range, meaning that no synchronisation is needed among the antennas and the inter-channel interference is avoided [8].

Another feature of spatial modulation is the possibility of increasing the number of transmitted bits; for instance, in the case of 8 transmit antennas being used, it is already recognised that there is the possibility of three ( $\log_2 8$ ) more bits with regards to the spatial modulation gain. Spatial modulation is also capable of transferring more data bits. This dependency is particularly significant if there are many antennas. This affects the performance due to the constraints on the spectral frequency. This leads to the idea that there is no competition allowed between this mechanism and the traditional mechanism; for instance, Vertical-Blast. In SM, there is a logarithmic increase in the spatial efficiency ( $\log_2 N_t$ ) in conjunction with an increasing number of antennas, compared to SMX, where there is a linear increase in spectral efficiency.

There are a number of limitations inherent in spatial modulation. Firstly, in the case of the input stream, the spatial modulation has to be coded with a Reed Muller code, which reduces capacity and improves the interference rejection adding to the simplicity of Reed Muller codes. Secondly, the spacing of antennas must be large enough to lessen the fading effect, or the severe multipath fading will cause complexity in the detection process. [8, 44, 69].

### **3.5 Spatial Complementary Code Keying Theory**

CCK codes are used in the spatial domain as a result of the Euclidean distances between codeword pairs in spatial CCK system is large with the majority of codes exhibiting large Euclidean distance. The more code words with large distances leads to lower BER performance since codewords with large Euclidean distances are less likely to be corrupted than other codewords. Increasing the spectral efficiency by increasing the phase order of CCK code generation is another benefit that is obtained by applying CCK codes in MIMO systems.

The first use of CCK block coding was in time domain environments with multipath delay spread up to 150 ns [70], where RAKE receivers were employed to effectively exploit the multipath. To

combat the multipath effect in cases where the delay spread exceeds the CCK code word length, it is important to use an equaliser for the channel effect.

The principle of spatial CCK is as follows. As shown in Fig 3.2 the  $B_c(k)$  represented the input binary sequence of  $c$  codewords, which is encoded to  $C_c(k)$  spatial CCK symbols where the number of transmit antennas depends on the CCK codeword length. For CCK codewords of length 2 there are 2 transmit antennas, 4 transmit antennas for length 4 CCK codewords, and so on.  $X_{N_t}(t)$  is the time domain OFDM symbol that is sent through  $N_t$  transmit antennas, where the number of OFDM modulators that can be utilised depends on the number of transmit antennas, with each row of this matrix including the CCK codes that will be OFDM modulated. These OFDM symbols are sent across the channel  $H$  where  $H$  is defined as frequency selective IEEE wireless channel as discussed in chapter 2. Then it faces Additive White Gaussian Noise (AWGN) and fading perturbs the signal during transmission. At the receive side  $r_{N_r}(t)$  is the time domain OFDM symbols that is received from  $N_r$  receive antennas. And  $r_c(k)$  is the received signal after the FFT process and after removing the cyclic prefix.

$g_c(k)$  are the received symbols after channel equalization, where the equalisation process in the frequency domain is carried out after the OFDM demodulation. In parallel with equalisation, the correlation of the signal with the codebook, including the original group of the code words of CCK, is done to choose the most appropriate corresponding CCK code with the minimum Euclidean distance compared with the equalized sequence, which is defined by  $\widehat{C}_c(k)$ . After that, estimation of the initial binary data occurs as  $\widehat{B}_c(k)$  delivered data [9].

### 3.5.1 Conventional Spatial Complementary Code Keying

Eight-chip CCK is the most frequently encountered conventional CCK modulation scheme, which is used in IEEE802.11b for Wi-Fi. 8-CCK has 256 codewords, which supports 8bit/s/Hz spectral efficiency and this represents polyphase codes with unity magnitude [16, 20]. The polyphase code generation is previously discussed in Chapter 2.

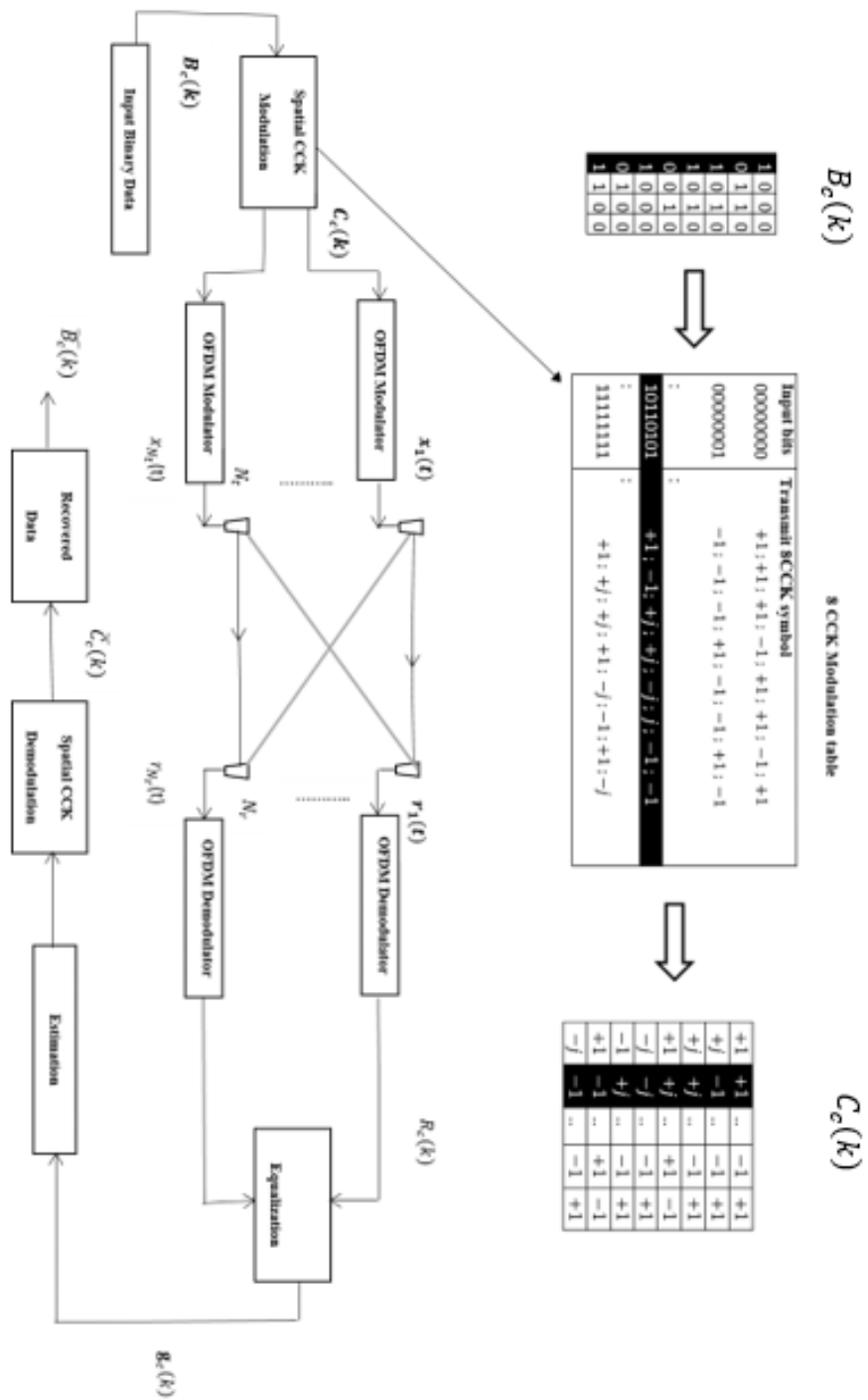


Figure 3.2: Block diagram of conventional spatial 8CCK modulation.

Using 4-phases results in 256 CCK codewords each of with length 8 symbols, which was discussed in Chapter 2. The phases ( $\phi_1, \phi_2, \phi_3, \phi_4$ ) are assigned according to the following tables (3.3), (3.4):

Bit Sequence	Phase
$a_0a_1$	$\phi_1$
$a_3a_2$	$\phi_2$
$a_5a_4$	$\phi_3$
$a_7a_6$	$\phi_4$

**Table 3. 3:** Phase Allocation for 8-bit CCK modulation

$a_{k+1}a_k$	Phase
00	0
01	$\pi/2$
10	$-\pi/2$
11	$\pi$

**Table 3. 4:** Bit phase correspondence

generate CCK codes with other possible lengths discussed in [9, 19]. It should be noted that for each CCK codeword, there is a corresponding column in the matrix with a minus sign for the fourth and seventh factors based on the complementary code generation in Chapter 2.

### 3.6 Contemporary WLAN Techniques

The demand for increasing data rates and spectral efficiency in WLANs are the main drivers behind research into wireless communications systems technologies [69]. Adaptive modulation and coding, space time coding (STC) and MIMO systems, multicarrier modulation, and ultra-wideband radio are the current techniques used for promoting systems for promising generations of wireless communication. A MIMO system enhances spectral efficiency by using multiple antennas to simultaneously send data to the receiver [41, 42, 71, 72]. Moreover, OFDM transforms a frequency-selective channel into a parallel collection of frequency flat-fading sub channels, in which the available bandwidth can be used in an efficient way [73]. The OFDM technique has been accepted in various wireless standards such as digital audio and video broadcasting, the IEEE

802.11 standard [14], the IEEE 802.16a metropolitan area network standard, and the IEEE local area network standards [74].

There are currently three major categories of MIMO techniques: One aims at improving power efficiency by maximising spatial diversity. This delivers full diversity and reduces BER, e.g., using time diversity [27, 47]. In these systems (e.g., STBC), diversity gain is the vital factor responsible for improving the capacity, which in turn maximises the SNR and reduces BER. For any number of transmit antennas with full-diversity STBC systems the maximum spectral efficiency is one symbol per symbol duration [47]. The design of these systems is flexible to achieve full diversity gain with reduced the complexity of the receiver. In addition, STBC has an advantage of combating channel imperfections that occur in real-time implementations of the MIMO technique [75, 76]. In the second category of MIMO techniques, the knowledge of the channel or channel state information (CSI) is exploited at the transmitter. The channel state information decomposes the channel matrix by using singular value decomposition and uses the resulting unitary matrices as pre-filters and post-filters at the transmitter and receiver, respectively, to obtain capacity gain [77, 78].

The third type of MIMO technique deploys a layered space–time algorithm to send several independent data streams over multiple antennas to raise capacity. A well-known technique is the Bell Labs layered space–time (BLAST) architecture [41]. The BLAST technique demultiplexes a user’s data stream into a number of sub-streams that are equal to the number of transmit antennas. Two kinds of BLAST realisations have been developed: 1) Diagonal BLAST (D-BLAST) [41] and 2) vertical BLAST (V-BLAST) [44].

The D-BLAST construction is taken as a reference point in terms of the performance of MIMO systems, as it can attain capacities close to the Shannon limit [79]. The D-BLAST system has a diagonal layered STBC implementation with sequential nulling and interference cancellation decoding. However, boundary wastage at the beginning and end of each packet is the main problem from which this technique suffers, and its complexity is very high for practical use [80].

The V-BLAST architecture is a simplified version of D-BLAST, which attempts to solve the problem of its limitations. It has been illustrated that, with the V-BLAST algorithm, spectral efficiencies of 20–40 bit/s/Hz can be obtained in an indoor rich scattering propagation environment, supposing a practical SNR range [44].

In terms of the two realisations explained here, various difficulties are encountered in the modeling and implementation of multiple antenna transmission algorithms. Firstly, BLAST transmission systems face the problem of high inter-channel interference (ICI) at the receiver side due to simultaneous transmission on same frequencies to multiple antennas. Secondly, high ICI necessitates a complex receiver mechanism, which raises the complexity of the entire system. Thirdly, the performance of the system is traded off with the complexity of the receiver. Moreover, although BLAST systems attain a relatively better performance in ideal channel conditions, this can result in degrading the BER performance [48, 81].

In terms of mitigating these negative effects, research has suggested the following. Broadly speaking, deploying mechanisms to obtain full-diversity STBCs can overcome a many of the limitations that this system may face. Secondly, orthogonal design of STBCs allows codewords to be more easily decoded at the receiver. STBCs also work efficiently even with channel imperfections present [75, 76]. STBC design for more than 2 transmit antennas must sacrifice a portion of the data rate to obtain a full orthogonality and, thereby, full diversity.

SM is an approach for dealing with these issues [63, 64, 67]. In this case, only a single antenna is active at the transmitter side at any one instant. The antenna selected to transmit is an additional source of information that is exploited by SM to increase the spectral efficiency. For this reason, SM is different from other MIMO techniques, such as space time bit interleaved coded modulation [82], in which the antenna pattern is known as a spatial constellation and is not utilised as an information source. In [8] SM, a set of number of bits is mapped into a constellation point in the signal domain and a constellation point in the spatial domain. At the receiver side, the maximum value is utilised to estimate the transmit antenna number.

The majority of existing SM research concentrates on flat fading channels [11, 83, 84]. However, to consider frequency selective fading channels, OFDM-based SM schemes have to be proposed [64, 85]. However, these schemes require a trade-off in spectral efficiency [86].

In [87] the effect of channel correlation on a general upper bounding for the average bit error probability of spatial modulation over Rayleigh and Rician channels is discussed by applying the exponential Kronecker model, this model will applied in the proposed system in this thesis.

In [88, 89] generalized spatial modulation (GNSM) is proposed to increase the spectral efficiency while decreasing the number of transmit antennas compared with conventional SM.

Reference [88] discusses the capacity and symbol error probability (SEP) of GNSM utilizing measured channels, which are attained at 60 GHz by channel sounding in an indoor office location. Non-line of sight factors are harmful and should be tackled by deploying practical detectors, this defines the need for more optimal and complicated receivers to consider the NLOS channel in appropriate means.

Reference [89] discusses the fully generalized special modulation (F-GNSM), by considering the complexity, the suggested F-GNSM method needs a higher computational complexity over the conventional spatial modulation to reduce the transmit antennas number from 7 to 5 for approximately the same spectral efficiency. Therefore, the assortment between the two suggested processes is basically according to the trade-off mechanism between the high computational complexity, spectral efficiency and ABER performance of the receiver.

A significant amount of SM research has focused on frequency-selective fading channels in a single-carrier (SC) system [86, 90-93]. In [90], linear frequency-domain equalisation (FDE) detection, time-frequency decision feedback equaliser (DFE) detection, and ML detection employing QR decomposition and M-algorithm (QRM-MLD) techniques are investigated for spatial modulation systems, where QRM-MLD technique resolves the channel matrix into Q and R matrices and utilises the M-algorithm to minimise the high complexity of the ML detection. In [91], a particular ML detector is developed with higher complexity for large channel delay spread.

In [92], the complexity of ML detector is reduced by a partial interference cancellation technique, this results in a receiver diversity in zero-padded (ZP) SC-SM, which offers full multipath diversity with ML detection. The SC-SM scheme receiver generates hard decisions not amenable to iterative detection, which is a familiar trait of this system. In [86], a minimum mean square error frequency-domain (MMSE-FDE) turbo equaliser is combined with SC-SM. However, the MMSE-FDE does not take advantage of a priori information. In general, most of the FDE algorithms require full-rank MIMO channels in which the number of transmit antennas (TAs) is smaller than the number of receive antennas (RAs).

To address the above limitations, [94] introduces a novel single-carrier spatial modulation SC-SM mechanism by introducing complementary code keying (CCK) modulation (CCK-SM) over frequency-selective fading channels. It develops a CCK-SM by employing the activated antenna index to code a proportion of the CCK chips to achieve joint CCK coding between transmitted symbols and antenna selection. At the receiver, frequency-domain processing is adopted for iterative block decision feedback equalisation (IBDFE) to enhance the performance. Moreover, this paper integrates a soft CCK decoder within the iterative equaliser to achieve a significant performance gain by taking advantage of the soft information from the decoder. This research also uses the standard 8CCK code and concentrates on improving the gain from the turbo receiver, but without exploiting the CCK characteristics to boost the spectral efficiency.

Reference [9] presents more robust and spectrally efficient transmission techniques for MIMO systems. In this reference, spatial complementary code keying modulation (SCCK) is considered exploiting the characteristics of complementary sequences. This system utilizing spatial CCK modulation scheme is based on different codeword lengths of SCCK modulation. The system was applied to a MIMO-OFDM system and its performance was compared to that of SM in some chosen simulation results.

The proposed phases in the system in [9] did not apply the 4-phases of the conventional CCK scheme, which is QPSK modulation except in case of 8-SCCK codeword length. Instead, it uses non-conventional phases which increased gradually in number with the increasing codeword length. Reference [9] focuses on improving BER performance compared to SM instead of spectral efficiency. The performance was evaluated for the wideband channel.

From [9] and the open literature then, there is a lack of work on spatial CCK codes in terms of increasing the spectral efficiency with improving bit error rate performance along with an ability to detect the original codeword at the receiver side. Add to that there is no analytical BER performance of SCCK in narrowband channels with which to validate simulation results.

Because of that, a SCCK system with conventional 4-phase with wideband channel and with employment of both ZF and MMSE detection at the receiver is carried out on the spatial CCK-OFDM receiver to mitigate the multipath effect of frequency selective. ML detection of the CCK codewords follows.

Applying Rayleigh and Rician wireless frequency selective fading channels with different RMS delay spreads tests this system under the effect of different environments and for more realistic scenarios by applying correlated channel models.

One of the main contributions of this thesis is to present the analytical BER of spatial CCK and compare the analytical results across existing systems such as SM and SMX under the same narrowband channels to validate the system performance compared with the state of art.

### **3.7 Summary**

An overview of the evolution of the spatial modulation has been presented in this chapter, followed by a discussion of the issues faced this system to increase the spectral efficiency in trade of the complexity and BER performance. In terms of improving BER performance the SCCK system is suggested in case of wideband channel and non-conventional phases with some results to compare with SM.

Before concluding this chapter, it is worthwhile mentioning that the right choice of conventional phases and developed analytical BER performance of SCCK validates the system compared with state of art, which will be defined in Chapter 4.

## Chapter 4      spatial complementary code keying

### 4.1 Chapter Overview

The purpose of this chapter is to characterize spatial complementary code keying applying code generating phases, which take the values of QPSK modulation for length 2, 4 and 8 CCK codewords, instead of the non-conventional phases proposed in [9]. The proposed MIMO-OFDM system model presents a new spatial coding modulation scheme based on complementary code keying (CCK) sequences, which is named spatial complementary code keying (SCCK). SCCK can achieve higher spectral efficiencies than state of art systems such as SM, through the deployment of large code sets, in addition to improvements in bit error rate performance due to coding gain compared with both SM and SMX systems. Conventional SCCK uses the same 4 codeword generating phases for all codeword lengths. These SCCK code words have a property that the number of code word pairs with large Euclidean distance generated by one SCCK equation is more than the number of pairs that have a small Euclidean distance, which here is exploited in the spatial domain. This property is maintained while having a large number of code words generated by each equation, increasing the spectral efficiency. CCK codes as mentioned in chapter 3 are quite resistant to the destructive effects of channel impairments, and as a result of that their BER performance is very desirable. As in [9], a MIMO-OFDM system in an IEEE wideband channel is examined in case of NLOS and LOS channels .

Moreover, to evaluate the proposed SCCK system in more realistic scenarios we apply channel correlation to this system. The Kronecker exponential model is used as a general model for correlation because of its popularity in many papers, which discuss MIMO signal processing and information theory for correlated channels.

Finally, the key contribution is the analytical BER performance, which is discussed mathematically in terms of a narrowband channel to validate the proposed system and compare with Monte Carlo simulation.

## 4.2 An investigation of CCK with different Spectral efficiencies

As a result of cooperation between Intersil [17] and the IEEE committee the amendment of the IEEE802.11 standard, which used for a long time Binary Phase Shift Keying “BPSK” and Quadrature Phase Shift Keying “QPSK” to get 1Mbit/s and 2Mbit/s data rates respectively [17] in IEEE802.11b, was one of the first definitions of Complementary Code Keying (CCK) modulation techniques. This standard used length 8-chip sequences representing either 8 or 4 bit/s/Hz spectral efficiency, to implement 11 Mbit/s or 5.5 Mbit/s in wireless local area networks (WLANs). The CCK codes which are most commonly discussed are 8 bit/s/Hz and 8 chip codewords, but there are many types that are rarely studied such as those which include length two, four and sixteen, here studied in the spatial domain.

### 4.2.1 4-bit/s/Hz Spatial Complementary Code Keying

This mechanism generates 4 bit/s/Hz spectral efficiency conventional SCCK modulation of codeword length 2.

Equation 4.1 is the matrix representation of equation 4.2.  $\phi_1$  and  $\phi_2$  can take on values from set(  $0, \pi, \pi/2, -\pi/2$ ), which are the QPSK code generating phases, giving 16 possible codewords. Relate bits to code generating phases.

Equation (4.2) manipulates 16-phase combinations to derive the 4-bit conventional phase SCCK codewords. This equation uses the same CCK kernel that is formed using Golay’s rule for length expansion that is mentioned in chapter 2.

$$M_2 = \begin{bmatrix} \phi_1 & \phi_1 \\ \phi_2 & 0 \end{bmatrix} \quad (4.1)$$

$$C_2 = (e^{j(\phi_1+\phi_2)}, -e^{j(\phi_1)}) \quad (4.2)$$

Where  $M_2$  defines the Hadamard like matrix of CCK with length two and  $C_2$  is the sequence rule to generate the 2-CCK codewords.

### 4.2.2 6- bit/s/Hz Spatial Complementary Code Keying.

In the case of 4-phase 4-SCCK with codewords of length 4, a spectral efficiency of 6-bit/s/Hz is obtained with 64 codewords.

The matrix presented in equation (4.3) describes the phase arrangement 4-SCCK, which uses four phases identified as  $(0, \pi, \pi/2, -\pi/2)$ .

The equation (4.4) with four phases generates 64 codewords with length of 4:

$$M_4 = \begin{bmatrix} \phi_1 & \phi_1 & \phi_1 & \phi_1 \\ \phi_2 & 0 & \phi_2 & 0 \\ \phi_3 & \phi_3 & 0 & 0 \end{bmatrix} \quad (4.3)$$

$$C_4 = \{e^{j(\phi_1+\phi_2+\phi_3)}, e^{j(\phi_1+\phi_3)}, e^{j(\phi_1+\phi_2)}, -e^{j(\phi_1)}\} \quad (4.4)$$

Where  $M_4$  defines the Hadamard like matrix of CCK with length four and  $C_4$  is the sequence rule to generate the 4-CCK codewords.

### 4.2.3 8-bit/s/Hz Spatial Complementary Code Keying.

Eight-bit CCK is the most common CCK modulation which is used in IEEE802.11b. An 8-bit input sequence can consist of four different phases that might be applied by using the Euler formula property, which achieves 8-bit CCK codewords because of an 8-bit input sequence[9, 17]

As the same trend of 2-SCCK and 4-SCCK cases, 4-phase 8-SCCK with codewords of length 8, a spectral efficiency of 8-bit/s/Hz is obtained with 256 codewords.

The matrix showed in equation (4.5) discussed the phase arrangement 8-SCCK, which uses four phases identified as  $(0, \pi, \pi/2, -\pi/2)$ .

The equation (4.6) with four phases generates 256 codewords with length of 8:

$$M_8 = \begin{bmatrix} \phi_1 & \phi_1 \\ \phi_2 & 0 & \phi_2 & 0 & \phi_2 & 0 & \phi_2 & 0 \\ \phi_3 & \phi_3 & 0 & 0 & \phi_3 & \phi_3 & 0 & 0 \\ \phi_4 & \phi_4 & \phi_4 & \phi_4 & 0 & 0 & 0 & 0 \end{bmatrix} \quad (4.5)$$

$$C_8 = \left\{ e^{j(\phi_1+\phi_2+\phi_3+\phi_4)}, e^{j(\phi_1+\phi_3+\phi_4)}, e^{j(\phi_1+\phi_2+\phi_4)}, -e^{j(\phi_1+\phi_4)}, e^{j(\phi_1+\phi_2+\phi_3)}, e^{j(\phi_1+\phi_3)}, -e^{j(\phi_1+\phi_2)}, e^{j(\phi_1)} \right\} \quad (4.6)$$

As mentioned previously, where  $M_8$  defines the Hadamard like matrix of CCK with length eight and  $C_8$  is the sequence rule to generate the 8-CCK codewords.

#### 4.2.4 10-bit/s/Hz Spatial Complementary Code Keying.

A novel mechanism utilizing a greater number of transmit antennas than the previous case of 8-SCCK, which is 16-SCCK and first time is presented in this thesis. 4-phase 16-SCCK with codewords of length 16, a spectral efficiency of 10-bit/s/Hz is obtained with 1024 codewords.

The matrix showed in equation (4.7) discussed the phase arrangement 16-SCCK, which uses four phases identified as  $(0, \pi, \pi/2, -\pi/2)$ .

The equation (4.8) with four phases generates 1024 codewords with length of 16:

$$M_{16} = \begin{bmatrix} \phi_1 & \phi_1 \\ \phi_2 & 0 & \phi_2 & 0 \\ \phi_3 & \phi_3 & 0 & 0 & \phi_3 & \phi_3 & 0 & 0 & \phi_3 & \phi_3 & 0 & 0 & \phi_3 & \phi_3 & 0 & 0 \\ \phi_4 & \phi_4 & \phi_4 & \phi_4 & 0 & 0 & 0 & 0 & \phi_4 & \phi_4 & \phi_4 & \phi_4 & 0 & 0 & 0 & 0 \\ \phi_5 & 0 & 0 & 0 & 0 & 0 & 0 & 0 & 0 \end{bmatrix} \quad (4.7)$$

$$C_{16} = (e^{j(\phi_1+\phi_2+\phi_3+\phi_4+\phi_5)}, e^{j(\phi_1+\phi_3+\phi_4+\phi_5)}, e^{j(\phi_1+\phi_2+\phi_4+\phi_5)}, \\ , -e^{j(\phi_1+\phi_4+\phi_5)}, e^{j(\phi_1+\phi_2+\phi_3+\phi_5)}, e^{j(\phi_1+\phi_3+\phi_5)}, -e^{j(\phi_1+\phi_2+\phi_5)}, e^{j(\phi_1+\phi_5)}, e^{j(\phi_1+\phi_2+\phi_3+\phi_4)}, e^{j(\phi_1+\phi_3+\phi_4)}, \\ , e^{j(\phi_1+\phi_2+\phi_4)}, -e^{j(\phi_1+\phi_4)}, -e^{j(\phi_1+\phi_2+\phi_3)}, -e^{j(\phi_1+\phi_3)}, e^{j(\phi_1+\phi_2)}, -e^{j(\phi_1)}) \quad (4.8)$$

Where  $M_{16}$  presents the Hadamard like matrix of CCK with length sixteen and  $C_{16}$  is the sequence rule to generate the 16-CCK codewords.

### 4.3 Largest minimum distance between Complementary Codes

The distinguishing property of SCCK codewords is of the large number of codewords that have large Euclidian distance, and then application of these codewords to the proposed system.

For instance, in the case of 8-SCCK applying equations (4.5) and (4.6) with 4 phase positions will result in 256 codewords each of length 8 chips. For each of the  $256 \times 256 = 65536$  possible pairs of codewords, the Euclidean distance was calculated in Table 4.1.

As shown in the Table 4.1 the codeword pairs which have large Euclidean distances is more than the codewords pairs with small Euclidean distances. For example, the number of code word pairs with Euclidean distance higher than or equal to 4 as an average number in Table 4.1, is 55040 compared to 9986 code word pairs with Euclidean distance less than 4.

Euclidean distance between each CCK code pair	Number of code word pairs
5.657	256
4.899	6144
4.472	4096
4.000	44544
3.464	3842
2.828	6144

**Table 4.1:** The Euclidean distance comparison between the code words of 8-SCCK

#### 4.4 Spatial Complementary Code Keying Modulation System

A block of random binary information bits is mapped into codewords in the spatial domain and presented with first a wideband channel, then discussed in a narrowband channel at the end of chapter.

As shown in Fig (4.1) the input binary sequence is represented by the matrix  $B_c(k)$  of size  $M \times N_{sub}$ , where,  $M$  describes the phase order of SCCK modulation system and  $N_{sub}$  denotes the number of OFDM sub-channels. The binary bits are coded to  $C_c(k)$  SCCK codewords as discussed previously in this chapter, and will result in CCK codewords of the required length (two, four and eight).

The number of bits that can be transmitted on each OFDM sub channel for a system that uses spatial SCCK modulation with  $m$  is:

$$m = (1 + \log_2 (N_T)) \log_2 (M) \text{ bit/s/Hz} \quad (4.9)$$

where  $m$  is number of bits and the number of transmit antennas is  $N_t$ , and  $M$  is the modulation constellation diagram size, which is equal to four in this conventional case.

The obtained SCCK codewords will be spatially spread through the transmit antennas, with one codeword chip transmitted from each antenna. The matrix  $C_c(k)$  is the output of SCCK codeword generator with dimensions  $N_t \times N_{sub}$ , as discussed previously, and small  $c$  denotes the transmitted codeword. At the side of the transmitter a bank of OFDM modulators is positioned with one aligned to every row of  $C_c(k)$ . Then, OFDM modulation is applied in each row vector  $C_c(k)$  and the output of the OFDM symbols is  $x_{N_t}(t)$ . At the same time the  $N_t$  transmit antennas will transmit

OFDM modulated vectors across the wireless wideband channel and the signals will be degraded by the AWGN and fading, this channel is described in more details in chapter 2.

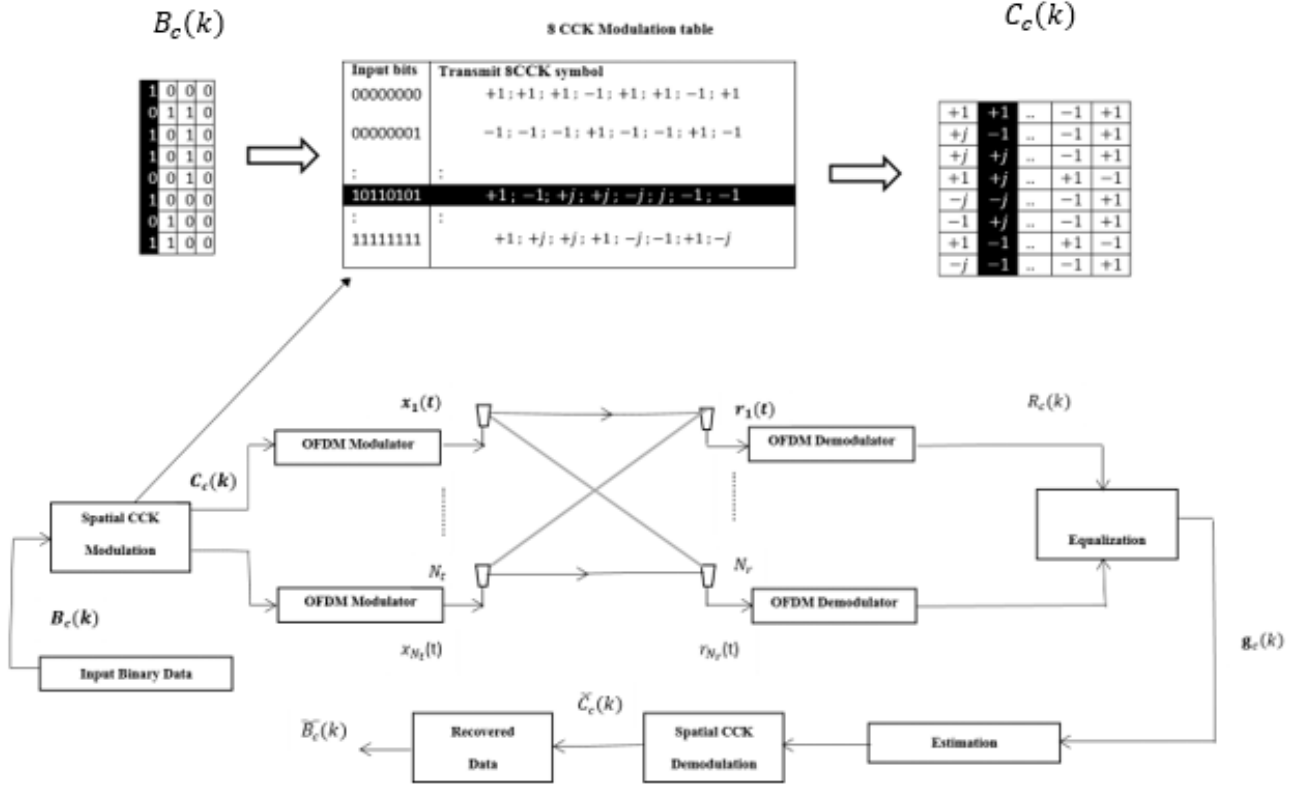


Figure 4.1: Block diagram of spatial CCK modulation with wideband channel

So:

$$r_{N_R}(t) = H(\tau, t) \otimes X_{N_T}(t) + n(t) \quad (4.10)$$

$r_{N_R}(t)$  presents the receive matrix of size  $N_R \times m$ , the OFDM symbols matrix and the AWGN matrix are denoted by  $X_{N_T}(t)$  and  $n(t)$  respectively, and  $\otimes$  represents the convolution in time domain, and note that the synchronous transmission by all antennas on each subcarrier helps to attain a spatial multiplexing advantage.

Different types of detection schemes are used, such as zero forcing (ZF) detection and minimum mean square error (MMSE), discussed previously in Chapter 2, on each of its column vectors. The result from OFDM demodulation is  $R_c(k)$ , detected in the frequency domain so as to minimize the impact of the channel impairments. It should be noted that the discrete time index is denoted by  $k$ , Note that  $k$  presents the discrete time index.

In the case of ZF:

$$g_c(k) = H(k)^{-1}R_c(k) \quad (4.11)$$

where  $g_c(k)$  defines the detecting receive signal. Most importantly, the pseudo-inverse is applied for ZF in the case of non-symmetrical MIMO systems.

The detected data stream will be split into sub-streams obtained on each sub-channel, and the computation of the Euclidean distance between the subjects of the CCK codebook (which include each produced SCCK codeword) and sub-stream obtained on each sub-channel.

The SCCK codebook in this case involves  $L = m^2$  SCCK codewords where  $m = (1 + \log_2(N_T))\log_2(M)$  bit/s/Hz.

The estimated codeword  $\widehat{C}_c(k)$  will be the one with the least Euclidean distance from the received signal  $g_c(k)$  at the end compared with the codebook. It is then de-mapped to the conforming estimated data sequence  $\widehat{B}_c(k)$ .

Mathematically [7]:

$$d_i^2(c_j, s_i) = (c_j - s_i)(c_j^* - s_i^*) \quad (4.12)$$

$$i = 1, 2, \dots, N_{sub} \quad j = 1, 2, \dots, L$$

Where  $L = m^2$  presents the number of code words in SCCK codebook

So, by choosing the codeword with minimum Euclidean distance compared with the codebook reference, then:

$$E_i(k) = \min(d_i^2) \quad (4.13)$$

Where, the Squared Euclidean distance between the obtained signal is on each sub-channel and each content of the SCCK codebook  $c_j$  is denoted by  $d_i^2(c_j, s_i)$ , and  $s_i$  is the received codeword. And the SCCK codeword with least Euclidean distance related with  $i^{th}$  sub-channel is denoted by  $E_i(k)$  [9] .

## 4.5 Simulation modeling.

MIMO-OFDM systems are considered and 100000 packets are transmitted where each packet contains 20 OFDM symbols. With delay spreads of 50, 100, or 150ns, the wireless channel is defined to be an IEEE time-variant frequency-selective multipath channel, the carrier frequency is considered to be 2.4 GHz because of it is the standard of Wi-Fi.  $(Eb/N0)$  is used for the standardized signal-to-interference-plus-noise ratio. Table 4.2 describes the parameters of the system simulation:

Parameter	Setting
Number of Packets	100000
Number of OFDM symbols	20
Number of OFDM sub-channels	256
Length of cyclic prefix	16
Channel delay spread (ns)	50,100,150
System Bandwidth (MHz)	20
Transmit Power (W)	1
Carrier Frequency (GHz)	2.4

**Table 4.2:** System Simulation Parameters

Bit Error Ratio (BER) is defined as a one of the most important ways to determine and measure the quality of a digital transmission system. It is calculated by made a comparison between the received bits and transmitted sequences of bits and counting the number of errors. The BER will defined as the ratio of how many bits received in error over the number of total bits received. This ratio is affected by many factors including: signal to noise, distortion.

$$BER = \frac{N_{Err}}{N_{bits}} \quad (4.14)$$

Where BER is the Bit Error Ratio and  $N E_{rr}$  is the number of errors and  $N bits$  is the number of bits.

One of the most common methods of measuring BER is calculating the BER after sending bits through the system. Since this is a statistical process, in this case this BER only approaches the actual BER as the number of bits tested approximates infinity. For the majority of cases there is a need only to test if the BER is less than a predefined threshold. The required confidence level and BER threshold are the main factors that the number of bits required to accomplish this process depends on. The confidence level is defined as the percentage of tests that the system's true BER is less than the specified BER. The confidence level will never reach 100%.

To calculate the confidence level (CL), we use the equation:

$$CL = 1 - e^{-N bits \times BER} \quad (4.15)$$

This means to reach typical confidence level of 0.95, which means (95%) in data with bit error rate of  $10^{-6}$  this requires around  $2.9957 \times 10^6$  number of transmit bits.

The Matlab modelling for SCCK-OFDM scheme is as follows:

- 1- Generate random binary data [0 1].
- 2- Modulate these data by using SCCK mapping data for four, six, eight and ten bit/s/Hz spectral efficiencies.
- 3- Mapping the data to antennas.
- 4- Applying OFDM modulation process by taking the inverse discrete fast Fourier transform of the modulated data using a fast Fourier transform algorithm and applying the length 16 cyclic prefix. The term cyclic prefix involves attaching the last 16 symbols to the front of an OFDM frame. Typically, at the receive side the system is implemented to discard the cyclic prefix. The cyclic prefix serves two aims: firstly, eliminating the inter-symbol-interference (ISI) from the previous OFDM frame because of the guard interval provided. Secondly, the CP converts the linear frame to a circular convolution. This approach provides a simple frequency domain processing, such as equalization and channel estimation by ZF.

- 5- The channel is convolved with the OFDM packets for each transmit/receive antenna pair and the white Gaussian noise is added, considering the channel power normalization.
- 6- At the receiver, the received vector is grouped into multiple symbols, the cyclic prefix is removed, and the desired subcarriers are converted from the time domain into the frequency domain using the FFT process.
- 7- Apply different detection schemes such as ZF, MMSE and the optimal ML detection.
- 8- Recover the data using the SCCK codebook.
- 9- Compare the recovered and input data to calculate BER performance.

### **4.5.1 Spatial CCK for different detection schemes Results.**

The purpose of this section is to investigate the bit error rate performance of the proposed system with both ZF and MMSE detectors at the receiver, as discussed previously in Chapter 2, where the detection scheme is one of the important parameters in the MIMO system regarding improving the performance and determining the complexity.

Moreover, different detectors are examined as they trade off performance with complexity. ZF suffers from noise enhancement, while MMSE trades off limited removal of ISI for improved noise performance. ML is the ideal in terms of error rate reduction. However, ML has a complexity increasing exponentially with the number of antennas. MMSE has moderate performance or "acceptable" with less complexity than ML. ZF has the worst performance compared with ML and MMSE, but is less complex than them.

#### **4.5.1.1 4-bit/s/Hz spatial CCK BER performance results**

In Fig 4.3 the BER is shown while employing 2 antennas at both the transmitter and receiver with different types of detectors. Evidently, performance of the both MMSE and ZF detectors schemes is almost equal and there is a noticeable improvement in the optimal detector case (ML), for example at 10 dB the bit error rate in ML optimal detector is nearly  $1.25 \times 10^{-3}$  compared with the BER in the same point with ZF detector  $1.45 \times 10^{-2}$  and MMSE detector  $1.393 \times 10^{-2}$ .

This means that the proposed system with a frequency selective IEEE channel and 50 ns RMS delay spread approaches the same performance in bit error rate with different detectors (ZF-MMSE) considering that the MMSE is more complex than ZF in its implementation.

The improvement with increasing the number of receive antennas is relatively high, and this can be attributed to the properties of complementary codes as well as the diversity at the receive side. As shown in Fig 4.4 and 4.5 respectively, there will be a noteworthy improvement in initial BER performance of SCCK with codeword length 2 due to the increased number of receive antennas. For example, in Fig 4.5, which shows the same comparison as Fig 4.3 but with 4 receive antennas, the BER performance of 2x4 SCCK, shown in Fig 4.4, outperforms 2x2 in Fig 4.3 with nearly 17 dB SNR gain in  $1.2 \times 10^{-4}$ . This increases to 31 dB in the case of 2x8 antennas in Fig 4.5 compared with Fig 4.3, or 8 dB improvement compared with Fig 4.4, which is a noticeable improvement, though in trade-off with the receiver complexity.

In the case of different detectors as shown in Figures 4.3, 4.4 and 4.5, the BER curve of MMSE detector is better than ZF detector by approximately 0.25 dB, but with nearly the similar performance in the case of 2x2 antennas as shown in Fig 4.3, which means the effect of the detectors is obvious with receiver diversity in case of SCCK with codeword of length 2.

In Fig. 4.6, the number of transmit antennas is kept as 2 and the number of receive antennas is set to 1, 2, 4 and 8 for comparison. Here it can be seen that due to the increase in the number of receive antennas, based on the optimal detector ML and as expected, the BER is greatly improved, which defines the receive diversity effect of the proposed system that helps to improve the overall BER performance significantly. For example, as shown in Fig 4.6 the BER performance of 2-SCCK 2x8 has nearly 18 dB SNR gain over the equivalent 2x2 system, in trade-off with increased receiver complexity.

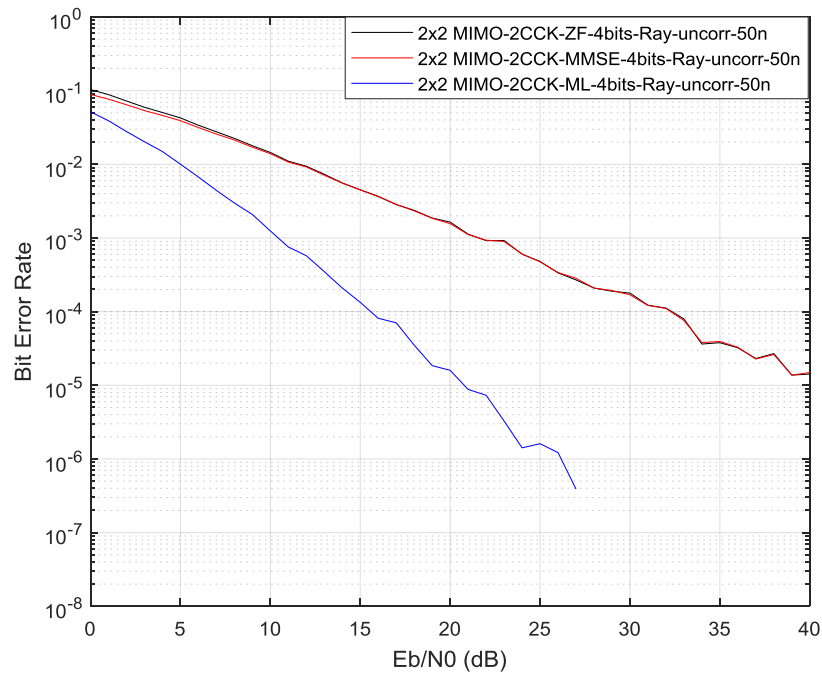


**Figure 4.2:** BER versus  $E_b/N_0$  for spatial conventional SCCK over uncorrelated Rayleigh channel and different detection schemes with  $m = 4$ , where  $N_t = 2$  and  $N_r = 2$  and RMS delay spread=50 ns.

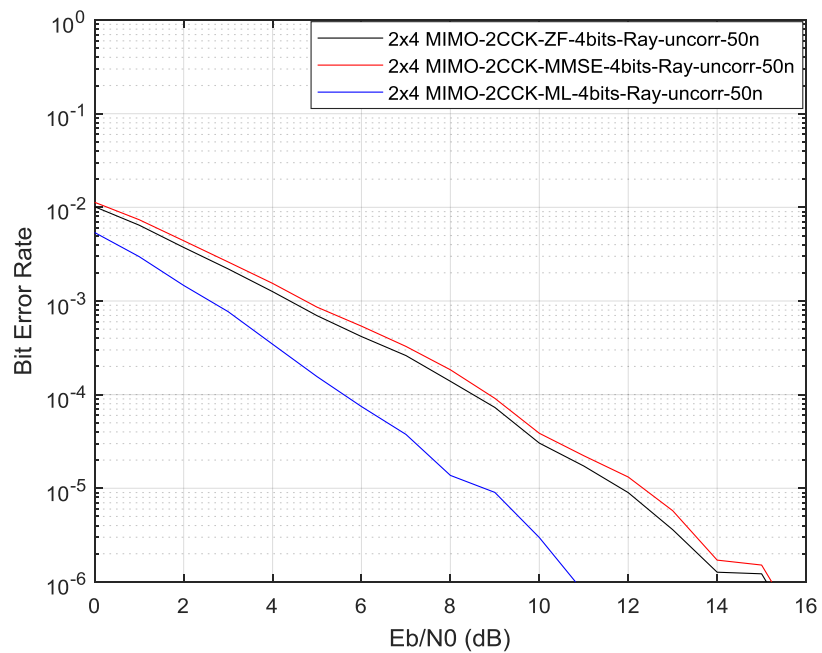


**Figure 4.3:** BER versus  $E_b/N_0$  for spatial conventional SCCK over uncorrelated Rayleigh channel and different detection schemes with  $m = 4$ , where  $N_t = 2$  and  $N_r = 4$  and RMS delay spread=50 ns.

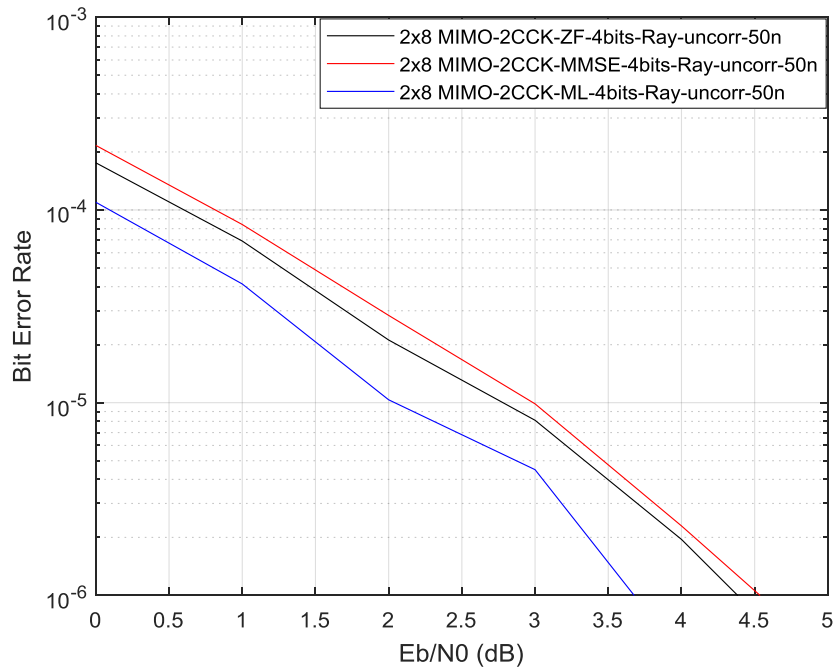


**Figure 4.4:** BER versus  $E_b/N_0$  for spatial conventional SCCK over uncorrelated Rayleigh channel and different detection schemes with  $m = 4$ , where  $N_t = 2$  and  $N_r = 8$  and RMS delay spread=50 ns.

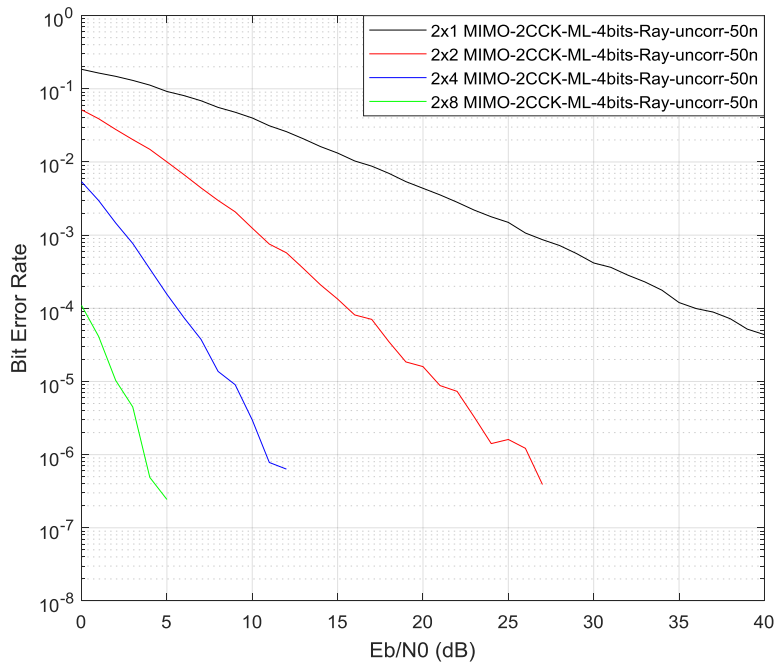


**Figure 4.5:** BER versus  $E_b/N_0$  for spatial conventional SCCK over uncorrelated Rayleigh channel and different receive antennas and ML detection with  $m = 4$ , where  $N_t = 2$  and  $N_r = 1, 2, 4$  and  $8$  and RMS delay spread=50 ns.

#### 4.5.1.2 6-bit/s/Hz spatial CCK BER performance results

In the case of 4-SCCK, which means codewords with length 4, higher spectral efficiency of  $m=6$  bit/s/Hz is achieved compared with 2-SCCK of  $m=4$  bit/s/Hz. This results from a high number of codewords.

In Fig. 4.7 and 4.8 the trend of the curves are similar to Fig. 4.3 and 4.4, where the BER performance is improved when the number of antenna receivers increased, and the BER difference between the ZF (black curve) and MMSE (red curve) is approximately 3dB.

In addition to that, applying more antennas at the receive side and keeping the transmit antennas to 4 antennas means more diversity and improvement in BER performance in trade-off with receiver complexity as shown in Fig 4.8, where the BER performance of the 4x8 system outperforms the same system but with 4 receive antennas presented in Fig 4.7 with nearly 22 dB SNR gain in both ZF and MMSE detectors.

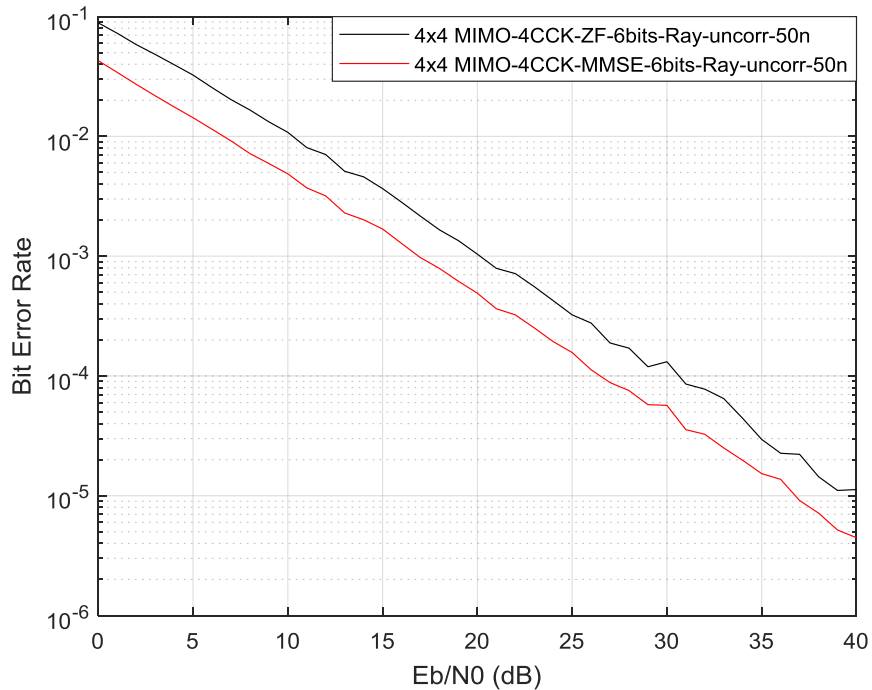


**Figure 4.6:** BER versus  $E_b/N_0$  for spatial conventional SCCK over uncorrelated Rayleigh channel and different detection schemes with  $m = 6$ , where  $N_t = 4$  and  $N_r = 4$  and RMS delay spread=50 ns.

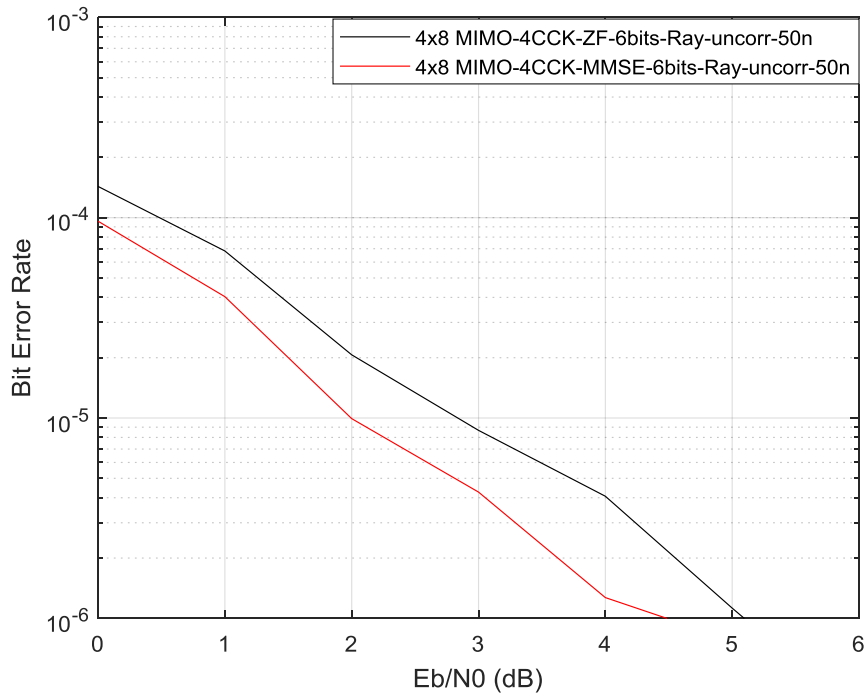


**Figure 4.7:** BER versus Eb/No for spatial conventional SCCK over uncorrelated Rayleigh channel and different detection schemes with  $m = 6$ , where  $N_t = 4$  and  $N_r = 8$  and RMS delay spread=50 ns.

In the case of ML optimal detection as shown in Fig 4.9, which presents the same trend as Fig 4.6, discussed previously, the number of transmit antennas is 4 and the number of receiver antennas is set to 1, 2 and 4 for comparison. Here it can be expected the BER is greatly reduced, which defines the receive diversity effect of the proposed SCCK system that helps to improve the overall BER performance significantly in trade off the receiver complexity.

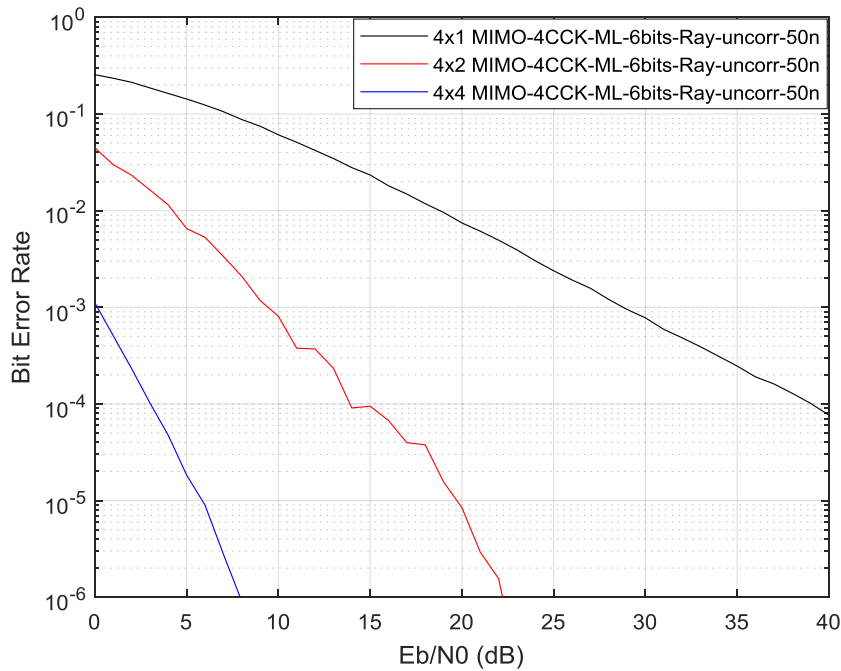


**Figure 4.8** BER versus  $E_b/N_0$  for spatial conventional SCCK over uncorrelated Rayleigh channel and different receive antennas and ML detection with  $m = 6$ , where  $N_t = 4$  and  $N_r = 1, 2$  and  $4$  and RMS delay spread=50 ns.

#### 4.5.1.3 8bit/s/Hz spatial CCK BER performance results

In the case of 8-SCCK, which had codeword of length 8, this means  $m=8$  bit/s/Hz spectral efficiency, and this system is again compared in terms of different detectors.

Fig 4.10 plots BER Vs  $E_b/N_0$  comparing 8-SCCK-ZF detection with 8-SCCK-MMSE detection. In an IEEE Rayleigh channel at  $10^{-4}$  BER, SCCK-MMSE achieves a SNR gain of 15 dB over SCCK-ZF, in trade-off with receiver complexity.

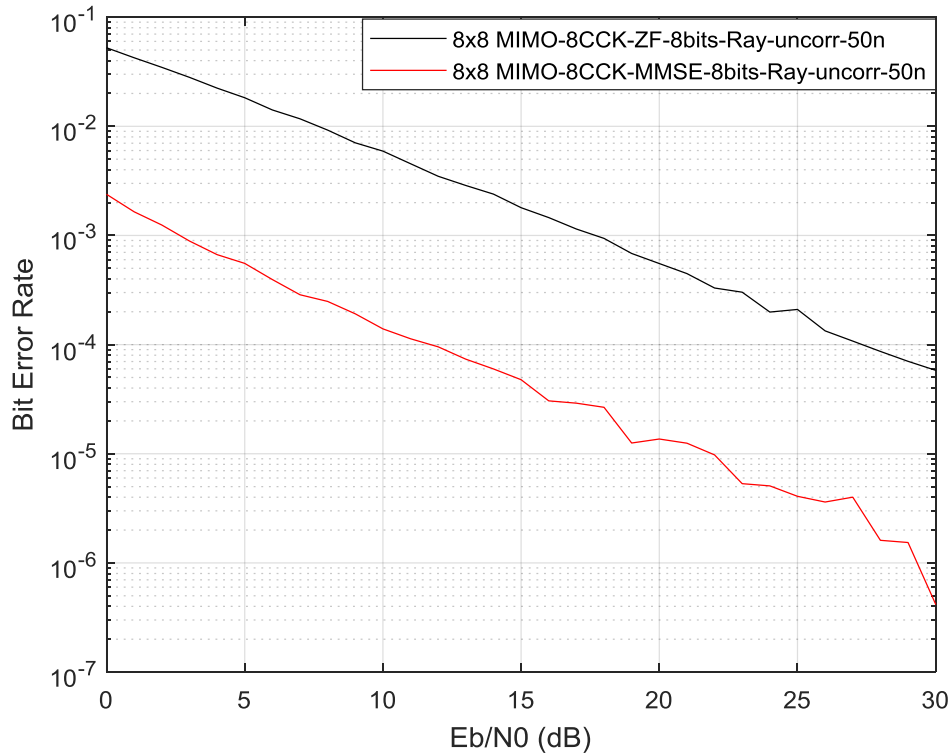


**Figure 4.9:** BER versus Eb/No for spatial conventional SCCK over uncorrelated Rayleigh channel and different detection schemes with  $m = 8$ , where  $N_t = 8$  and  $N_r = 8$  and RMS delay spread=50 ns.

#### 4.5.1.4 10-bit/s/Hz spatial CCK BER performance results

The 16-SCCK scheme defines SCCK with codewords of length 16, giving 10 bits/Hz spectral efficiency. As such, the 16-SCCK has a high spectral efficiency compared with the previous SCCK cases but with increasing the number of transmit antennas, which means more cost than 2, 4, 8 SCCK systems.

This 16x16 MIMO-OFDM system is compared with different detection schemes such as ZF and MMSE detectors. In detail, Fig 4.11 shows BER vs Eb/No compared 16-SCCK-ZF detection with 16-SCCK-MMSE detection for both the same spectral efficiency 10bit/s/Hz. In IEEE Rayleigh channel at  $10^{-3}$  BER, SCCK-MMSE achieves a SNR gain of 7 dB over SCCK-ZF in trade-off with receiver complexity.

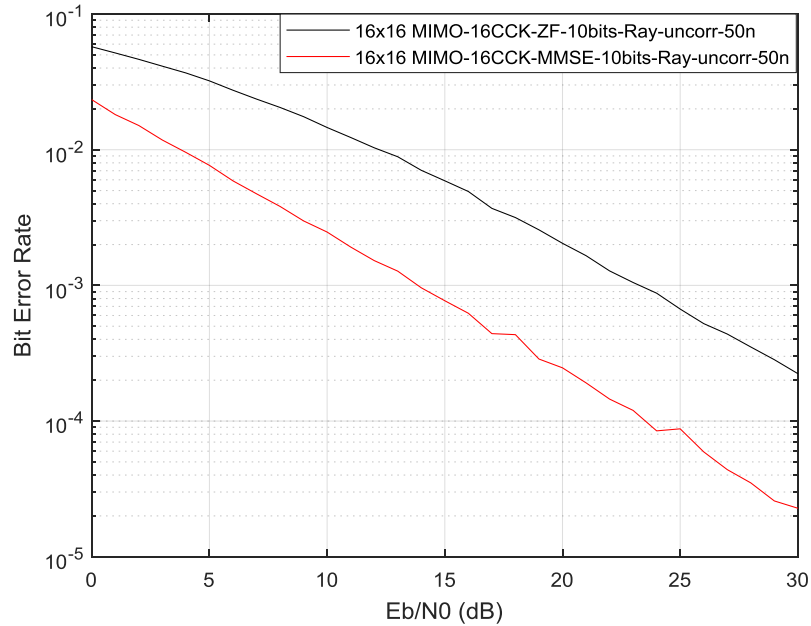


**Figure 4.10:** BER versus Eb/No for spatial conventional SCCK over uncorrelated Rayleigh channel and different detection schemes with  $m = 10$ , where  $N_t = 16$  and  $N_r = 16$  and RMS delay spread=50 n.

## 4.5.2 Spatial CCK under different wireless channels with different RMS delay spread results

In the case of different wireless channels (Rayleigh, Rician) with different RMS delay spreads the IEEE channel is modified to Rician fading channel with Rician K-factor.

### 4.5.2.1 4-bit/s/Hz spatial CCK in Rician channel BER performance results

Conventional SCCK-MIMO-OFDM systems with 2, 4, 8 and 16 transmit and receive antennas are considered. The simulation transmission schemes will apply spectral efficiencies of  $m = 4$  bit/s/Hz,  $m = 6$  bit/s/Hz,  $m = 8$  bit/s/Hz and  $m = 10$  bit/s/Hz respectively.

Fig. 4.12 plots results where an  $N_t = 2$  and  $N_r = 2$  SCCK system is used for both Rayleigh and Rician fading channels and different detectors. Solid curves define the Rician uncorrelated channel and the dashed curves show the Rayleigh uncorrelated channel. The detectors are presented with different colors.

This Figure shows approximately similar performance in terms of different wireless channels under the same RMS delay spread, which is 50ns. In the case of different detectors the similarity of BER performance is kept when comparing between ZF and MMSE detectors and considering the MMSE detector is more complex than the ZF detector.

The ML detector shows improvement of 16 dB over the other detectors at a BER of  $10^{-4}$ .

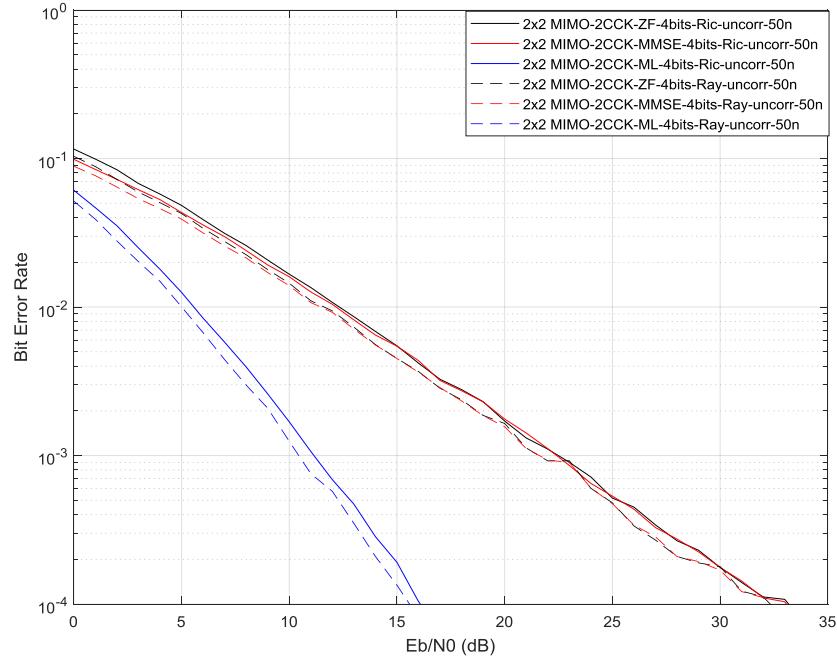


**Figure 4.11:** BER versus  $E_b/N_0$  for spatial conventional SCCK over uncorrelated Rayleigh/Rician channel and different detection schemes with  $m = 4$ , where  $N_t = 2$  and  $N_r = 2$  and RMS delay spread = 50 ns.

Figs 4.13 and 4.14 presents the proposed system with RMS delay spreads of 50, 100 and 150 ns in the case of IEEE channel. In detail, Fig 4.13 and 4.14 plots the BER performance with ZF and MMSE detection and different RMS delay spreads and shows deterioration in BER performance in high  $E_b/N_0$  ranges in the case of RMS delay spread of 150 ns.

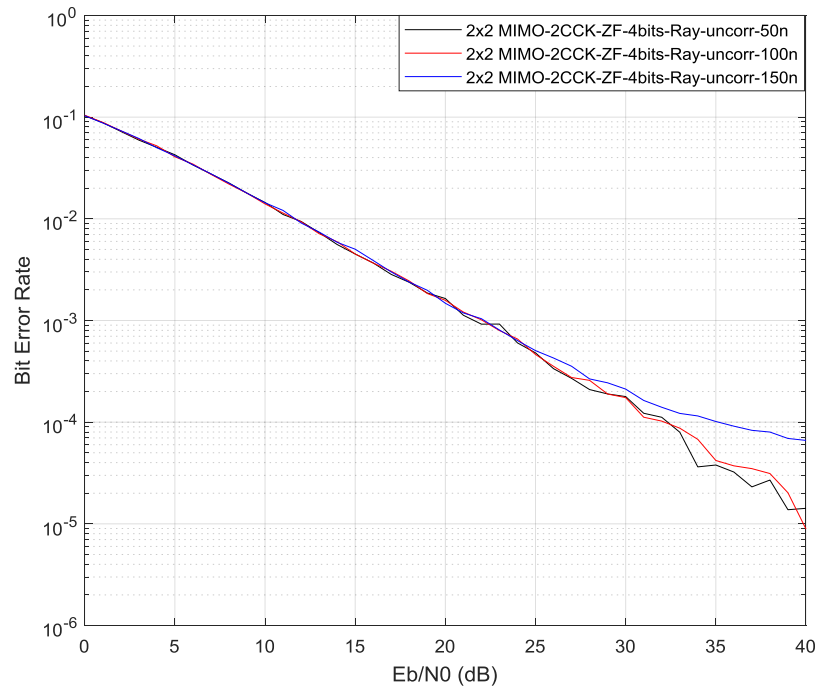


**Figure 4.12:** BER versus  $E_b/N_0$  for spatial conventional SCCK over uncorrelated Rayleigh channel and ZF detection scheme with  $m = 4$ , where  $N_t = 2$  and  $N_r = 2$  and RMS delay spread=50,100,150 ns.

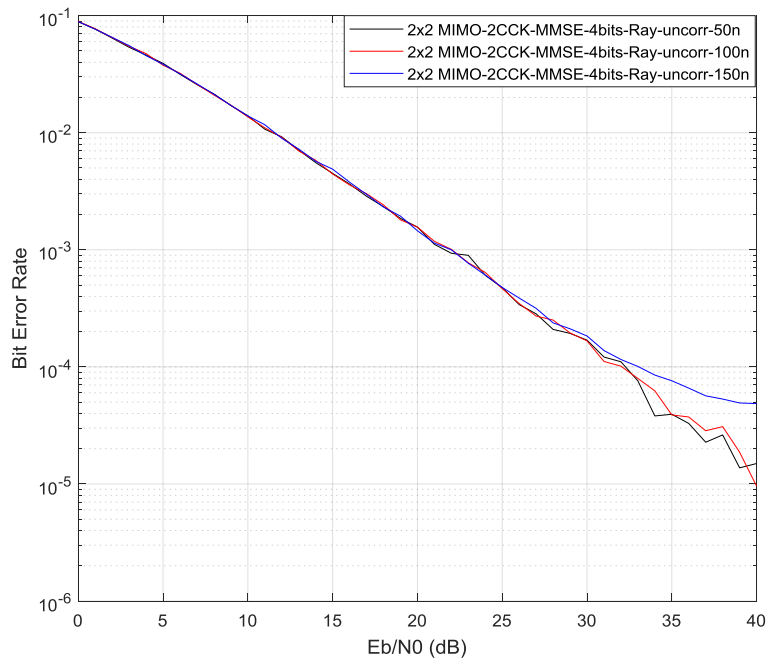


**Figure 4.13:** BER versus  $E_b/N_0$  for spatial conventional SCCK over uncorrelated Rayleigh channel and MMSE detection scheme with  $m = 4$ , where  $N_t = 2$  and  $N_r = 2$  and RMS delay spread=50,100,150 ns.

In the case of Rician channels the degradation of performance with different RMS is small compared with Rayleigh fading as shown in Figs 4.15 with ZF detector. This figure plots the same trend as the previous figures but with a Rician fading channel, the BER performance in 50,100 and 150ns delay spreads and the Fig 4.15 show that the performance is maintained in the Rician channel with no real effect of the performance of different RMS delay spreads, but with degradation in BER performance compared with Rayleigh channel.

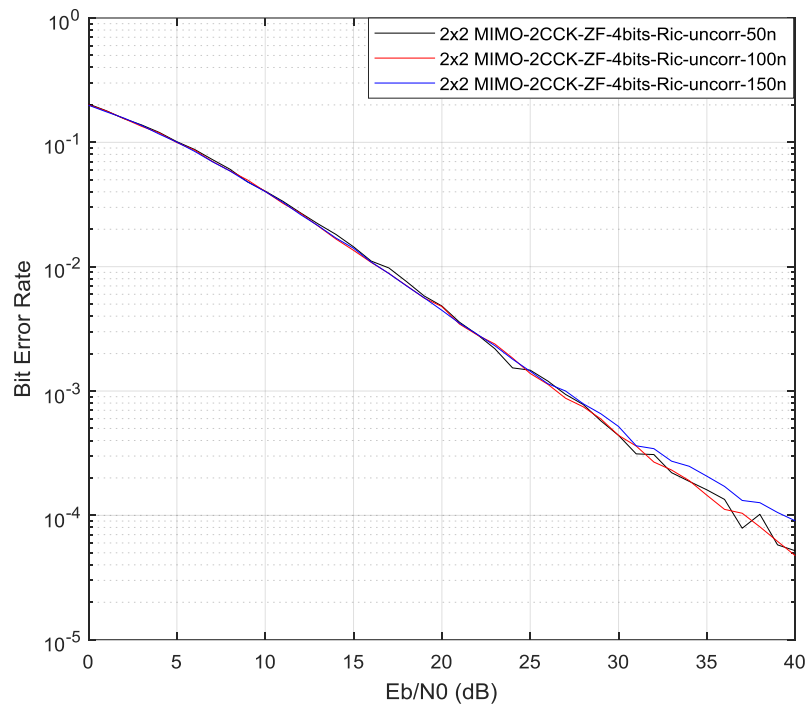


**Figure 4.14:** BER versus  $E_b/N_0$  for spatial conventional SCCK over uncorrelated Rician IEEE channel and ZF detection scheme with  $m = 4$ , where  $N_t = 2$  and  $N_r = 2$  and RMS delay spread=50,100,150 ns.

#### 4.5.2.2 6-bit/s/Hz spatial CCK in Rician channel BER performance results

The simulation results of Fig 4.16 will follow the same trend as Fig 4.12 results except the difference in both SCCK codeword length and spectral efficiency, which are four and six respectively, with  $N_t=N_r=4$ .

In detail, Fig 4.16 plots a 4-SCCK system with different detection schemes and different wireless uncorrelated channel. Solid curves show the Rician uncorrelated channel and the dashed curves presents the Rayleigh uncorrelated channel. The detectors are plotted with different colors.

This Fig 4.16 shows approximately the similar performance in terms of different wireless channels with 50ns RMS delay spread. The results confirm that the BER performance of 4-SCCK with MMSE detector outperforms the same system with ZF detector with nearly 3 dB SNR gain in both Rayleigh and Rician uncorrelated channels.

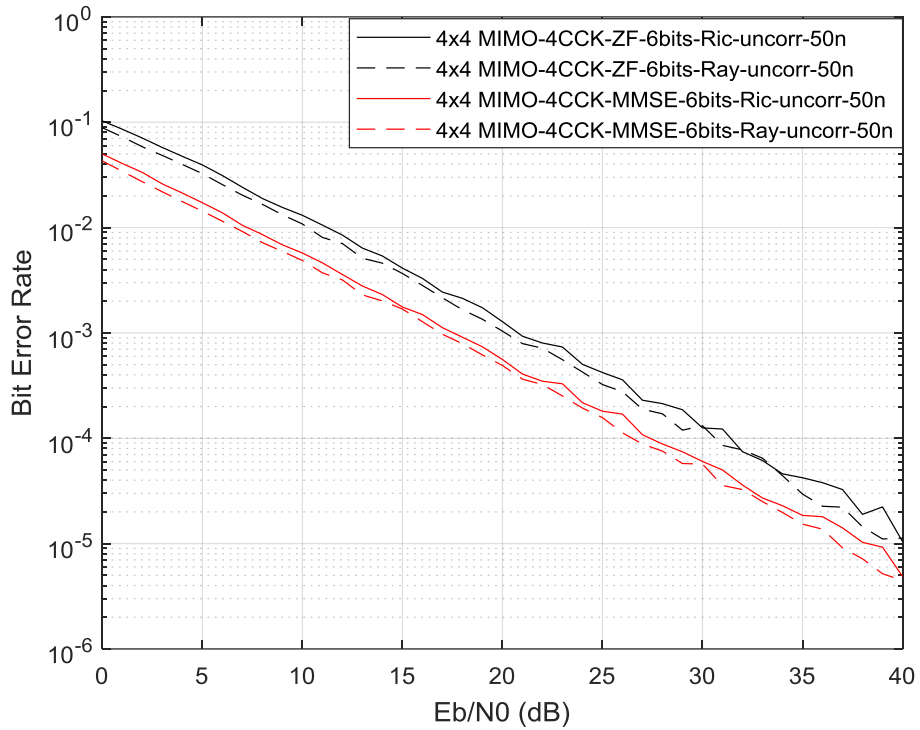


**Figure 4.15:** BER versus  $E_b/N_0$  for spatial conventional SCCK over uncorrelated Rayleigh/Rician IEEE channel and different detection schemes with  $m = 6$ , where  $N_t = 4$  and  $N_r = 4$  and RMS delay spread = 50 ns.

Fig 4.17 and 4.18 illustrate the same trend as Fig 4.16 except with different RMS delay spreads which are 50, 100 and 150 ns. In this case there is noticeable difference between Rayleigh and Rician channels in terms of the RMS delay spread effect. The BER performance of Rayleigh channels will be affected more by increasing the RMS delay than Rician channel, for example; as shown in Fig 4.17 the deterioration of BER performance of 4x4-MIMO-OFDM-SCCK with ZF detection and Rayleigh channel and RMS delay spread 150ns (blue dashed curve) start from approximately 21 dB  $E_b/N_0$ ; but this deterioration will start in the case of Rician channel (blue solid curve) at nearly 27 dB, which means that the system performance with IEEE channel is more effective outdoors in the case of Rician channel than indoors in the case of Rayleigh channel. This result will show the same trend in Fig. 4.18 with MMSE detection schemes.

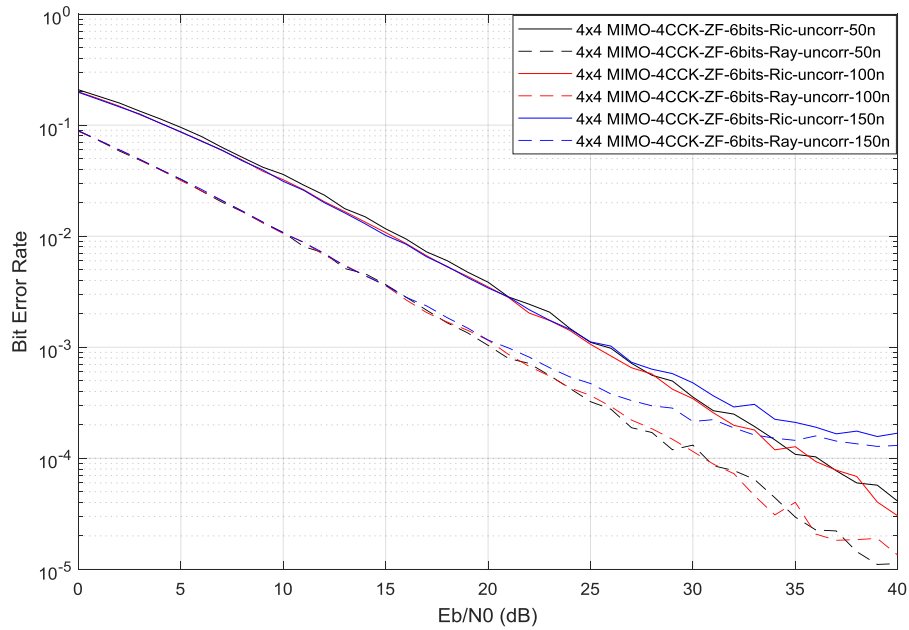


**Figure 4.16:** BER versus  $E_b/N_0$  for spatial conventional SCCK over uncorrelated Rayleigh/Rician IEEE channel and ZF detection scheme with  $m = 6$ , where  $N_t = 4$  and  $N_r = 4$  and RMS delay spread=50,100,150 ns.

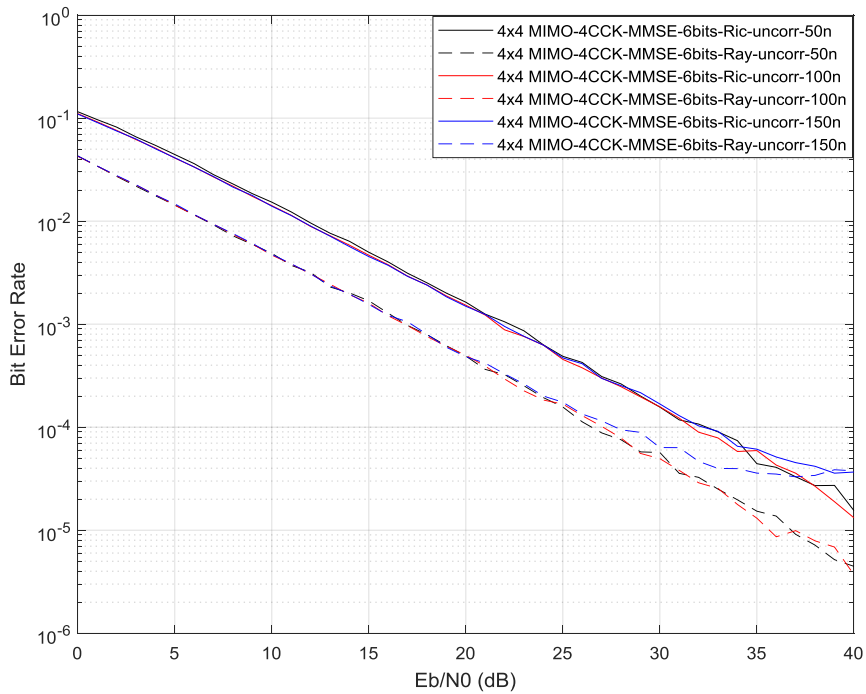


**Figure 4.17:** BER versus  $E_b/N_0$  for spatial conventional SCCK over uncorrelated Rayleigh/Rician IEEE channel and MMSE detection scheme with  $m = 6$ , where  $N_t = 4$  and  $N_r = 4$  and RMS delay spread=50,100,150 ns.

### 4.5.2.3 8- bit/s/Hz spatial CCK in Rician channel BER performance results

As shown in Fig. 4.19, SCCK system with 8 transmit/receive antennas and  $m= 8$ bit/s/Hz spectral efficiency and with codeword length of 8; this comparison illustrates the BER performance in terms of Rayleigh and Rician uncorrelated channels and ZF detection scheme and with RMS delay spreads of 50, 100 and 150 ns.

In detail, the effect of high RMS delay is presented in both Rayleigh (dashed curves) and Rician (solid curves) in high  $E_b/N_0$ , and this deterioration starts where  $E_b/N_0$  is higher than 25 dB in Rician uncorrelated channel and higher than 19 dB in the case of Rayleigh uncorrelated channel, which means the SCCK system is effected by outdoors environments in case of IEEE frequency selective channel.

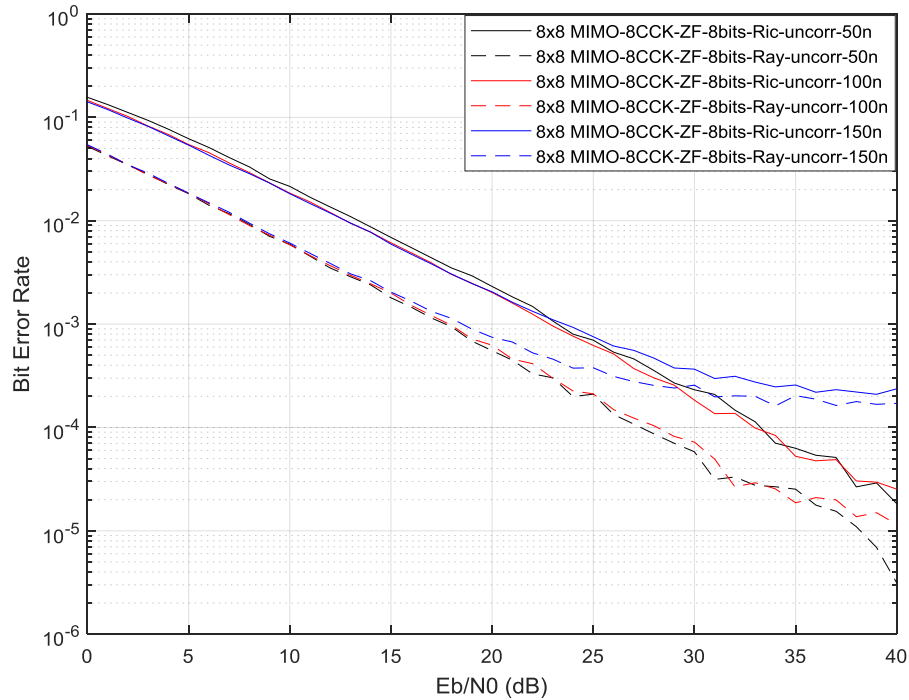


**Figure 4.18:** BER versus  $E_b/N_0$  for spatial conventional CCK over uncorrelated Rayleigh/Rician channel and ZF detection scheme with  $m = 8$ , where  $N_t = 8$  and  $N_r = 8$  and RMS delay spread=50,100,150 ns.

### 4.5.2.4 10- bit/s/Hz spatial CCK in Rician channel BER performance results

Fig 4.19 shows the same trend of Fig 4.18 except with different SCCK codeword length which here is 16, meaning the number of transmit antennas is also 16. Therefore, the proposed system can be suitable only for use in low  $E_b/N_0$  (<10 dB) when the RMS delay spread is >150 ns in

IEEE Rayleigh/Rician channels (the blue solid and the blue dashed curves), this is because of the IEEE channel model causes degradation in performance for delay spreads of  $\geq 150$ nsec [9]. When the RMS delay spread is this great, the inter symbol interference cannot be mitigated successfully with the CP length 16 in the case of MIMO-OFDM systems, which affects the BER performance as seen in Fig 4.18 and 4.19.

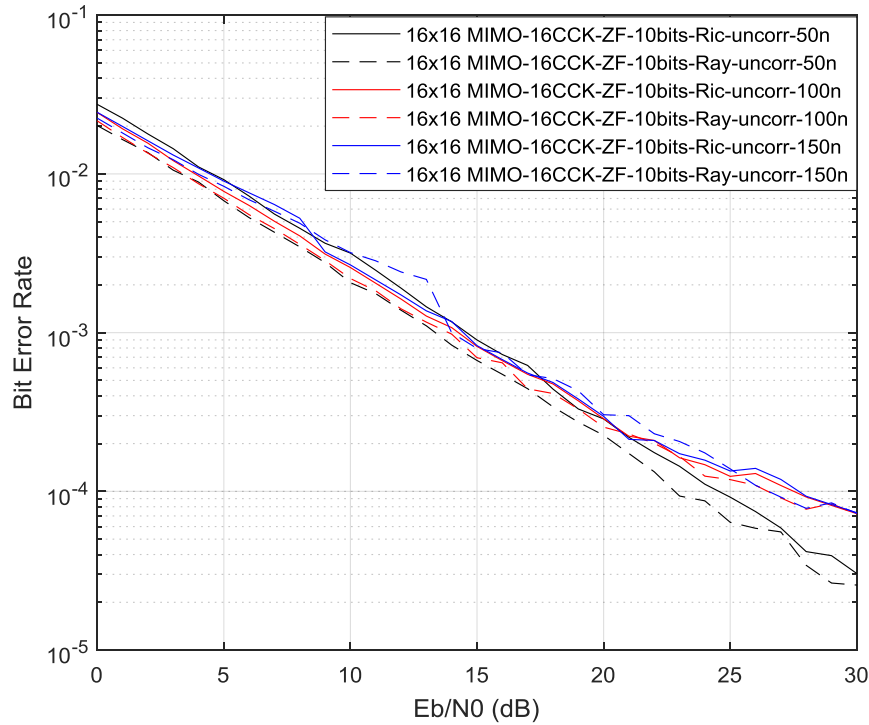


**Figure 4.19:** BER versus  $E_b/N_0$  for spatial conventional SCCK over uncorrelated Rayleigh/Rician channel and ZF detection scheme with  $m = 10$ , where  $N_t = 16$  and  $N_r = 16$  and RMS delay spread=50,100,150 ns.

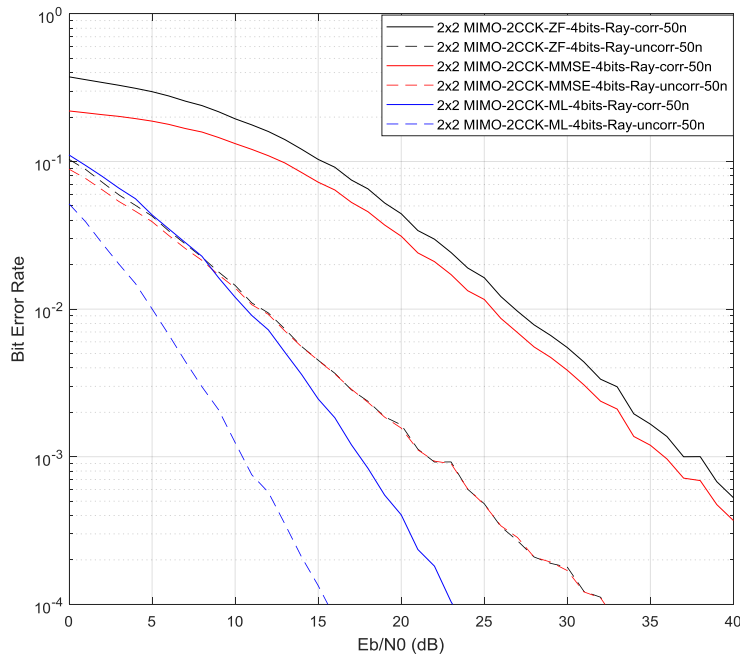
### 4.5.3 Correlated channel effect results

The purpose of this section is to evaluate the proposed SCCK system in more realistic scenarios by applying channel correlation in the MIMO-OFDM system. The correlation matrix is modelled using the exponential Kronecker channel model for its straightforward mathematical description [11]

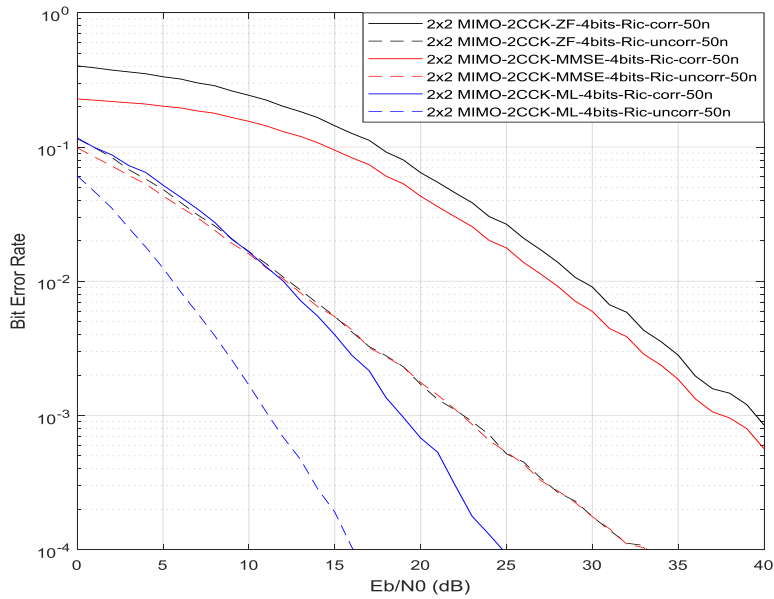
#### 4.5.3.1 4-bit/s/Hz spatial CCK results

Fig 4.20 and 4.21 show the simulation results of BER performance of the proposed SCCK system using ZF and MMSE detection schemes over correlated and uncorrelated, Rayleigh and Rician

channels with different RMS delay spreads. Note that, in these figures the number of both transmit and receive antennas and the spectral efficiency are the same but the difference is in the type of channel and the detector schemes. In detail, Fig 4.20 plots BER vs  $E_b/N_0$  compared SCCK with correlated Rayleigh channel (solid curves) with SCCK with uncorrelated Rayleigh channel (dashed curves) for 4 bit/s/Hz spectral efficiencies, and ZF, MMSE and ML detection schemes respectively with correlation coefficient ( $c=0.5$ ) in both transmit/receive sides. At  $10^{-2}$  BER SCCK with uncorrelated Rayleigh channel and ZF detector achieves a SNR gain of 12 dB over the same system under the channel correlation effect. The same trend can be seen in the case of the Rician channel as shown in Fig 4.21, which describes the effect of correlation that degrades the BER performance and describes the system in more realistic scenarios.



**Figure 4.20:** BER versus  $E_b/N_0$  for spatial conventional SCCK over correlated/uncorrelated Rayleigh channel and different detection schemes with  $m = 4$ , where  $N_t = 2$  and  $N_r = 2$  and RMS delay spread=50 ns and  $c=0.5$ .

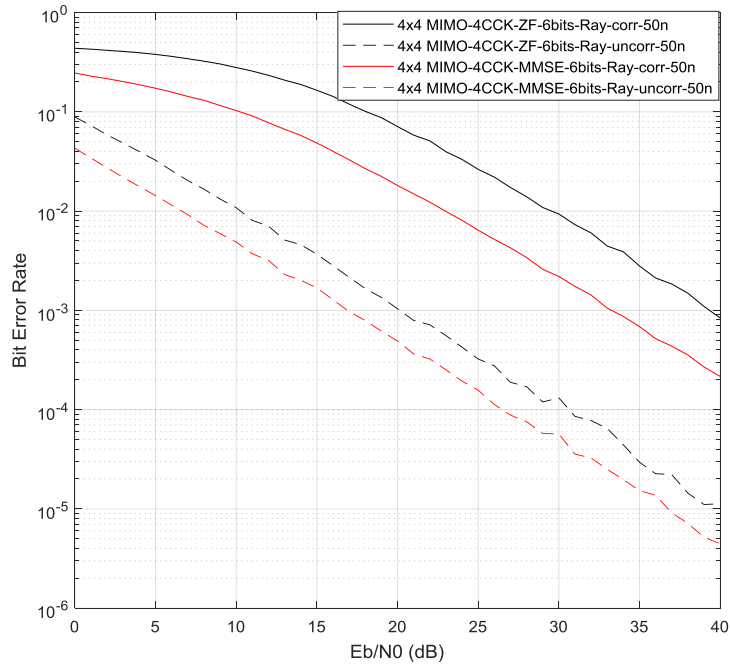


**Figure 4.21:** BER versus  $E_b/N_0$  for spatial conventional SCCK over correlated/uncorrelated Rician channel and different detection schemes with  $m = 4$ , where  $N_t = 2$  and  $N_r = 2$  and RMS delay spread=50 ns and  $c=0.5$ .

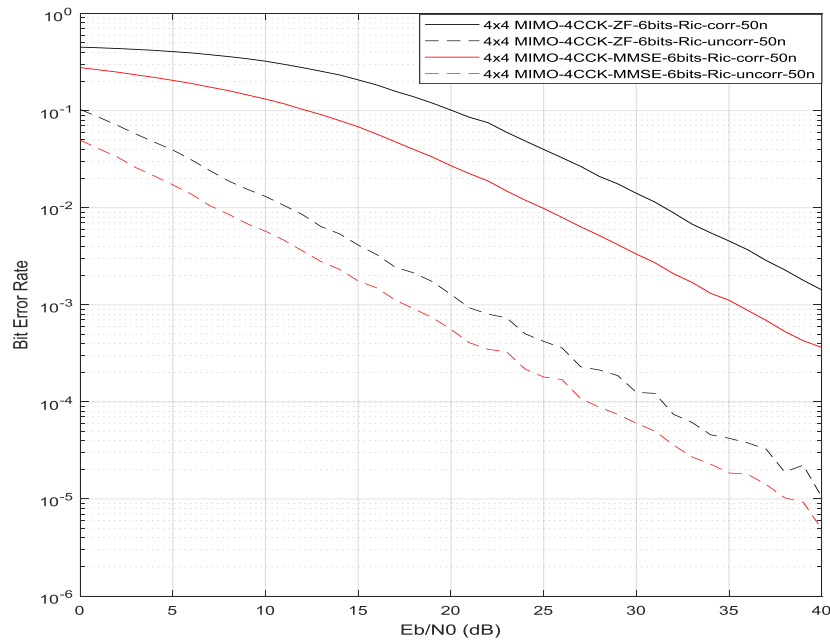
#### 4.5.3.2 6-bit/s/Hz spatial CCK results

Fig 4.22 presents the effect of correlation that degrades the BER performance with 4-SCCK codeword length.

In detail, Fig 4.22 presents BER vs  $E_b/N_0$  SCCK with correlated Rayleigh channel (solid curves) compared with SCCK with uncorrelated Rayleigh channel (dashed curves) for 6 bit/s/Hz spectral efficiencies, and ZF and MMSE detection schemes with correlation coefficient ( $c=0.5$ ) in both transmit and receive sides. At  $10^{-3}$  BER, SCCK with uncorrelated Rayleigh channel and ZF detector achieves a SNR gain of a 19 dB over the same system under the channel correlation effect. The same trend can be seen in the case of the Rician channel as shown in Fig 4.23, which describes the effect of correlation that degrades the BER performance, again describing the system in more realistic scenarios.



**Figure 4.22:** BER versus  $E_b/N_0$  for spatial conventional SCCK over correlated/uncorrelated Rayleigh channel and different detection schemes with  $m = 6$ , where  $N_t = 4$  and  $N_r = 4$  and RMS delay spread = 50 ns and  $c = 0.5$ .



**Figure 4.23:** BER versus  $E_b/N_0$  for spatial conventional SCCK over correlated/uncorrelated Rayleigh channel and different detection schemes with  $m = 6$ , where  $N_t = 4$  and  $N_r = 4$  and RMS delay spread = 50 ns and  $c = 0.5$ .

### 4.5.3.3 8-bit/s/Hz spatial CCK results

Figs 4.24 and 4.25 plot the BER system performance as a function of the  $E_b/N_0$  for 8x8 MIMO-OFDM-SCCK system. Bold lines represent the correlated channels while the dashed lines denote the uncorrelated channels. The degree of the correlation in the channels is defined by  $c=0.5$  for both the transmitter and the receiver.

In detail, Fig 4.24 shows BER vs  $E_b/N_0$  compares SCCK with correlated Rayleigh channel (solid curves), with SCCK with uncorrelated Rayleigh channel (dashed curves), for 8 bit/s/Hz spectral efficiencies, and ZF, MMSE detection schemes respectively. The correlation effect decreased the BER performance in both ZF and MMSE detectors by approximately 19 dB. The same trend can be seen in the case of the Rician channel as shown in Fig 4.25, which presents the effect of correlation that degraded the BER performance in trade off and describing the system in more realistic scenarios.

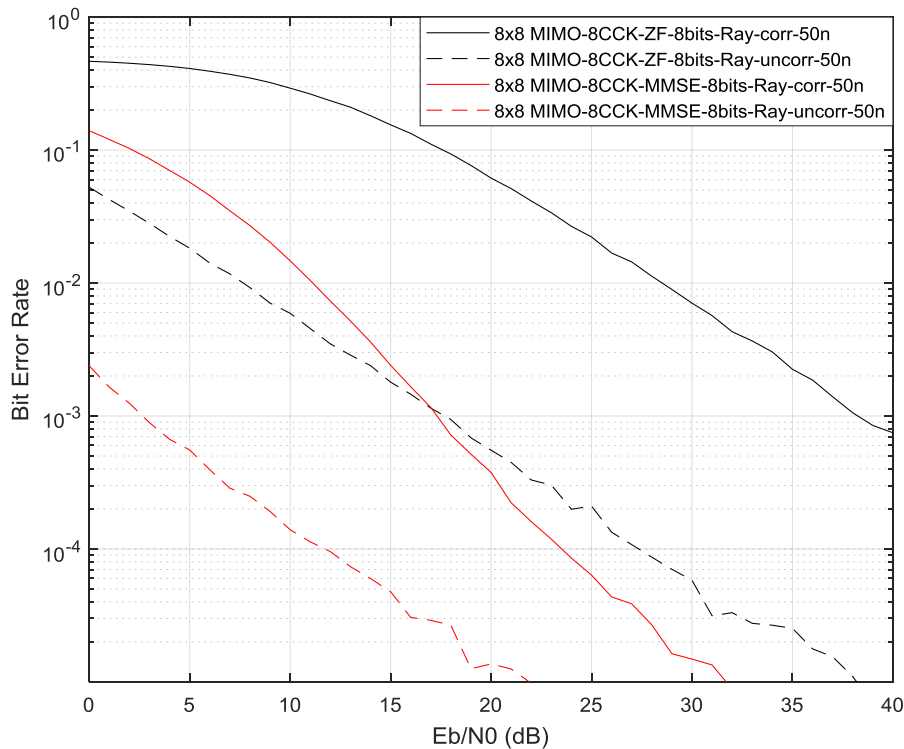


**Figure 4.24:** BER versus  $E_b/N_0$  for spatial conventional SCCK over correlated/uncorrelated Rayleigh channel and different detection schemes with  $m = 8$ , where  $N_t = 8$  and  $N_r = 8$  and RMS delay spread=50 ns and correlation factor=0.5.

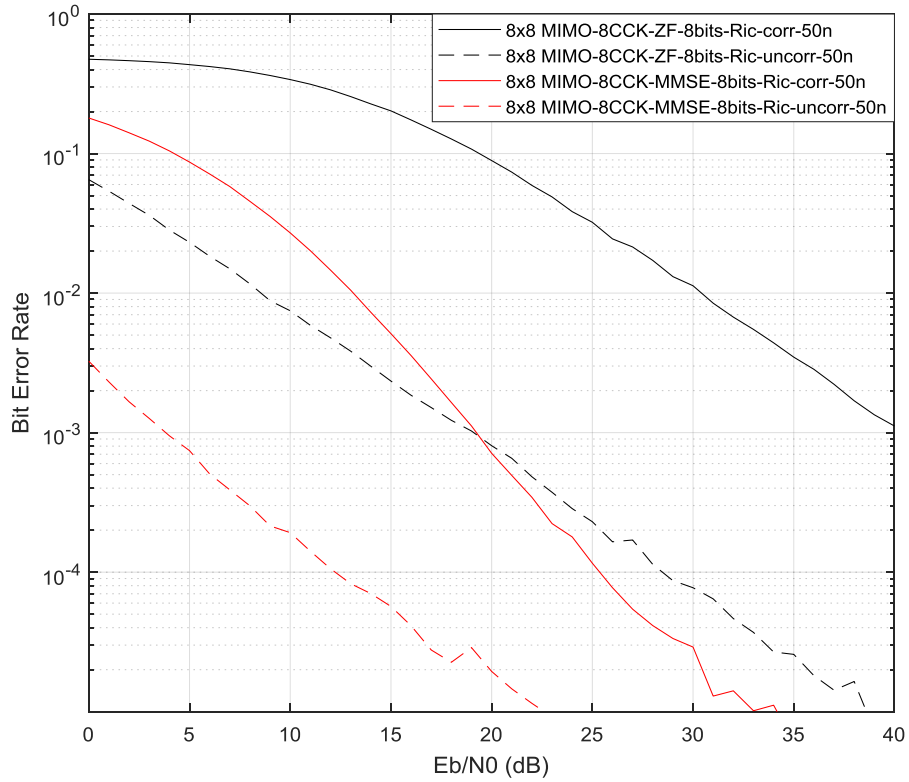


**Figure 4.25:** BER versus  $E_b/N_0$  for spatial conventional CCK over correlated/uncorrelated Rician channel and different detection schemes with  $m = 8$ , where  $N_t = 8$  and  $N_r = 8$  and RMS delay spread=50 ns and  $c=0.5$ .

Fig 4.26 plots the proposed SCCK system with different RMS delay spreads, under the ZF detection scheme and Rician fading channels with spreads of 50, 100 and 150 ns. It shows BER vs  $E_b/N_0$  for SCCK with correlated Rician channel (solid curves), compared with SCCK with uncorrelated Rician channel (dashed curves) for 8 bit/s/Hz spectral efficiencies, and ZF detection scheme with correlation coefficient ( $c=0.5$ ) in both transmit and receive sides. The BER performance is deteriorated in the case of RMS delay spreads of 150 ns when the  $E_b/N_0$  is higher than 22 dB, with no obvious effect in terms of RMS delay spreads of 50 and 100 ns. For instance, the BER performance is approximately flat at the point  $10^{-3}$  in case of Rician uncorrelated channel with RMS delay spreads of 150 ns.

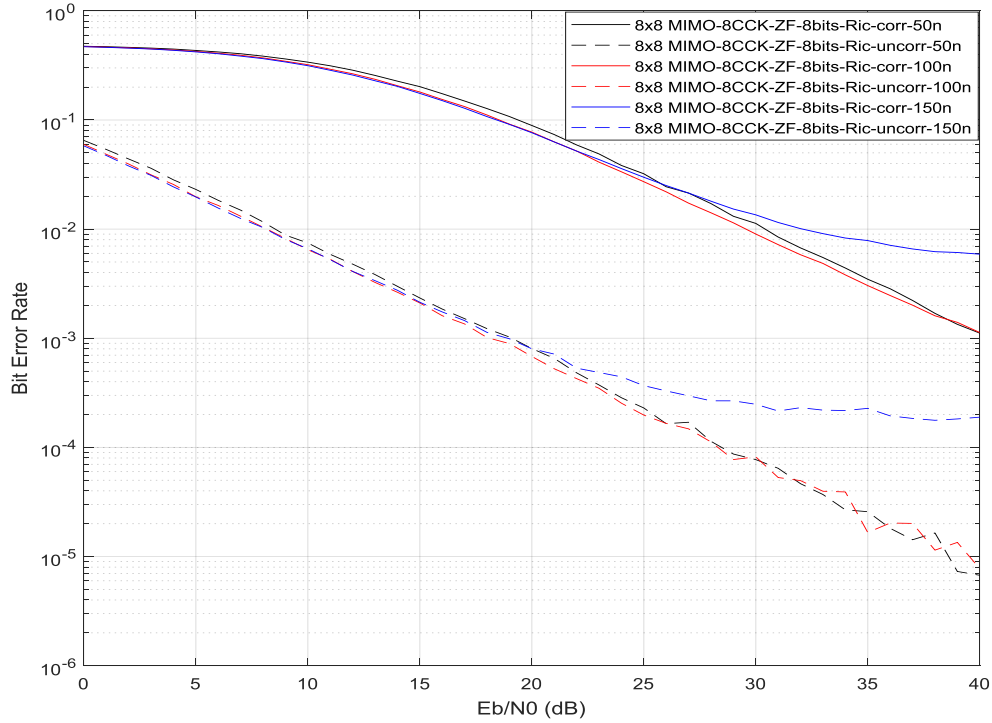


**Figure 4.26:** BER versus  $E_b/N_0$  for spatial conventional SCCK over correlated/unrelated Rician channel and ZF detection scheme with  $m = 8$ , where  $N_t = 8$  and  $N_r = 8$  and RMS delay spread=50,100,150 ns and  $c=0.5$ .

#### 4.5.3.4 10-bit/s/Hz spatial CCK results

Fig 4.27 shows the simulation results of BER performance of the proposed SCCK system with codeword length 16 and using ZF and MMSE detection schemes over correlated and uncorrelated, Rayleigh and Rician channels with 50ns RMS delay spreads. Correlation coefficient ( $c=0.5$ ) is used in both transmit and receive sides. For instance, at  $10^{-2}$  BER 16-SCCK with uncorrelated Rayleigh channel and MMSE detector achieve a SNR gain of 20 dB over the same system under the channel correlation effect. This suggests this type of IEEE fading channel is not suitable for SCCK with large codeword numbers. Different, more suitable channels will be suggested in future work, after discussing the analytical BER performance of spatial CCK system with narrowband channel in the next section and leaving the analytical BER of wideband channel to the future work as well.

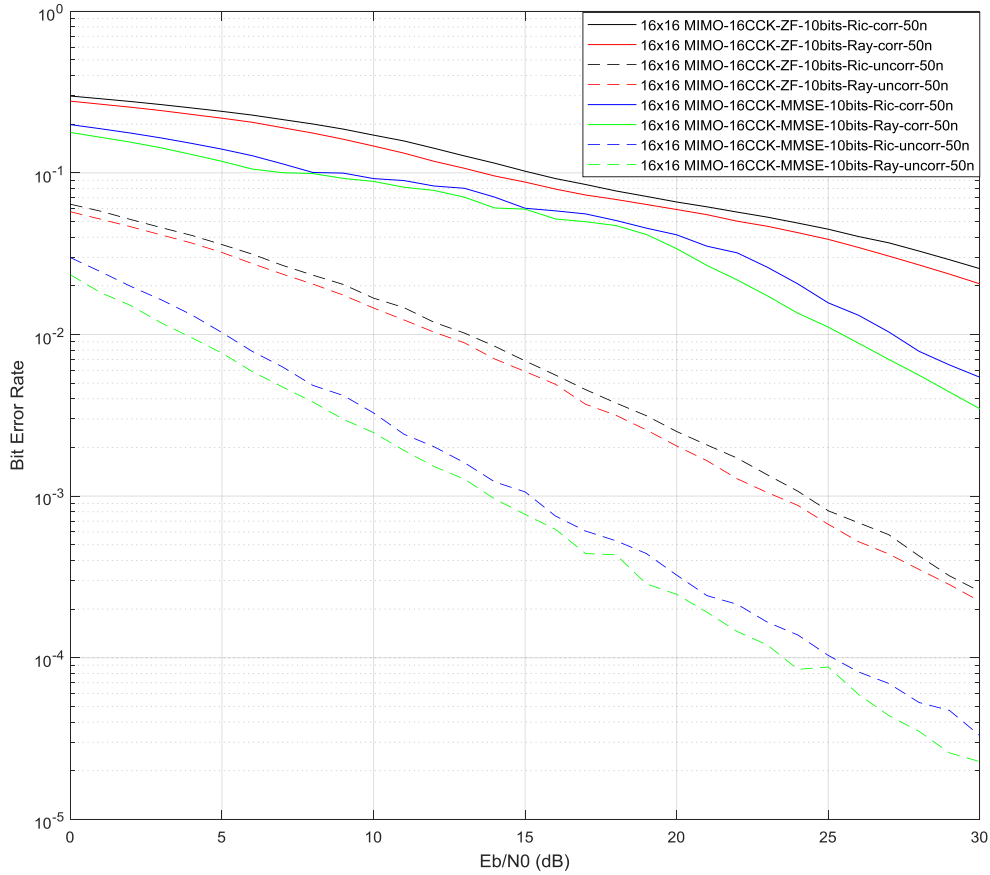


**Figure 4.27:** BER versus Eb/No for spatial conventional SCCK over correlated/uncorrelated Rician-Rayleigh channel and ZF, MMSE detection schemes with  $m = 10$ , where  $N_t = 16$  and  $N_r = 16$  and RMS = 50 ns and  $c=0.5$ .

## 4.6 Bit error rate analysis of Spatial Complementary Code Keying compared to SMX and SM with narrowband fading channels.

This section discusses the analytical model of SCCK system with narrowband channel and ML detector at the receiver.

A brief description of Fig 4.28 follows:  $B_c(k)$  is the input binary sequence of  $c$  codewords which presents as an example 2-SCCK with  $B_c(k) = [a_0, a_1, a_2, a_3]$ , and is divided into streams of  $(1 + \log_2(N_T)) \times \log_2(M)$  bits, where  $N_t$  the number of transmit antennas and  $M$  is the number of code generating phases, here 4. These streams are encoded into SCCK codewords defined by  $C_c(k) = [C_c(0), C_c(1), C_c(2), C_c(3)]$ . these codewords that is sent through the Rayleigh fading

channel  $H(t)$ . At the receive side the noise  $n(t)$  is added to the signal to result  $y(t)$ , after ML detection stage the estimated date  $\widehat{B}_c(k)$  is compared with the transmit data to calculate the BER performance of the system. Note that the synchronisation is considered at the receiver.

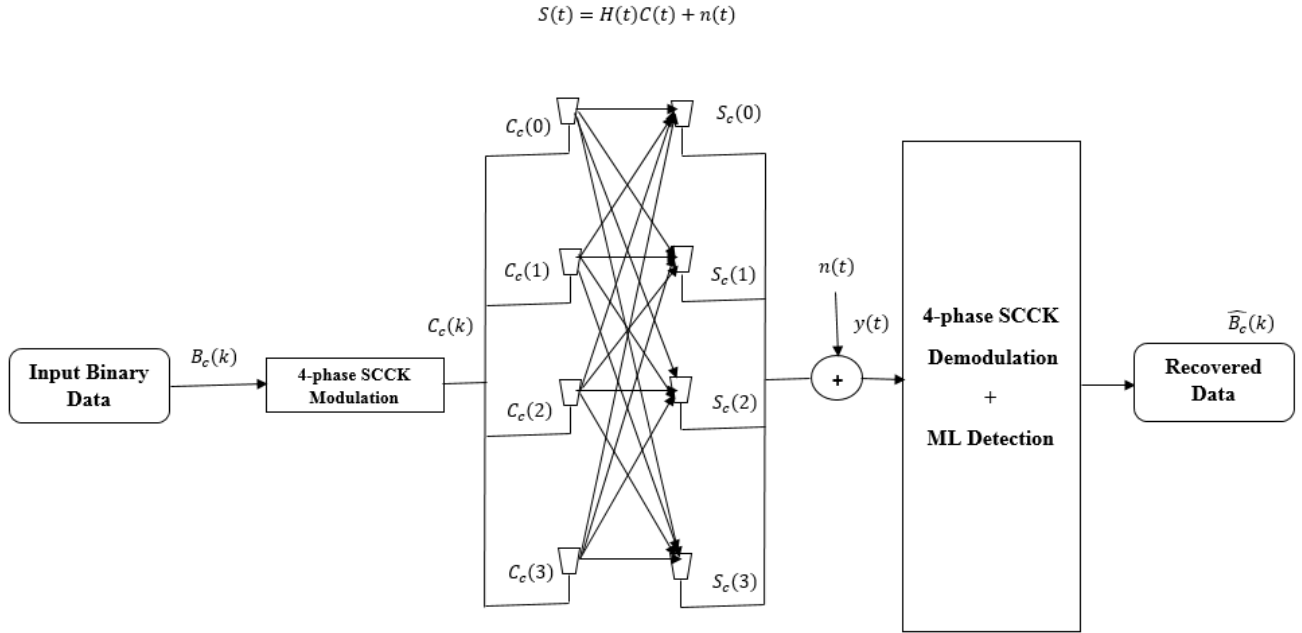


**Figure 4.28:** spatial CCK modulation system with 4-phases and narrowband Rayleigh channel

Over the bandwidth of interest of frequency-flat fading, the  $N_T \times N_R$  MIMO channel matrix at a particular moment of time may be described as the following[31]:

$$\tilde{H} = \begin{bmatrix} h_{1,1} & h_{1,2} & \dots & h_{1,N_T} \\ h_{2,1} & h_{2,2} & \dots & h_{2,N_T} \\ \vdots & \vdots & \ddots & \vdots \\ h_{N_R,1} & h_{N_R,2} & \dots & h_{N_R,N_T} \end{bmatrix} \quad (4.16)$$

where  $h_{ij}$  is the SISO channel gain between the  $j^{th}$  transmit and  $i^{th}$  receive antenna pair. The  $j^{th}$  column of  $\tilde{H}$  is often represented by the spatial signature of the  $j^{th}$  transmit antenna through the receive antenna array. As with SISO channels, the common model that includes the MIMO channel

with independent gains is known as zero-mean AWGN in which the Rayleigh distributed random variables' amplitudes are  $h_{ij}$ . Thus, the following equation represents the receiving signal.

$$y = \tilde{H}x + n \quad (4.17)$$

where  $y$  is the received vector of the signal of size  $N_R \times 1$ ,  $x$  is the  $N_T \times 1$  transmitted vector of the signal,  $n$  is the AWGN.

The correlation channel matrix is [49, 95, 96]:

$$H = R_{N_r}^{\frac{1}{2}} \tilde{H} R_{N_t}^{\frac{1}{2}} \quad (4.18)$$

where  $\tilde{H}$  is the uncorrelated channel defined in equation (4.16), which can be Rayleigh, Rician fading channel;  $R_{N_T}$  is the transmitter correlation matrix; and  $R_{N_R}$  is the receiver correlation matrix. Moreover, the correlation matrices can be produced using an exponential decay model:

$$R_c = \begin{bmatrix} 1 & r_c & r_c^2 & \dots & r_c^{n-1} \\ r_c & 1 & r_c & \ddots & \vdots \\ r_c^2 & r_c & 1 & \ddots & r_c^2 \\ \vdots & \ddots & \ddots & \ddots & r_c \\ r_c^{n-1} & \dots & r_c^2 & r_c & 1 \end{bmatrix} \quad (4.19)$$

Where  $r_c = \exp(-\beta)$  and  $\beta$  is the correlation decay coefficient and  $n$  is the number of transmit receive antennas. At the receiver the ML optimum detector is used, which can be written as [97]:

$$\hat{x}_t = \arg \min_{x \in Q} \{ \|y - \tilde{H}x\|_F^2 \} \quad (4.20)$$

where  $Q$  contains every possible  $(N_T - 1)$  transmit vector, and  $\hat{x}$  denotes the estimated transmission vector. The approximation equation that defends the overall rates [98] is:

$$P_e \leq \sum_x P(x) \sum_{\tilde{x} \neq x} P(x \rightarrow \tilde{x}) \quad (4.21)$$

Where  $P(x)$  is defined as the probability of codeword  $x$ , assumed uniform, and  $P(x \rightarrow \tilde{x})$  is defined the pairwise error probability that a code word  $x$  is decoded as  $\tilde{x}$ .

The ABER for MIMO SM -SMX systems can be computed using the union bound technique, which can be expressed as follows [99]:

where  $N(x, \tilde{x})$  is defined the number of bits in error between  $x$  and  $\tilde{x}$ ;  $E_H\{\cdot\}$  is the expectation across the channel  $H$ ; and  $P_r$  is presents the conditional pairwise error probability *PEP* of deciding on  $\tilde{x}$  given that  $x$  is transmitted; and  $Q^m$  is a  $2^m$  space containing all possible transmitted vectors ( $N_T \times 1$ ), and  $m$  defined the spectral efficiency which defined in details in chapter 1.

The *PEP* of space modulation system can be written as:

$$P_r = P_r \left( \|y - \tilde{H}x_t\|_F^2 > \|y - \tilde{H}x\|_F^2 \right) \quad (4.22)$$

To clarify (4.22) for simple case of AWGN channel[100]:

In general:

$$\text{If } y = x + n, n \sim \mathcal{N}\left(0, \frac{N_0}{2} I_n\right) \quad (4.23)$$

Where  $y$  is represented the series of outputs of the AWGN channel in  $n$  defined the noise vector where  $\mathcal{N}\left(0, \frac{N_0}{2} I_n\right)$  is independent and identically distributed and shown from a zero mean normal distribution with variance  $\frac{N_0}{2} I_n$  (the noise). And  $I_n$  is identity matrix with  $n$  size.

The close form of *PEP* is defined as:

$$P_r (x \neq \tilde{x}) = P_r (\|y - x\|_F^2 \neq \|y - \tilde{x}\|_F^2) \quad (4.24)$$

$$= P_r (\|(x + n) - x_t\|_F^2 \neq \|(x + n) - \tilde{x}\|_F^2)$$

$$= P_r (\|n\|_F^2 \neq \|(x - \tilde{x}) + n\|_F^2)$$

$$= P_r (\|n\|_F^2 \neq \|x_t - \tilde{x}\|_F^2 + \|n\|_F^2 + 2(n, x - \tilde{x}))$$

$$= P_r (-\|x - \tilde{x}\|_F^2 \neq +2(n, x - \tilde{x})) \quad (4.25)$$

So:

$$P_r (x \neq \tilde{x}) = P_r \left( (n, x - \tilde{x}) \neq \frac{-\|x - \tilde{x}\|_F^2}{2} \right) \quad (4.26)$$

$(n, x - \tilde{x})$  is the Gaussian random variable with mean Zero and variance  $\frac{N_0 \|x - \tilde{x}\|_F^2}{2}$

For zero mean variance  $\sigma^2 = 1$  Gaussian random variable and from the Q-function equation definition in [101]:

For general random variable  $x$  with mean  $\mu$  and variance  $\delta^2$  so:

$$P_{\text{error}}(x \neq \tilde{x}) = Q(x) \quad (4.27)$$

$$\text{Where } x = \frac{x - \mu}{\sqrt{\delta^2}}$$

Hence, applying 4.26 in 4.27

$$P_{\text{error}}(x \neq \tilde{x}) = Q\left(\frac{\frac{\|x - \tilde{x}\|_F^2}{2}}{\sqrt{\frac{N_0 \|x - \tilde{x}\|_F^2}{2}}}\right) \quad (4.28)$$

$$P_{\text{error}}(x \neq \tilde{x}) = Q\left(\frac{\|x - \tilde{x}\|_F^2}{2} \cdot \sqrt{\frac{2}{N_0 \|x - \tilde{x}\|_F^2}}\right) \quad (4.29)$$

So:

$$P_{\text{error}}(x \neq \tilde{x}) = Q\left(\frac{\|x - \tilde{x}\|_F^2}{\sqrt{2N_0}}\right) \quad (4.30)$$

By applying this result (4.28) with Rayleigh channel instead of AWGN channel[11]:

$$P_{\text{error}} = Q\left(\frac{\|\tilde{H}(x - \tilde{x})\|_F^2}{\sqrt{2N_0 N_R}}\right) \quad (4.31)$$

$$P_{\text{error}} = Q\left(\frac{\|\tilde{H}\Psi\|_F^2}{\sqrt{2N_0 N_R}}\right) \quad (4.32)$$

Where  $\tilde{H}$  defined the channel matrix if Rayleigh and Rician and  $\Psi = x - \tilde{x}$  is the Euclidean distance between transmit and receive codewords of SM, SMX code words.

For the proposed spatial CCK system these code words generated by applying the general CCK equations with QPSK modulation order (discussed in the section of spatial CCK code words generation) which are mentioned in chapters 2, 3.

From[102]

by using the alternative integral expression of Q-function defined as *Craig's formula* as:

$$Q(x) = \frac{1}{\pi} \int_0^{\frac{\pi}{2}} \exp\left(-\frac{x^2}{2 \sin^2 \theta}\right) d\theta \quad (4.33)$$

So substituting 4.32 in 4.33:

$$Q\left(\frac{\|\tilde{H}\Psi\|_F^2}{\sqrt{2N_0 N_R}}\right) = \frac{1}{\pi} \int_0^{\frac{\pi}{2}} \exp\left(-\frac{\|\tilde{H}\Psi\|_F^2}{4 N_0 N_R \sin^2 \theta}\right) d\theta \quad (4.34)$$

And  $\Psi = x - \tilde{x}$

Then:

$$P_{r_{error}} = \frac{1}{\pi} \int_0^{\frac{\pi}{2}} \exp\left(-\frac{\|\tilde{H}\Psi\|_F^2}{4 N_0 N_R \sin^2 \theta}\right) d\theta \quad (4.35)$$

Taking the expectation of both sides of the equation[97]:

$$\begin{aligned} E_H \left\{ P_{r_{error}} \right\} &= E_H \left\{ \frac{1}{\pi} \int_0^{\frac{\pi}{2}} \exp\left(-\frac{\|\tilde{H}\Psi\|_F^2}{4 N_0 N_R \sin^2 \theta}\right) d\theta \right\} \\ &= \frac{1}{\pi} \int_0^{\frac{\pi}{2}} \Phi\left(-\frac{1}{4 N_0 N_R \sin^2 \theta}\right) d\theta \end{aligned} \quad (4.36)$$

where  $\Phi(\cdot)$  is defined the moment generation function of a random variable of  $\|\tilde{H}\Psi\|_F^2$

As a general definition of the moment generation function so:

From[98] the argument of the MGF in (4.36) can be written as:

For channel  $H_n = H$  for  $n = 1, \dots, N$ . And  $N$  is  $N$  is the total code word length. Denote the difference of two code word matrices with  $\Delta = [\mathbf{e}_1 \cdots \mathbf{e}_N]$ . Then, the argument of the MGF in (4.34) can be described in terms of  $R_{N_T}$  and  $R_{N_R}$  will discussed as:

$$\begin{aligned} \|\tilde{H}\Psi\|_F^2 &= \sum_{n=1}^N \|H_n e_n\|^2 \\ &= \|H\Delta\|^2 \\ &= \text{tr}(H\Delta\Delta^H H^H) \\ &= \text{vec}(H^H)^H (I_{N_R} \otimes \Delta\Delta^H) \text{vec}(H^H) \end{aligned} \quad (4.37)$$

So with correlation effect this equation will be:

$$= \text{vec}(\tilde{H}^H)^H (R_S^{\frac{1}{2}})^H (I_{N_R} \otimes \Delta\Delta^H) R_S^{\frac{1}{2}} \text{vec}(\tilde{H}^H)^H \quad (4.38)$$

$$\text{And } R_S = R_{N_R} \otimes R_{N_T} \quad (4.39)$$

where  $I_{N_R}$  is an identity matrix;  $(\cdot)^H$  denotes the Hermitian; and in general  $\text{vec}(B)$  is the vectorization operator, where the matrix columns  $B$  are accumulated in column vector; and  $R_S = R_{N_R} \otimes R_{N_T}$ , with  $\otimes$  being the Kronecker product between  $R_{N_R}$  and  $R_{N_T}$ .

Fact [103]: Let  $A$  be a Hermitian matrix and  $u$  a circularly symmetric complex Gaussian vector with mean  $\bar{u}$  and covariance matrix  $R_u$ .

The MGF of the quadratic form  $y = u\Lambda u^H$  is given as:

$$\Phi_y(s) = \int_0^\infty e^{-sy} pY(y) dy = \frac{\exp(s\bar{u} \Lambda (I - sR_u \Lambda)^{-1} \bar{u}^H)}{|I - sR_u \Lambda|} \quad (4.40)$$

where  $I$  is the identity matrix with appropriate size.

By applying this fact in equation (4.36), So the moment generation function (MGF) will be:

$$\Phi(s) = \frac{\exp(s\bar{u} \Lambda (I - sR_u \Lambda)^{-1} \bar{u}^H)}{|I - sR_u \Lambda|} \quad (4.41)$$

Clearly  $u = \text{vec}(\tilde{H}^H)^H$  is the zero mean Gaussian vector with covariance matrix  $R_u = I_{nRnT}$  and  $(R_s^2)^H (I_{nR} \otimes \Delta \Delta^H) R_s^2$  is a Hermitian matrix and  $\Lambda = \Psi \Psi^H$ , hence, using the properties of the Kronecker product [97]:

$$\Phi(s) = \frac{\exp(sx \text{vec}(\tilde{H}^H)^H \Lambda (I_{nRnT} - sR_u \Lambda)^{-1} \text{vec}(H^H))}{|I_{nRnT} - sR_u \Lambda|} \quad (4.44)$$

Now plugging (4.42) into (4.36) yields:

$$E_H \left\{ P_{r_{error}} \right\} = \frac{1}{\pi} \int_0^{\frac{\pi}{2}} \frac{\exp\left(-\frac{1}{4N_0N_R \sin^2 \theta} x \text{vec}(\tilde{H}^H)^H \Lambda \left(I_{nRnT} - \left(-\frac{1}{4N_0N_R \sin^2 \theta}\right) R_u \Lambda\right)^{-1} \text{vec}(H^H)\right)}{\left|I_{nRnT} - \left(-\frac{1}{4N_0N_R \sin^2 \theta}\right) R_u \Lambda\right|} d\theta \quad (4.43)$$

So:

$$E_H \left\{ P_{r_{error}} \right\} = \frac{1}{\pi} \int_0^{\frac{\pi}{2}} \frac{\exp\left(-\frac{1}{4N_0N_R \sin^2 \theta} x \text{vec}(\tilde{H}^H)^H \Lambda \left(I_{nRnT} + \frac{1}{4N_0N_R \sin^2 \theta} R_u \Lambda\right)^{-1} \text{vec}(H^H)\right)}{\left|I_{nRnT} - \left(-\frac{1}{4N_0N_R \sin^2 \theta}\right) R_u \Lambda\right|} d\theta \quad (4.44)$$

From (4.21) and (4.44), and using the Chernoff bound[11] the general PEP is:

$$P_r(x_t \neq x) \leq \frac{1}{2} \frac{\exp\left(-\frac{1}{4N_0N_R} \text{vec}(\tilde{H}^H)^H \Lambda \left(I_{nRnT} + \frac{R_u \Lambda}{4N_0N_R}\right)^{-1} \text{vec}(H^H)\right)}{\left|I_{nRnT} + \frac{R_u \Lambda}{4N_0N_R}\right|} \quad (4.45)$$

Then, the average BER of spatial CCK modulation is:

$$ABER \leq \frac{1}{2^m} \sum_{x_t \in Q^m} \sum_{x \in Q^m} \frac{N(x_t, x)}{m} \frac{1}{2} \frac{\exp\left(-\frac{1}{4N_0N_R} \text{vec}(\tilde{H}^H)^H \Lambda \left(I_{nRnT} + \frac{R_u \Lambda}{4N_0N_R}\right)^{-1} \text{vec}(H^H)\right)}{\left|I_{nRnT} + \frac{R_u \Lambda}{4N_0N_R}\right|} \quad (4.46)$$

Now for a given fading channel, the mean matrix  $\tilde{H}$  and the covariance matrix  $C$  can be expressed as[104]:

$$\tilde{H} = w \times \mathbf{1}_{nRnT} \quad (4.47)$$

$$C = \sigma_n^2 \times I_{nRnT} \quad (4.48)$$

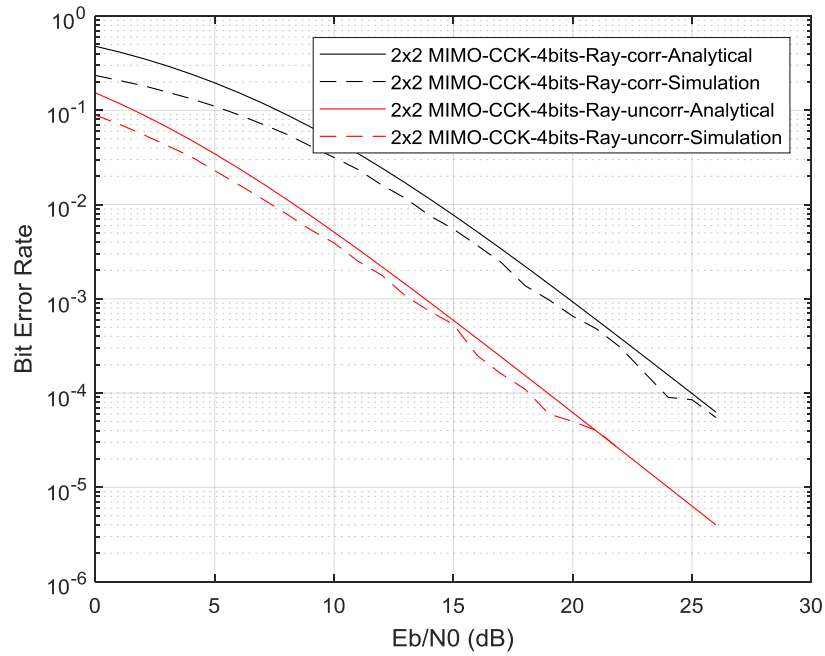
Where  $\mathbf{1}_{nRnT}$  is an  $N_T \times N_R$  all ones matrix and  $I_{nRnT}$  is identity matrix with  $N_T \times N_R$  matrix  
And  $\sigma_n^2 = N_0 \times N_R$

#### 4.6.1 BER performance results discussion

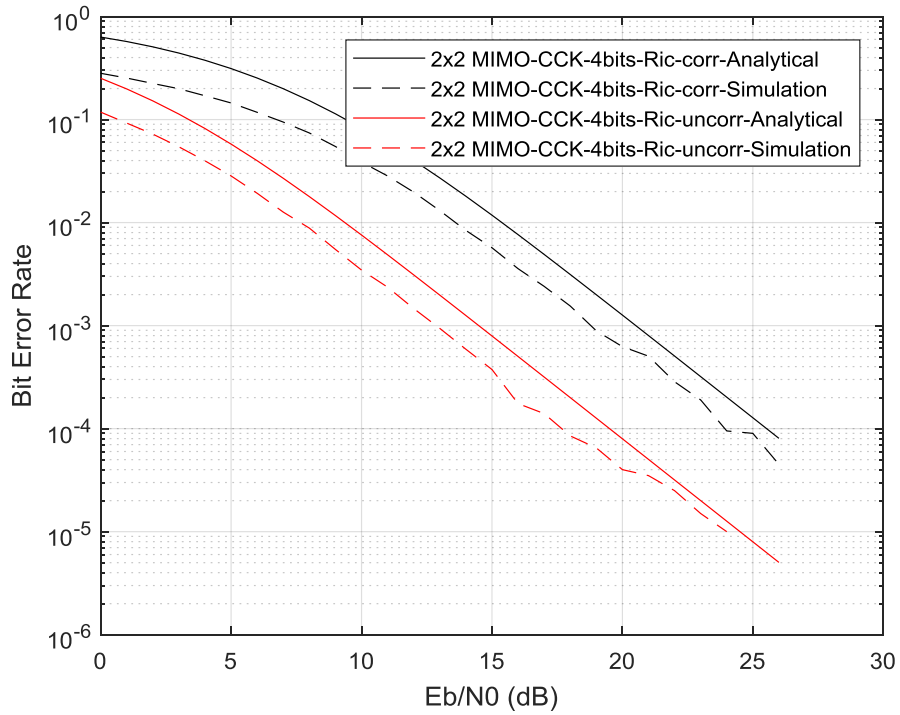
The results for the analytical and simulated BER of SCCK over i.i.d. uncorrelated and correlated, Rayleigh and Rician fading channels for the system configuration of two transmit and receive antennas and  $m= 4$  bit/s/Hz spectral efficiency and Rician factor  $K=3$  dB is depicted in Fig 4.29 and 4.30.

In Fig 4.29 and 4.30, analytical and simulation results show a close match for a wide and pragmatic range of  $E_b/N_0$  values and for different wireless channel conditions, and thus validates the derived analysis in this thesis.

Moreover, the effect of the correlation in both transmit receive sides is clear in both figures which reaches approximately 5 dB compared with uncorrelated case in both Rayleigh Rician channels. The dashed curves show the Monte Carlo simulation and the bold lines presents the analytical results and it shows that the simulation results is approximately the same with analytical results in high  $E_b/N_0$  comparing with low  $E_b/N_0$  this is because of the bound approximation calculation.



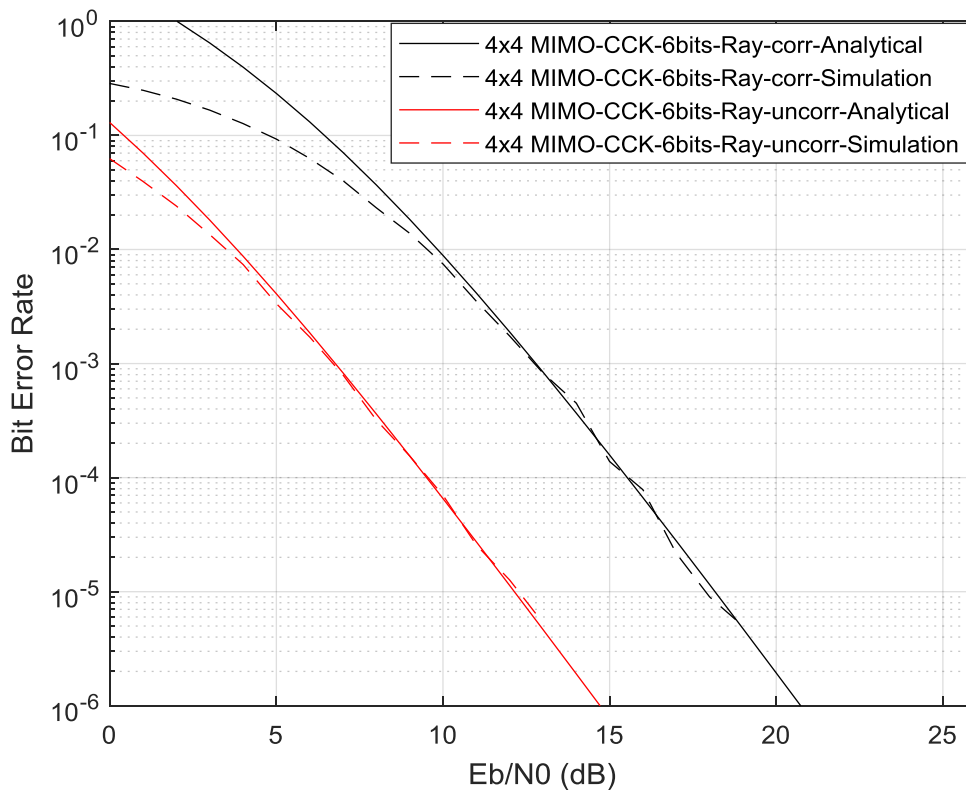
**Figure 4.29:** BER versus  $E_b/N_0$  for SCCK over uncorrelated/correlated Rayleigh channel, where  $m=4$  and  $N_t=N_r=2$ . (Dashed line) Simulation, (solid line) Analytical



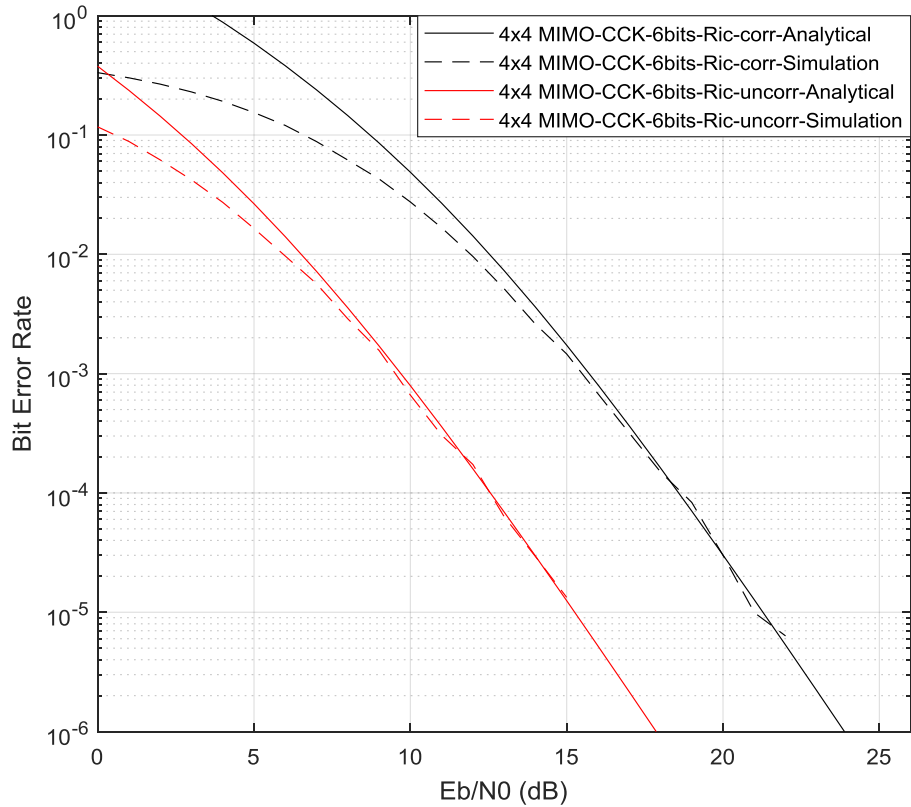
**Figure 4.30:** BER versus  $E_b/N_0$  for SCCK over uncorrelated/correlated Rician channel, where  $m=4$  and  $N_t=N_r=2$ . (Dashed line) simulation, (solid line) Analytical.

In the case of the 4 SCCK system, which means 4 transmit and receive antennas, the BER simulation results over uncorrelated and correlated, Rayleigh and Rician channels with  $K=3\text{dB}$  and with correlation decay coefficient  $c=0.5$  at both transmit and receive sides, together with the analytical results gained from the bound in the previous section are shown in Fig 4.29 and 4.30.

The same trend of the results as described in Fig 4.31 and 4.32 is presented, except the difference in the number of transmit and receive antennas and the spectral efficiency which is  $m=6$  bit/s/Hz. The correlation effect with moderate correlation factor in both Rayleigh and Rician wireless channel cases will affect the BER by approximately 5 dB. The dashed curves in Fig 4.31 represent the Monte Carlo simulation and the bold lines are the analytical results. The simulation matches the analytical results in high  $E_b/N_0$  and differs when  $E_b/N_0$  is low. The simulation is less accurate due to the bound approximation calculation in low SNR.



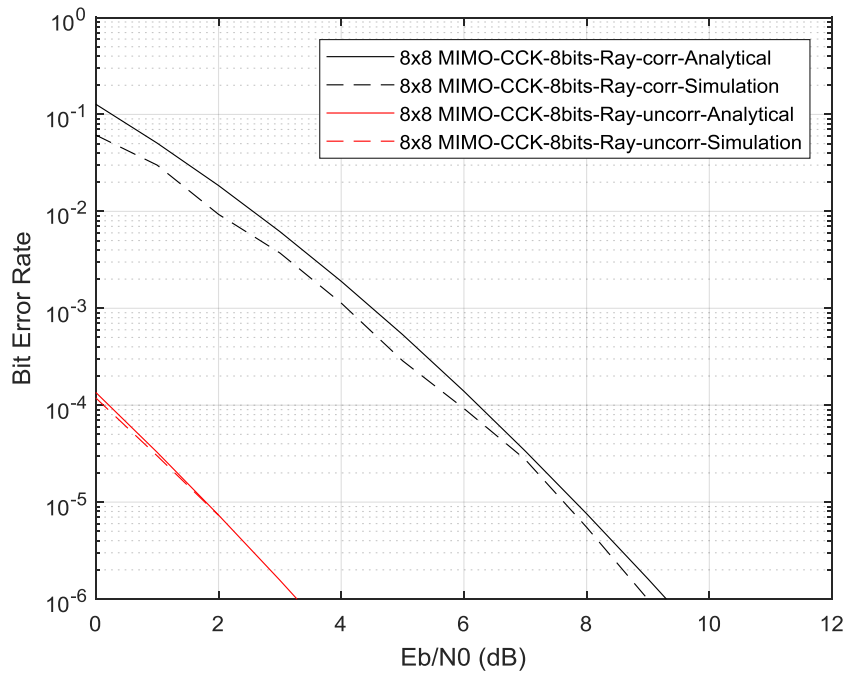
**Figure 4.31:** BER versus  $E_b/N_0$  for SCCK over uncorrelated/correlated Rayleigh channel, where  $m = 6$  and  $N_t=N_r = 4$ . (Dashed line) Simulation, (solid line) Analytical.



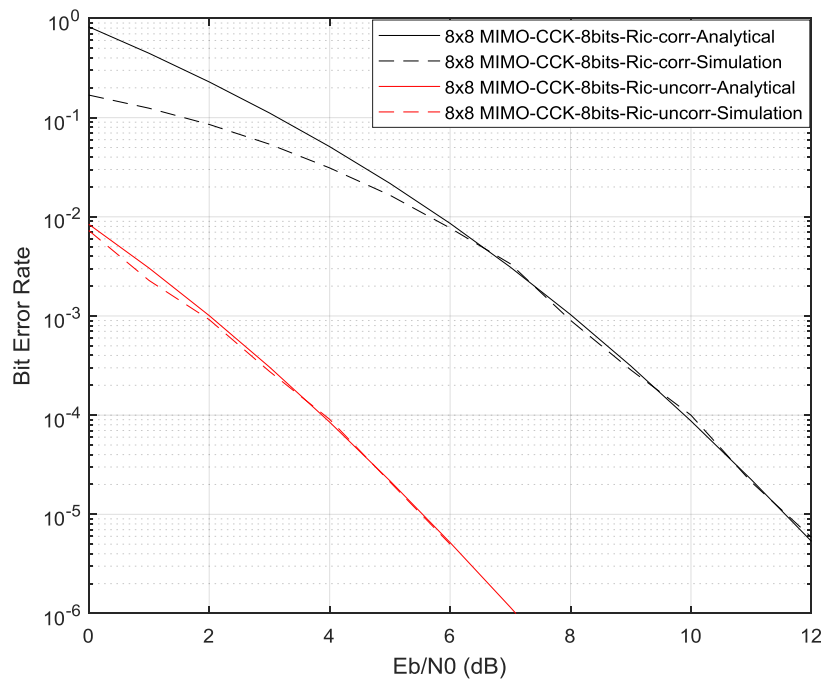
**Figure 4.32:** BER versus EbNo for SCCK over uncorrelated/correlated Rician channel, where  $m=6$  and  $N_t=N_r = 4$ .  
(Dashed line) Simulation, (solid line) Analytical

Fig 4.33 and 4.34 present the BER performance of the proposed SCCK system in terms of  $m= 8$  bit/s/Hz spectral efficiency and eight transmit receive antennas with same trend of the previous figures.

There is noticeable difference between uncorrelated and correlated channels in both Rayleigh and Rician cases, where the BER is decreased by approximately 6 dB by the correlation effect.



**Figure 4.33:** BER versus EbNo for SCCK over uncorrelated/correlated Rayleigh channel, where  $m = 8$  and  $N_t=N_r = 8$ . (Dashed line) Simulation, (solid line) Analytical



**Figure 4.34:** BER versus EbNo for SCCK over uncorrelated/correlated Rician channel, where  $m = 8$  and  $N_t=N_r = 8$ . (Dashed line) Simulation, (solid line) Analytical

The key results are shown in Fig 4.35 and 4.36, in the case of Rayleigh correlated and uncorrelated channels with 16 SCCK, which means 16 transmit antennas and  $m= 10$  bit/s/Hz spectral efficiency. The BER performance shows further improvement compared with the previous 8 SCCK cases, especially in the case of the signal power being less than the noise power, which is a promising result in the case of applications in noisy environments. The effect of the correlation will reach approximately 6 dB degradation compared with uncorrelated Rayleigh channel. The results of the Monte Carlo simulation (dashed lines) perform close to the analytical results (solid lines) at high  $E_b/N_0$ . At low  $E_b/N_0$ , the simulation diverges because of the bound approximation calculation. In addition to that the comparison with the state of the art is done by using the spatial modulation scheme; this comparison is applied by using the same number of transmit and receive antennas and four phases. In the case of Rayleigh fading channels, where the black and blue curves present the SM scheme and the red and magenta the SCCK scheme results, the results show that there is approximately 8 dB improvement in SCCK compared with SM in both correlated and uncorrelated channel cases. In addition there is a noticeable increase in spectral efficiency in SCCK, which is 10 bits, compared with SM, where the spectral efficiency is equal to 6 bits. In chapter 5 the comparison with the state of the art will be discussed in more detail.

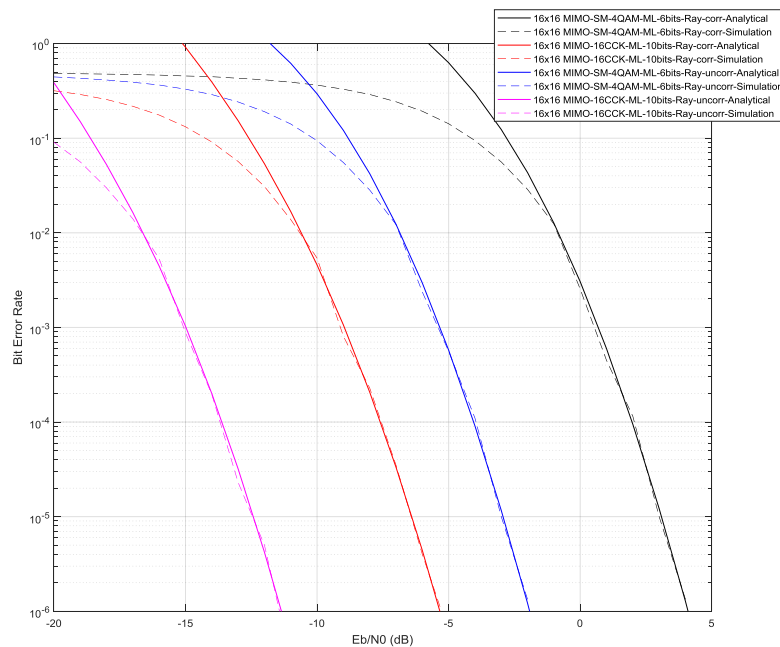


**Figure 4.35:** BER versus  $E_b/N_0$  for SCCK over uncorrelated/correlated Rayleigh channel compared with SM, where  $m = 6, 10$  and  $N_t=N_r = 16$ . (Dashed line) Simulation, (solid line) Analytical

Fig 4.36 presents the analytical and Monte Carlo simulation of 16-SCCK system with Rician uncorrelated and correlated fading channels with Rician factor  $K = 3$  dB, compared with SM results with the same number of transmit and receive antennas and number of phases. The results show approximately the same BER performance at high  $E_b/N_0$  as a result of the bound approximation. It is clear to see that SCCK (red and magenta curves) is more effective and workable at low  $E_b/N_0$  compared with SM (black and blue curves) and this means that this system is promising in noisy environments. For example, in the case of SM with a Rician correlated channel it is clear that this system is not effective with low SNR (black curve ) compared with SCCK result with the same channel and phase condition (red curve) with noticeable improvement in BER performance. This result is one of the key novelties in the research.

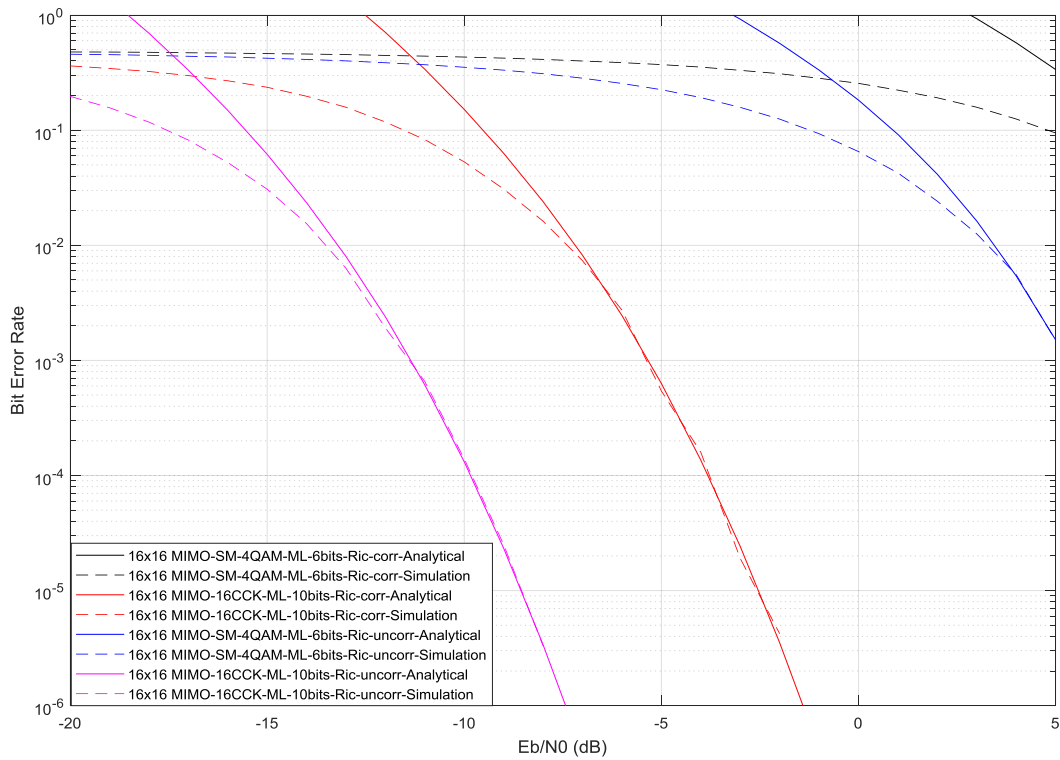


**Figure 4.36:** BER versus  $E_b/N_0$  for SCCK over uncorrelated Rician channel compared with SM, where  $m = 6, 10$  and  $N_t = N_r = 16$ . (Dashed line) Simulation, (solid line) Analytical

## 4.7 Summary

To conclude, it has been well proved that the conventional SCCK modulation is a promising system for various MIMO systems. This system is evaluated firstly with 4 phases to achieve better system capacity and better BER performance with wideband IEEE channel compared with the first application of this system in [9]. The result of applying the proposed SCCK system in a wireless IEEE wideband channel is discussed for different SCCK code word lengths, here 2, 4, 8 and 16-SCCK. A Rician channel with LOS path is also applied to expand the study in terms of different wireless channels and the results are discussed.

It has been noticed that the BER performance of the system in an IEEE wideband channel is obviously degraded in correlated channels and different detectors at high values of  $E_b/N_0$ , especially with large code sets such as 16-SCCK compared with uncorrelated IEEE channel. In future work testing this system with different wideband channels is recommended. The detection procedure is hypothesized that the combined effect of this ZF and MMSE detection, along with diversity gain accomplished through increasing the number of receive antennas can improve the BER in both schemes compared with small number of receive antennas. An important point about the proposed scheme is the noticeable improvements accomplished in the BER through increasing the number of receive antennas, which improve the BER performance by strengthening the desired signal components, in trade off with receiver complexity.

The exponential Kronecker correlation is applied to describe the system in more realistic scenarios. The correlation coefficient is chosen as  $c=0.5$  at both the transmit and receive antennas, and the results show that the system in case of the IEEE channel is obviously affected by correlation.

Keeping the same 4 phases in all modulation schemes, because of applying a QPSK modulation scheme for all codeword lengths, while still increasing the spectral efficiency as a result of increasing the number of transmit antennas, is one of the advantages of the proposed system in the case of transmitter complexity.

The outcomes of this chapter introduced a novel use of the union bound approximation in SCCK system. The chapter firstly characterizes the SCCK for different length codes. Then, the novel analytical BER performance of SCCK system was presented mathematically and compared to the results obtained by Monte Carlo simulation, which showed good agreement especially at high  $E_b/N_0$  range. At the end, a comparison of some of the key results in this chapter with the state of the art was made. This will be expanded in more detail in chapter 5.

# Chapter 5 System performance comparison of spatial CCK, SM and SMX

## 5.1 Chapter overview

In this chapter, the results of both SM and SMX MIMO systems for the narrowband channel as represented in reference [11, 97, 105], which is an upper bound closed form average bit error rate (ABER), are regenerated.

In [11, 97], which discussed spatial modulation (SM) systems over uncorrelated and correlated fading channels, and compared the framework with Monte Carlo simulations, the upper bound has three advantages:

- 1) gives an accurate estimation of the average BER;
- 2) gives upper bound closed form that is easy to calculate;
- 3) Suitable for uncorrelated and correlated, Rayleigh and Rician channels.

Moreover, the performance of SM was compared with that of the spatial multiplexing (SMX), where the SM offers better performance than SMX. The results of reference [97] are compared to the analytical and simulation results, which were presented in Chapter 4 for the proposed conventional spatial CCK system for a narrowband channel, with noticeable improvement in BER performance compared with both SM and SMX.

Finally, the SCCK system with wideband IEEE channel MIMO-OFDM system is compared with SM with some exemplar results, which were obtained by simulation only.

## 5.2 Introduction

In [11, 97, 105] the ABER performance of SM over different fading channels was studied analytically. References [8, 84, 106] present a study of the analytical average BER performance of SM over Rayleigh fading channels. In [106] an analytical upper bound of the system ABER was proposed but was complex. In [8] there is computation of the uncorrelated probability of transmit-antenna detection and in [11, 97, 105] an expression of pairwise error probability (PEP) of both SM and SMX with uncorrelated and correlated wireless channels is presented.

In all previous analyses, derivation of a closed-form expression of the PEP derivation needs the probability distribution function (PDF) of the signal to noise ratio ( $E_b/N_0$ ) at the receiver, considering the specific channel model.

Therefore, based on the literature, the contributions of the chapter include:

1. A general comparison of the PEP of SCCK in correlated/uncorrelated channels with SM and SMX as applied in [11, 97, 105] under the same channel and ML detection.
2. Comparison of SCCK with SM and SMX based on spectral efficiencies in narrowband fading channels by simulation and analysis.
3. Comparison of the simulation results for the BER of SCCK with MIMO OFDM over correlated and uncorrelated, Rayleigh and Rician wideband channel with SM-MIMO-OFDM system under the same channel conditions.

### **5.3 Spatial Multiplexing (SMX)**

SMX is described as a one of the most important MIMO techniques for increasing spectral efficiency [41].

The SMX modulation scheme can be summed up as:

- 1- The data bits to be transmitted are divided into a number of sub-streams, where the number of sub-streams is equal to the number of transmit antennas, and each one of these sub-streams consists of the data bits to be sent from each transmit antenna.
- 2- Each sub stream is modulated using any proposed modulation scheme, such as BPSK or QAM modulation.
- 3- The sub-streams are sent simultaneously from the transmit antennas. Because of this the SE increases linearly with the number of transmit antennas.

However, these advantages come in trade off with an increase in:

- 1- The inter channel interference (ICI), which results from transmitting from all antennas simultaneously, which requires computation by a complex receiver.
- 2- Due to the equality between the number of radio frequency (RF) chains and the number of transmit antennas, the hardware complexity increases with the antenna dimension.
- 3- Power consumption is high as a result of the linear increase in the power requirements with the added number of RF chains [107, 108].

Consequently, in modern wireless communication, SMX may not always be practically feasible, where energy efficiency is of fundamental concern. Modern solutions look for a trade-off between energy efficiency, spatial multiplexing gain, and computational complexity.

### 5.3.1 Maximum-Likelihood Receiver for SMX

The ML optimum detection receiver for SMX can be expressed as [11, 97, 105]

$$\hat{x}_t^{ML} = \underset{x \in Q^m}{\operatorname{argmin}} \{ \|y - Hx\|_F^2 \} \quad (5.1)$$

Where  $Q^m$  is a  $2^m$  space containing all possible transmitted vectors ( $Nt \times 1$ ),  $\|\cdot\|_F^2$  is the Frobenius norm, and  $\hat{\cdot}$  indicates the estimated spatial and constellation symbols.

## 5.4 Spatial Modulation

Spatial modulation is a transmission technology proposed for modern MIMO wireless systems, which aims to minimise the receiver complexity in trade off with spectral efficiency compared with SMX, while ICI is avoided [109]. As shown in Fig 5.1, this works as follows:

- i) A single active antenna sends a given data symbol (constellation symbol).
- ii) The spatial position of the active antenna is utilised as an additional dimension for data transmission, which acts as a spatial symbol based on the antenna index [8].

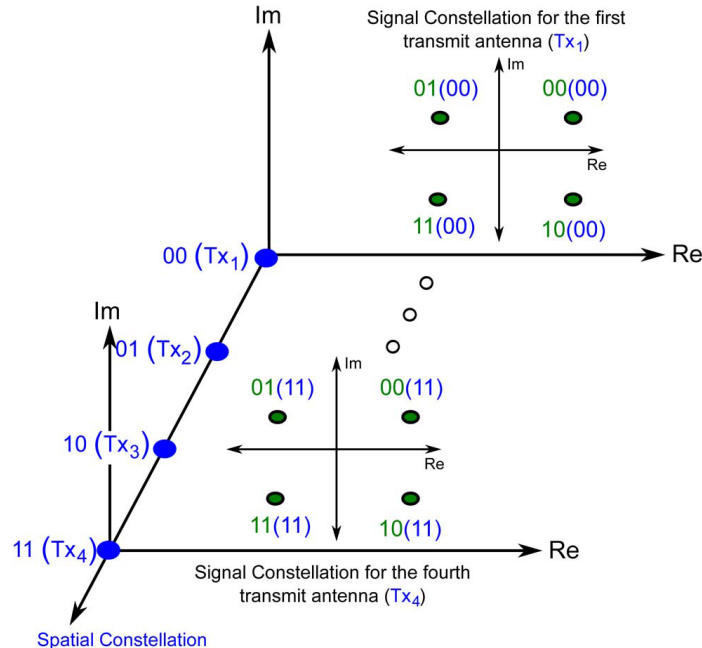


**Figure 5.1:** The SM unique three dimensional constellation diagram, where the second two bits from left to right identify the active antenna, which describes the spatial constellation. These are represented in parentheses. The signal constellation point that is to be transmitted is defined by the remaining two bit set [99]

### 5.4.1 SM Operating Principle

The SM modulation scheme can be summed up by [110]:

- 1- The transmit data bits are divided into blocks where each block contains  $\log_2(N_t) + \log_2(M)$  bits.  $N_t$  is defined as the number of transmit antennas, and  $M$  is defined as the constellation size.
- 2- The first  $\log_2(N_t)$  bits are utilised to choose the antenna, which is switched on for data transmission, whereas the other transmit antennas are kept inactive. In this chapter,  $\ell_t$  will represent the transmit antenna which is active for transmission for  $\ell_t \in \{1, 2, \dots, N_t\}$ .
- 3- The second  $\log_2(M)$  bits are used to select the symbol in the signal–constellation diagram. In this chapter, the actual complex symbol emitted by the transmit antenna  $\ell_t$  will be represented with  $s_t \in \{s_1, s_2, \dots, s_M\}$ .

### 5.4.2 Maximum–Likelihood Receiver for SM

In SM, at a given time, only one transmit antenna is active. Therefore, the optimal detector at the receiver can be presented as [11, 97, 105]:

$$\begin{aligned}
 \left[ \hat{\ell}_t^{(ML)}, \hat{s}_t^{(ML)} \right] &= \underset{\substack{\ell \in \{1, 2, \dots, N_t\} \\ s \in \{s_1, s_2, \dots, s_M\}}}{\text{argmin}} \left\{ \|y - \hat{h}_\ell s_t\|_F^2 \right\} \\
 &= \underset{\substack{\ell \in \{1, 2, \dots, N_t\} \\ s \in \{s_1, s_2, \dots, s_M\}}}{\text{argmin}} \left\{ \sum_{r=1}^{N_r} |y_r - \hat{h}_{\ell, r} s_t|^2 \right\} \tag{5.2}
 \end{aligned}$$

where  $y_r$  is the  $r$ -th entry of  $y$  receive antennas,  $\hat{h}_\ell$  represents the uncorrelated fading channel matrix,  $\hat{\ell}_t^{(ML)}$  is the estimated transmit antenna by ML detection, and  $\hat{s}_t^{(ML)}$  is the estimated transmitted symbol.

## **5.5 Analytical ABER performance of SM and SMX**

The ABER for MIMO systems using SM and SMX can be computed utilising the union bound technique, which can be represented and discussed in [11, 97, 104, 105]:

## **5.6 Results discussion**

This section compares analytical and simulation BER performance of SCCK with SM and SMX. The number of symbols that used to obtain this results is the same as chapter four which equals 2000000 symbol.

### **5.6.1 Analytical performance of SM, SMX**

In this section, Monte Carlo simulation results in [11, 97, 104, 105] for the ABER performance of SM and SMX are regenerated, and the performance in Rayleigh and Rician, uncorrelated and correlated channels are presented and compared with the derived analytical bound of SCCK.

The ABER simulation results are given for SM and SMX over uncorrelated and correlated, Rayleigh fading channel and Rician fading channels with a Rician K-factor of 3 dB, and correlation coefficient  $c = 0.5$  in both transmit and receive antennas. This is chosen as a moderate correlation, and is the same as with analytical results obtained from Chapter 4.

Analytical and simulated regenerated results of both SM and SMX demonstrate close match for different channel conditions and a wide pragmatic range of  $E_b/N_0$  values, which validates the derived analysis and comparison in this chapter.

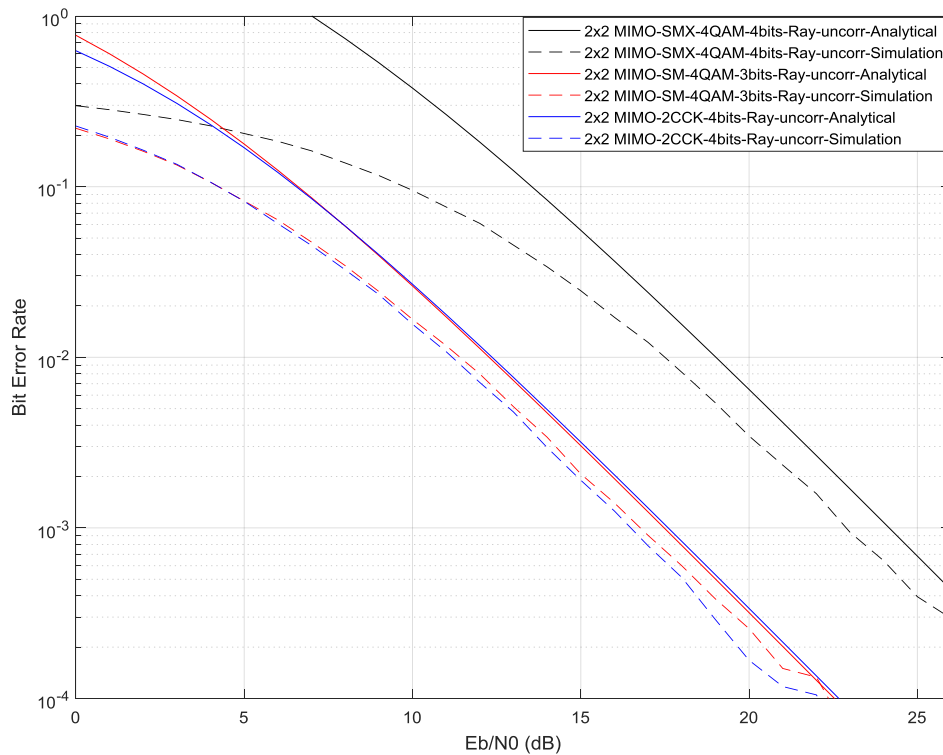
### **5.6.2 Comparing the ABER performance of SCCK, SM and SMX**

This section compares the ABER performance of SCCK with SM and SMX for  $N_t = 2, 4, 8$  and 16, over correlated and uncorrelated, Rayleigh and Rician channels, with similar parameters as discussed in Section 5.6.1.

### 5.6.2.1 Rayleigh Fading channel

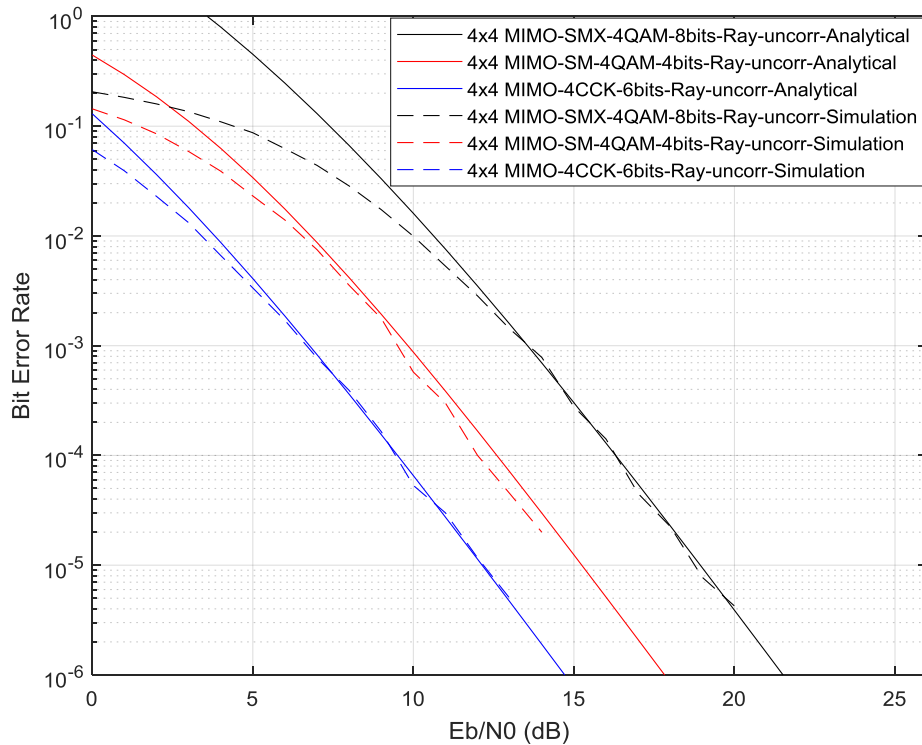
In Figs. 5.2-5.10 the ABER Vs EbNo for SCCK, SMX and SM over correlated and uncorrelated Rayleigh channels are presented, with spectral efficiency as a parameter. The dependence on the number of transmit antennas and the constellation size for ABER performance can be seen.

For the same constellation size, which is four phases, the performance of the proposed conventional SCCK with 4 bits in Fig 5.2 is better than the SMX with the same spectral efficiency by approximately 7 dB. Another result is that SCCK and SM offer approximately the same BER performance when utilising the same constellation size but with spectral efficiency  $m=4$  bit/s/Hz for SCCK, compared with  $m= 3$  bit/s/Hz for SM. The main point of this comparison is to present the performance with same number of phases and transmit and receive antennas, which results in different spectral efficiencies for each of the three techniques, as discussed previously. The results show that SCCK performs better than both SM and SMX in terms of BER performance and better than SM in terms of spectral efficiency with the same modulation order.



**Figure 5.2:** BER versus Eb/No for SMX and SM and SCCK over uncorrelated Rayleigh channel, where  $m = 4, 3, 4$  respectively and  $N_t = N_r = 2$ . (Dashed line) Simulation, (solid line) Analytical

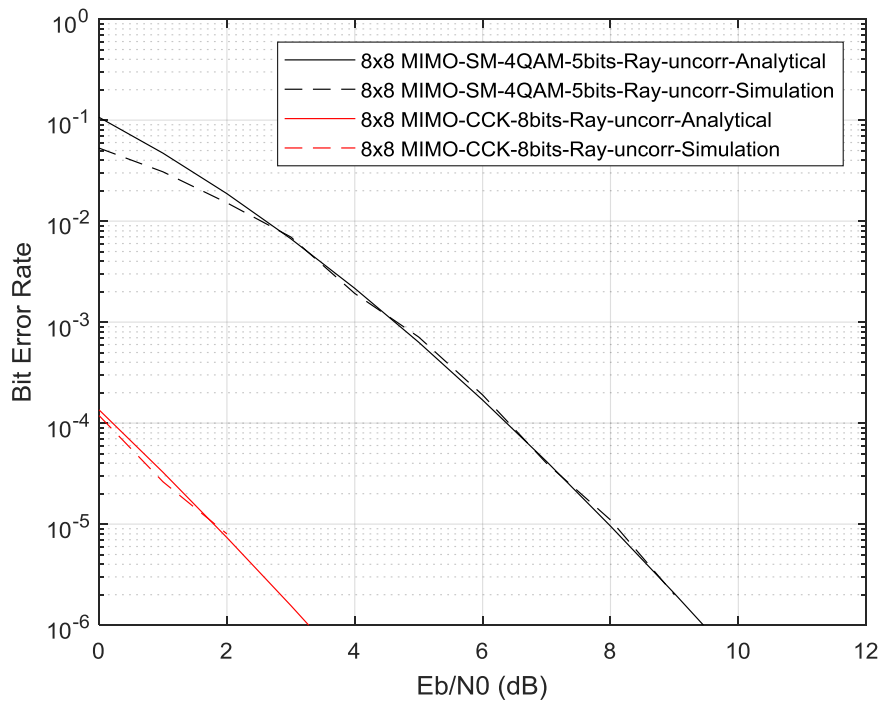
With the same constant constellation size as in Fig 5.2, Fig 5.3 presents a comparison between SMX, SM and SCCK with 4 transmit and receive antennas with different spectral efficiencies. The results confirm that the BER performance of SCCK outperforms both SM and SMX, with lower spectral efficiency than SMX, but greater spectral efficiency than SM. There is nearly 8 dB SNR gain for SCCK compared with SMX, and about 4 dB SNR gain compared to SM.



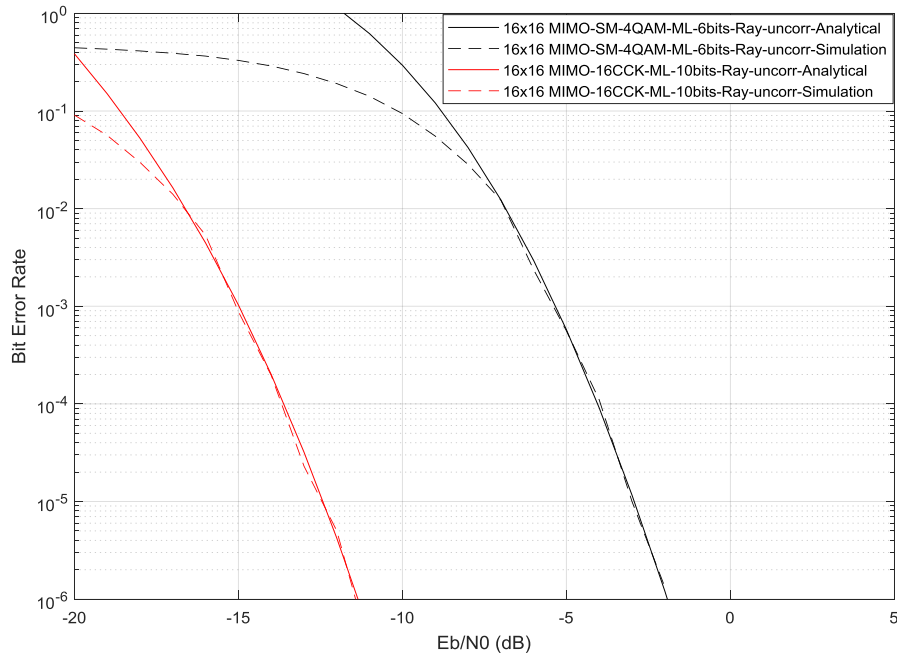
**Figure 5.3:** BER versus  $E_b/N_0$  for SMX and SM and SCCK over uncorrelated Rayleigh channel, where  $m= 8, 4, 6$  respectively and  $N_t=N_r = 4$ , (Dashed line) Simulation, (solid line) Analytical

Fig 5.4 shows the results of SCCK and SM with 8 transmit and receive antennas, and again applying the same 4-phase modulation order. The BER performance of SCCK outperforms SM in both spectral efficiency and BER performance, with about 7 dB SNR gain.

In the case of 16 SCCK codeword length, i.e. 16 transmit and receive antennas with a spectral efficiency of 10 bit/s/Hz, and in a Rayleigh uncorrelated channel, the system BER performance is increased dramatically compared with 2, 4 and 8-SCCK. This is shown in Fig 5.5, where it is demonstrated that the system can work effectively with using low signal power, and the SNR improvement will reach approximately 10 dB compared with SM, which has 6 bit/s/Hz spectral efficiency.



**Figure 5.4:** BER versus  $E_b/N_0$  SM and SCCK over uncorrelated Rayleigh channel, where  $m=5, 8$  respectively and  $N_t=N_r=8$ . (Dashed line) Simulation, (solid line) Analytical



**Figure 5.5:** BER versus  $E_b/N_0$  SM and SCCK over uncorrelated Rayleigh channel, where  $m=6, 10$  respectively and  $N_t = N_r = 16$ . (Dashed line) Simulation, (solid line) Analytical

Comparing results for uncorrelated channels with correlated channels, SCCK is more robust to channel correlation than SM. For the uncorrelated case, SM with  $N_t = 2$  offers nearly the same performance as SCCK with  $N_t = 2$ . However, for the correlated case SCCK offers 5 dB better performance than SM as shown in Fig 5.6.

Fig 5.7 presents the same comparison as Fig 5.6 between SCCK and SM with 4 transmit and receive antennas for a correlated channel, where the proposed SCCK outperforms the SM by approximately 5 dB.

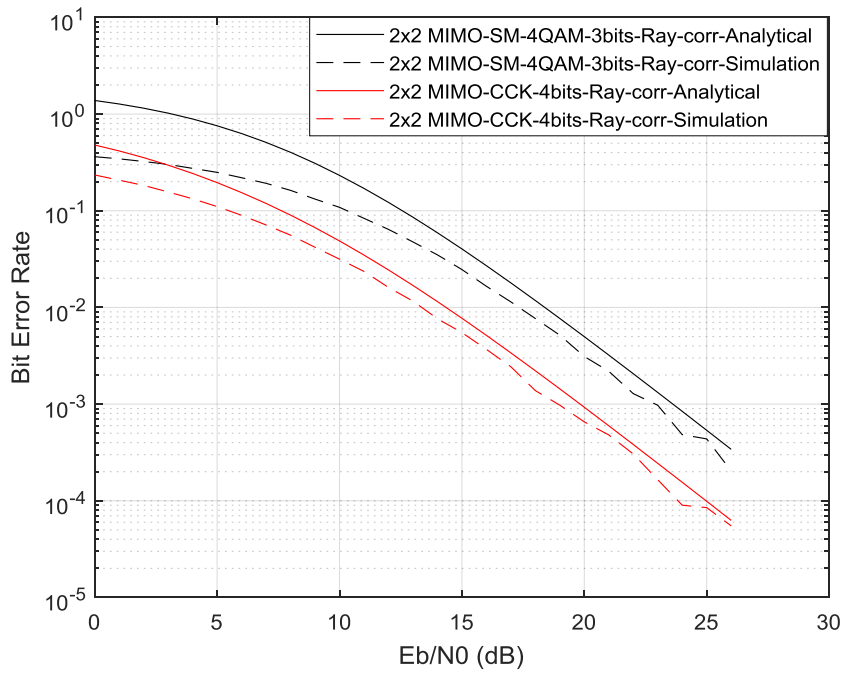


**Figure 5.6:** BER versus  $E_b/N_0$  for SM and SCCK over correlated Rayleigh channel, where  $m=3, 4$  respectively and  $N_t=N_r=2$ . (Dashed line) Simulation, (solid line) Analytical

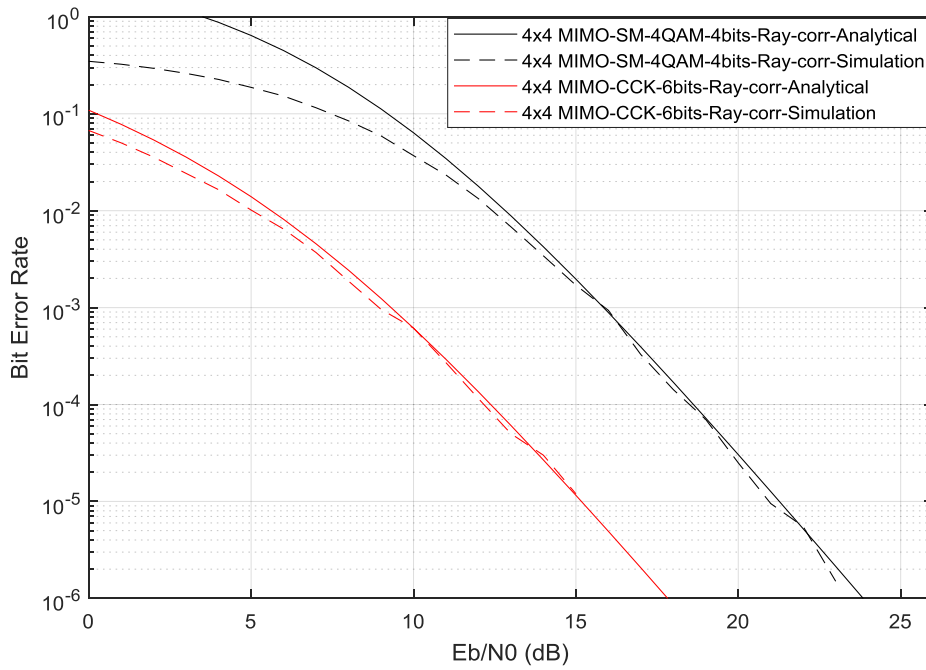


**Figure 5.7:** BER versus  $E_b/N_0$  for SM and SCCK over correlated Rayleigh channel, where  $m=4, 6$  respectively and  $N_t=N_r=4$ . (Dashed line) Simulation, (solid line) Analytical

A SCCK system with 8 transmit receive and antenna will keep the same BER improvement compared with SM in Rayleigh correlated channel as showed in Fig 5.8. For instance at a BER of  $10^{-4}$  the  $E_b/N_0$  is approximately 6 dB in SCCK system compared with 12.5 dB in SM system, which means system improvement in both spectral efficiency and BER performance in both uncorrelated and correlated channels.

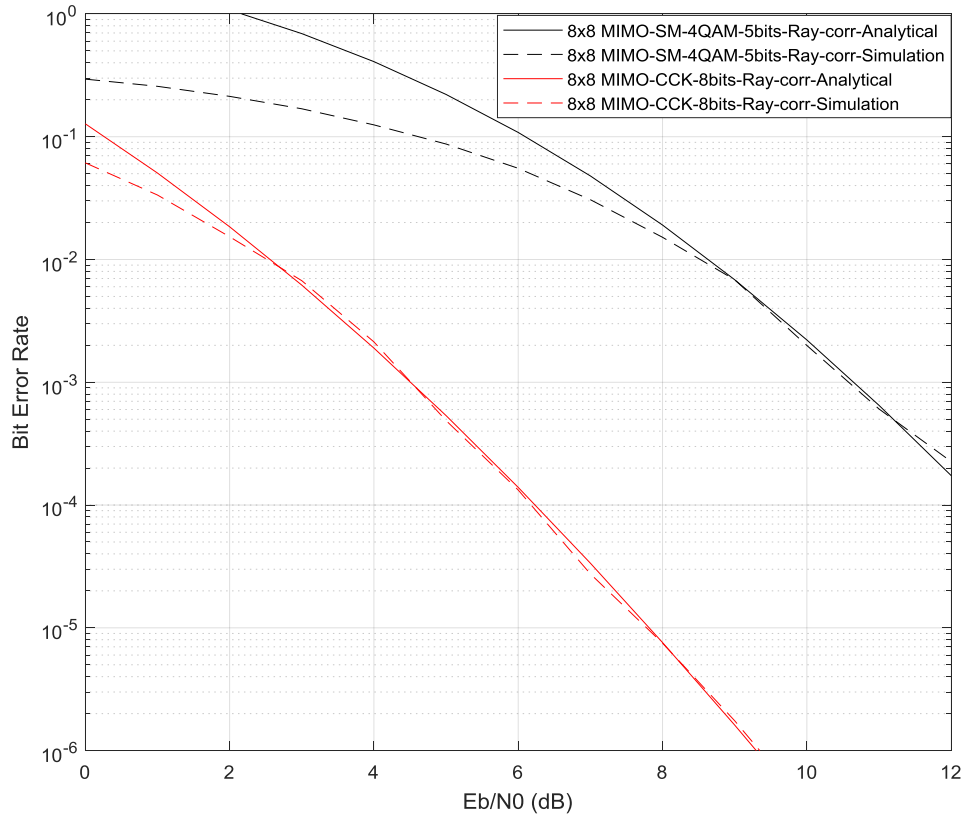


**Figure 5.8:** BER versus  $E_b/N_0$  SM and SCCK over correlated Rayleigh channel, where  $m=5, 8$  respectively and  $N_t = N_r = 8$ . (Dashed line) Simulation, (solid line) Analytical

Fig 5.9 shows the same trend as Fig 5.8 except using 16-SCCK, and this results in 10 bit/s/Hz spectral efficiency. The system improvement is still clear compared with SM in terms of spectral efficiency and BER performance.

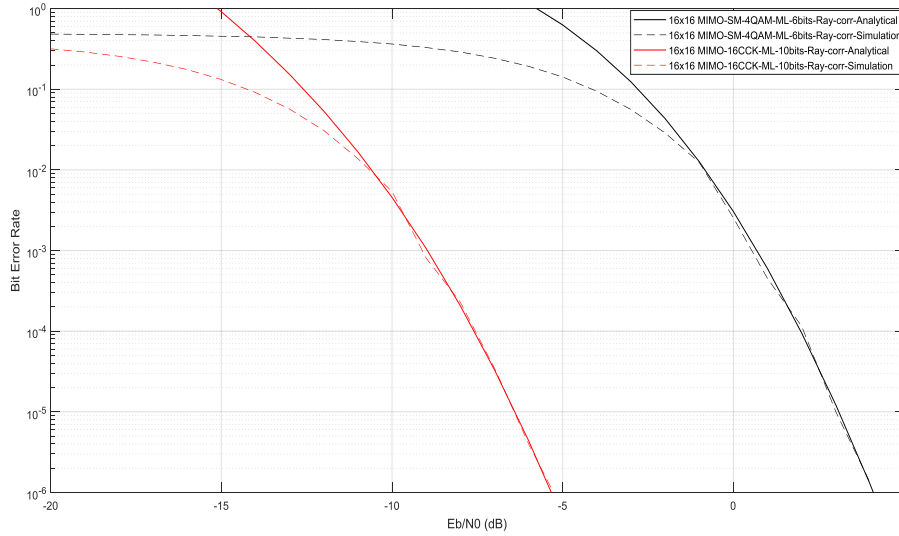


**Figure 5.9:** BER versus  $E_b/N_0$  SM and SCCK over correlated Rayleigh channel, where  $m=6, 10$  respectively and  $N_t=N_r=16$ . (Dashed line) Simulation, (solid line) Analytical

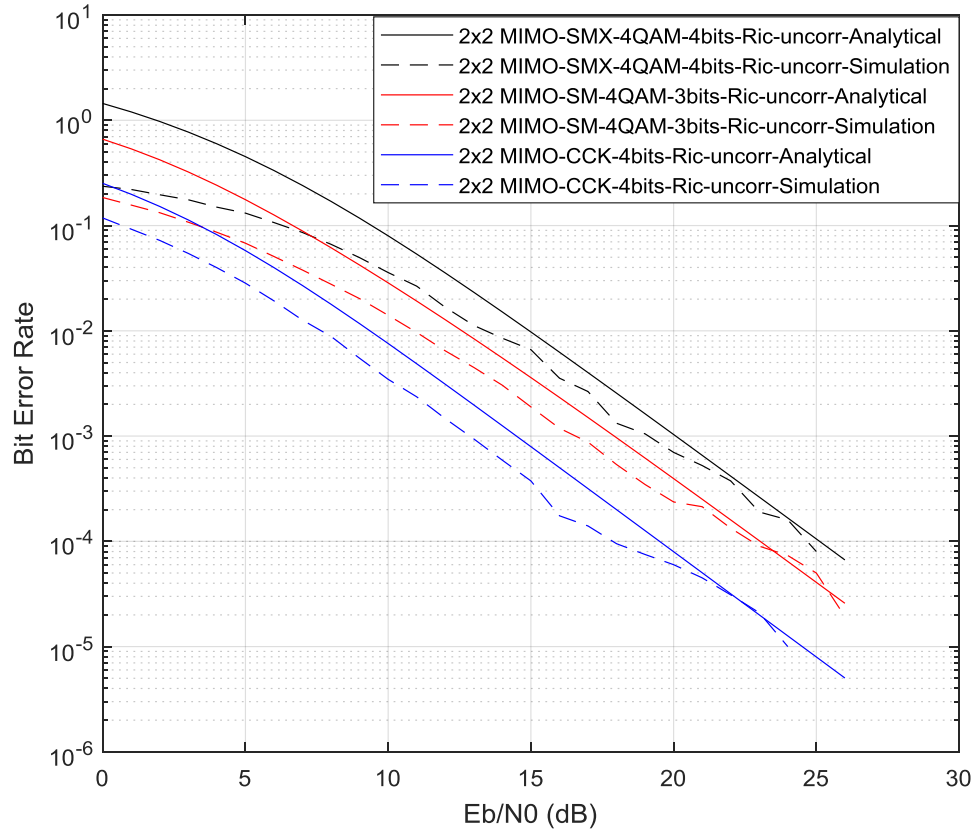
### 5.6.2.2 Rician Fading channel

BER performance comparison of SCCK with SM and SMX over correlated and uncorrelated Rician channels are presented in Fig. 5.10 in the case of 4bit/s/Hz spectral efficiency for SMX and SCCK, and 3 bit/s/Hz for SM. For the uncorrelated case, the same results trend as in an uncorrelated Rayleigh channel is obtained, where SCCK with  $N_t=2$  outperforms both SMX and SM with  $N_t=2$ .

The Rician K factor is applied as 3 dB as a result of the study [110], which estimates the values of the K-factor for most of the segmented tracks in the urban area are below 3dB. We choose the maximum value in this case and leave the other areas to future study.

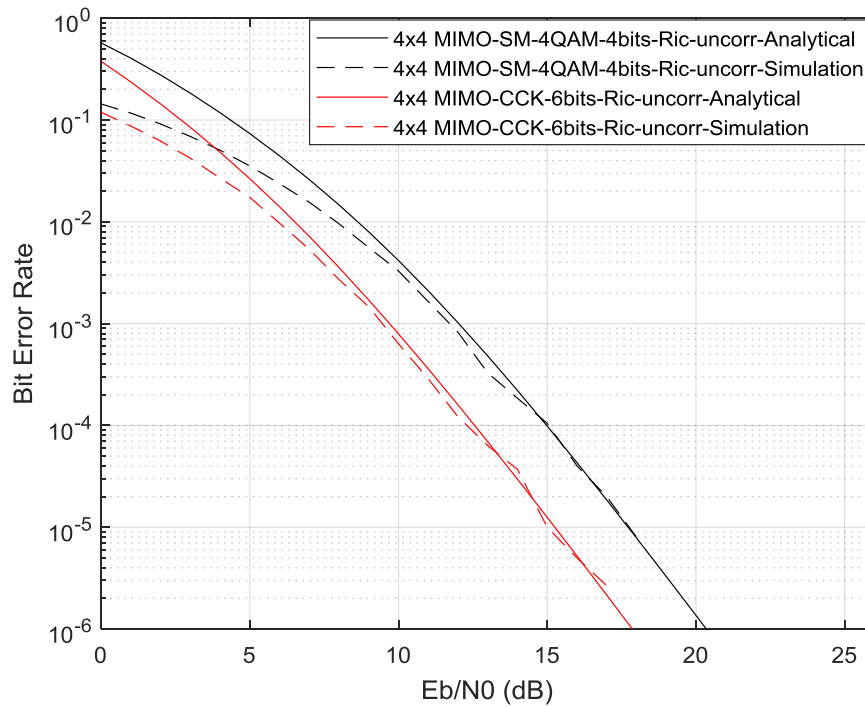
Fig 5.10 presents the improvement of BER performance by applying the LOS Rician channel in case of SCCK with codeword length 2, compared with a SM system with same modulation order and  $N_t=N_r=2$  in all cases, which is affected by the LOS in the Rician channel which decreases

the BER performance. SCCK keeps the BER performance improvement compared with SM and SMX system in Rician channels.



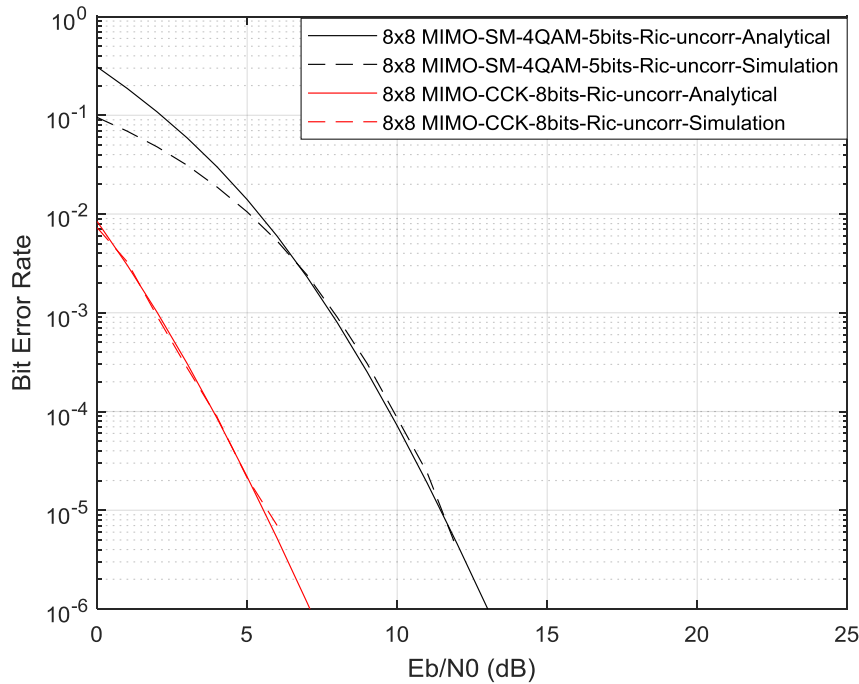
**Figure 5.10:** BER versus  $E_b/N_0$  for SMX and SM and SCCK over uncorrelated Rician channel, where  $m = 4, 3, 4$  respectively and  $N_t = N_r = 2$  and  $K=3$ dB. (Dashed line) Simulation, (solid line) Analytical

Fig 5.11 presents a comparison between SM and SCCK for 4 transmit and receive antennas with different spectral efficiencies in an uncorrelated Rician channel, and the results confirm that the BER performance of SCCK outperforms SM, with greater spectral efficiency than SM.



**Figure 5.11:** BER versus  $E_b/N_0$  for SM and SCCK over uncorrelated Rician channel, where  $m=4, 6$  respectively and  $N_t=N_r=4$  and  $K=3$ dB. (Dashed line) Simulation, (solid line) Analytical

A SCCK system with 8 transmit and receive antennas will increase the BER improvement dramatically compared with SM as showed in Fig 5.12. For instance, at  $10^{-4}$  BER the  $E_b/N_0$  is approximately 4dB in the SCCK system compared with 10 dB in the SM system, which means system improvement of 6 dB in BER performance in uncorrelated Rician channels. SCCK also has greater spectral efficiency here than SM.



**Figure 5.12:** BER versus  $E_b/N_0$  for SM and SCCK over uncorrelated Rician channel, where  $m = 5, 8$  respectively and  $N_t = N_r = 8$  and  $K=3$ dB. (Dashed line) Simulation, (solid line) Analytical

In the case of correlated channels, Fig. 5.13 shows the BER performance of SCCK with codeword length 2 compared with SM under the same number of transmit and receive antennas and the same constellation order under the same Rician channel conditions, where the Rician  $K$ -factor = 3 dB and the correlation coefficient in both transmit and receive antennas is  $c=0.5$ .

However, the system improvement of SCCK compared with SM is maintained, which confirms that SCCK improves on SM for the same number of phases and transmit and receive antennas. In addition, for the correlated Rician case SCCKM performs nearly 3 dB better than SM. Also, SCCK with  $N_t = 4$  outperforms SM with  $N_t = 4$  for the same correlated case by approximately 2.5dB, as shown in Fig 5.15.

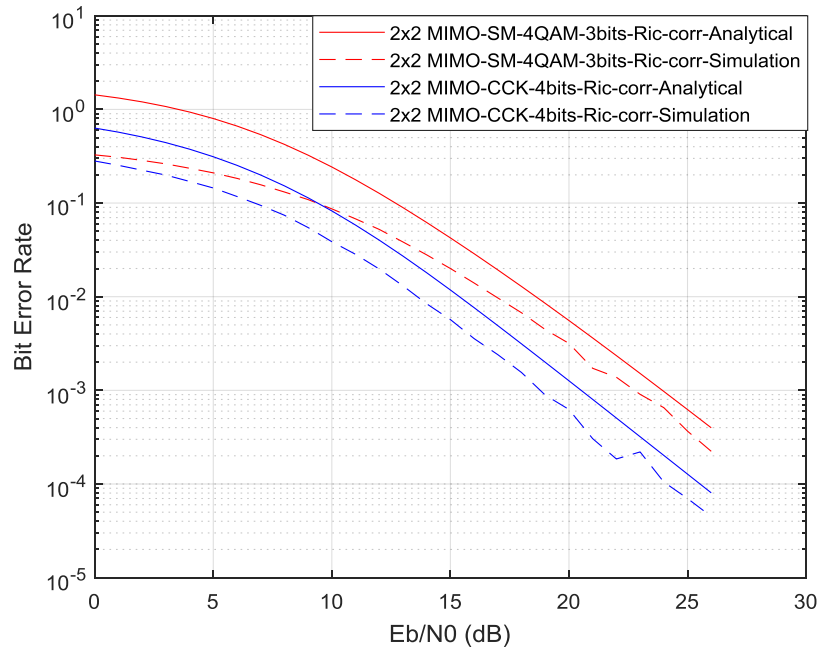


**Figure 5.13:** BER versus  $E_b/N_0$  for SM and SCCK over correlated Rician channel, where  $m = 4$  and  $N_t = N_r = 2$  and  $K=3$ dB. (Dashed line) Simulation, (solid line) Analytical

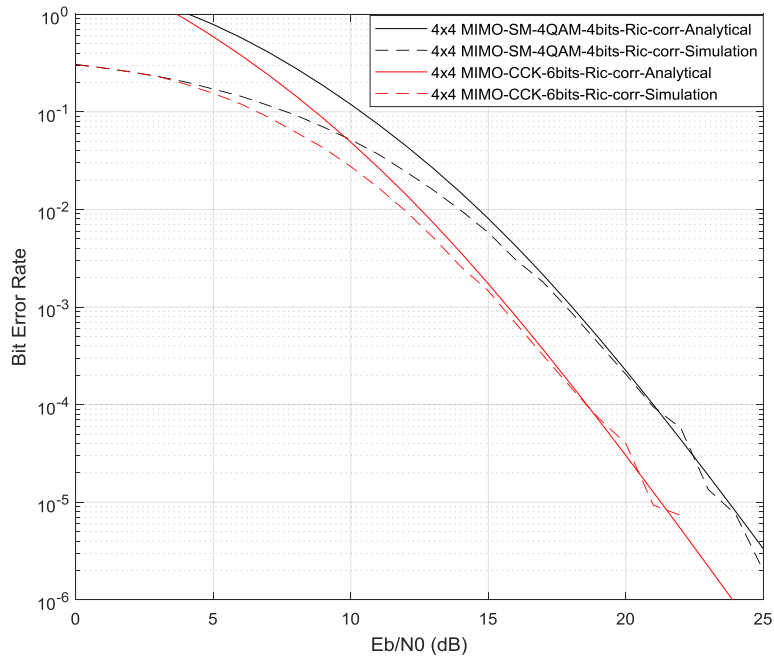


**Figure 5.14:** BER versus  $E_b/N_0$  for SM and SCCK over correlated Rician channel, where  $m = 4, 6$  respectively and  $N_t = N_r = 4$  and  $K=3$ dB. (Dashed line) Simulation, (solid line) Analytical

Figure 5.15 presents the comparison between SM and SCCK for 8 transmit and receive antennas. The results show the BER performance of SCCK with 8 bit/s/Hz spectral efficiency is better than SM with 8 transmit and receive antennas by approximately 6 dB. The high spectral efficiency of 8-SCCK, which is 8 bit/s/Hz, should also be noted, compared with SM with 5 bit/s/Hz spectral efficiency.

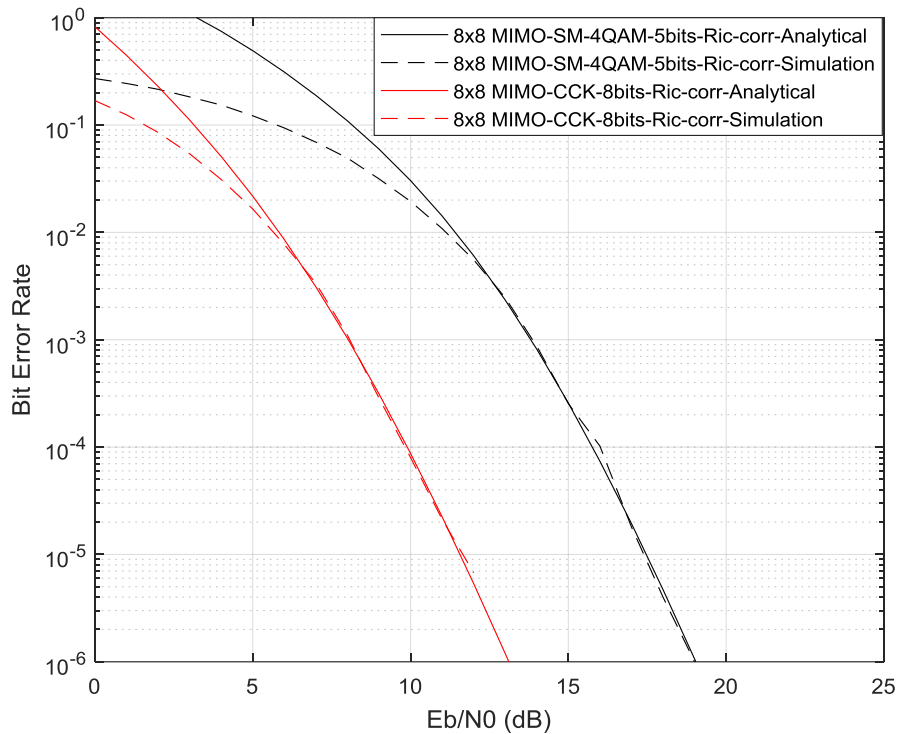


**Figure 5.15:** BER versus  $E_b/N_0$  for SM and SCCK over correlated Rician channel, where  $m = 5, 8$  respectively and  $N_t = N_r = 8$  and  $K=3$ dB. (Dashed line) Simulation, (solid line) Analytical

### 5.6.3 Comparing exemplar results of CCK-SM MIMO-OFDM systems with different spectral efficiency results with Rayleigh wideband channel and different detection schemes

For the MIMO-OFDM system, which is discussed in Chapter 4, as shown in Fig 5.16, the BER of the proposed spatial CCK system design with the ML detector (blue curve) is lower than the red curve which represented SM based on the same detector, but with different spectral efficiency.

This conforms to the analytical results of SCCK in narrowband channels in terms of the improving of BER performance of SCCK compared with SM. The BER of the proposed design is also lower than the black curve of the SM with the maximum value (MV) detector, which is less complex than the ML detector of SCCK system. All of these results are justified by simulation only, with analytical results in wideband channels left to the future work.

As discussed in [8] the MV detector depends on taking the maximum value of the magnitude of the received signal, and take it as the signal from the active antenna as a result of the null in the other antennas. This detector is simpler than the others in this thesis, but decrease the BER performance.

As shown in Fig 5.17, based on the same design parameters, the BER of the proposed SCCK method with four phases is lower than the SM method with 16QAM. With the small number of modulation phases, which means low detection complexity, the  $E_b/N_0$  of the proposed design is around 9dB less than the counterpart at a BER of  $10^{-3}$ .

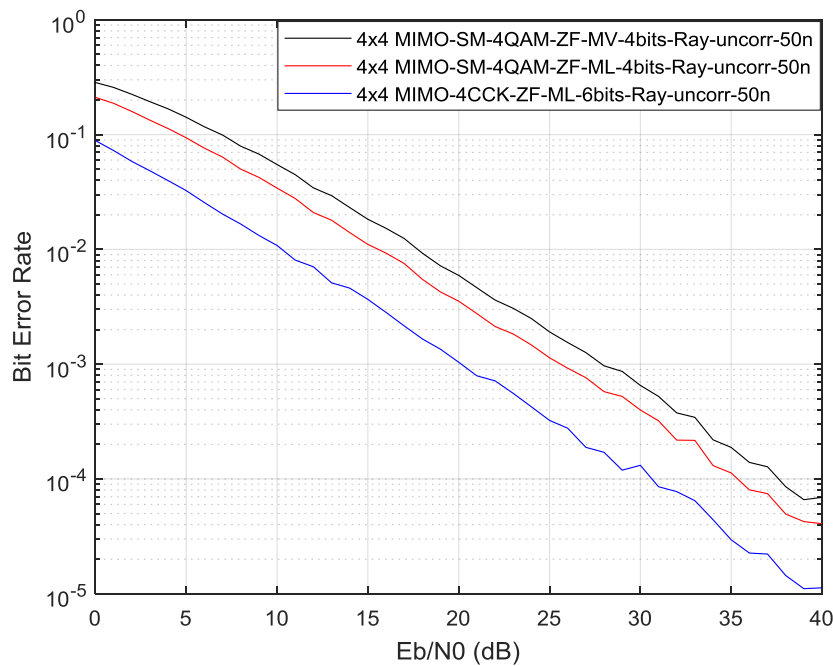


**Figure 5.16:** BER versus  $E_b/N_0$  for MIMO-OFDM-SM and MIMO-OFDM-SCCK over uncorrelated IEEE channel, where  $m = 4, 6$  respectively and  $N_t = N_r = 4$  and different detection scheme for SM with same modulation order

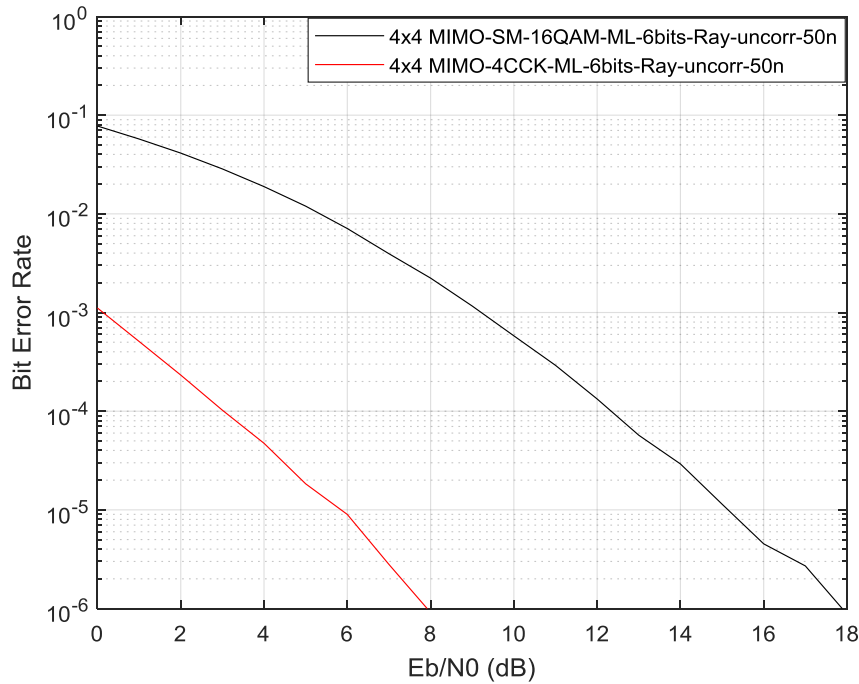
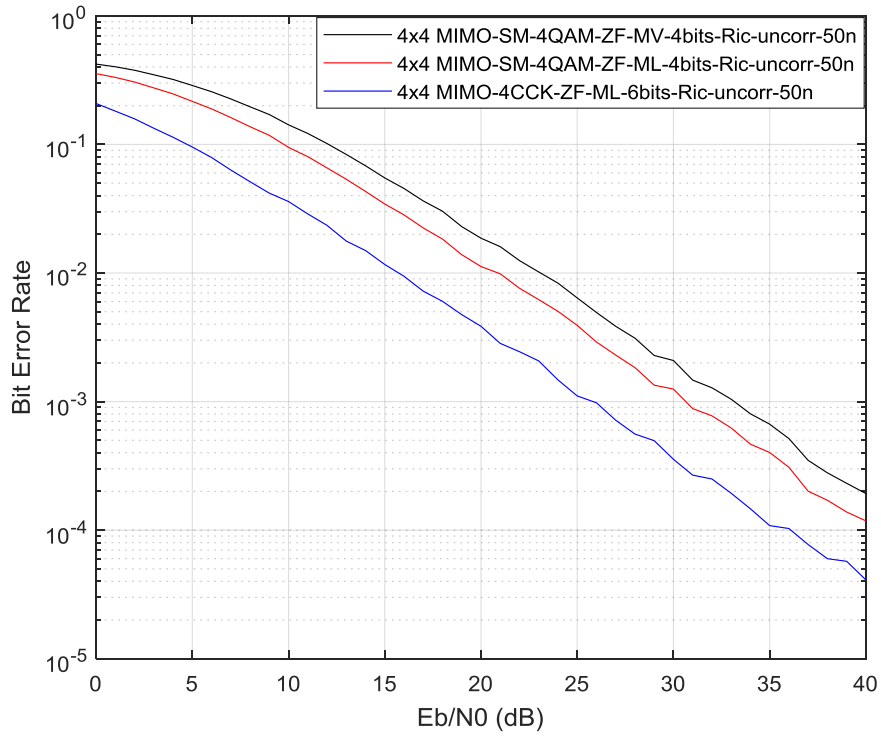


**Figure 5.17:** BER versus EbNo for MIMO-OFDM-SM and MIMO-OFDM-SCCK over uncorrelated IEEE channel, where  $m = 6$  and  $N_t = N_r = 4$  with different modulation order

Comparing Rayleigh fading results, Fig. 5.17, with Rician fading results, Fig. 5.18, obviously highlights the negative effect of the LOS component of Rician channels. The system performance with Rayleigh outperforms the Rician channel, which can be explained as the degrees of freedom in Rayleigh fading can be beneficial, while in the Rician channel the LOS component dominates, which negatively affects the system performance.

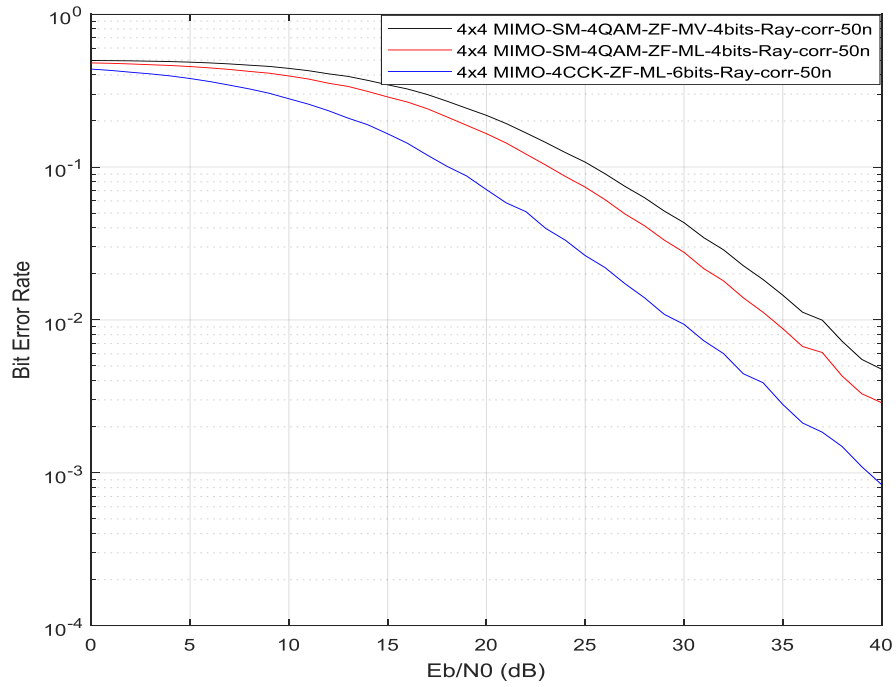
The existence of the LOS component increases the correlation between different wireless channel paths, and that leads to degradation in the BER performance of both SM and SCCK systems. This performance degradation of about 5 dB can be seen in the figures below. Similar degradation is noticed for correlated SCCK systems.

Moreover, the SCCK shown in the blue curve shows the lowest BER even with a higher spectral efficiency. For example, when the BER is  $10^{-3}$ , the blue line is approximately 5dB less than the red one and nearly 8dB lower than the black one, representing the effectiveness of the proposed design.



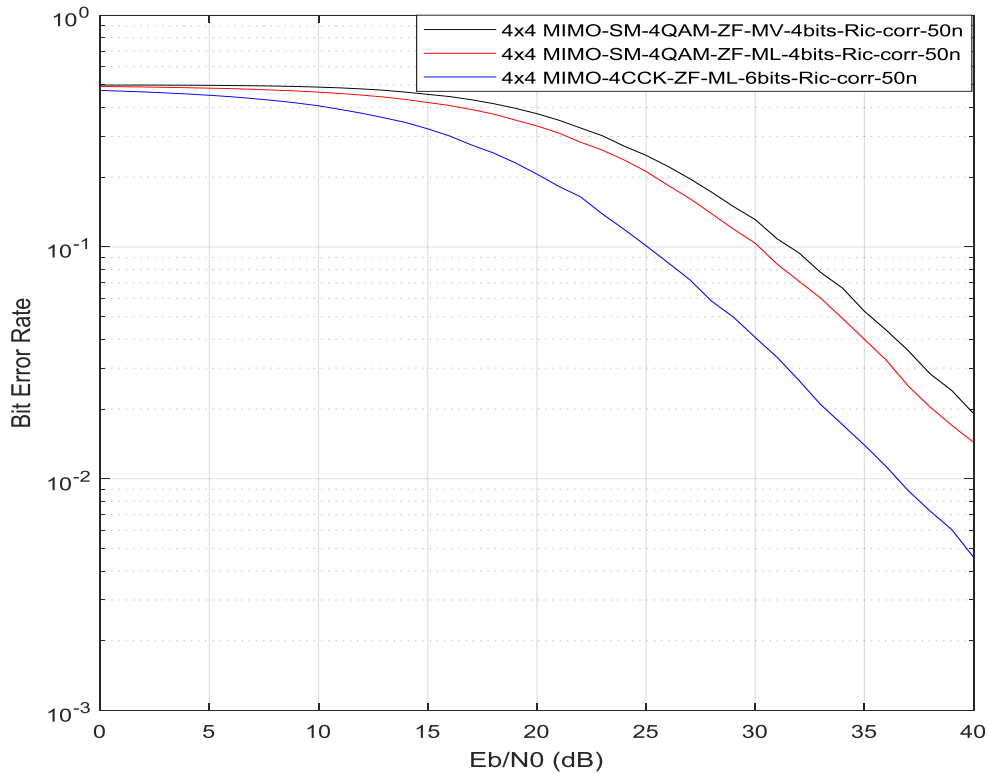
**Figure 5.18:** BER versus  $E_b/N_0$  for MIMO-OFDM-SM and MIMO-OFDM-SCCK over uncorrelated IEEE Rician channel, where  $m = 4, 4, 6$  respectively and  $N_t = N_r = 4$ , ZF detection scheme and  $K=3$ dB for SM with same modulation order

For correlated wideband channels as shown in Fig 5.19, based on an IEEE channel with  $c=0.5$  correlation factor for both transmit and receive sides, the BER displayed in red with the ML detector is lower than the counterpart in black which is for MV detector. Moreover, SCCK in blue shows the lowest BER even with a higher spectral efficiency. For example, when the BER is  $10^{-2}$ , the blue line is 4dB lower than the red one, and 6dB lower than the black one, representing the effectiveness of the proposed design.



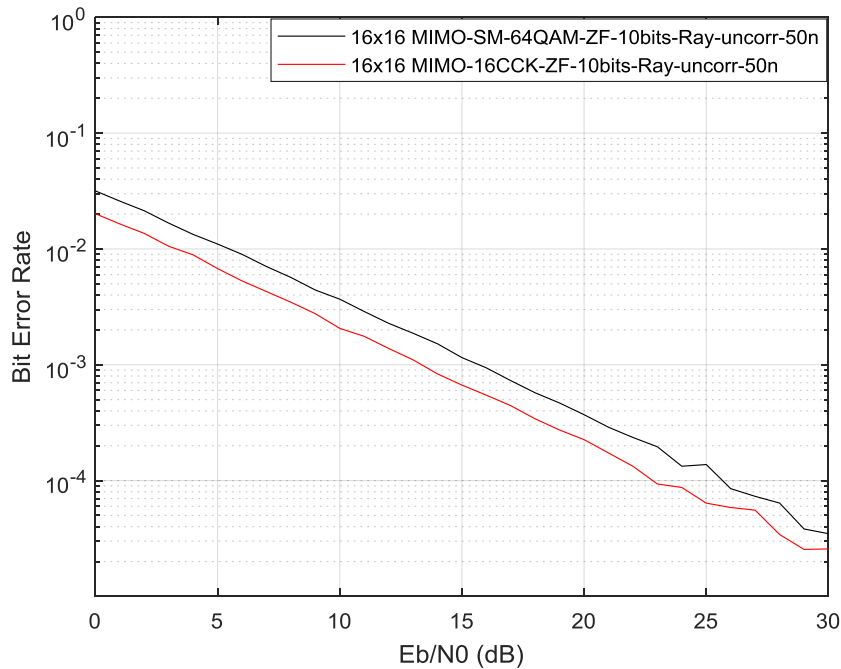
**Figure 5.19:** BER versus  $E_b/N_0$  for MIMO-OFDM-SM and MIMO-OFDM-SCCK over correlated IEEE channel, where  $m = 4, 6$  respectively and  $N_t = N_r = 4$  and ZF detection scheme for SM with same modulation order

Fig 5.20 plots BER Vs  $E_b/N_0$  for SM compared with SCCK for 4 and 6 bit/s/Hz spectral efficiencies respectively, in a correlated Rician channel ( $c=0.5$ ). At  $10^{-2}$  BER SCCK achieves a SNR gain of 4 dB over SM with ML detection, and 6 dB over SM with MV detection.



**Figure 5.20:** BER versus EbNo for MIMO-OFDM-SM and MIMO-OFDM-SCCK over correlated Rician IEEE channel, where  $m = 4, 4, 6$  respectively and  $N_t = N_r = 4$ , ZF detection scheme and  $K=3$ dB for SM with same modulation order

Fig 5.21 shows the BER Vs Eb/No comparing SM with SCCK for 10 bit/s/Hz spectral efficiencies, in an uncorrelated Rayleigh channel. At  $10^{-4}$  BER, SCCK achieves a SNR gain of approximately 3 dB over SM with ML detection, taking into account the different modulation order, which is 64 constellation points for SM to reach the same spectral efficiency as SCCK with the same number of both transmit and receive antennas, which is a key result.



**Figure 5.21:** BER versus EbNo for MIMO-OFDM-SM and MIMO-OFDM-SCCK over uncorrelated wideband Rayleigh channel, where  $m = 10$  and  $N_t = N_r = 16$  and ZF detection scheme with different modulation order

## 5.7 Summary

In this chapter, the BER performance of the novel, simple and analytical upper bound of proposed SCCK system, which was discussed in Chapter 4, is compared with regenerated analytical and simulated results of SM and SMX [11, 97, 104, 105].

The comparison between SMX, SM and SCCK over Rayleigh fading and Rician fading channels has been carried out. These results shown that SCCK system provides noticeably better performance than SM and SMX for similar or higher spectral efficiencies.

Another confirmed outcome of this chapter is the higher spectral efficiency of the proposed SCCK system compared with SM for the same phase constellation order, giving a noticeable improvement in BER performance.

Moreover, evaluating and investigating the performance of SCCK to achieve better system capacity and better BER performance with wideband IEEE channel is carried out. The result of applying the proposed SCCK system in wireless IEEE wideband channel shows the trend of the BER performance improvement of SCCK system compared with a MIMO-OFDM-SM system under the same conditions.

## Chapter 6 Modified spatial complementary code keying

### 6.1 Chapter Overview

The purpose of this chapter is to reproduce the modified spatial complementary code keying as discussed in [9]. The key point of the proposed system discussed in reference [9] is to exploit the properties of the SCCK codewords in the spatial domain. In this system CCK codewords of various lengths (2, 4 and 8) are generated using non-conventional input phases, and are used in SCCK modulation. These are applied in a MIMO-OFDM system with an IEEE fading channel, and the BER performance results are discussed. Because of the non-conventional phases used to generate the SCCK codewords, the name modified SCCK system is chosen for this system. Modified SCCK depends on choosing specific phases that generate codewords with the large Euclidian distance property that improves the BER performance of the system. On the other hand, the enhancement of the BER performance comes at the cost of decreasing the spectral efficiency. These non-conventional phases are described in reference [9] as a standard SCCK, which is not precise, as discussed previously in Chapter 4. The number of these non-conventional phases increases in parallel with the increasing SCCK codeword length. For example, for 2-SCCK there are 2 phases, for 4-SCCK there are 3-phases and for 8-SCCK there are 4-phases. Extending this, for 16-SCCK there are 5-phases, and this case is discussed and evaluated in this chapter.

In this chapter a modified SCCK system with codeword lengths 2, 4 and 8, using the same MIMO-OFDM system discussed in [9] and an IEEE fading channel, is discussed. In addition, the SCCK with length 16 codeword is investigated in terms of BER performance and with different detectors, here ZF, MMSE and ML.

As in Chapters 4 and 5 the Kronecker exponential model is used in both transmit and receive antennas to evaluate the proposed SCCK system in more realistic scenarios.

The main contribution in this chapter is a mathematical analytical model of the modified SCCK system in narrowband channels with a ML detector. Also, simulation results are compared with conventional SCCK results, discussed in Chapter 4.

## 6.2 Modified spatial Complementary Code Keying Modulation system

The same system will be applied as in Chapter 4, with all the same conditions except the SCCK codeword generation, which will be with non-conventional phases.

### 6.2.1 2-bit/s/Hz Modified Spatial Complementary Code Keying with codeword length 2-Chip.

As discussed in [9], in a 2 bit/s/Hz spectral efficiency modified SCCK system uses codewords of length of 2, and so uses only 2 transmit antennas. To enable a codeword set with symmetry, there is a selection of two phases as  $\{0, \pi\}$  which produces four SCCK codewords, which represent 2 bits, previously discussed in Chapters 2 and 3.

### 6.2.2 4-bit/s/Hz Modified Spatial Complementary Code Keying with code word length 4-Chip

In contrast to modified 2-SCCK where two phases were engaged in codeword computation, the case of modified SCCK with codewords of length 4 only deals with 3 phases, which makes it more challenging than the straightforward case of codeword length 2. The extended Euler equation for 4-bit SCCK codeword is presented in equation (6.2).

$$M_4 = \begin{bmatrix} \phi_1 & \phi_1 & \phi_1 & \phi_1 \\ \phi_2 & 0 & \phi_2 & 0 \\ \phi_3 & \phi_3 & 0 & 0 \end{bmatrix} \quad (6.1)$$

$$C_4 = \{e^{j(\phi_1+\phi_2+\phi_3)}, e^{j(\phi_1+\phi_3)}, e^{j(\phi_1+\phi_2)}, -e^{j(\phi_1)}\} \quad (6.2)$$

Where  $M_4$  defines the Hadamard matrix of the SCCK case with length four and  $C_4$  is the equation generated by the CCK codewords with length 4.

The use of the typical modulation mechanism has been limited by applying the three phases. To maintain the symmetry property of the modulation, the three phases will be selected as  $(0, \frac{2\pi}{3}, \frac{4\pi}{3})$ . It is demonstrated that in the case of three phases there is the possibility of having 27 combinations. As shown in Fig 6.1, to have 27 combinations refers to having 27 4-chip SCCK codewords calculated based on equations (6.1) and (6.2). It is crucial to select a subset, which consists of 16 input codewords, from the 27 codewords to maintain the one to one relation among all 16 inputs to get 4 bit/s/Hz spectral efficiency. The purpose is to choose the most suitable subset comprising 16 codewords.

1	1	1	-1
$1-0i$	$-0.5-0.866i$	$-0.5+0.866i$	-1
$1-0i$	$-0.5+0.866i$	$-0.5-0.866i$	-1
$-0.5+0.866i$	$-0.5+0.866i$	1	-1
$-0.5-0.866i$	$-0.5-0.866i$	1	-1
$-0.5+0.866i$	1	$-0.5+0.866i$	-1
$-0.5-0.866i$	1	$-0.5-0.866i$	-1
$-0.5-0.866i$	$-0.5+0.866i$	$-0.5+0.866i$	-1
$-0.5+0.866i$	$-0.5-0.866i$	$-0.5-0.866i$	-1
1	$-0.5-0.866i$	$-0.5-0.866i$	$0.5-0.866i$
1	1	$-0.5+0.866i$	$0.5-0.866i$
1	$-0.5+0.866i$	1	$0.5-0.866i$
$-0.5+0.866i$	1	$-0.5-0.866i$	$0.5-0.866i$
$-0.5+0.866i$	$-0.5-0.866i$	1	$0.5-0.866i$
$-0.5-0.866i$	$-0.5+0.866i$	$-0.5-0.866i$	$0.5-0.866i$
$-0.5-0.866i$	$-0.5-0.866i$	$-0.5+0.866i$	$0.5-0.866i$
$-0.5+0.866i$	$-0.5+0.866i$	$-0.5+0.866i$	$0.5-0.866i$
$-0.5-0.866i$	1	1	$0.5-0.866i$
1	$-0.5+0.866i$	$-0.5+0.866i$	$0.5+0.866i$
1	1	$-0.5-0.866i$	$0.5+0.866i$
1	$-0.5-0.866i$	1	$0.5+0.866i$
$-0.5+0.866i$	$-0.5-0.866i$	$-0.5+0.866i$	$0.5+0.866i$
$-0.5-0.866i$	1	$-0.5+0.866i$	$0.5+0.866i$
$-0.5+0.866i$	$-0.5+0.866i$	$-0.5-0.866i$	$0.5+0.866i$
$-0.5-0.866i$	$-0.5+0.866i$	1	$0.5+0.866i$
$-0.5+0.866i$	1	1	$0.5+0.866i$
$-0.5-0.866i$	$-0.5-0.866i$	$-0.510.866i$	$0.5+0.866i$

**Figure 6.1:** Matrix shows all possible 4-bit/s/Hz spectral efficiency for modified SCCK with code word length 4 [7]

As discussed in [6] there can be a random selection of the 16 codewords out of 27 possible codewords. There would be calculations for four dimensional complex Euclidean distances among all potential pairs as presented in Fig 6.2. There could be another random selection for another 16 codewords. This will follow the same procedure to achieve the minimum Euclidean distance for the current subset. The comparison is made between two components and the component with a smaller value is removed. This strategy is re-used many times since each will result in a selection of a new subset. Then, after deriving the minimum Euclidean distance, the comparison will be applied to them. The sub-optimal subset is selected to maximize the minimum Euclidean distance. This subset presents the SCCK of length 4 chip [9].

$$\begin{bmatrix}
 1 & 1 & 1 & -1 \\
 1-0i & -0.5+0.866i & -0.5-0.866i & -1 \\
 -0.5+0.866i & -0.5+0.866i & 1 & -1 \\
 -0.5-0.866i & -0.5-0.866i & 1 & -1 \\
 -0.5-0.866i & 1 & -0.5-0.866i & -1 \\
 -0.5-0.866i & -0.5+0.866i & -0.5+0.866i & -1 \\
 -0.5+0.866i & -0.5-0.866i & -0.5-0.866i & -1 \\
 1 & -0.5-0.866i & -0.5-0.866i & 0.5-0.866i \\
 1 & 1 & -0.5+0.866i & 0.5-0.866i \\
 -0.5+0.866i & 1 & -0.5-0.866i & 0.5-0.866i \\
 -0.5-0.866i & -0.5+0.866i & -0.5-0.866i & 0.5-0.866i \\
 -0.5+0.866i & -0.5+0.866i & -0.5+0.866i & 0.5-0.866i \\
 1 & -0.5-0.866i & 1 & 0.5+0.866i \\
 -0.5+0.866i & -0.5-0.866i & -0.5+0.866i & 0.5+0.866i \\
 -0.5-0.866i & 1 & -0.5+0.866i & 0.5+0.866i \\
 -0.5+0.866i & 1 & 1 & 0.5+0.866i
 \end{bmatrix}$$

**Figure 6.2:** Matrix showing the selected 4-bit/s/Hz spectral efficiency for modified SCCK subset [7]

It was noticed that the performance of a size 16 subset of codeword is related to maximizing the minimum Euclidean distance. It has the potential to have further expansion by sorting the codewords according to the specified criterion and the number of minimum Euclidean distances. It has been calculated as 2.445 and therefore the procedure can be made to work out the result of this minimum Euclidean distance. The 2.445 is the appropriate result that was selected.

### 6.2.3 8-bit/s/Hz Modified Spatial Complementary Code Keying with code word length 8-Chip

In the case of 8-SCCK with the same 4-phases of conventional SCCK, reviewed in Chapter 4 and mathematically [9] , previously discussed in Chapters 2 and 3.

### 6.2.4 11-bit/s/Hz Modified Spatial Complementary Code Keying with code word length 16-Chip

In 11-bit modified Spatial CCK, there is an approximate compatibility between this case and the case of SCCK using codewords of length 4. The SCCK with codeword length 16 offers 11 bit/s/Hz by selecting five phases as  $(0, \frac{2\pi}{5}, \frac{4\pi}{5}, \frac{6\pi}{5}, \frac{8\pi}{5})$  . The same process for finding a subset of codewords for 4-SCCK, discussed previously, is performed in the case of 16-SCCK. The process is done by choosing the codewords with large Euclidean distance, choosing 2048 codewords to apply in the proposed system. This means that higher spectral efficiency, 11 bit/s/Hz, is achieved compared with the conventional SCCK of 10 bit/s/Hz, which is discussed in Chapter 4.

## 6.3 The Minimum Euclidean Distance between Complementary Codes

The assumption is made to have  $M$  phases corresponding to the code. This leads to the derivation of the set of bits for each codeword as  $(1+\log_2 N_T)\log_2 M$  bits. In the case of having 16, 4 and 2 length codewords, this will contain 5, 3 and 2 phases, respectively. The following calculation shows the number of bits per codeword.

- Length 16-SCCK codeword

If  $M_c$  presents the number of bits per codeword then:

$$M_c = (1+\log_2 N_T) \log_2 M \quad (6.3)$$

$$M_c = (1+\log_2 16) \times \log_2 5 = 11.6096 \text{ and } \lfloor 11.6096 \rfloor = 11 \text{ bits per codeword}$$

- Length 4-SCCK codeword

$$M_c = (1+\log_2 N_T) \log_2 M \quad (6.4)$$

$$M_c = (1 + \log_2 4) \times \log_2 3 = 4.754 \text{ and } \lfloor 4.754 \rfloor = 4 \text{ bits per codeword}$$

- Length 2-SCCK codeword

$$M_c = (1 + \log_2 N_T) \log_2 M \quad (6.5)$$

$$M_c = (1 + \log_2 2) \times \log_2 2 = 2 \text{ bits per codeword}$$

It is fundamental to calculate the number of symbols which is enough for producing SCCK phases. It can be demonstrated that  $1 + N/2$  symbols are sufficient because  $1 + \log_2 N_T$  number of phases can be gained through  $1 + \log_2 N_T$  independent equations limited by the condition that all produced phases are at least used once in one of these equations. The equations emphasise that each phase is utilized in  $\frac{N_T}{2}$  equations and therefore  $(1 + \frac{N_T}{2})$  symbols would be enough. The minimum Euclidean distance  $d_{min}$  between any two codewords, if the least phasor rotation between  $\frac{N_T}{2}$  symbols is  $\frac{2\pi}{M}$ , is given by [9]:

$$d_{min} = \sqrt{\frac{N_T}{2} \left\| 1 - \exp(j \frac{2\pi}{M}) \right\|^2} \quad (6.6)$$

## 6.4. Results and Discussions

MIMO-OFDM systems are considered and 2000000 packets are transmitted, where each packet includes 20 OFDM symbols. With delay spreads of 50, 100 and 150 ns, the channel is defined as a time-variant frequency-selective multipath channel. Eb/N0 is used for the standardized signal-to-interference-plus-noise ratio. Table (6.1) describes the parameters of the system simulation:

Parameter	Setting
Number of Packets	100000
Number of OFDM symbols	20
Number of sub-channels	256
Length of cyclic prefix	16
Channel delay spread (ns)	50,100,150
System Bandwidth (MHz)	20
Transmit Power (W)	1
Carrier Frequency (GHz)	2.4

**Table 6.1:** System Simulation Parameters

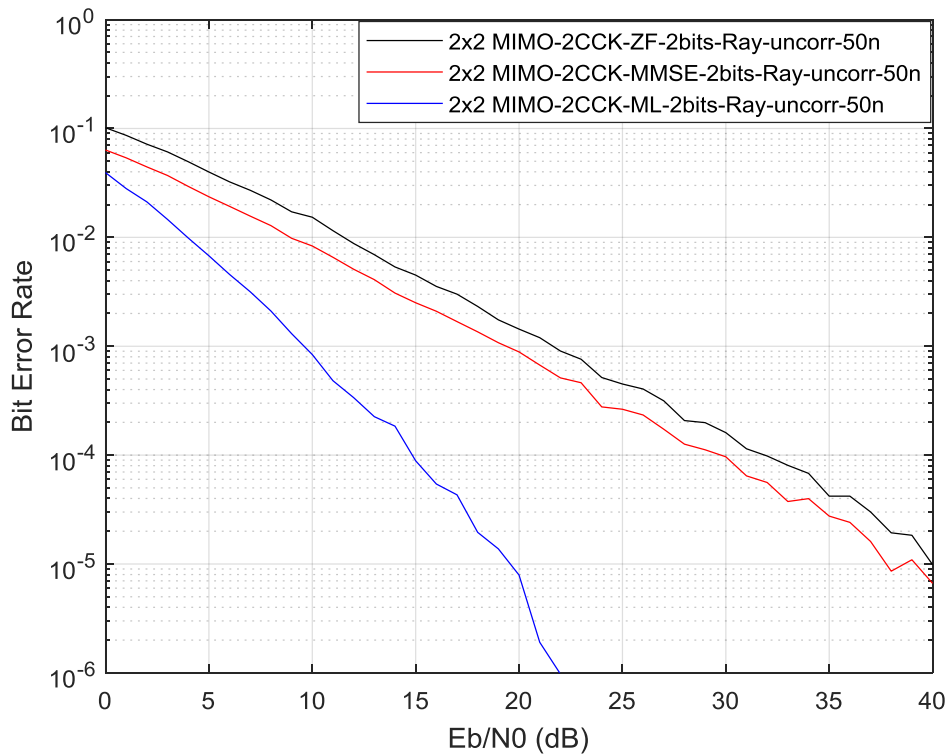
The Matlab modelling of modified SCCK-OFDM follows the same steps as discussed in Chapter 4.

### 6.4.1 Spatial CCK for different detection schemes Results

The purpose of this section is to investigate the bit error rate performance of the proposed system with different detectors, zero forcing (ZF) and minimum mean square error (MMSE), at the receiver.

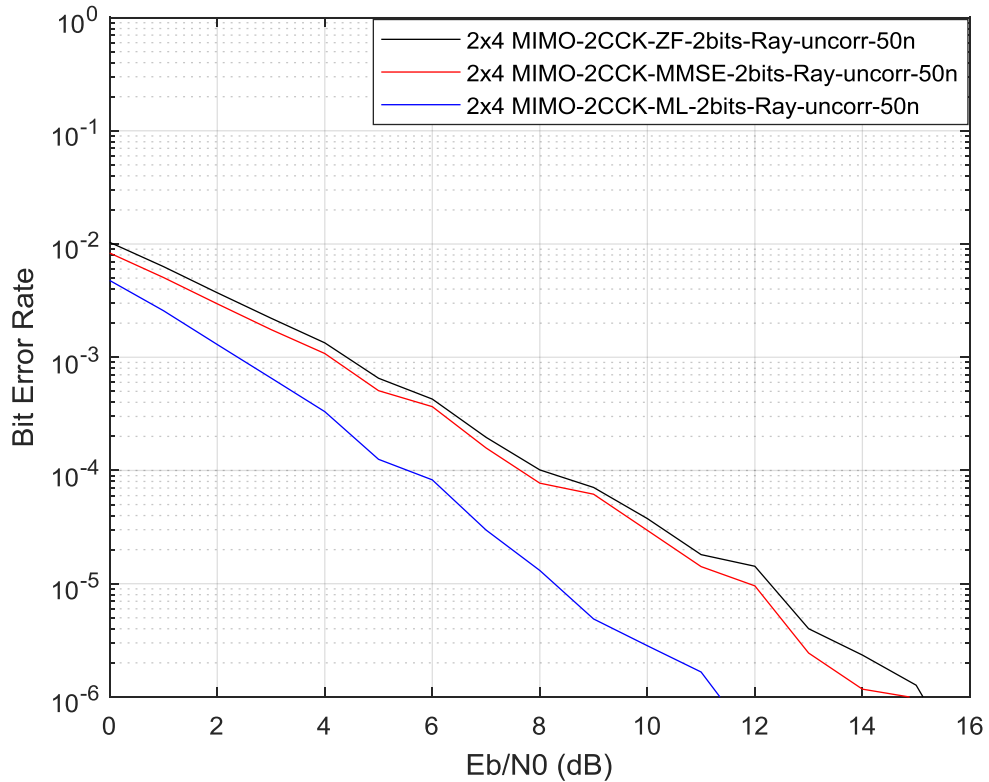
#### 6.4.1.1 2 bit/s/Hz Modified SCCK results

Fig 6.3 shows the performance of BER versus the  $E_b/N_0$  comparing different detectors in a 2x2 MIMO-OFDM-SCCK modified system under uncorrelated Rayleigh fading channels, with RMS delay spread equal to 50 ns. As expected, the optimal BER performance is obtained by the ML detector at the cost of complexity. Clearly, the MMSE detector outperforms the ZF across all the  $E_b/N_0$  considered. There is approximately a 3 dB SNR gain achieved.



**Figure 6.3:** BER versus  $E_b/N_0$  for spatial modified CCK over uncorrelated Rayleigh channel and different detection schemes with  $m = 2$ , where  $N_t = 2$  and  $N_r = 2$  and RMS delay spread=50 ns

Evidently, BER performance of both schemes is largely affected by the receiver diversity as shown in Fig 6.4. For instance, there is clear improvement in BER in all different detection schemes when the number of receive antennas increases. This improvement reaches 9 dB SNR gain between 2x2-SCCK in Fig 6.4 and 2x4-SCCK with ML detector.



**Figure 6.4:** BER versus  $E_b/N_0$  for spatial modified SCCK over uncorrelated Rayleigh channel and different detection schemes with  $m = 2$ , where  $N_t = 2$  and  $N_r = 4$  and RMS delay spread=50 ns

Comparing the results shown in Fig 6.3 with the conventional SCCK system discussed in Chapter 4 under the same codeword length conditions gives the curves shown in Fig 6.5. In detail, for a ZF detector the BER curve for both 2 bit/s/Hz and 4 bit/s/Hz are almost the same, while for MMSE and ML detectors the system with 2 bit/s/Hz spectral efficiency gains 1 dB in  $E_b/N_0$  compared with the system of 4 bit/s/Hz.

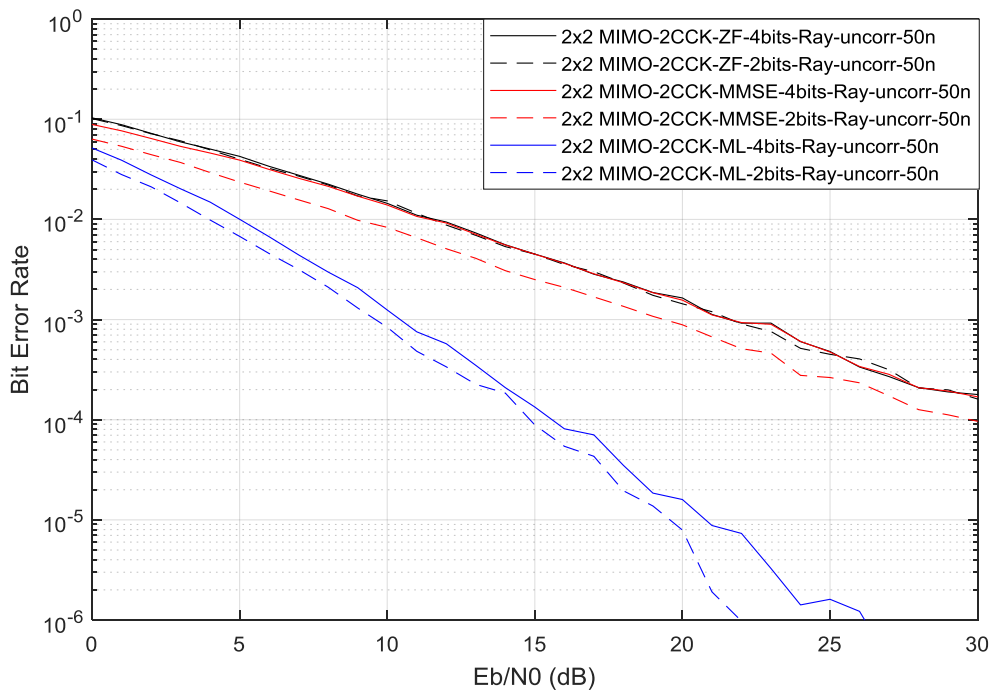
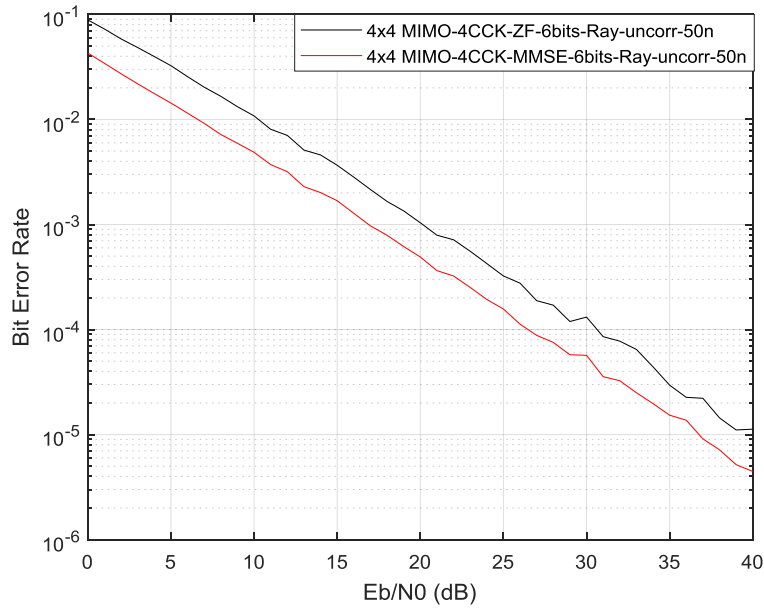


**Figure 6.5:** BER versus  $E_b/N_0$  comparison between for spatial conventional/modified 2CCK over uncorrelated Rayleigh channel and different detection schemes with  $m = 2, 4$  respectively, where  $N_t = 2$  and  $N_r = 2$  and RMS delay spread=50 ns

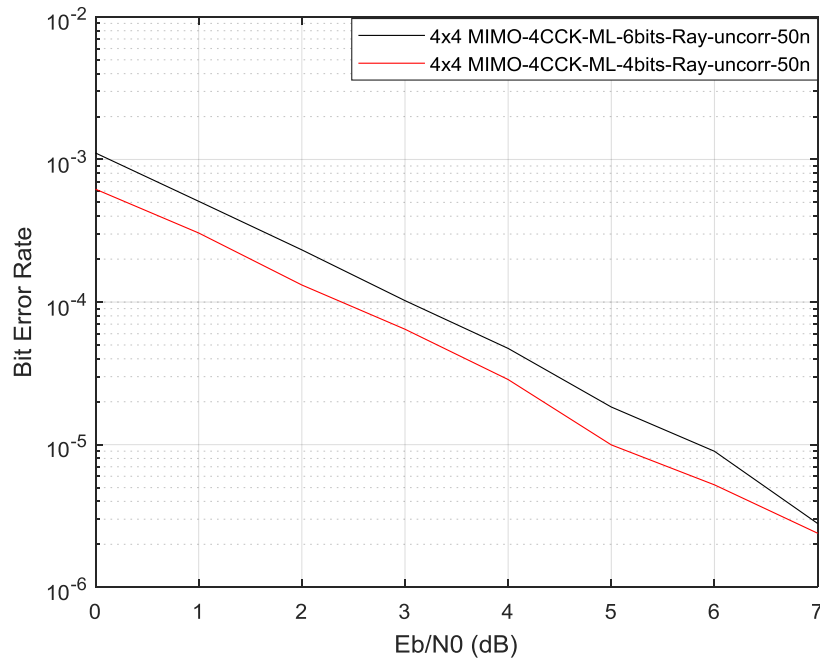
#### 6.4.1.2 4-bit/s/Hz Modified SCCK results

In the case of 4 bit/s/Hz modified SCCK, the BER performance noticeably improves in the case of the MMSE detector compared to the ZF detector, which reaches approximately 9 dB for a 4-SCCK system with 4 transmit and receive antennas, as presented in Fig 6.6.

Fig 6.7 presents a comparison between conventional MIMO-OFDM-4SCCK with 4 phases and modified MIMO-OFDM-4SCCK with 3 phases, both of which use 4 transmit and receive antennas with 6 bit/s/Hz and 4 bit/s/Hz spectral efficiency respectively, in an uncorrelated IEEE channel with a ML detector. The results confirm that the BER performance of modified 4-SCCK system outperforms conventional 4-SCCK by approximately 1 dB in trade off with spectral efficiency.



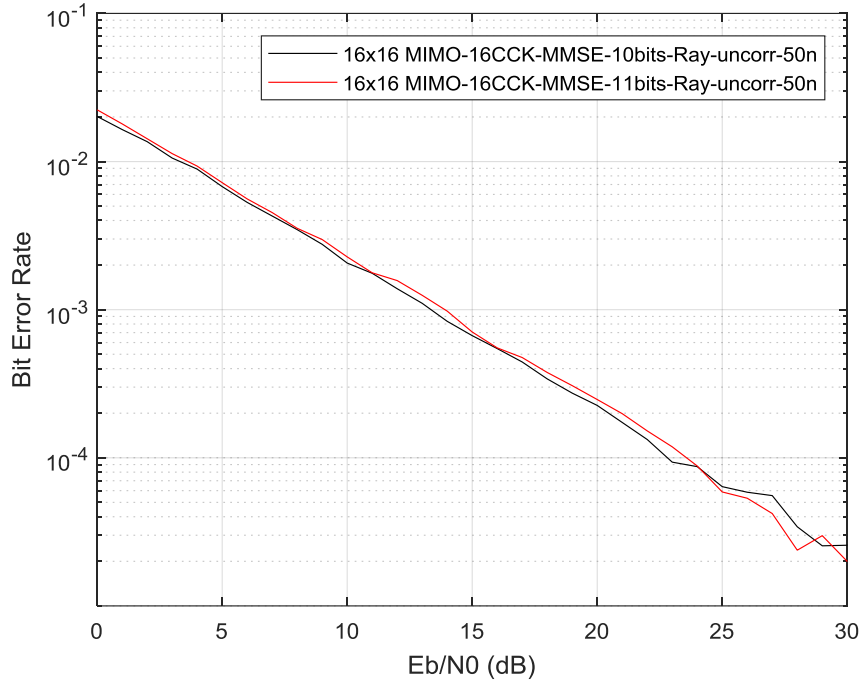
**Figure 6.6:** BER versus  $E_b/N_0$  for spatial modified CCK over uncorrelated Rayleigh channel and different detection schemes with  $m = 4$ , where  $N_t = 4$  and  $N_r = 4$  and RMS delay spread = 50 ns



**Figure 6.7:** BER versus  $E_b/N_0$  comparison between for spatial conventional/modified 4-SCCK over uncorrelated Rayleigh channel and optimal detection schemes with  $m = 4, 6$  respectively, where  $N_t = 4$  and  $N_r = 4$  and RMS delay spread = 50 ns

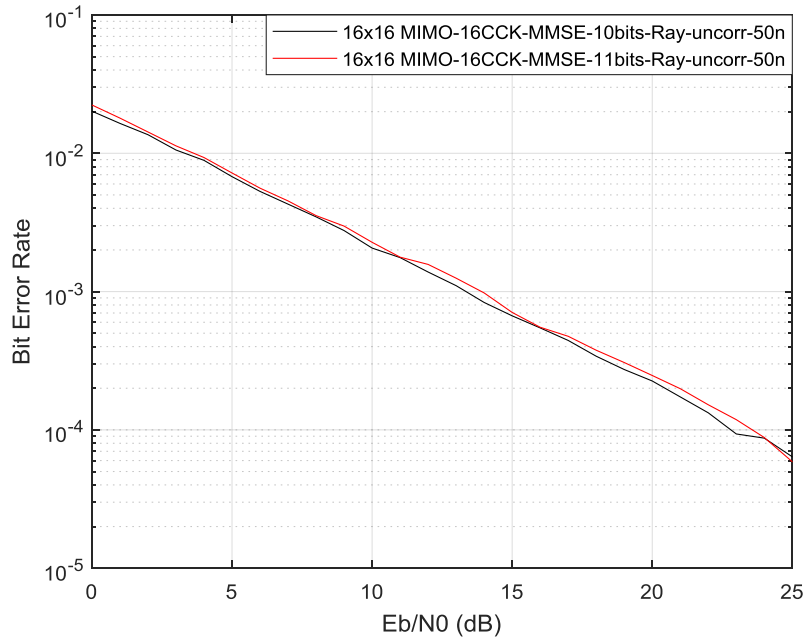
### 6.4.1.3 11- bit/s/Hz Modified SCCK results

Fig 6.8 shows the BER performance of the MMSE detector (red curve) is approximately the same with BER of the ZF detector (black curve), despite being a more complex receiver.



**Figure 6.8:** BER versus Eb/No for spatial modified CCK over uncorrelated Rayleigh channel and different detection schemes with  $m = 11$ , where  $N_t = 16$  and  $N_r = 16$  and RMS delay spread=50 ns

Fig 6.9 plots BER Vs Eb/No comparing modified 16-SCCK with conventional 16-SCCK for 11 and 10 bit/s/Hz spectral efficiencies respectively, in an uncorrelated Rayleigh channel using MMSE detection scheme. The results show approximately the same BER performance with higher spectral efficiency in the case of modified 16-SCCK compared to conventional 16-SCCK.



**Figure 6.9:** BER versus  $E_b/N_0$  comparison between for spatial conventional/modified 16-SCCK over uncorrelated Rayleigh channel and optimal detection schemes with  $m = 10, 11$ , where  $N_t = 16$  and  $N_r = 16$  and RMS delay spread = 50 ns

## 6.4.2 Modified Spatial CCK under different wireless channels with different RMS delay spread results

The purpose of this section is to evaluate the system performance under different types of Rayleigh and Rician wireless channels to quantify the fading effect on the system in comparison with the conventional SCCK system. Different RMS delay spreads will be examined, and the BER performance evaluated.

### 6.4.2.1 2-bit/s/Hz Modified SCCK results

Fig 6.10 shows the BER performance of the system in the case of ZF, MMSE and ML detectors in both Rician and Rayleigh channels, where the solid curves represent the Rician uncorrelated channel and the dashed curves plot the Rayleigh uncorrelated channel. The results show the same trend discussed in Chapter 4; the ML detector has the best performance compared with MMSE

and ZF results, and the system keeps the same BER performance in the case of different RMS delay spreads when using a ML detector, as shown in Fig 6.11.

The key comparison is BER performance of modified SCCK (black curves) system with conventional SCCK (red curves), discussed in Chapter 4 and as shown in Fig 6.12. The BER performance of modified SCCK gains approximately 0.75 dB in trade off with spectral efficiency.

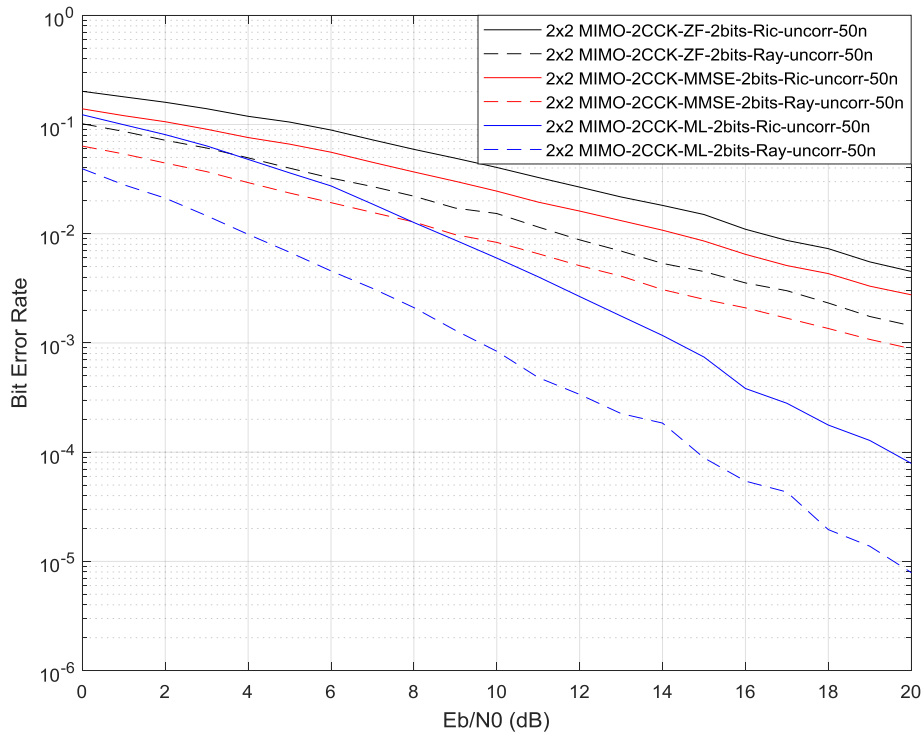


**Figure 6.10:** BER versus  $E_b/N_0$  for spatial modified SCCK over uncorrelated Rayleigh/Rician channel and different detection schemes with  $m = 2$ , where  $N_t = 2$  and  $N_r = 2$  and RMS delay spread = 50 ns

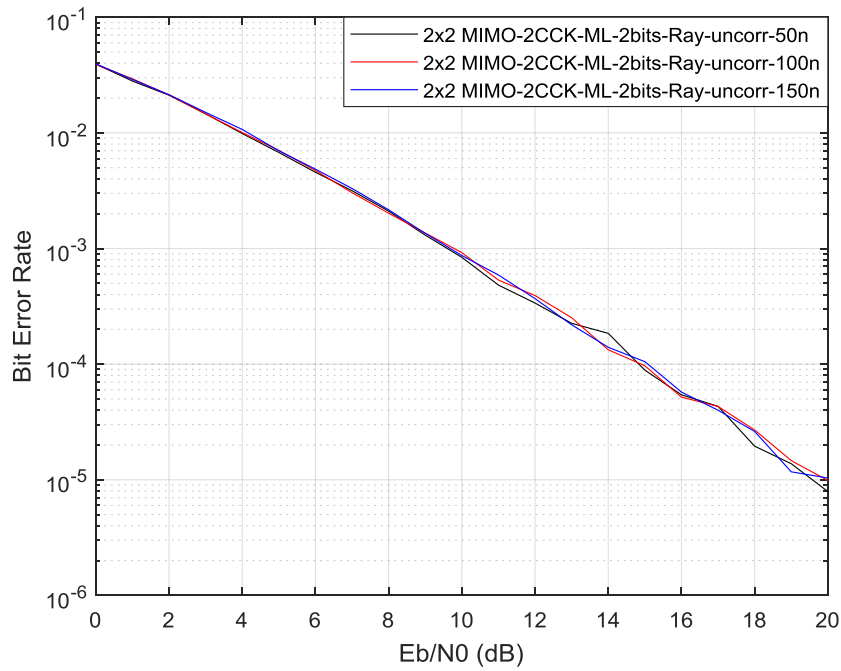


**Figure 6.11:** BER versus  $E_b/N_0$  for spatial modified SCCK over uncorrelated Rayleigh channel and optimal detection scheme with  $m = 2$ , where  $N_t = 2$  and  $N_r = 2$  and RMS delay spread=50,100,150 ns

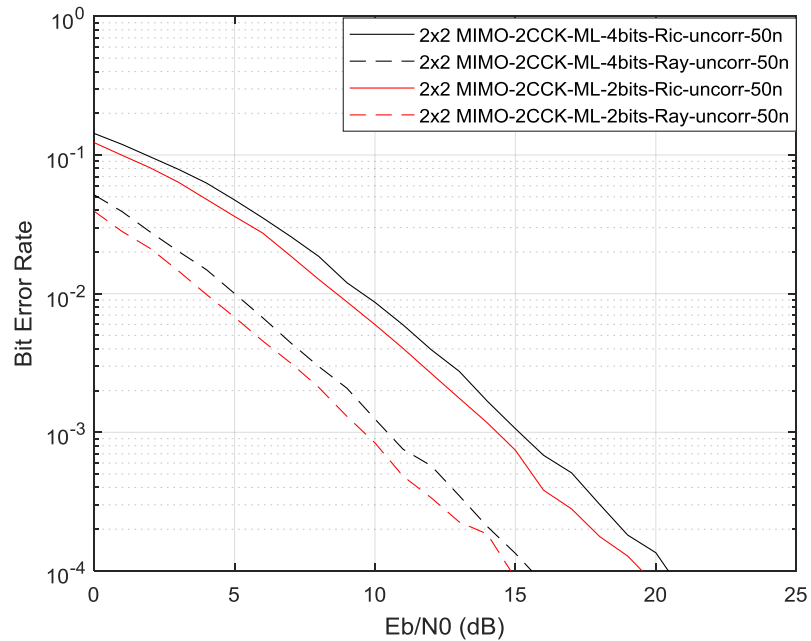
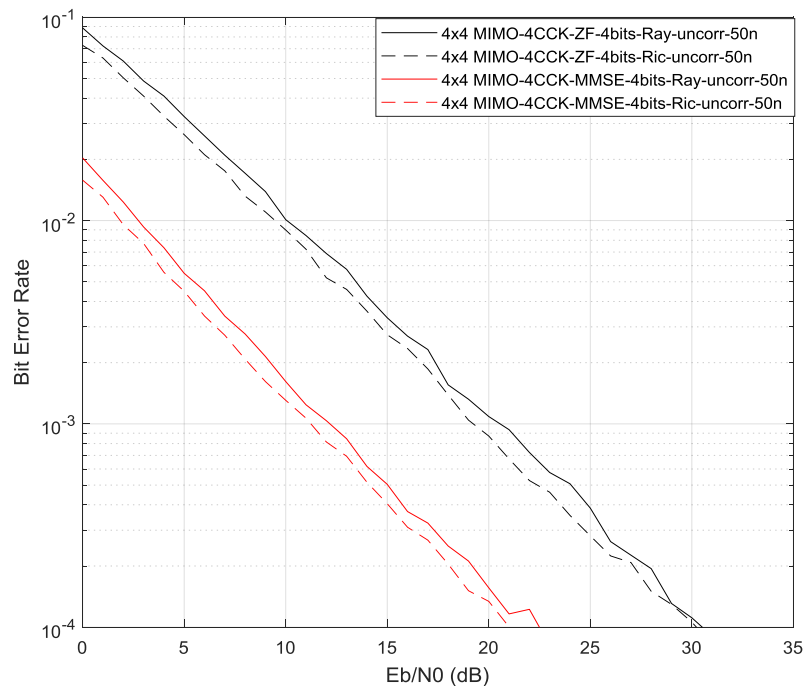


**Figure 6.12:** BER versus  $E_b/N_0$  comparison between spatial conventional/modified 2CCK over uncorrelated Rayleigh/Rician channel and optimal detection schemes with  $m = 4, 2$  respectively, where  $N_t = 2$  and  $N_r = 2$  and RMS delay spread=50 ns

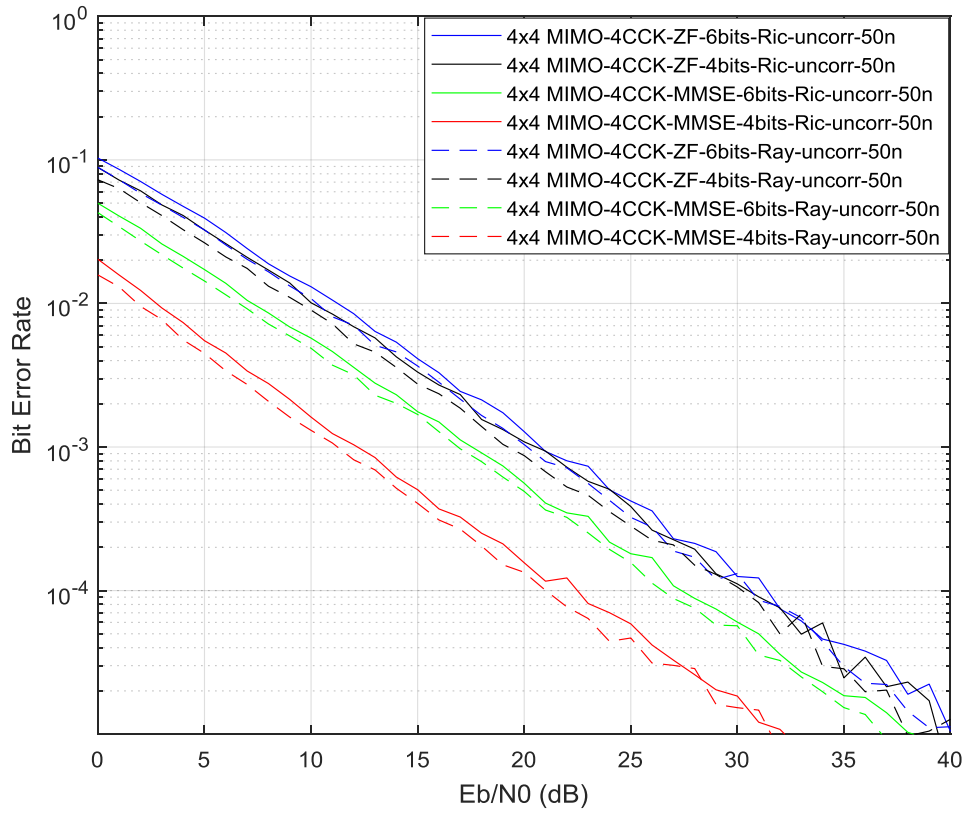
### 6.4.2.2 4- bit/s/Hz Modified SCCK results

Fig 6.13 plots BER Vs  $E_b/N_0$  comparing modified 4-SCCK in a Rician uncorrelated channel (solid curves), with 4-SCCK in a Rayleigh uncorrelated channel (dashed curves) for 4 bit/s/Hz spectral efficiency, with different detection schemes. At  $10^{-3}$  BER, 4-SCCK in a Rayleigh uncorrelated channel using a ZF detector (dashed black curve) achieves a SNR gain of 0.5 dB over 4-SCCK in a Rician uncorrelated channel, also using a ZF detector (solid black curve).

In the case of comparing modified SCCK results with 4-phase conventional SCCK using the same codeword lengths, Fig 6.14 shows this comparison in terms of different wireless channels. The results show that the BER performance of modified 4-SCCK with both Rayleigh and Rician uncorrelated channels and ZF, MMSE detectors achieve a SNR gain of approximately 0.5 dB over conventional 4-SCCK under the same channel and detection schemes conditions in trade off with spectral efficiency. It is worthy mentioned that the modified SCCK is outperformed the conventional SCCK in case of MMSE detector and the BER performance in case of ZF is approximately the same.



**Figure 6.13:** BER versus  $E_b/N_0$  for modified 4-SCCK over uncorrelated Rayleigh/Rician channel and different detection schemes with  $m = 4$ , where  $N_t = 4$  and  $N_r = 4$  and RMS delay spread = 50 ns



**Figure 6.14:** BER versus  $E_b/N_0$  comparison between for spatial conventional/modified 4-SCCK over uncorrelated Rayleigh/Rician channel and different detection schemes with  $m = 6, 4$  respectively, where  $N_t = 4$  and  $N_r = 4$  and RMS delay spread=50 ns

### 6.4.2.3 11- bit/s/Hz Modified SCCK results

Fig 6.15 plots BER Vs  $E_b/N_0$  comparing modified 16-SCCK in Rician uncorrelated channels (solid curves), with 4-SCCK in Rayleigh uncorrelated channels (dashed curves) for 11 bit/s/Hz spectral efficiency, with ML detector. At  $10^{-4}$  BER, 16-SCCK with Rayleigh uncorrelated channel and ZF detector (solid red curve) achieves a SNR gain of 0.75 dB over 16-SCCK with Rician uncorrelated channel and ZF detector (solid black curve). The figure also shows that the system is effective in noisy environment with very low  $E_b/N_0$ .

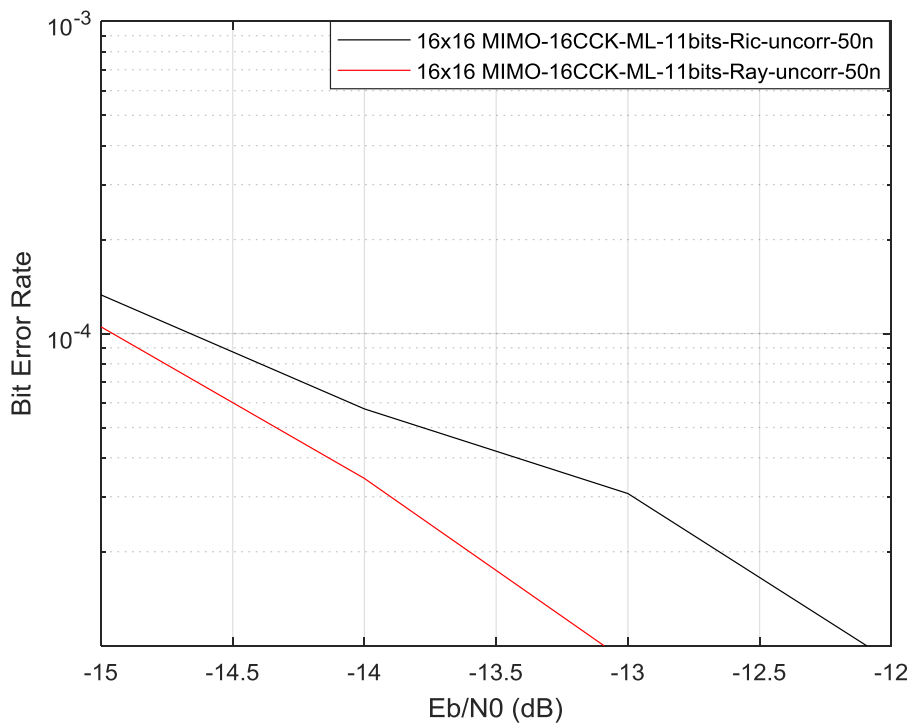


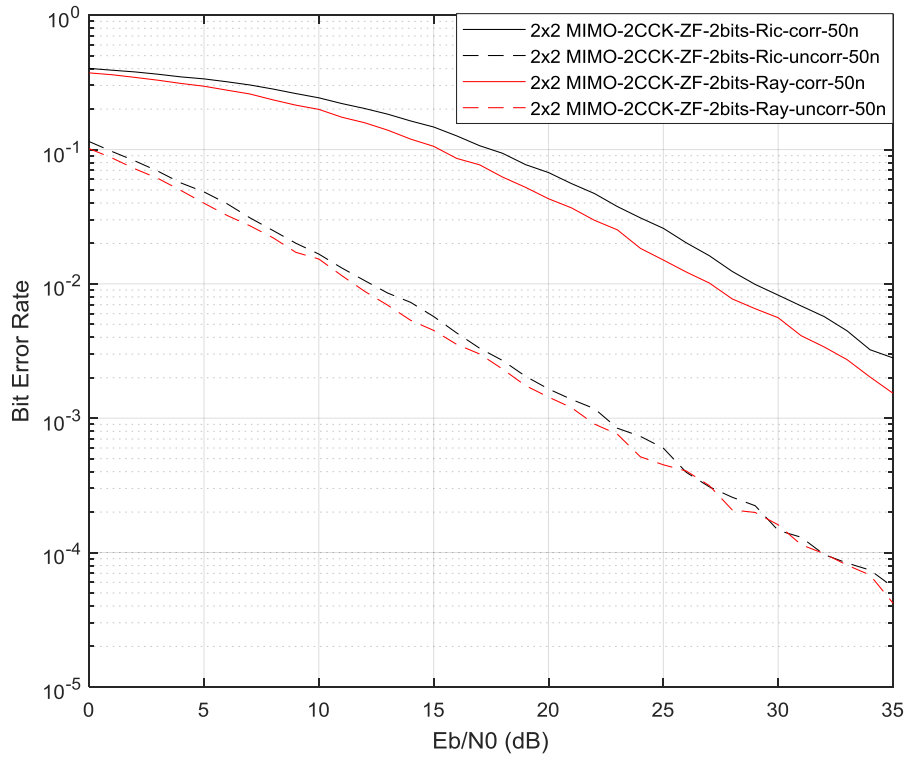
**Figure 6.15:** BER versus Eb/No for modified 16-SCCK over uncorrelated Rayleigh/Rician channel and different detection schemes with  $m = 11$ , where  $N_t = 12$  and  $N_r = 12$  and RMS delay spread = 50 ns

### 6.4.3 Correlated channel effect Results

To evaluate the SCCK in more realistic scenarios, the Kronecker exponential correlation is applied and compares the results with conventional 4-phase SCCK under the same channel and detection schemes conditions.

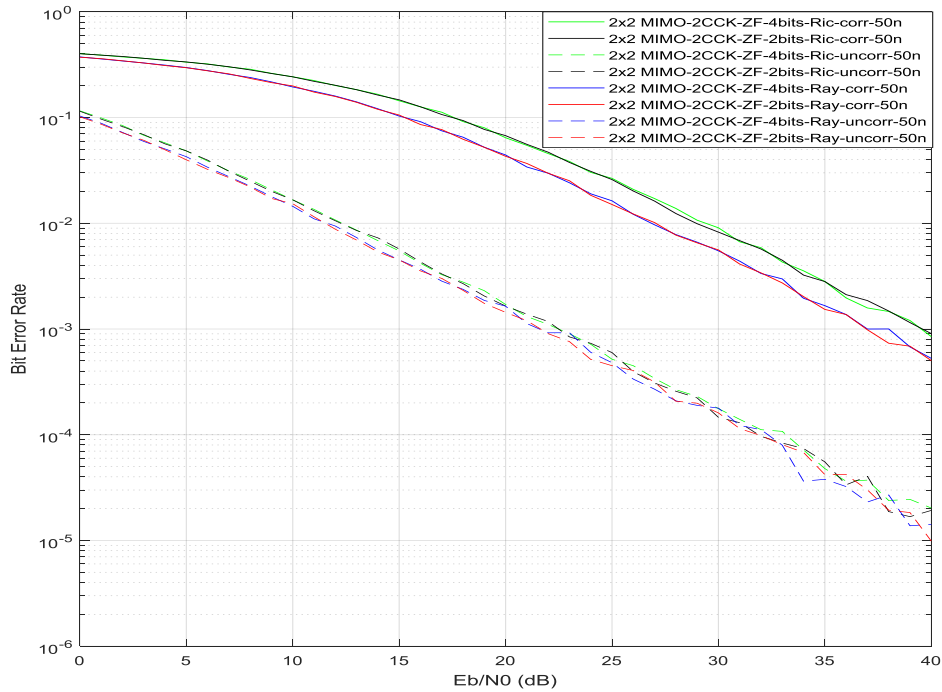
#### 6.4.3.1 2- bit/s/Hz Modified SCCK results

Fig 6.16 shows a comparison between correlated and uncorrelated Rician and Rayleigh channel with a ZF detector, based on the 2x2 transmitter and receiver structure. In detail, Fig 6.16 plots BER vs Eb/No comparing 2-SCCK in a Rician correlated channel (solid curves), with 2-SCCK in Rician uncorrelated channel (dashed curves). Both systems have 2 bit/s/Hz spectral efficiencies, with correlation coefficient of ( $c=0.5$ ) applied. At  $10^{-2}$  BER 2-SCCK with Rician uncorrelated channel achieves a SNR gain of a 15 dB over 2-SCCK with Rician correlated channel.



**Figure 6.16:** BER versus Eb/No for modified 2-SCCK over correlated/uncorrelated Rician channel and ZF detection schemes with  $m = 2$ , where  $N_t = 2$  and  $N_r = 2$  and RMS delay spread=50 ns and correlation factor=0.5

In the case of comparing modified 2-SCCK results with 4-phase conventional 2-SCCK results under the same codeword length, Fig. 6.17 plots this comparison in terms of different wireless uncorrelated and correlated channels using the ZF detection scheme. The results show that under the channel correlation effect the BER performance of modified 4-SCCK in Rayleigh and Rician uncorrelated channel is similar to the conventional 4-SCCK in trade off with spectral efficiency. This is an advantage in the conventional SCCK system in the case with higher spectral efficiency than modified SCCK.

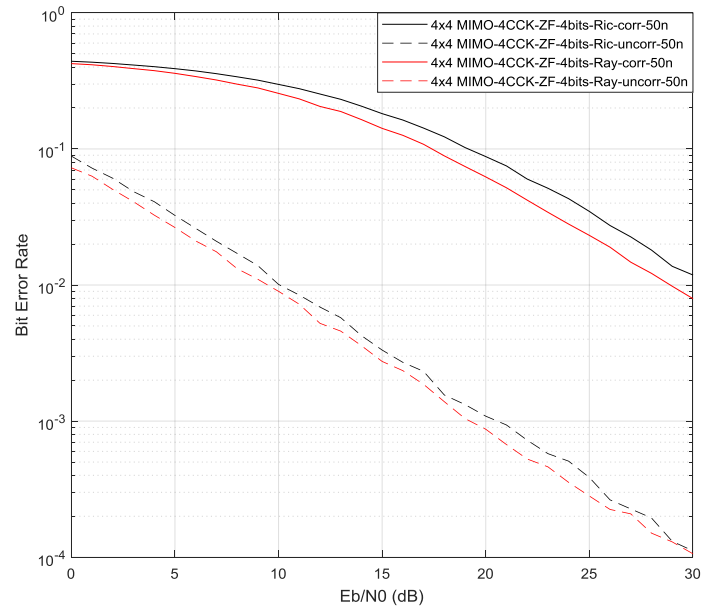


**Figure 6.17:** BER versus  $E_b/N_0$  comparison between for conventional/modified 4-SCCK over uncorrelated/correlated Rayleigh/Rician channel and different detection schemes with  $m = 4, 2$  respectively, where  $N_t = 2$  and  $N_r = 2$  and RMS delay spread = 50 ns

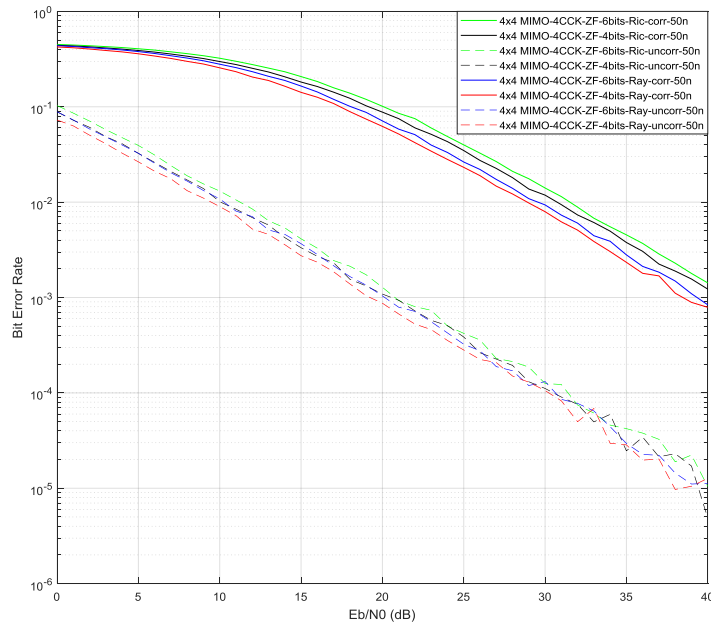
#### 6.4.3.2 4- bit/s/Hz Modified SCCK results

Fig 6.18 and 6.19 show the same system as Figs 6.16 and 6.17 except with different numbers of transmit and receive antennas, which is 4, and the correlation effect is found to remain at 15 dB when using a ZF detector, as shown in Fig 6.18.

Fig 6.19 shows that under the correlation effect with  $c=0.5$  in both transmit and receive antennas, the BER is approximately the same in conventional and modified SCCK systems, but with 4 bit/s/Hz spectral efficiency in conventional SCCK, compared with 2 bit/s/Hz in the case of the modified SCCK system.



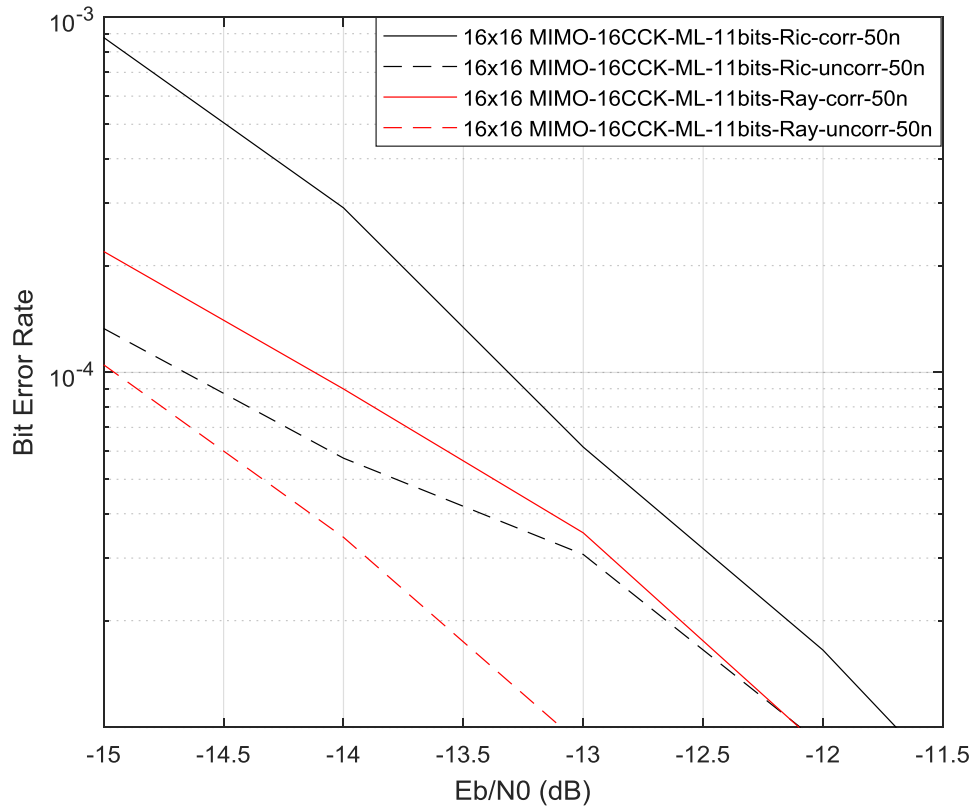
**Figure 6.18:** BER versus  $E_b/N_0$  for modified 4-SCCK over correlated/uncorrelated Rician channel and ZF detection schemes with  $m = 4$ , where  $N_t = 4$  and  $N_r = 4$  and RMS delay spread=50 ns and  $c=0.5$



**Figure 6.19:** BER versus  $E_b/N_0$  comparison between for conventional/modified 4-SCCK over uncorrelated/correlated Rayleigh/Rician channel and different detection schemes with  $m = 6, 4$  respectively, where  $N_t = 4$  and  $N_r = 4$  and RMS delay spread=50 ns and  $c=0.5$

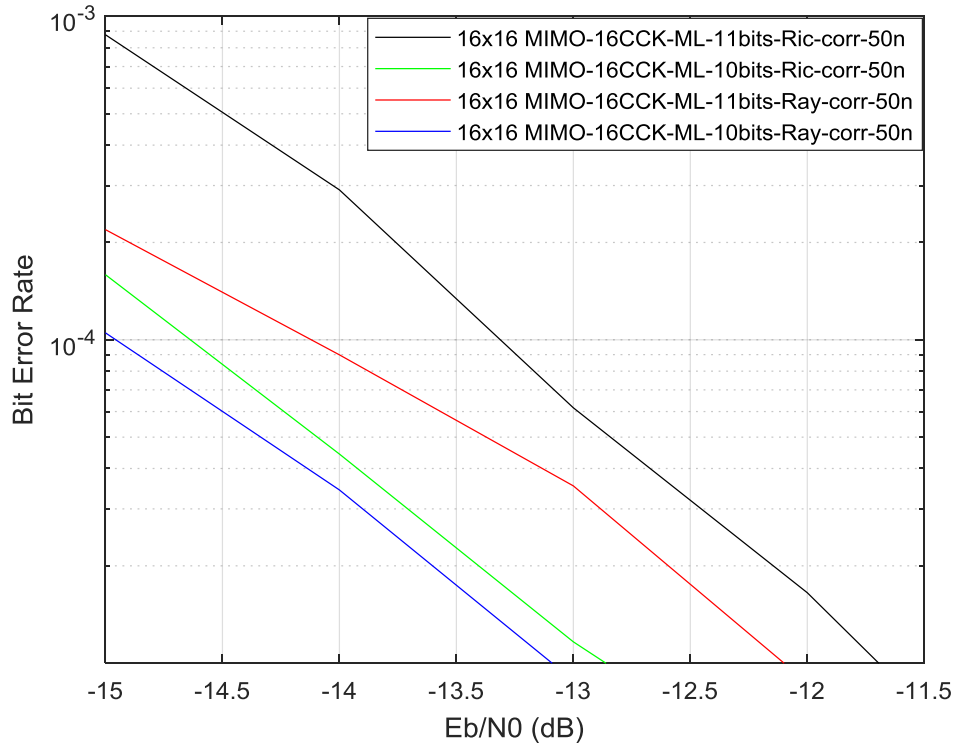
### 6.4.3.3 11- bit/s/Hz Modified SCCK results

Fig. 6.20 shows the BER of the modified 16-SCCK system under correlated and uncorrelated Rayleigh and Rician channels using a ML detector, with  $c=0.5$  in both transmit and receive antennas. At  $10^{-4}$  BER, modified 16-SCCK in an uncorrelated Rician channel achieves a SNR gain of 2 dB over modified 16-SCCK in a correlated Rician channel.



**Figure 6.20:** BER versus  $E_b/N_0$  for spatial modified 4-SCCK over correlated/uncorrelated Rician channel and ZF detection schemes with  $m = 11$ , where  $N_t = 16$  and  $N_r = 16$  and RMS delay spread=50 ns and correlation factor=0.5

Fig 6.21 plots BER vs  $E_b/N_0$  comparing the conventional 16-SCCK system under a correlated Rician channel and  $c=0.5$  in both transmit and receive antennas (black curve), with modified 16-SCCK system under correlated Rician channel and  $c=0.5$  in both transmit and receive antennas (green curve). The BER of conventional 16-SCCK system achieves a SNR gain of approximately 2 dB over the modified 16-SCCK system, in trade off with spectral efficiency.



**Figure 6.21:** BER versus  $E_b/N_0$  comparison between for conventional/modified 16-SCCK over correlated Rician channel and ML detection scheme with  $m = 11$ , where  $N_t = 16$  and  $N_r = 16$  and RMS delay spread=50 ns

## 6.5 Bit error rate analysis of Modified SCCK system for narrow band channel

The analytical average BER of spatial modified complementary code keying modulation derived here is based on the union bound, similarly to conventional SCCK as discussed in Chapter 4, but with different transmit codewords. This is due to using non-conventional phases and different spectral efficiencies

### 6.5.1 Modified SCCK results discussion

The results for the analytical and simulated BER of modified SCCK over i.i.d. uncorrelated and correlated, Rayleigh and Rician fading channels, for the system configurations of 2, 4 and 16 transmit and receive antennas, giving  $m = 2, 4$  and 11 bit/s/Hz spectral efficiency respectively, and Rician factor  $K = 3$  dB and  $c = 0.5$  are presented below.

In Fig 6.22 and 6.23, analytical and simulated results show a close match for a wide and pragmatic range of  $E_b/N_0$  values and for different channel conditions, and thus validates the derived analysis

in this thesis. In detail, Figure 6.22 shows this comparison of modified SCCK system with conventional SCCK system in terms of uncorrelated and correlated Rayleigh channels. Solid curves represent Rayleigh correlated channels and dashed lines show Rayleigh uncorrelated channels, and the results show that BER performance of modified 2-SCCK in Rayleigh uncorrelated channels with a ML detector achieve a SNR gain of approximately 1 dB over conventional 4-SCCK under the same channel conditions and detection scheme, in trade off with spectral efficiency.

The same trend of results is shown in Fig 6.23 except the channel is a Rician fading channel with  $K=3$  dB. Moreover, the effect of the correlation in both transmit and receive sides is clear in both figures, which reaches approximately 5 dB loss compared with the uncorrelated case in both Rayleigh and Rician channels.

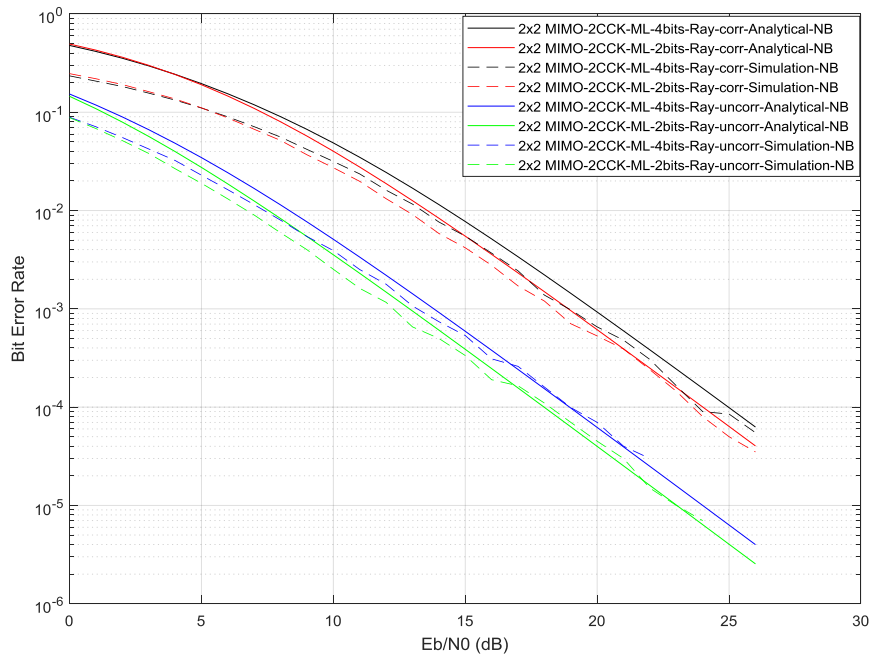


**Figure 6.22:** BER versus  $E_b/N_0$  for SCCK over uncorrelated/correlated Rayleigh channel,  $m = 4, 2$  respectively, where  $N_t=N_r = 2$ . (Dashed line) Simulation, (solid line) Analytical

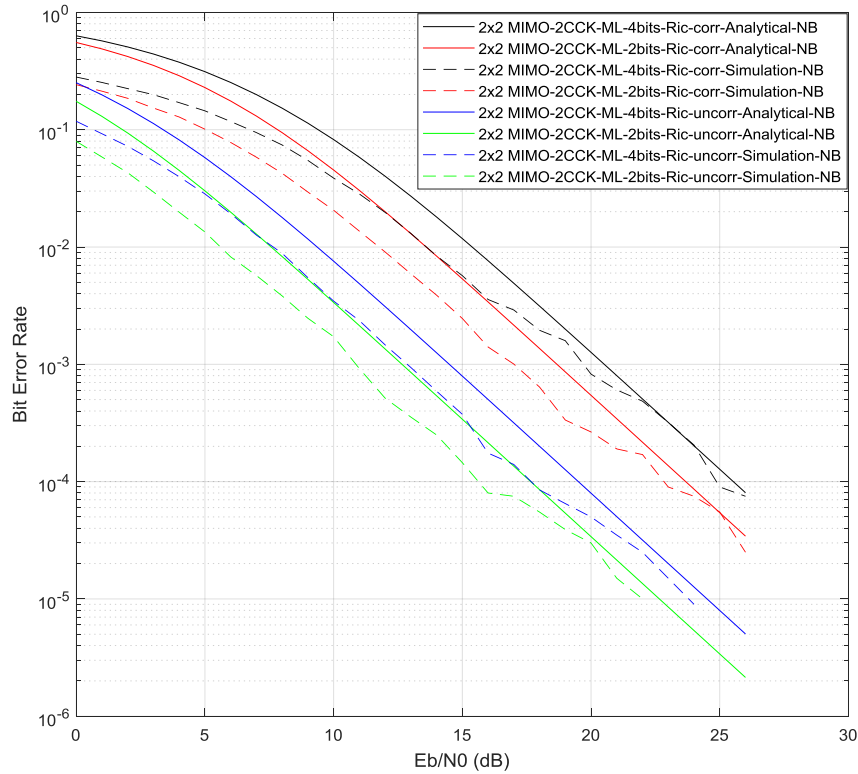


**Figure 6.23:** BER versus  $E_b/N_0$  for SCCK over uncorrelated/correlated Rician channel, where  $m = 4, 2$  respectively and  $N_t=N_r = 2$ . (Dashed line) Simulation, (solid line) Analytical

Fig 6.24 plots BER Vs  $E_b/N_0$  comparing a modified 4-SCCK system in Rayleigh uncorrelated and correlated channels, with conventional 4-SCCK system in Rayleigh uncorrelated and correlated channels, with 4 and 6 bit/s/Hz spectral efficiencies respectively, with  $c=0.5$ . The BER performance of the modified 4-SCCK system achieves a SNR gain of nearly 2 dB over conventional 4-SCCK under the same channel conditions and detection scheme in trade off with spectral efficiency. The same trend of results is shown in Fig 6.25 but with Rician fading channels with  $K=3$  dB. Moreover, the effect of the correlation in both transmit and receive sides is clear in both figures which reaches approximately 5 dB compared with the uncorrelated case in both Rayleigh and Rician channels.

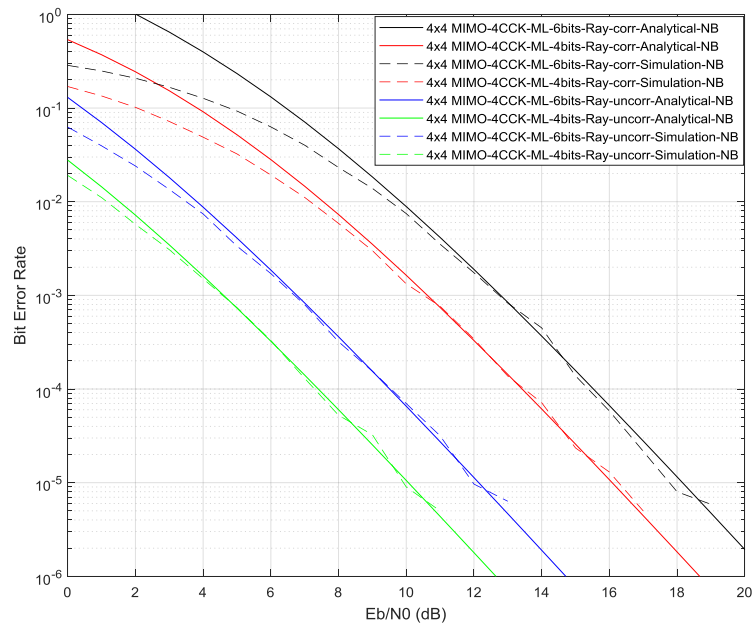


**Figure 6.24:** BER versus  $E_b/N_0$  for SCCK over uncorrelated/correlated Rayleigh channel, where  $m = 6, 4$  respectively and  $N_t=N_r = 4$ . (Dashed line) Simulation, (solid line) Analytical

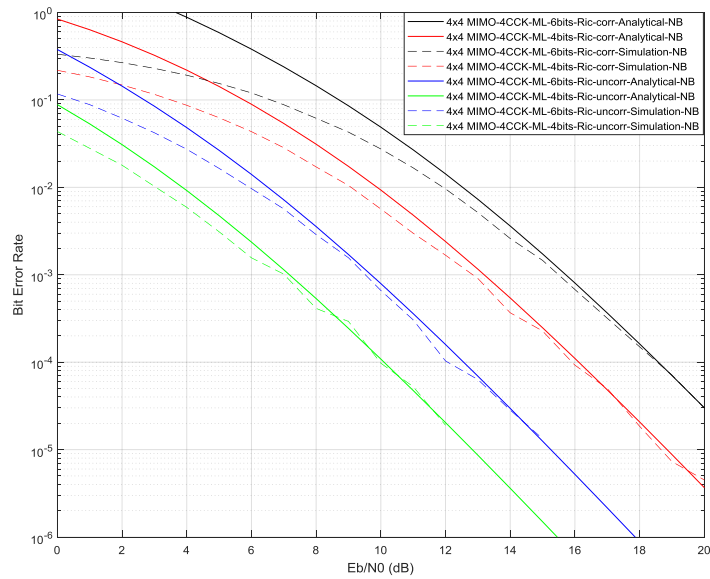


**Figure 6.25:** BER versus  $E_b/N_0$  for SCCK over uncorrelated/correlated Rician channel, where  $m = 6, 4$  respectively and  $N_t=N_r = 4$ . (Dashed line) Simulation, (solid line) Analytical

In the case of analytical BER results of comparing modified and conventional 16-CCK under Rayleigh fading channels with  $c=0.5$ , Fig 6.26 shows that the BER performance of conventional 16-SCCK achieves a SNR gain of a 2.5 dB over modified 16-SCCK system in trade off with spectral efficiency.

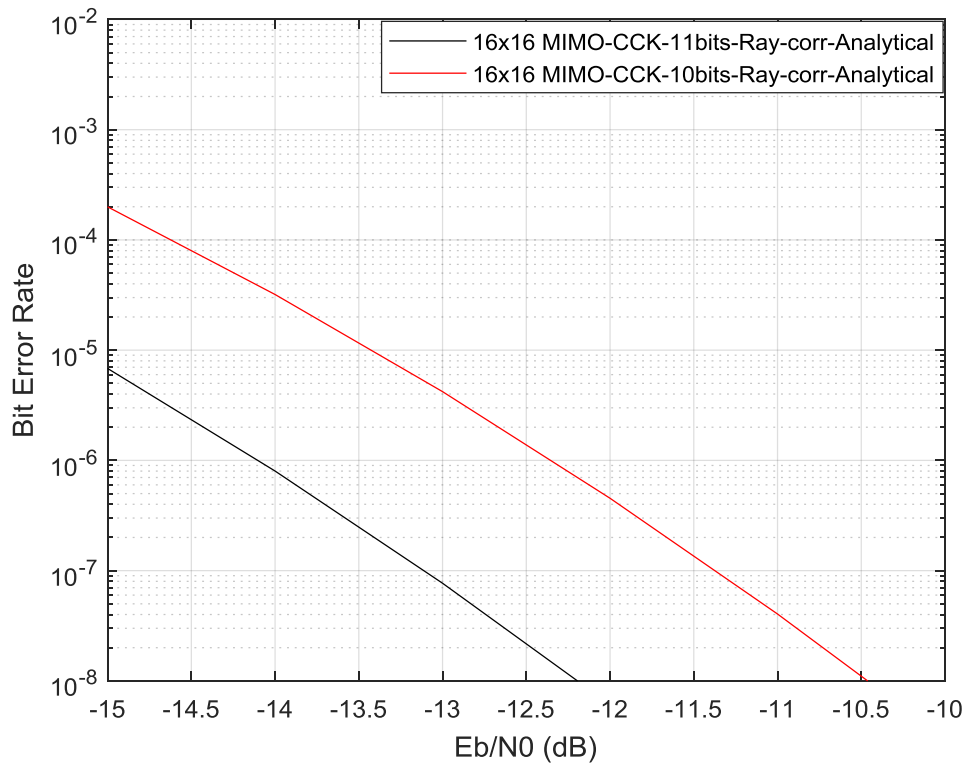


**Figure 6.26:** analytical BER versus  $E_b/N_0$  for conventional/modified SCCK over correlated Rayleigh channel, where  $m = 10, 11$  respectively and  $N_t=N_r = 16$ .

## 6.6 Summary

The result of this simulation shows an improvement in the BER performance of modified SCCK compared to conventional SCCK, which was discussed in Chapter 4, at the expense of spectral efficiency.

It is noted that the regeneration of modified SCCK BER for length 2 and 4 codewords is done as in reference [9].

When comparing the modified SCCK with conventional 2 and 4-SCCK systems with the same codeword lengths, there is a slight improvement in BER for modified SCCK at cost of reduction in spectral efficiency. Note that the modified system applied non-conventional phases, which is different to the conventional SCCK case, where the same four phases are applied in all 2, 4, 8 and 16-SCCK codeword lengths.

The chapter also extended the work in [9] to modified 16-SCCK with 11 bit/s/Hz spectral efficiency. 3125 code words of length 16 were generated and 2048 code words with the largest Euclidean distances between them were chosen to get 11 bit/s/Hz spectral efficiency.

Comparing the modified 16-SCCK system with conventional 16-SCCK shows a decrease in BER performance of modified 16-SCCK, in trade off against an increase in the spectral efficiency.

The main contribution is the analytical BER performance of a modified SCCK system in narrowband Rayleigh and Rician, uncorrelated and correlated channels. Comparing the results with conventional SCCK confirms the slight improvement of modified SCCK systems compared with conventional SCCK, in trade off with decreased spectral efficiency.

# Chapter 7 High order phase spatial complementary code keying

## 7.1 Chapter Overview

This chapter aims at modifying the SCCK model to work at even higher spectral efficiencies. This technique is applied by utilizing 8-phases instead of the 4-phases system that is used in Chapter 4.

Using 8-phases results in having more codewords than that for the 4-phases and the modified SCCK schemes. This technique achieves more codewords with a large Euclidian distance, which results in higher spectral efficiency with noticeable improvement in BER performance.

This chapter also discusses and validates the higher order SCCK results analytically and with Monte Carlo simulation, based on a MIMO system with narrowband Rayleigh and Rician fading channels with ML detection. It also compares some examplar results with the SM system previously discussed in Chapter 5 under the same channel conditions and ML detection scheme.

Finally, this chapter aims to evaluate a higher order SCCK system in frequency selective wideband IEEE Rayleigh and Rician channels, by applying MIMO-OFDM with different detector schemes and different numbers of receive antennas, to see how the receive diversity affects the proposed system performance. For more realistic scenarios, an exponential channel correlation is used to assess and evaluate the proposed SCCK system.

## 7.2 High order phase spatial Complementary Code Keying Modulation system

As illustrated in Chapter 4, the same system will be applied using the same conditions except the codeword generation will have 8 phases. A narrowband channel with Rayleigh fading is used in the system with ML detection schemes at the receiver.

A brief description of Fig 7.1 follows where:  $B_c(k)$  is the input binary sequence of  $c$  codewords which represents, as an example, 2-SCCK with  $B_c(k) = [a_0, a_1, a_2, a_3]$ , and is divided into streams of  $(1 + \log_2(N_T)) \times \log_2(M)$  bits, where  $N_t$  the number of is transmit antennas and  $M$  is the number of code generating phases, here 8. These streams are encoded into SCCK codewords defined

by  $C_c(k) = [C_c(0), C_c(1), C_c(2), C_c(3)]$ . These codewords are transmitted through the Rayleigh fading channel  $H(t)$ . At the receive side the noise  $n(t)$  is added to the signal to result  $y(t)$ . After ML detection stage the estimated data  $\widehat{B}_c(k)$  is compared with the transmit data to calculate the BER performance of the system.

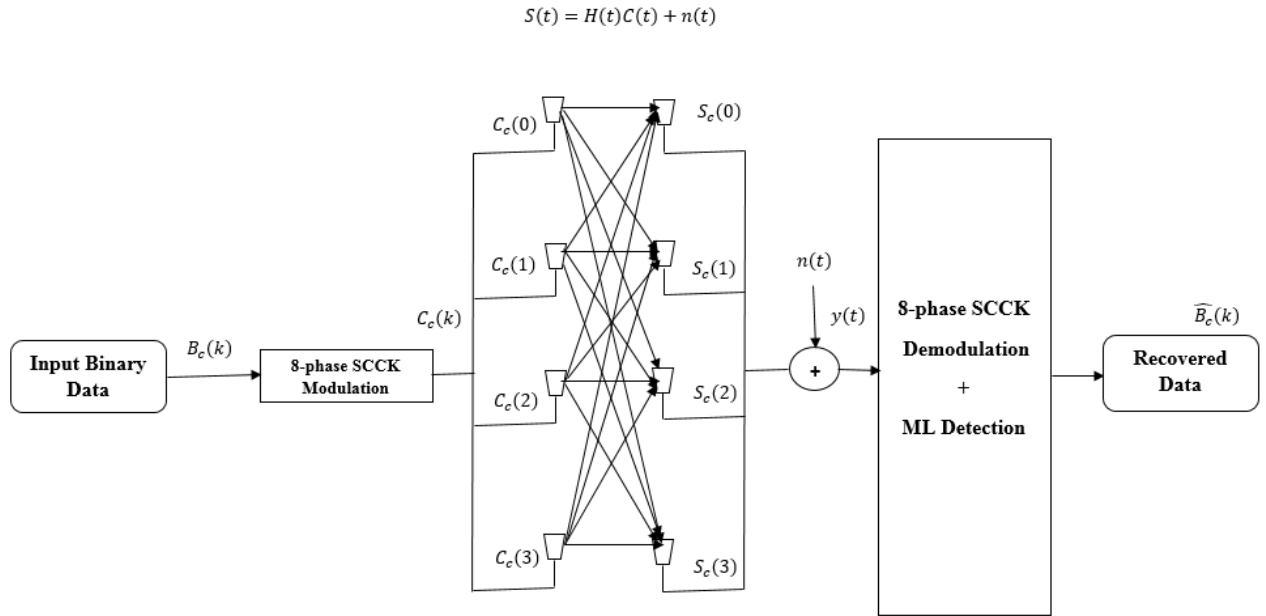


**Figure 7.1:** spatial CCK modulation system with 8-phases and narrowband Rayleigh channel

### 7.2.1 6-bit/s/Hz High order Spatial Complementary Code Keying

This mechanism generates 6 bit/s/Hz spectral efficiency higher order SCCK modulation of codeword length 2. As stated before, coded modulated data follows the same trend as Chapter 4, except with 8 phases instead of 4-phases.

Equation (7.1) is the matrix representation of equation (7.2).  $\phi_1$  and  $\phi_2$  can take on values from the set  $(0, \frac{\pi}{4}, \pi/2, 3\pi/2, \pi, -\frac{\pi}{4}, -\pi/2, -3\pi/2)$ , which are the 8-PSK code generating phases, giving 64 possible codewords.

Equation (7.2) manipulates 64 phase combinations to derive the 6-bit higher order phase SCCK codewords. This equation uses the same CCK kernel that is formed using Golay's rule for length expansion that is mentioned in Chapter 2.

### **7.2.2 9- bit/s/Hz High order Spatial Complementary Code Keying**

In the case of 8-phase 4-SCCK, with codewords of length 4, a spectral efficiency of 9 bit/s/Hz is obtained with 512 codewords, which is higher than the previous 8-SCCK case with four phases with 6 bit/s/Hz spectral efficiency.

### **7.2.3 12- bit/s/Hz High order Spatial Complementary Code Keying.**

For 8-phase 8-SCCK with codewords of length 8, a spectral efficiency of 12-bit/s/Hz is obtained with 4096 codewords, which is higher than the previous 8-SCCK case with four phases, which gave 12 bit/s/Hz spectral efficiency.

The phase arrangement of 8-SCCK, which uses eight phases identified as  $(0, \frac{\pi}{4}, \pi/2, 3\pi/2, \pi, -\frac{\pi}{4}, -\pi/2, -3\pi/2)$ .

### **7.2.4 15- bit/s/Hz High order Spatial Complementary Code Keying.**

A new mechanism utilizing a greater number of transmit antennas than the previous case of 8-SCCK is 16-SCCK, which has been presented for the first time in this thesis. 8-phase 16-SCCK with codewords of length 16 produces a spectral efficiency of 15-bit/s/Hz, with 32768 codewords being generated. This is higher than the previous 16-SCCK case with four phases, with 10 bit/s/Hz spectral efficiency.

The phase arrangement of 16-SCCK, which uses eight phases identified as  $(0, \frac{\pi}{4}, \pi/2, 3\pi/2, \pi, -\frac{\pi}{4}, -\pi/2, -3\pi/2)$ . And the eight phases generates 32768 codewords with length 16

### **7.2.5 Minimum Distance Characteristics between Complementary Codewords.**

The distinguishing property of SCCK codewords is of the large number of codewords that have large Euclidian distance, and the application of these codewords to the proposed system.

For instance, in the case of 2-SCCK, by applying 8 phase positions will result in 64 codewords each of length 2 chips. For each of the  $64 \times 64 = 4096$  possible pairs of codewords, the Euclidean distance was calculated in Table (7.1).

As shown in the Table 7.1 the codeword pairs which have large Euclidean distances is more than the codewords pairs with small Euclidean distances. For example, the number of codeword pairs with Euclidean distance higher than or equal to 1.6 as an average number in the Table 7.1 is 3242, compared to 742 codeword pairs with Euclidean distance less than 1.6.

<b>Euclidean distance</b>	<b>Number of codewords pairs</b>
2.82	64
2.72	256
2.61	256
2.45	256
2.32	490
2.14	256
2	896
1.85	256
1.6	512
1.4	244
1.08	256
0.765	242

**Table 7.1:**The Euclidean distance comparison between the codewords of high order 2-SCCK

### **7.3 Theoretical and simulations BER performance results for 8-phase SCCK with narrowband channel**

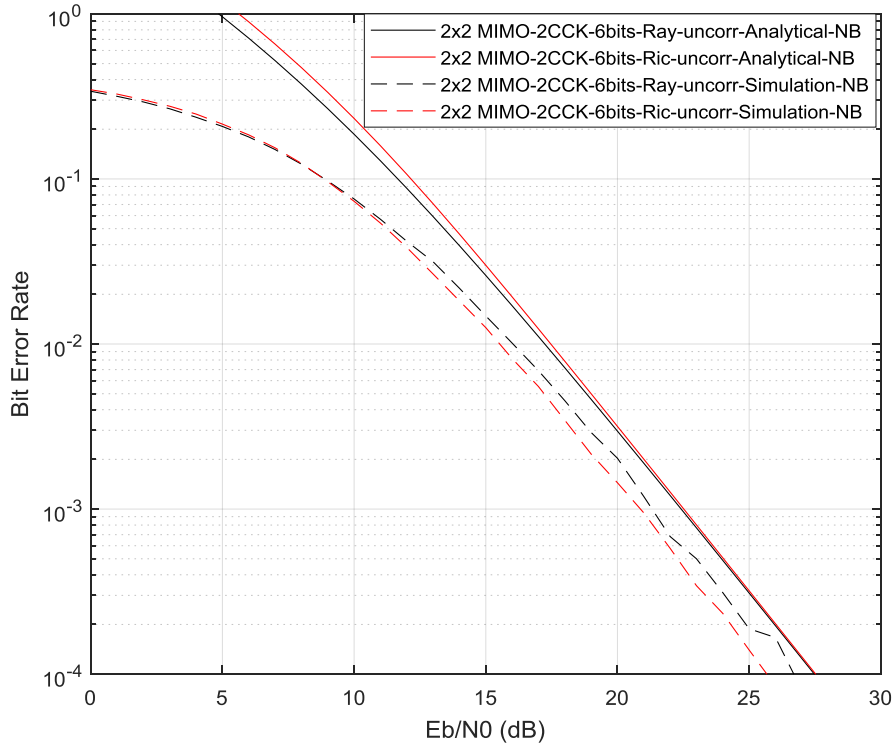
As discussed in Chapter 4 the average BER of SCCK modulation as given by the union bound but with 8 phases instead of four phases [6]

#### **7.3.1 Analytical and simulation results comparison.**

In this section the analytical and Monte Carlo simulation results are discussed based on narrowband Rayleigh and Rician wireless channels, and with different SCCK codeword lengths. The K factor in terms of the Rician channel is set as  $K= 3$  dB, the correlation factor in both transmit and receive antennas is set to be  $c= 0.5$  as a moderate quantity to test the system under more realistic environment conditions.

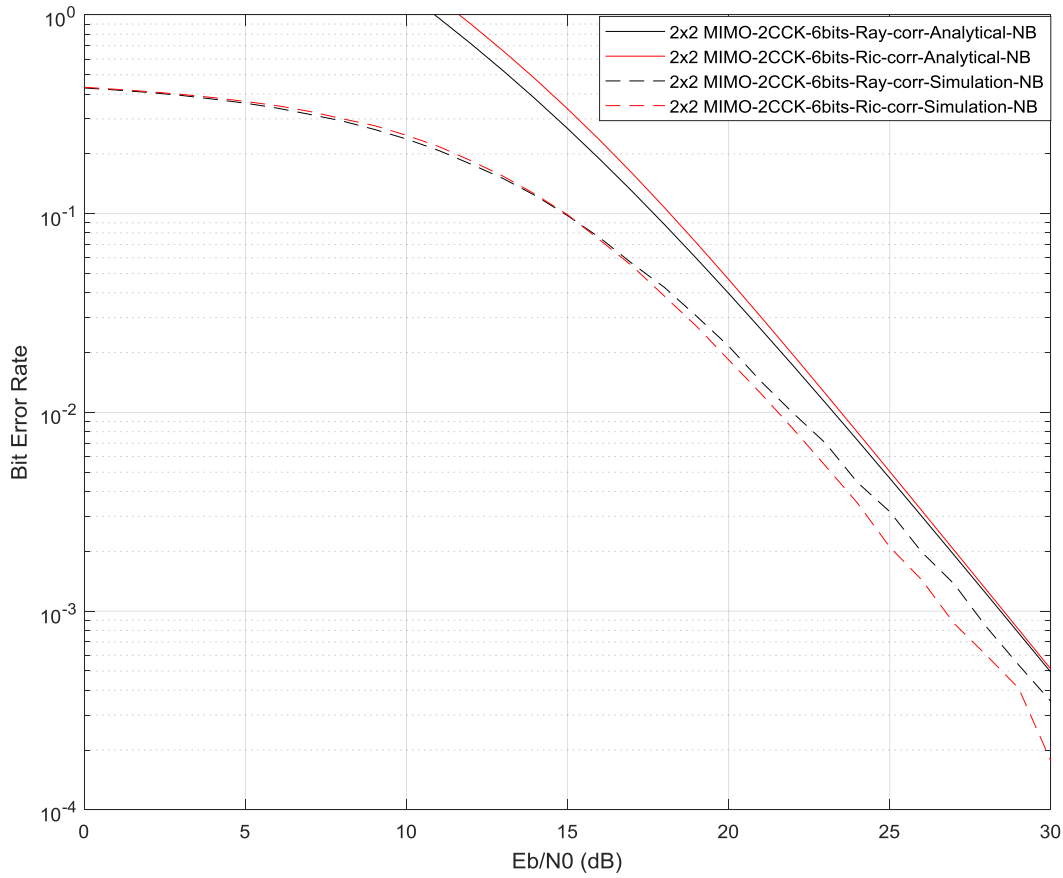
### 7.3.1.1 6 bit/s/Hz High order phase 2-SCCK with Rayleigh/Rician uncorrelated fading channel

Fig 7.2 plots the theoretical BER versus  $E_b/N_0$  for 2-SCCK high order modulation phases over uncorrelated Rayleigh and Rician channels with  $K = 3$  dB, and the spectral efficiency is  $m= 6$ . It shows the similarity between theoretical and simulated results. It is also seen that there is considerable improvement in BER performance over a  $E_b/N_0$  range of high order phases SCCK system.



**Figure 7.2:** Theoretical BER versus  $E_b/N_0$  for SCCK modulation over uncorrelated Rayleigh/Rician channels with  $K = 3$  dB, where  $m = 6$  and  $N_t = N_r = 2$ . (Solid line) analytical, (Dashed line) simulation

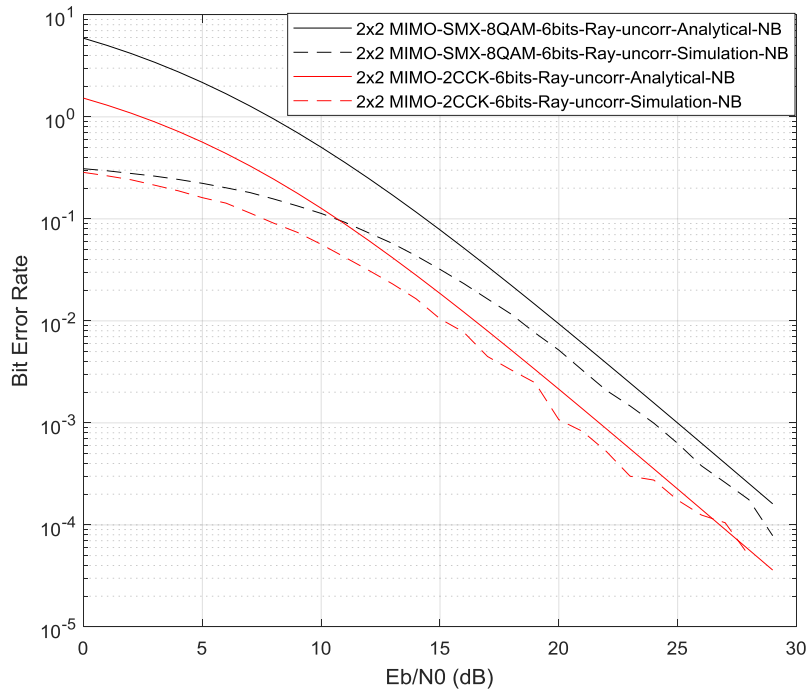
In the case of including channel correlation effects, Fig. 7.3 presents the comparison with the same trend as Fig. 7.2, but including the correlation effect of  $c=0.5$  in both transmit and receive sides. The comparison shows the effect of correlation, which reaches 6 dB of degradation compared with uncorrelated channel in Fig. 7.2



**Figure 7.3:** Theoretical BER versus  $E_b/N_0$  for SCCK modulation over correlated Rayleigh/Rician channels with  $K = 3$  dB, where  $m = 6$  and  $N_t = N_r = 2$ . (Solid line) analytical, (Dashed line) simulation

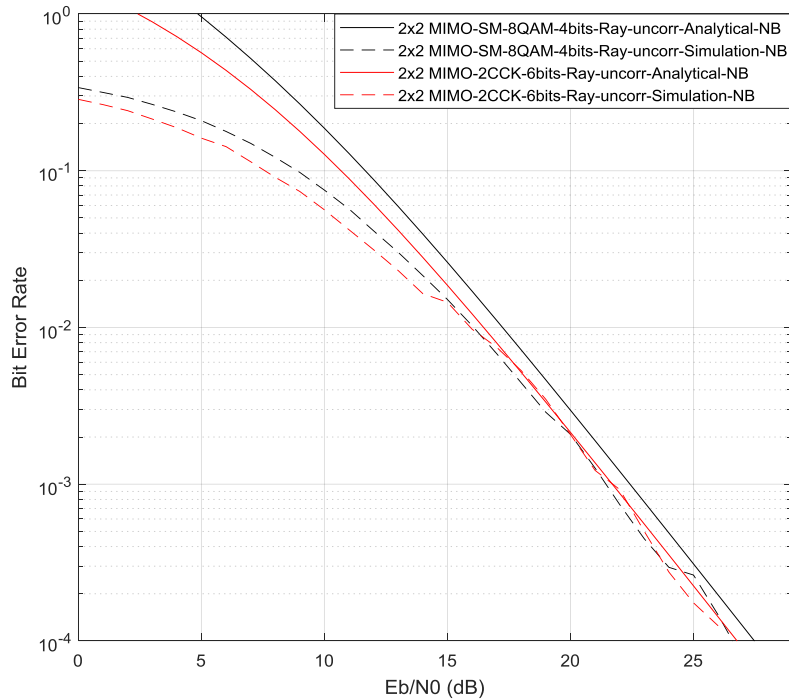
### 7.3.1.2 2-SCCK High order phase compared with SM system

Fig. 7.4 shows the theoretical BER versus  $E_b/N_0$  for SCCK compared to SMX over uncorrelated Rayleigh channels, where  $m = 6$  bit/s/Hz in both systems and  $N_T = N_R = 2$ , using ML for signal detection. The SMX use 8-QAM, so the simulated results for 2-SCCK with ML detection and 8 phases displays better BER performance than that for SMX with the same phase order. This is despite the higher complexity of SMX compared with SCCK system.



**Figure 7.4:** Theoretical BER versus  $E_b/N_0$  for SCCKM and SMX over uncorrelated Rayleigh channels, where  $m = 6$  and  $N_t = N_r = 2$ . (Dashed line) simulation, (Solid line) Analytical

In the case of comparing SCCK systems with SM systems under the same channel conditions and detection scheme, Fig 7.5 presents the theoretical BER versus  $E_b/N_0$  over uncorrelated Rayleigh channels. Here  $m = 6$  bit/s/Hz in the SCCK system and  $m=4$  bit/s/Hz in the SM system, and  $N_T = N_R = 2$ . The simulated results for SCCK system with codeword length 2 displays slight improvement over that for SM with the same number of constellation points, also with greater spectral efficiency than SM.

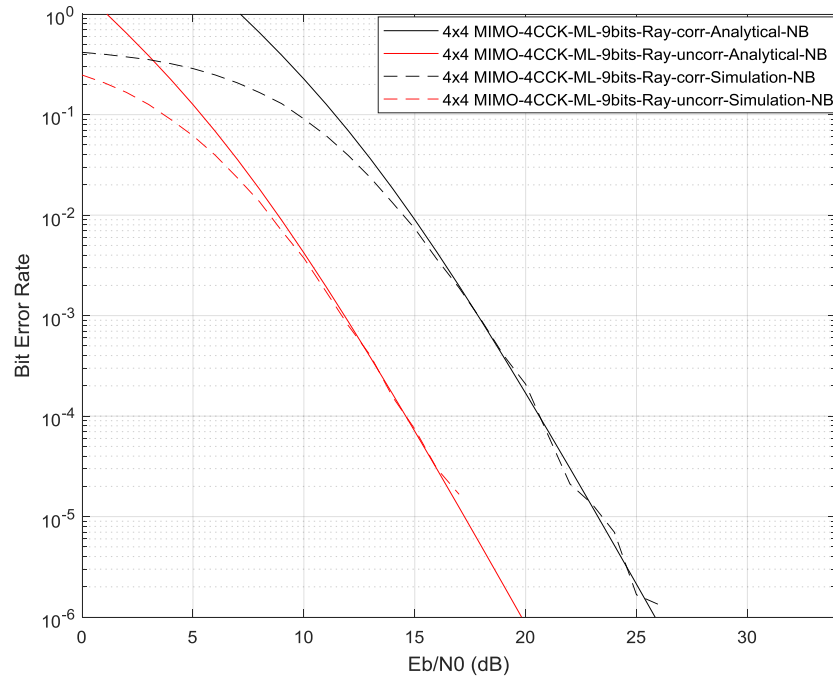


**Figure 7.5:** Theoretical BER versus  $E_b/N_0$  for SCCK and SM over uncorrelated Rayleigh channels, where  $N_t = N_r = 2$ . (Dashed line) simulation, (Solid line) Analytical

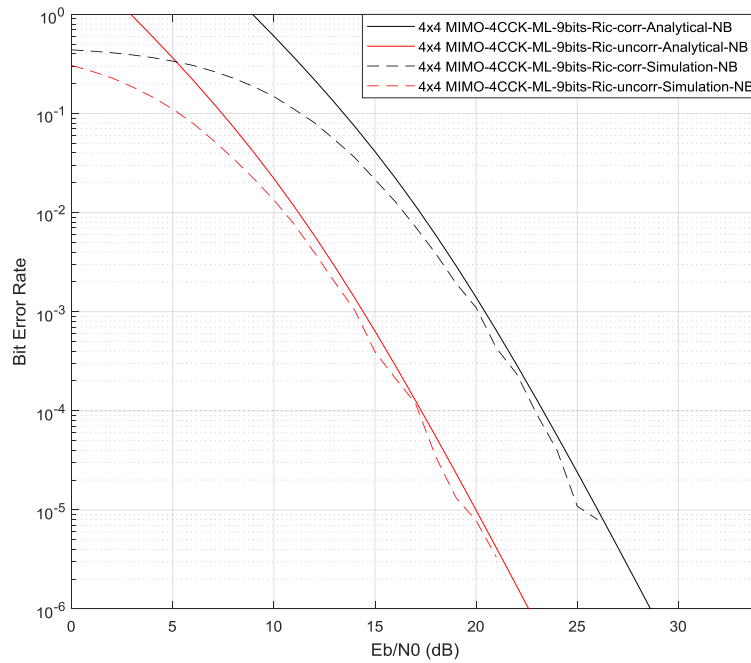
### 7.3.1.3 9 bit/s/Hz High order phase 4-SCCK with Rayleigh/Rician uncorrelated fading channel

Fig 7.6 shows the theoretical BER versus  $E_b/N_0$  of Spatial CCK modulation system with 4-SCCK and 8 modulation phases, meaning 9 bit/s/Hz, under uncorrelated and correlated Rayleigh channels with correlation factor  $c=0.5$  at both transmit and receive sides. The correlation effect is obvious in this case, where the BER performance degradation of the correlated channel reaches approximately 5 dB compared with the uncorrelated case.

Fig. 7.7 presents the same trend as Fig. 7.6 with a different wireless channel, here a Rician channel with K factor equal to 3 dB. The results show a degradation by 5 dB compared with the Rician uncorrelated channel.



**Figure 7.6:** Theoretical BER versus  $E_b/N_0$  for SCCK modulation over uncorrelated/correlated Rayleigh channels, where  $m = 9$  and  $N_t = N_r = 4$ . (Solid line) analytical, (Dashed line) simulation



**Figure 7.7:** Theoretical BER versus  $E_b/N_0$  for SCCK modulation over uncorrelated/correlated Rician channels, where  $m = 9$  and  $N_t = N_r = 4$ . (Solid line) analytical, (Dashed line) simulation

### 7.3.1.4 4-SCCK High order phase compared with SM system

To compare 4-SCCK results with the state of the art, Fig. 7.8 shows the comparison between the 4-SCCK system and the SM scheme discussed previously in Chapter 5 under the same channel conditions and detection scheme. The same number of transmit and receive antennas are used, as well as the same number of constellation points. In terms of the different spectral efficiencies of both systems, discussed in Chapter 5, the proposed system results in higher spectral efficiency under the same number of constellation points as well as the same transmit and receive antennas.

In addition to improving the spectral efficiency, the system BER performance is improved by approximately 2.2 dB compared with SM.

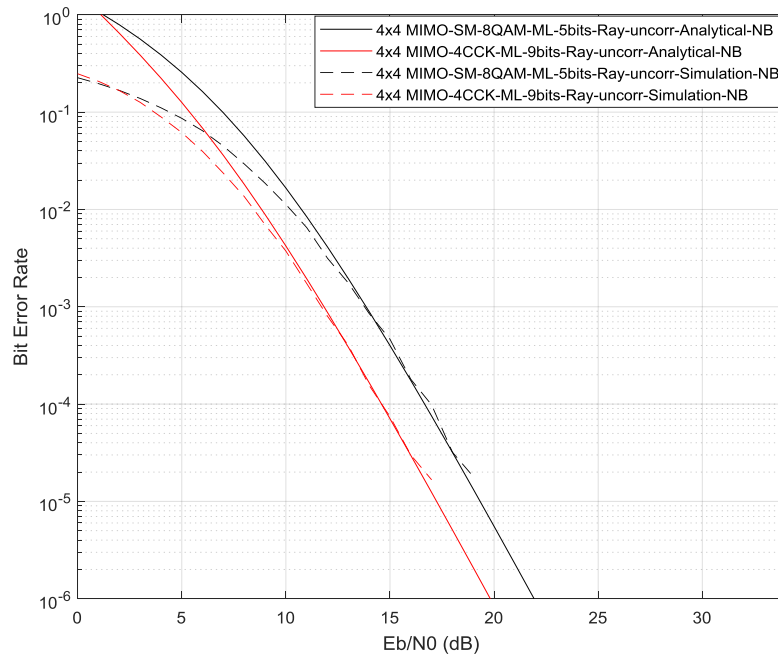


**Figure 7.8:** Theoretical BER versus  $E_b/N_0$  for SCCKM and SM over uncorrelated Rayleigh channels, where  $N_t = N_r = 4$ . (Dashed line) simulation, (Solid line) Analytical

### 7.3.1.5 12 bit/s/Hz High order phase 8-SCCK with Rayleigh uncorrelated fading channel

As with the same trend as discussed above, Fig. 7.9 shows the theoretical BER versus  $E_b/N_0$  for 8-SCCK modulation over an uncorrelated Rayleigh channel, with higher spectral efficiency  $m=12$  bit/s/Hz and higher number of transmit and receive antennas  $N_T = N_R=8$  than the previous 2 and 4-SCCK cases. It shows the same difference between theoretical (solid black curve) and simulated

(dash black curve) results. It is also seen that there is considerable improvement in BER performance over a range of  $E_b/N_0$  for the proposed higher order SCCK system, and this trend of results indicates that the system is effective in noisy environment in the case of increasing the number of antennas at the transmitter and receiver, in parallel with the noticeable improvement in BER performance at low  $E_b/N_0$  ranges.

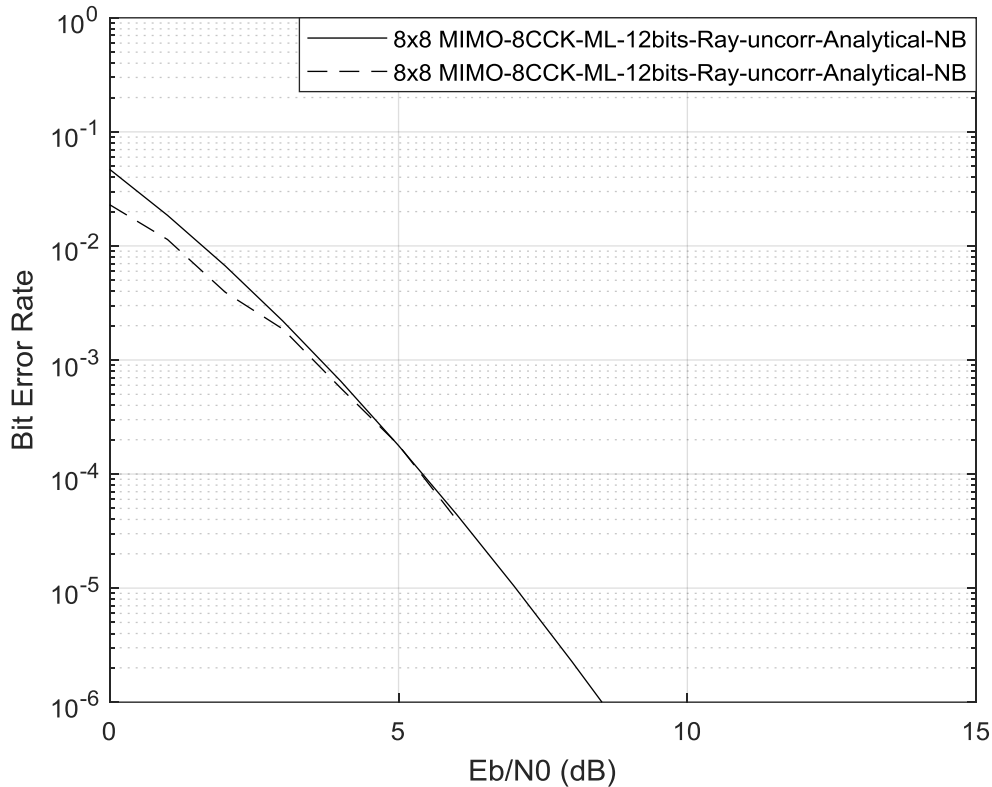


**Figure 7.9:** Theoretical BER versus  $E_b/N_0$  for SCCK modulation over uncorrelated Rayleigh channel, where  $N_t = N_r = 8$ . (Solid line) analytical, (Dashed line) simulation

### 7.3.1.6 8-SCCK High order phase compared with SM system

In the case of comparing with the SM results discussed in Chapter 5, Fig. 7.10 compares the same systems under the same Rayleigh channel conditions and the same detection schemes as well as the same number of constellation points, which here is equal to 8. The contribution shows the proposed system completely exceeds the SM system in terms of higher spectral efficiency and the noticeable improvement in BER performance, that reaches approximately 5 dB both analytically (solid curve) and in Monte Carlo simulations (dashed line). For example, the SM scheme with 8

transmit and receive antennas needs a modulation order of 512 QAM to reach 12 bit/s/Hz spectral efficiency, which 8x8 MIMO 8-SCCK system achieves with just 8-phases. The higher modulation order in the SM case leads to more complexity in detecting symbols, leading to degradation in BER performance.

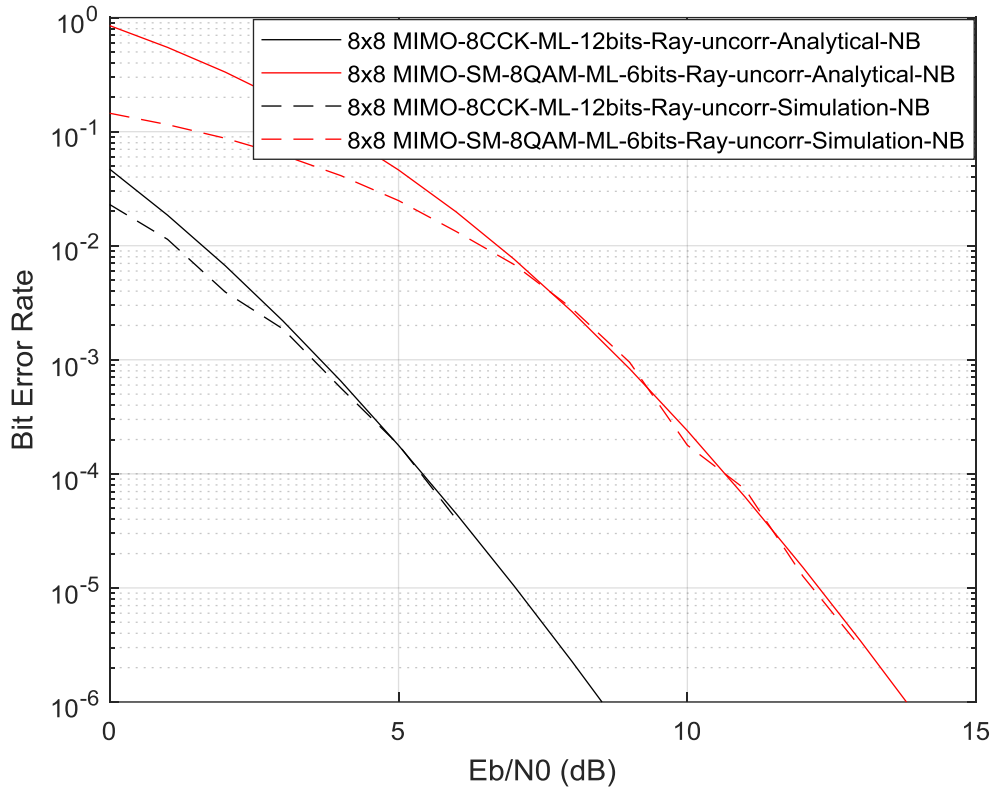


**Figure 7.10:** Theoretical BER versus  $E_b/N_0$  for SCCK and SM modulation comparison over uncorrelated Rayleigh channel, where  $N_t = N_r = 8$ . (Solid line) analytical, (Dashed line) simulation

## 7.4 Simulations results for 8-phase SCCK with wideband IEEE fading channels.

Various MIMO systems are considered, and 1000 packets are transmitted, each packet containing 20 OFDM symbols. With RMS delay spreads of 50, 100 and 150 ns, the channel is an IEEE time-variant frequency-selective multipath channel, which changes every packet. Additionally, these channels are statistically independent. The noise is AWGN. It is assumed that there is perfect time and frequency synchronization, and full knowledge of the channel is accessible at the receiver.  $E_b/N_0$  is used for the normalized signal-to-noise ratio.

### 7.4.1 Comparison between conventional 4-phase and 8-phase SCCK with detection schemes under wideband IEEE fading channel.

This section studies the comparison between the 8-phase SCCK systems and the 4-phase SCCK discussed in Chapter 4, in terms of the same SCCK codeword lengths and the same ZF detection schemes, as well as the same Rayleigh and Rician fading wireless channels. However, the spectral efficiencies are different because of the different modulation order phases.

#### 7.4.1.1: 4-8 phases BER performance comparison of 2x2 conventional SCCK

Fig. 7.11 shows BER versus  $E_b/N_0$  to compare between conventional 4 and 8 phases 2-SCCK systems, over an uncorrelated wideband IEEE Rician channel using ZF detection schemes. The systems give  $m = 2$  and 6 bit/s/Hz respectively, and with  $N_T = N_R = 2$  and RMS delay spread of 50 ns. The 2-SCCK system with 4-phases is gained approximately 7 dB at  $10^{-3}$  BER in trade off with spectral efficiency, compared with 2-SCCK with 8-phases.

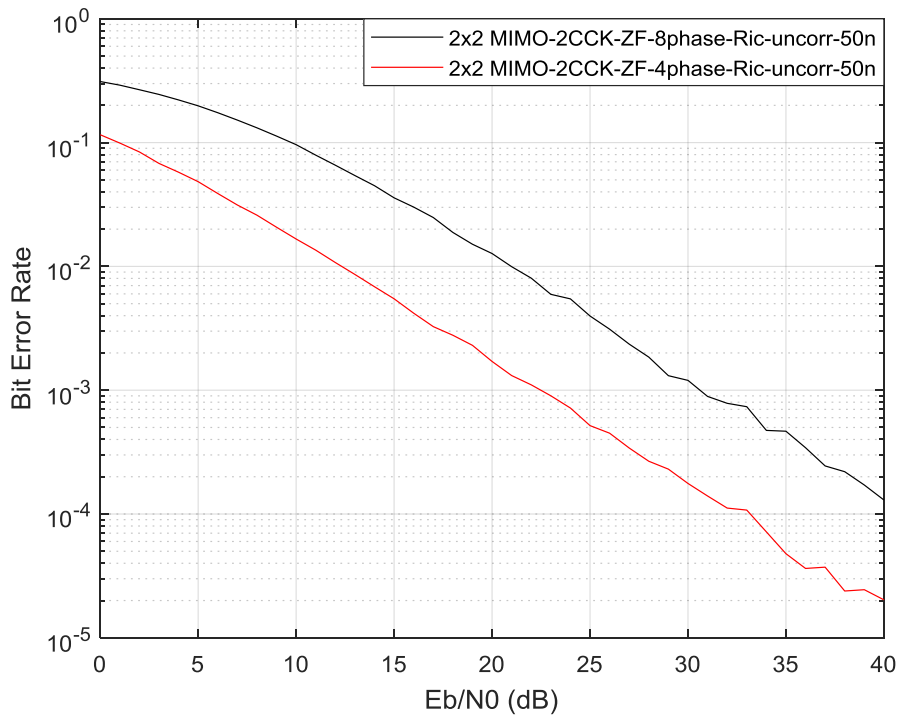


**Figure 7.11:** BER versus  $E_b/N_0$  comparison between conventional 4 and 8 phase SCCK over uncorrelated Rician channel and ZF detection scheme with  $m = 4, 6$  respectively, where  $N_t = N_r = 2$  and RMS delay spread=50 ns.

### 7.4.1.2: 4-8 phases BER performance comparison of 4x4 conventional SCCK

Fig. 7.12 plots BER Vs  $E_b/N_0$  comparing 4-phase SCCK with 8-phase SCCK for 4 transmit and receive antennas, in a uncorrelated Rayleigh channel. At  $10^{-3}$  BER, 4-phase SCCK achieves a SNR gain of approximately 5 dB over 8-phase SCCK with ZF detection, in trade off with the spectral efficiency.

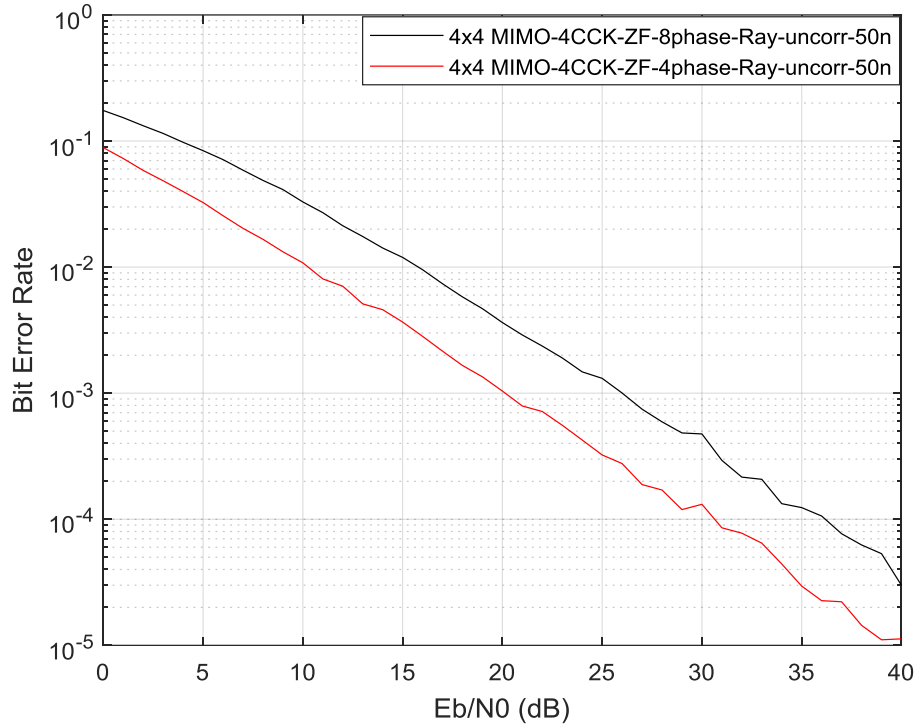


**Figure 7.12:** BER versus  $E_b/N_0$  comparison between conventional 4 and 8 phase SCCK over uncorrelated Rayleigh channel and ZF detection scheme with  $m = 6, 9$  respectively, where  $N_t = N_r = 4$  and RMS delay spread=50 ns

### 7.4.1.3: 4-8 phases BER performance comparison of 8x8 conventional SCCK

Fig 7.13 shows the BER performance comparison between 4 phase 8-SCCK (black curve) and 8 phase 8-SCCK (red curve) with  $m= 8$  and 12 bit/s/Hz respectively, while using a ZF detection scheme. The BER performance in terms of 4-phases gained nearly 2.5 dB at  $10^{-3}$  BER compared with 8-phases, in trade off with spectral efficiency.

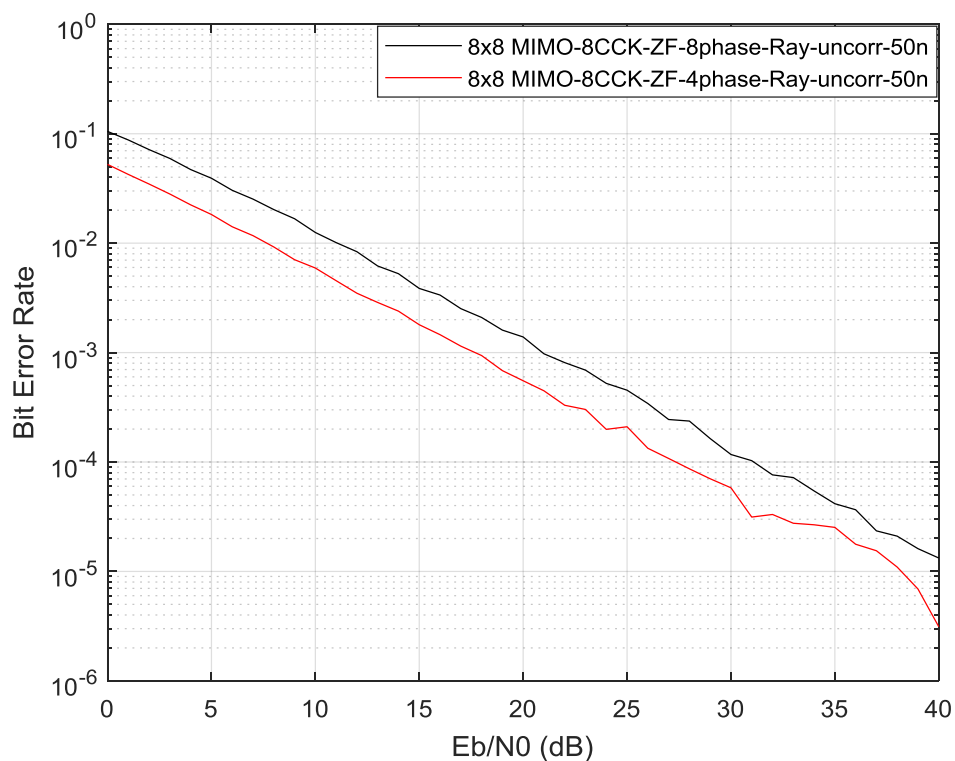


**Figure 7.13:** BER versus Eb/No comparison between conventional 4-8 phase SCCK over uncorrelated Rayleigh channel and ZF detection schemes with  $m = 8, 12$  respectively, where  $N_t = N_r = 8$  and RMS delay spread=50 ns

#### 7.4.1.4: 4-8 phases BER performance comparison of 16x16 conventional SCCK

Fig. 7.14 presents a key contribution, with 8-phase 16-SCCK system in the case of a wideband IEEE uncorrelated Rayleigh channel, which results in approximately the same BER performance, with increased spectral efficiency, as the 4-phase 16-SCCK system.

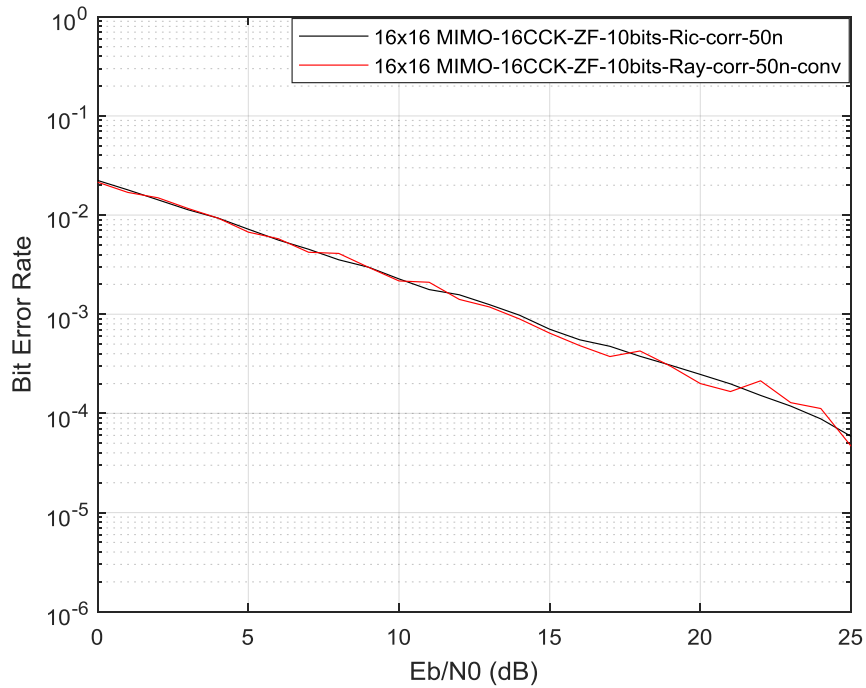


**Figure 7.14:** BER versus Eb/No comparison between conventional 4 and 8 phase SCCK over uncorrelated Rayleigh channel and ZF detection scheme with  $m = 10, 15$  respectively, where  $N_t = N_r = 16$  and RMS delay spread=50 ns

## 7.5. Summary

It is concluded that SCCK is a promising spatial block coded modulation scheme based on different codeword lengths of CCK, which shows a significant enhancement in system throughput. SCCK modulation benefits from large Euclidean distances between codeword pairs, which enhances its resistance to interference and improves BER performance. The system was tested and evaluated with 8-phases, which results in high spectral efficiency compared with the previous 4-phase SCCK and modified SCCK, discussed in Chapters 4 and 6 respectively, over both correlated and uncorrelated Rayleigh and Rician channels, using different detection techniques such as ZF, MMSE and ML. However, some results show obvious BER performance degradation in correlated channels and with different ZF and MMSE detection schemes in the case of wideband IEEE channels, especially in large SCCK code sets. Future work will check with different wideband channels. An important contribution in this chapter is the analytical BER performance of a 8-phase SCCK system for narrowband channels with ML detection scheme. The comparison with SM and SMX shows fundamental gains.

## Chapter 8                      Conclusions and Future Work

### 8.1 Conclusions

Beneficial code sets for spatial communications applications require large Euclidean distance properties. Complementary codewords in the spatial domain have the useful property that a large number of codeword pairs have large Euclidean distances compared with the number of codeword pairs with small Euclidean distance in each CCK code set. This leads to improved BER performance.

In terms of the spatial domain, the large Euclidean distance between the majorities of codeword pairs generated in each SCCK set makes them more distinct to detect at the receiver with less interference than comparable codes.

Each SCCK code is characterised by a fixed phase order. Four and eight phase SCCK have been studied in the thesis but 2, 16, 32 and further phases are also possible. Such higher order phases increase spectral efficiency.

In this regard, this thesis began with the aim of providing a collection of general guidelines and recommendations on spatial modulation techniques to support the rapid growth in mobile data traffic in parallel with less complexity in system implementation in either the transmitter or receiver.

First, the thesis, aims, objectives and motivation were introduced in Chapter 1. Chapter 2 presented an extensive discussion of MIMO-OFDM system stages and the CCK code generation.

Chapter 3 discussed a review of the open literature related to a spatial block coding based on complementary code keying (CCK) sequences. It has shown that CCK techniques can achieve higher spectral efficiencies through the deployment of larger code sets and BER improvement compared with spatial modulation (SM). This chapter included a brief discussion of both SM and SMX, which are the systems we compare with the proposed spatial CCK in terms of both BER performance and spectral efficiency.

Chapter 4 discusses conventional spatial CCK (i.e. 4-phase) in terms of codeword lengths 2, 4, 8 and 16 elements. This system is firstly applied in a MIMO-OFDM system with an IEEE multipath

channel. ZF, MMSE and ML detection schemes are applied. An important result is the BER improvement achieved through increasing the number of receive antennas. Rician fading channels were applied in the same system to examine the performance when a LOS component is present. The results showed that the system performance in Rayleigh channels is slightly better compared with in Rician channels as the latter has less diversity. The exponential Kronecker correlation model is applied for a more realistic evaluation and the results showed that correlation at both transmit and receive sides substantially degrade the BER performance. Another important contribution from chapter 4 was the union bound analytical model SCCK in narrowband channels characterised by Rayleigh, Rician, correlated or uncorrelated fading channels. The analytical results were compared with Monte Carlo simulation, which gives approximately similar BERs especially at high  $E_b/N_0$  values.

Chapter 5 compared the BER performance of the proposed SCCK system, with SM and SMX. The comparison between SMX, SM and SCCK over Rayleigh and Rician fading was studied. These results show that the SCCK system provides noticeably better performance than both SM and SMX for the same spectral efficiency. SCCK exhibits a BER performance that improves with the increase of the number of transmit antennas, and a reduction in receiver complexity when compared to SMX.

Chapter 6 in this thesis reproduces the modified SCCK system in [6], which uses a non-conventional code-generating phases. Chapter 6 regenerates the results for modified SCCK under the same channel conditions. The results from simulation demonstrate a noticeable improvement in the BER performance of modified spatial CCK compared to conventional SCCK.

The chapter also extended the work in [6] to include a modified 16-SCCK codeword length with 11 bit/s/Hz spectral efficiency. A total of 3125 codewords of length 16 were generated and 2048 codewords with the largest Euclidean distance were chosen to get an 11 bit/s/Hz spectral efficiency.

Comparing the modified 16-SCCK system with the conventional 4-phase 16-SCCK and 10 bit/s/Hz spectral efficiency shows a decrease in BER performance of modified 16-SCCK, in trade off against an increase in the spectral efficiency.

A key contribution in chapter 6 is the analytical BER performance of the modified SCCK system in narrowband Rayleigh and Rician, uncorrelated and correlated channels. Comparing the results

with conventional SCCK confirms the slight improvement of modified SCCK while SE is decreased.

In Chapter 7 an SCCK system with 8-phases was tested and evaluated, which results in high spectral efficiency compared with the 4-phase SCCK discussed in Chapter 4. Comparisons over both correlated and uncorrelated Rayleigh and Rician channels, using different detection techniques such as ZF, MMSE and ML optimum detection were carried out.

There is a noticeable improvement in BER performance compared with the state of the art such as SM, SMX schemes under the same Rayleigh and Rician, correlated and uncorrelated channels, especially with 16-SCCK codeword length.

The key contribution is the analytical BER of 8-phase SCCK system in the case of narrowband channels and ML detection, the results shows noticeable improvement in BER performance compared to SM and SMX schemes.

The main contributions of this thesis are:

1. Evaluating the SCCK system with conventional 4-phases in case of wideband fading channel to compare the results with state of art (modified SCCK).
2. Extending both the phases from 4 to 8 phases and the SCCK codeword length from 2,4 and 8 to 16 SCCK and left the 32,64 and 128...etc and phases 16,32 and 64...etc to the future work.
3. The key contribution is an analytical model of 4 and 8 phase and modified SCCK in the case of narrowband channels, in both Rayleigh and Rician, correlated and uncorrelated fading channels, and comparing that with SM and SMX state of art system.

All in all, it has been shown that spatial CCK modulation is a promising system for P2P MIMO schemes and these results suggest the system as a promising system in future wireless communications applications.

## 8.2 Future work

1. To compare the SCCK scheme with generalised spatial modulation (GSM) in terms of spectral efficiency and number of transmit and receive antennas, accounting for the computational complexity of both schemes is the first future suggestion. GSM is proposed to increase the spectral efficiency while decreasing the overall number of transmit antennas compared with conventional SM. GSM is defined as the activation of more than one transmit antenna at a time to simultaneously transmit same data symbols.

In GSM, the information is transmitted in both the activated combination of transmit antennas, and the transmitted modulated signal. As a result, the number of transmit antennas needed to achieve a certain spectral efficiency is reduced by more than half compared with conventional SM. Transmitting the same data symbol from more than one antenna at a time keeps the key advantage of SM, which is the complete avoidance of inter channel interference ICI at the receiver. Moreover, GSM offers spatial diversity gains and increases the reliability of the wireless channel, by providing replicas of the transmitted signal to the receiver [10]. At the receiver, a maximum likelihood (ML) detection algorithm estimates the activated combination of transmit antennas and the transmitted constellation symbol. Additionally, comparing the SCCK system with GSM for the same spectral efficiency and modulation order in terms of BER and PER will show if the SCCK is still competitive compared with GSM.

2. Evaluating sensitivity to imperfect matrix inversion when reducing detector complexity.

The linear detectors need to invert the channel matrix i.e. ( $Z = HH^H$  find  $Z^{-1}$ ).

This inversion is computationally intensive for large arrays. To reduce complexity, evaluating the performance of the SCCK when matrix inversion algorithms of low complexity such as Neumann series, Gauss Sidel, Jacobi, conjugate Gradient and steepest decent are used.

3. Extending the narrowband NB analysis to include the Nakagami model and compare with Rayleigh/ Rician channels. The Nakagami-m distribution is a generalised approach to model small scale fading. Nakagami-m distribution is applied by trying to approximate the

amplitude/power of a received signal using a suitable distribution. Rayleigh distribution is sufficient to model amplitude in urban areas, Rician distribution suits better in sub-urban areas where LOS components exist, and Hoyt distribution models scintillation effects. Nakagami-m distribution is a generalised case and includes the three distributions as special cases. Therefore, Nakagami-m fading is equally applicable in any of the above mentioned fading environments ( $m < 1$  for Hoyt,  $m = 1$  for Rayleigh, and  $m > 1$  for Rician). As such, analysis with Nakagami-m fading aids understanding of SCCK performance in broad range of channels.

Reducing the complexity of the ML receiver using Fast Walsh Transform (FWT) with CCK codes.

Two stages describe the typical FWT CCK demodulator, accepts all eight chips of the CCK codeword simultaneously, which results sixty-four values outputs, the second stage is upon deploying the suggested systolic array design with its pipelining nature, instead of processing all eight chips of CCK in parallel during the first stage, every two chips can be processed immediately. At each stage, the resulted values are moved instantly to the next stage upon multiplying the appropriate constants. There are many advantages as a result of systolic array architecture over the conventional design. Firstly, a serial-to-parallel converter to convert serial incoming data to parallel blocks of eight chips is not required. This reduces hardware complexity. Secondly, every stage in the architecture is continuously processing data; whereas, in the conventional design, the hardware in each stage is left idle until inputs from the next eight chips block arrives. Thirdly, 28 butterflies are needed in a conventional design, but, only 13 butterflies are needed due to hardware reuse in the suggested architecture [111]. If this structure can be used for SCCK receivers, the implementation complexity could drop significantly compared with the ML receiver.

## References

- [1] S. Malisuwan, J. Sivaraks, N. Tiamnara, and Y. Thamachareon, "Performance Analysis of MIMO-OFDM Systems on Coexistence Environment in FDD-LTE Networks," *International Journal of Computer and Communication Engineering*, vol. 3, no. 5, p. 321, 2014.
- [2] H. Donelan and T. O'Farrell, "Families of ternary sequences with aperiodic zero correlation zones for MC-DS-CDMA," *Electronics Letters*, vol. 38, no. 25, pp. 1660-1661, 2002.
- [3] S. Sharma, M. Chakraborty, M. Singhal, and M. Jha, "A Review of 4G and 5G in Context of Future of Wireless Communication," *International Journal of Computer Applications*, vol. 95, no. 22, 2014.
- [4] A. Kafaltiya and P. Sharma, "Performance Improvement in MIMO-OFDM using BCH Coding and Interleaving," *International Journal of Computer Applications*, vol. 97, no. 2, 2014.
- [5] P. Sharma, "Evolution of mobile wireless communication networks-1G to 5G as well as future prospective of next generation communication network," *International Journal of Computer Science and Mobile Computing*, vol. 2, no. 8, pp. 47-53, 2013.
- [6] J. Thompson *et al.*, "5G wireless communication systems: Prospects and challenges," *IEEE Commun. Mag*, vol. 52, no. 2, pp. 62-64, 2014.
- [7] R. MacKenzie and T. O'Farrell, "Throughput and delay analysis for p-persistent CSMA with heterogeneous traffic," *IEEE Transactions on Communications*, vol. 58, no. 10, pp. 2881-2891, 2010.
- [8] R. Mesleh, H. Haas, S. Sinanovic, C. W. Ahn, and S. Yun, "Spatial modulation," *IEEE Transactions on Vehicular Technology*, vol. 57, no. 4, p. 2228, 2008.
- [9] A. H. Jafari and T. O'Farrell, "Performance Evaluation of Spatial Complementary Code Keying Modulation in MIMO Systems," *arXiv preprint arXiv:1709.05525*, 2017.
- [10] J. Mitola *et al.*, "Accelerating 5G QoE via public-private spectrum sharing," *IEEE Communications Magazine*, vol. 52, no. 5, pp. 77-85, 2014.
- [11] A. Younis *et al.*, "Performance of spatial modulation using measured real-world channels," in *Vehicular Technology Conference (VTC Fall), 2013 IEEE 78th*, 2013, pp. 1-5: IEEE.
- [12] C. U. Ndujiuba, O. Oshin, and N. Nkordeh, "MIMO deficiencies due to antenna coupling," *International Journal of Networks and Communications*, vol. 5, no. 1, pp. 10-17, 2015.

- [13] R. Khanduri and S. Rattan, "Performance Comparison Analysis between IEEE 802.11 a/b/g/n Standards," *International Journal of Computer Applications*, vol. 78, no. 1, pp. 13-20, 2013.
- [14] L. Verma, M. Fakharzadeh, and S. Choi, "Wifi on steroids: 802.11 ac and 802.11 ad," *IEEE Wireless Communications*, vol. 20, no. 6, pp. 30-35, 2013.
- [15] C. Andren, "CCK, the new IEEE 802.11 standard for 2.4 GHz wireless LANs," in *International IC Conf. Proceedings May 3, 2000*, 2000.
- [16] S.-b. Liu, A. Huang, Z.-y. Zhang, and Z. Zhang, "Performance analysis of cck modulation under multipath fading channel," in *Signal Processing Symposium, 2004. NORISIG 2004. Proceedings of the 6th Nordic*, 2004, pp. 276-279: IEEE.
- [17] B. Pearson, "Complementary code keying made simple," *Intersil, Milpitas, CA, USA, Application Notes AN9850*, vol. 1, 2000.
- [18] R. D. Van Nee, "OFDM codes for peak-to-average power reduction and error correction," in *Global Telecommunications Conference, 1996. GLOBECOM'96. Communications: The Key to Global Prosperity*, 1996, vol. 1, pp. 740-744: IEEE.
- [19] K. Halford, S. Halford, M. Webster, and C. Andren, "Complementary code keying for RAKE-based indoor wireless communication," in *Circuits and Systems, 1999. ISCAS'99. Proceedings of the 1999 IEEE International Symposium on*, 1999, vol. 4, pp. 427-430: IEEE.
- [20] R. Frank, "Polyphase complementary codes," *IEEE Transactions on Information theory*, vol. 26, no. 6, pp. 641-647, 1980.
- [21] R. Handayani, A. Muayyadi, and R. Pudjiastuti, "Performance analysis of CCK-OFDM over fading channel," in *2013 19th Asia-Pacific Conference on Communications (APCC)*, 2013, pp. 63-68.
- [22] C. Andren, "CCK modulation delivers 11Mbps for high rate IEEE 802.11 extention," in *Wireless Symposium/Portable by Design Conference Spring, 1999*, 1999.
- [23] J. Wu, N.-J. Tai, Z.-H. Zhang, and W.-J. Tian, "Performance Analysis of M-ary Multi-Orthogonal Keying," in *Wireless Communications, Networking and Mobile Computing, 2008. WiCOM'08. 4th International Conference on*, 2008, pp. 1-4: IEEE.
- [24] Y. S. Cho, J. Kim, W. Y. Yang, and C. G. Kang, *MIMO-OFDM wireless communications with MATLAB*. John Wiley & Sons, 2010.

- [25] V. Kuhn, *Wireless communications over MIMO channels: applications to CDMA and multiple antenna systems*. John Wiley & Sons, 2006.
- [26] G. L. STÜBER, "Principles of Mobile Communication, Georgia Institute of Technology," *Atlanta. Kluwer Academic Publishers. Georgia. USA*, 2002.
- [27] S. M. Alamouti, "A simple transmit diversity technique for wireless communications," *IEEE Journal on selected areas in communications*, vol. 16, no. 8, pp. 1451-1458, 1998.
- [28] M. Jankiraman, *Space-time codes and MIMO systems*. Artech House, 2004.
- [29] A. Neubauer, J. Freudenberger, and V. Kuhn, *Coding theory: algorithms, architectures and applications*. John Wiley & Sons, 2007.
- [30] B. Vucetic and J. Yuan, *Space-time coding*. John Wiley & Sons, 2003.
- [31] A. Goldsmith, *Wireless communications*. Cambridge university press, 2005.
- [32] S. A. Joshi, T. Rukmini, and H. Mahesh, "Performance analysis of MIMO technology using V-BLAST technique for different linear detectors in a slow fading channel," in *Computational Intelligence and Computing Research (ICCIC), 2010 IEEE International Conference on*, 2010, pp. 1-4: IEEE.
- [33] M. Viswanathan, "Simulation of digital communication systems using Matlab," *Mathuranathan Viswanathan at Smashwords*, 2013.
- [34] B. Sklar, *Digital communications*. Prentice Hall Upper Saddle River, 2001.
- [35] A. F. Molisch and M. Z. Win, "MIMO systems with antenna selection," *IEEE microwave magazine*, vol. 5, no. 1, pp. 46-56, 2004.
- [36] J. Mietzner, "Spatial diversity in MIMO communication systems with distributed or co-located antennas," *Universitätsbibliothek Kiel*, 2006.
- [37] E. Biglieri, R. Calderbank, A. Constantinides, A. Goldsmith, A. Paulraj, and H. V. Poor, *MIMO wireless communications*. Cambridge university press, 2007.
- [38] J. G. Andrews, A. Ghosh, and R. Muhamed, *Fundamentals of WiMAX: understanding broadband wireless networking*. Pearson Education, 2007.
- [39] R. Xu, "Study of multiple-input multiple-output systems over fading channels," *The Hong Kong Polytechnic University*, 2007.
- [40] F. De Flaviis, L. Jofre, J. Romeu, and A. Grau, "Multiantenna systems for MIMO communications," *Synthesis Lectures on Antennas*, vol. 3, no. 1, pp. 1-250, 2008.

- [41] G. J. Foschini, "Layered space-time architecture for wireless communication in a fading environment when using multi-element antennas," *Bell labs technical journal*, vol. 1, no. 2, pp. 41-59, 1996.
- [42] G. J. Foschini and M. J. Gans, "On limits of wireless communications in a fading environment when using multiple antennas," *Wireless personal communications*, vol. 6, no. 3, pp. 311-335, 1998.
- [43] G. Golden, C. Foschini, R. A. Valenzuela, and P. Wolniansky, "Detection algorithm and initial laboratory results using V-BLAST space-time communication architecture," *Electronics letters*, vol. 35, no. 1, pp. 14-16, 1999.
- [44] P. W. Wolniansky, G. J. Foschini, G. Golden, and R. A. Valenzuela, "V-BLAST: An architecture for realizing very high data rates over the rich-scattering wireless channel," in *Signals, Systems, and Electronics, 1998. ISSSE 98. 1998 URSI International Symposium on*, 1998, pp. 295-300: IEEE.
- [45] M. Sellathurai and S. Haykin, "TURBO-BLAST for high-speed wireless communications," in *Wireless Communications and Networking Conference, 2000. WCNC. 2000 IEEE*, 2000, vol. 1, pp. 315-320: IEEE.
- [46] M. Sellathurai and S. Haykin, "A simplified diagonal BLAST architecture with iterative parallel-interference cancellation receivers," in *Communications, 2001. ICC 2001. IEEE International Conference on*, 2001, vol. 10, pp. 3067-3071: IEEE.
- [47] V. Tarokh, N. Seshadri, and A. R. Calderbank, "Space-time codes for high data rate wireless communication: Performance criterion and code construction," *IEEE transactions on information theory*, vol. 44, no. 2, pp. 744-765, 1998.
- [48] A. Goldsmith, S. A. Jafar, N. Jindal, and S. Vishwanath, "Capacity limits of MIMO channels," *IEEE Journal on selected areas in Communications*, vol. 21, no. 5, pp. 684-702, 2003.
- [49] A. Van Zelst and J. Hammerschmidt, "A single coefficient spatial correlation model for multiple-input multiple-output (MIMO) radio channels," *Proc. 27th General Assembly of the International Union of Radio Science*, 2002.
- [50] D.-S. Shiu, G. J. Foschini, M. J. Gans, and J. M. Kahn, "Fading correlation and its effect on the capacity of multielement antenna systems," *IEEE Transactions on communications*, vol. 48, no. 3, pp. 502-513, 2000.

- [51] G. D. Durgin and T. S. Rappaport, "Effects of multipath angular spread on the spatial cross-correlation of received voltage envelopes," in *Vehicular Technology Conference, 1999 IEEE 49th*, 1999, vol. 2, pp. 996-1000: IEEE.
- [52] T. S. Rappaport, *Wireless communications: principles and practice*. prentice hall PTR New Jersey, 1996.
- [53] P. Stavroulakis, *Interference analysis and reduction for wireless systems*. Artech House, 2003.
- [54] S. Plevel, S. Tomazic, T. Javornik, and G. Kandus, "MIMO: Wireless communications," *Encyclopedia of Wireless and Mobile Communications*, 2008.
- [55] P. Dahiya, I. Student, and K. Gate, "Turbo coded MIMO-OFDM systems," *simulation*, vol. 3, no. 3, 2013.
- [56] S. H. Krishnamurthy, "Fundamental Limits and Joint Design of Wireless Systems with Vector Antennas," 2005.
- [57] C. Oestges and B. Clerckx, *MIMO wireless communications: from real-world propagation to space-time code design*. Academic Press, 2010.
- [58] S. Wu, W. Tong, and L. Strawczynski, "Adaptive time diversity and spatial diversity for OFDM," ed: Google Patents, 2006.
- [59] A. Arbi and T. O'Farrell, "Energy efficiency in 5G access networks: Small cell densification and high order sectorisation," in *2015 IEEE International Conference on Communication Workshop (ICCW)*, 2015, pp. 2806-2811: IEEE.
- [60] W. Nie, Y. Zhong, F.-C. Zheng, W. Zhang, and T. O'Farrell, "Hetnets with random dtx scheme: Local delay and energy efficiency," *IEEE Transactions on Vehicular Technology*, vol. 65, no. 8, pp. 6601-6613, 2016.
- [61] W. Guo and T. O'Farrell, "Capacity-energy-cost tradeoff in small cell networks," in *2012 IEEE 75th Vehicular Technology Conference (VTC Spring)*, 2012, pp. 1-5: IEEE.
- [62] M. Di Renzo, H. Haas, A. Ghayeb, S. Sugiura, and L. Hanzo, "Spatial modulation for generalized MIMO: Challenges, opportunities, and implementation," *Proceedings of the IEEE*, vol. 102, no. 1, pp. 56-103, 2014.
- [63] R. Mesleh, H. Haas, C. W. Ahn, and S. Yun, "Spatial modulation-a new low complexity spectral efficiency enhancing technique," in *Communications and Networking in China, 2006. ChinaCom'06. First International Conference on*, 2006, pp. 1-5: IEEE.

- [64] S. Ganesan, R. Mesleh, H. Ho, C. W. Ahn, and S. Yun, "On the performance of spatial modulation OFDM," in *Signals, Systems and Computers, 2006. ACSSC'06. Fortieth Asilomar Conference on*, 2006, pp. 1825-1829: IEEE.
- [65] A. Younis, N. Serafimovski, R. Mesleh, and H. Haas, "Generalised spatial modulation," in *Signals, Systems and Computers (ASILOMAR), 2010 Conference Record of the Forty Fourth Asilomar Conference on*, 2010, pp. 1498-1502: IEEE.
- [66] M. Maleki, H. R. Bahrami, A. Alizadeh, and N. H. Tran, "On the performance of spatial modulation: Optimal constellation breakdown," *IEEE Transactions on Communications*, vol. 62, no. 1, pp. 144-157, 2014.
- [67] R. Mesleh, H. Haas, C. Ahn, and S. Yun, "Spatial modulation-OFDM," in *Proc. of the International OFDM Workshop*, 2006, pp. 30-31.
- [68] M. Di Renzo, H. Haas, and P. M. Grant, "Spatial modulation for multiple-antenna wireless systems: A survey," *IEEE Communications Magazine*, vol. 49, no. 12, 2011.
- [69] H. Haas and S. McLaughlin, *Next generation mobile access technologies: Implementing TDD*. Cambridge University Press, 2007.
- [70] W. Jeong, H. Park, H. Lee, and S. Hwang, "Performance improvement techniques for CCK-OFDM WLAN modem," *IEEE Transactions on Consumer Electronics*, vol. 49, no. 3, pp. 602-605, 2003.
- [71] E. Telatar, "Capacity of multi-antenna Gaussian channels," *European transactions on telecommunications*, vol. 10, no. 6, pp. 585-595, 1999.
- [72] Y. J. Zhang and K. B. Letaief, "Adaptive resource allocation for multiaccess MIMO/OFDM systems with matched filtering," *IEEE Transactions on Communications*, vol. 53, no. 11, pp. 1810-1816, 2005.
- [73] Y. G. Li, J. H. Winters, and N. R. Sollenberger, "MIMO-OFDM for wireless communications: signal detection with enhanced channel estimation," *IEEE Transactions on communications*, vol. 50, no. 9, pp. 1471-1477, 2002.
- [74] I. W. Group, "IEEE 802.16-2004 Local and metropolitan area networks-Part 16: Air interface for fixed broadband wireless access systems IEEE Standard for Local and Metropolitan Area Networks [S]," ed: IEEE Computer Society Press, 2004.
- [75] H. El Gamal, "On the robustness of space-time coding," *IEEE Transactions on Signal Processing*, vol. 50, no. 10, pp. 2417-2428, 2002.

- [76] M. Godavarti, T. L. Marzetta, and S. Shamai, "Capacity of a mobile multiple-antenna wireless link with isotropically random Rician fading," *IEEE Transactions on Information Theory*, vol. 49, no. 12, pp. 3330-3334, 2003.
- [77] P. Viswanath, D. N. C. Tse, and V. Anantharam, "Asymptotically optimal water-filling in vector multiple-access channels," *IEEE Transactions on Information Theory*, vol. 47, no. 1, pp. 241-267, 2001.
- [78] G. G. Raleigh and J. M. Cioffi, "Spatio-temporal coding for wireless communication," *IEEE Transactions on communications*, vol. 46, no. 3, pp. 357-366, 1998.
- [79] S. Haykin and M. Moher, "In Modern Wireless Communications, 2005," ed: Prentice Hall.
- [80] H. Jafarkhani, *Space-time coding: theory and practice*. Cambridge university press, 2005.
- [81] M. O. Damen, A. Abdi, and M. Kaveh, "On the effect of correlated fading on several space-time coding and detection schemes," in *Vehicular Technology Conference, 2001. VTC 2001 Fall. IEEE VTS 54th*, 2001, vol. 1, pp. 13-16: IEEE.
- [82] A. M. Tonello, "Space-time bit-interleaved coded modulation with an iterative decoding strategy," in *Vehicular Technology Conference, 2000. IEEE-VTS Fall VTC 2000. 52nd*, 2000, vol. 1, pp. 473-478: IEEE.
- [83] J. Wang, S. Jia, and J. Song, "Generalised spatial modulation system with multiple active transmit antennas and low complexity detection scheme," *IEEE Transactions on Wireless Communications*, vol. 11, no. 4, pp. 1605-1615, 2012.
- [84] J. Jeganathan, A. Ghrayeb, and L. Szczecinski, "Spatial modulation: Optimal detection and performance analysis," *IEEE Communications Letters*, vol. 12, no. 8, 2008.
- [85] S. U. Hwang, S. Jeon, S. Lee, and J. Seo, "Soft-output ML detector for spatial modulation OFDM systems," *IEICE Electronics Express*, vol. 6, no. 19, pp. 1426-1431, 2009.
- [86] S. Sugiura and L. Hanzo, "Single-RF spatial modulation requires single-carrier transmission: Frequency-domain turbo equalization for dispersive channels," *IEEE Transactions on Vehicular Technology*, vol. 64, no. 10, pp. 4870-4875, 2015.
- [87] M. Koca and H. Sari, "Performance analysis of spatial modulation over correlated fading channels," in *Vehicular Technology Conference (VTC Fall), 2012 IEEE*, 2012, pp. 1-5: IEEE.

- [88] P. Liu, J. Blumenstein, N. S. Perović, M. Di Renzo, and A. Springer, "Performance of Generalized Spatial Modulation MIMO Over Measured 60GHz Indoor Channels," *IEEE Transactions on Communications*, vol. 66, no. 1, pp. 133-148, 2018.
- [89] M. Elsayed, H. S. Hussein, and U. S. Mohamed, "Fully generalised spatial modulation," in *National Radio Science Conference (NRSC), 2018 35th*, 2018, pp. 274-282: IEEE.
- [90] B. Zhou, Y. Xiao, P. Yang, J. Wang, and S. Li, "Spatial modulation for single carrier wireless transmission systems," in *Communications and Networking in China (CHINACOM), 2011 6th International ICST Conference on*, 2011, pp. 11-15: IEEE.
- [91] P. Som and A. Chockalingam, "Spatial modulation and space shift keying in single carrier communication," in *Personal Indoor and Mobile Radio Communications (PIMRC), 2012 IEEE 23rd International Symposium on*, 2012, pp. 1962-1967: IEEE.
- [92] R. Rajashekar, K. Hari, and L. Hanzo, "Spatial modulation aided zero-padded single carrier transmission for dispersive channels," *IEEE Transactions on Communications*, vol. 61, no. 6, pp. 2318-2329, 2013.
- [93] P. Yang *et al.*, "Single-carrier SM-MIMO: A promising design for broadband large-scale antenna systems," *IEEE Communications Surveys & Tutorials*, vol. 18, no. 3, pp. 1687-1716, 2016.
- [94] L. Jing, H. Wang, C. He, and Z. Ding, "Spatial CCK Modulation and Iterative Detection Over Frequency-Selective Fading Channels," *IEEE Wireless Communications Letters*, vol. 6, no. 4, pp. 506-509, 2017.
- [95] J.-P. Kermoal, L. Schumacher, K. I. Pedersen, P. E. Mogensen, and F. Frederiksen, "A stochastic MIMO radio channel model with experimental validation," *IEEE Journal on selected areas in Communications*, vol. 20, no. 6, pp. 1211-1226, 2002.
- [96] K. Yu, M. Bengtsson, B. Ottersten, D. McNamara, P. Karlsson, and M. Beach, "Second order statistics of NLOS indoor MIMO channels based on 5.2 GHz measurements," in *Global Telecommunications Conference, 2001. GLOBECOM'01. IEEE*, 2001, vol. 1, pp. 156-160: IEEE.
- [97] A. Younis, "Spatial modulation: Theory to practice," 2014.
- [98] A. Hedayat, H. Shah, and A. Nosratinia, "Analysis of space-time coding in correlated fading channels," *IEEE Transactions on Wireless Communications*, vol. 4, no. 6, pp. 2882-2891, 2005.

- [99] N. Serafimovski *et al.*, "Practical implementation of spatial modulation," *IEEE Trans. Veh. Technol.*, vol. 62, no. 9, pp. 4511-4523, 2013.
- [100] A. Martinez, A. G. i Fabregas, and G. Caire, "A closed-form approximation for the error probability of coded BPSK fading channels," in *Communications Theory Workshop, 2006. Proceedings. 7th Australian*, 2006, pp. 15-18: IEEE.
- [101] M. Chiani, D. Dardari, and M. K. Simon, "New exponential bounds and approximations for the computation of error probability in fading channels," *IEEE Transactions on Wireless Communications*, vol. 2, no. 4, pp. 840-845, 2003.
- [102] J. W. Craig, "A new, simple and exact result for calculating the probability of error for two-dimensional signal constellations," in *Proc. IEEE Milcom*, 1991, vol. 91, pp. 571-575.
- [103] G. L. Turin, "The characteristic function of Hermitian quadratic forms in complex normal variables," *Biometrika*, vol. 47, no. 1/2, pp. 199-201, 1960.
- [104] R. Mesleh, O. S. Badarneh, A. Younis, and F. S. Almeahadi, "How significant is the assumption of the uniform channel phase distribution on the performance of spatial multiplexing MIMO system?," *Wireless Networks*, vol. 23, no. 7, pp. 2281-2288, 2017.
- [105] A. Younis, R. Mesleh, and H. Haas, "Quadrature Spatial Modulation Performance Over Nakagami- $m$  Fading Channels," *IEEE Transactions on Vehicular Technology*, vol. 65, no. 12, pp. 10227-10231, 2016.
- [106] M. Di Renzo, R. Y. Mesleh, H. Haas, and P. M. Grant, "Upper bounds for the analysis of trellis coded spatial modulation over correlated fading channels," in *Vehicular Technology Conference (VTC 2010-Spring), 2010 IEEE 71st*, 2010, pp. 1-5: IEEE.
- [107] G. Auer *et al.*, "How much energy is needed to run a wireless network?," *IEEE Wireless Communications*, vol. 18, no. 5, 2011.
- [108] C. Desset *et al.*, "Flexible power modeling of LTE base stations," in *Wireless Communications and Networking Conference (WCNC), 2012 IEEE*, 2012, pp. 2858-2862: IEEE.
- [109] Y. Lee and S. Yun, "Interchannel interference avoidance in MIMO transmission by exploiting spatial information," in *Personal, Indoor and Mobile Radio Communications, 2005. PIMRC 2005. IEEE 16th International Symposium on*, 2005, vol. 1, pp. 141-145: IEEE.

- [110] S. Medawar, P. Handel, and P. Zetterberg, "Approximate maximum likelihood estimation of Rician K-factor and investigation of urban wireless measurements," *IEEE Transactions on Wireless Communications*, vol. 12, no. 6, pp. 2545-2555, 2013.
- [111] A. Y. Kok and K. E. Law, "Systolic Array-based Pipelining Design of CCK Demodulators," in *2007 Canadian Conference on Electrical and Computer Engineering*, 2007, pp. 70-73: IEEE.